Introduction of novel artificial pathways in
Escherichia coli with fructose 6-phosphate aldolase (FSA)

Von der Fakultät für Energie-, Verfahrens- und Biotechnik der Universität Stuttgart
zur Erlangung der Würde eines Doktors der Naturwissenschaften (Dr. rer. nat.)
genehmigte Abhandlung

Vorgelegt von
Emma Guitart Font
aus Esplugues de Llobregat (Spanien)

Hauptberichter:	Prof. Dr. Georg A. Sprenger
Mitberichter:	Apl. Prof. Dr. Siemann-Herzberg
Tag der mündlichen Prüfung:	06. Februar 2024

Institut für Mikrobiologie der Universität Stuttgart

2024

Declaration of Authorship

I hereby certify that the dissertation with the title "Introduction of novel artificial pathways in Escherichia coli with fructose 6-phosphate aldolase (FSA)" is entirely my own work except where otherwise indicated. Passages and ideas from other sources have been clearly referenced.

Erklärung über die Eigenständigkeit der Dissertation

Ich versichere, dass ich die vorliegende Arbeit mit dem Titel "Introduction of novel artificial pathways in Escherichia coli with fructose 6-phosphate aldolase (FSA)" selbständig verfasst und keine anderen als die angegebenen Quellen und Hilfsmittel benutzt habe; aus fremden Quellen entnommene Passagen und Gedanken sind als solche kenntlich gemacht.

Bad Säckingen, 20.05.2023

Emma Guitart Font

Table of contents

Publications on the subject of this dissertation

1) **Guitart Font E., Sprenger G.A.** 2020. Opening a novel biosynthetic pathway to dihydroxyacetone and glycerol in *Escherichia coli* mutants through expression of a gene variant (*fsaA^{A129S}*) for fructose 6-phosphate aldolase. *International Journal of Molecular Sciences* **21**: 9625

   Submitted on 15 November 2020

   Published on 17 December 2020

2) **Guitart Font E., Sprenger G.A.** 2024. Complementation of an *Escherichia coli* K-12 mutant strain deficient in KDO synthesis by forming D-arabinose 5-phosphate from glycolaldehyde with fructose 6-phosphate aldolase (FSA). *Applied Microbiology* **4**: 470-480

   Submitted on 27 January 2024

   Published on 03 March 2024

Figures

Tables

Abbreviations

3PGA	3-phosphoglycerate
1x	1-fold
A5P	D-arabinose 5-phosphate
Abe	Abequose
ADP	adenosine diphosphate
Ala; A	alanine
ALE	adaptive laboratory evolution
Amp/AMP	ampicillin / adenosine monophosphate
APS	ammonium persulphate
API	arabinose 5-phosphate isomerase
ATP	adenosine triphosphate
bp	base pairs
BSA	bovine serum albumin
C	carbon
Cas9	CRISPR associated protein 9
cat	chloramphenicol resistance gene
CCR	carbon catabolite repression
cDNA	complementary DNA
CDW	cell dry weight
CE	cell-free extract
Cm	chloramphenicol
CMP	cytidine monophosphate
CoA	coenzyme A
CRISPR	Clustered Regularly Interspaced Short Palindromic Repeats
CRP	cAMP receptor protein
crr	gene that codes for EIIA^{Glc}
CSR	carbon storage regulator
CV	column volumes
DeoC	deoxyribose-phosphate aldolase
dH$_2$O	destilled water
DHA	dihydroxyacetone
dhaKLM	genes that code for dihydroxyacetone kinase in *E. coli* (DHAK)
DHAP	dihydroxyacetone phosphate
DMSO	dimethyl sulfoxide
DNA	deoxyribonucleic acid
dNTP	deoxynucleotides
ds	double-stranded
DTT	dithiothreitol
E4P	D-erythrose 4-phosphate
EI	enzyme I of the PTS
EII^{Glc}	glucose-specific enzyme II of the PTS
EII^{Fru}	fructose-specific enzyme II of the PTS

EII^{Man}	mannose-specific enzyme II of the PTS
E. coli	*Escherichia coli*
EDTA	ethylenediamine tetraacetic acid
EMP	Embden-Meyerhof-Parnas
eno	gene that codes for enolase
EtBr	ethidium bromide
EtN	ethanolamine
EtOAc	ethyl acetate
EtOH	ethanol
F1,6BP	fructose 1,6-bisphosphate
F6P	fructose 6-phosphate
FA	formaldehyde
FLP	flippase
FRT	FLP recognition site
Fru	fructose
fbaA / *fbaB*	genes that code for fructose 1,6-bisphosphate aldolase
fsaA / *fsaB*	genes that code for fructose 6-phosphate aldolase (FSAA wt / FSAB)
fsaA^{A129S}	gene that codes for FSAA A129S
FSA	fructose 6-phosphate aldolase
G1P	glucose 1-phosphate
G3P	glyceraldehyde 3-phosphate
G6P	glucose 6-phosphate
GA	glyceraldehyde
Gal	D-galactose
GalP	galactose permease
gapA	gene that codes for glyceraldehyde 3-phosphate dehydrogenase (G3P DH)
Glc	D-glucose
GlcN	glucoseamine
GlcNAc	*N*-acetyl-glucosamine
gldA	gene that codes for glycerol dehydrogenase (GldA)
glpD	gene that codes for glycerol 3-phosphate dehydrogenase
glpF	gene that codes for glycerol facilitator (GlpF)
glpK	gene that codes for glycerol kinase (GlpK)
Gly3P	glycerol 3-phosphate
gnd	gene that codes for 6-phosphogluconate dehydrogenase (Gnd)
GoA	glycolaldehyde
gpmM / *gpmA*	genes that codes for phosphoglycerate mutases
gpsA	gene that codes for glycerol 3-phosphate dehydrogenase (Gly3P DH)
gutQ	gene that codes for arabinose 5-phosphate isomerase (GutQ)
H$_2$O	water
HA	hydroxyacetone
HB	1-hydroxy-2-butanone
Hep	L-glycero-D-mannoheptose
Hi-Fi	High-Fidelity
His; H	histidine

XVIII

Hfq	RNA chaperone
HOAc	acetic acid
HPLC	High Performance Liquid Chromatography
HPr	histidine phosphocarrier protein
HT	heat-treated enriched fraction
IM	inner membrane
IPTG	isopropyl-β-D-thiogalactopyranosid
kan	kanamycin resistance gene
kb	kilobases
KDO	2-keto-3-deoxymanno-octulosonic acid
kdsA	gene that codes for KDO 8-phosphate synthetase (KdsA)
kdsD	gene that codes for arabinose 5-phosphate isomerase (KdsD)
K_M	Michaelis-Menten constant
Km	kanamycin
K_S	substrate concentration to reach half of the $OD_{600\ nm\ max}$
lacA	gene that codes for thiogalactoside acetyltransferase
lacI	gene that codes for the lactose inhibitor
lacI'	3' region of the *lacI* gene
lacY	gene that codes for the lactose permease
lacZ	gene that codes for the *β*-galactosidase
'lacZ	5' region of the *lacZ* gene
lacZ'	3' region of the *lacZ* gene
LB	Luria-Bertani
LC	lethal concentration
LPS	lipopolysaccharide
Lys; K	lysine
Man	mannose
max.	maximal
MeOH	methanol
mercaptoEtOH	2-mercaptoethanol
MG	methylglyoxal
Mlc	glucose repressor, makes large colonies
MM	minimal medium
MOPS	3-(N-Morpholino) propane sulfonic acid
MQ	deionised water
MS	mass spectrometry
MtfA	Mlc titration factor A
NAD^+/NADH	nicotinamide adenine dinucleotide oxidised/reduced
$NADP^+$/NADPH	nicotinamide adenine dinucleotide phosphate oxidised/reduced
Nag	*N*-acetyl-glucosamine
NEB	New England Biolabs GmbH
Ni^{2+}-NTA	Nickel (II) - Nitrilotriacetic
$OD_{xyz\ nm}$	optical density measured at the specified wavelength
OM	outer membrane

ONP	o-nitrophenol
ONPG	o-nitrophenyl-β-D-galactopyranoside
P	promoter/phosphate
PAGE	polyacrylamide gel electrophoresis
PCR	polymerase chain reaction
PEP	phosphoenolpyruvate
pfkA / *pfkB*	genes that code for phosphofructokinase (PfkA / PfkB)
P_{fsaA*}	promoter for *fsaA* or *fsaB*
pgi	gene that codes for phosphoglucose isomerase (PGI)
pgk	gene that codes for phosphoglycerate kinase (Pgk)
pgl	gene that codes for 6-phosphogluconolactonase (Pgl)
pH	negative of the base 10 logarithm of the molar concentration of hydrogen ions
Phe; F	phenylalanine
P_i	inorganic phosphate
P_{lac}	promoter for *lac* operon
PPP	pentose phosphate pathway
ppsA	gene that codes for the PEP synthetase (PpsA)
P_{tac}	*tac* promoter
PTS	phosphoenolpyruvate transport system
ptsG	gene that codes for EIIBC^{Glc}
pykF / *pykA*	genes that code for pyruvate kinase (PykF / PykA)
Pyr	pyruvate
qPCR	quantitative real-time PCR
antibiotic^R	resistant to the corresponding antibiotic
R5P	ribose 5-phosphate
RBS	ribosome binding site
RCF	relative centrifugal force
R_f	retention factor
Rha	rhamnose
RID	refractive index detector
RNA	ribonucleic acid
rpe	gene that codes for ribulose-phosphate 3-epimerase
rpiA / *rpiB*	genes that code for ribose 5-phosphate isomerase
rpm	revolutions per minute
RT	room temperature
Ru5P	ribulose 5-phosphate
antibiotic^S	sensitive to the corresponding antibiotic
S7P	D-sedoheptulose 7-phosphate
SDS	sodium dodecyl sulphate
sec	seconds
Ser; S	serine
SgrR	transcription factor
sgRNA	single-guide RNA
SgrS	sugar transport-related sRNA

XX

SgrT	protein, represses EII^{Glc} activity
Spc	spectinomycin
ss	single-stranded
T6P	tagatose 6-phosphate
TAE	Tris-acetate-EDTA
talB	gene that codes for transaldolase B
TCA	tricarboxylic acid
TEMED	N,N,N',N'-tetramethylethylenediamine
TFB I	transformation buffer I
TFB II	transformation buffer II
tktA / *tktB*	genes that codes for transketolase
TLC	Thin Layer Chromatography
tpiA	gene that codes for triose-phosphate isomerase (TPI)
tricine	N-Tris(hydroxymethyl)-methyl-glycine
Tris	tris(hydroxymethyl)-aminomethane
Tyr; Y	tyrosine
U	units
uhpT	hexose phosphate transport system
UQ/UQH$_2$	ubiquinone oxidised/reduced
USA	United States of America
V_{max}	maximal velocity
UV	ultraviolet
v/v	volume percent
vs.	versus
wt	wild-type
xfp	gene that codes for the X5P/F6P phosphoketolase (Xfp)
× *g*	times gravity
X-gal	5-bromo-4-chloro-3-indolyl-β-D-galactopyranoside
Xu5P	xylulose 5-phosphate
YigL	haloacid dehalogenase phosphatase
zwf	gene that codes for the glucose 6-phosphate dehydrogenase (G6P DH)

1 Summary

1.1 Summary

In *Escherichia coli* (*E. coli*) K-12 there are only two known genes that code for enzymes with fructose 6-phosphate aldolase (FSA) activities, *fsaA* codes for FSAA wt and *fsaB* for FSAB. These isoenzymes belong to class I aldolases and can use dihydroxyacetone (DHA) instead of dihydroxyacetone 3-phosphate (DHAP) as donor substrates (Schürmann and Sprenger, 2001). Furthermore, their first, but not solely, known reaction *in vitro* is the reversible cleavage of fructose 6-phosphate (F6P) to DHA and glyceraldehyde 3-phosphate (G3P). Due to the weak expression of the native promoters of *fsaA* and *fsaB*, only enzymatic data from recombinant FSA have been reported so far. Moreover, FSAA wt and its variant FSAA A129S have been reported to use a broad range of substrates, such as DHA and hydroxyacetone as donors and erythrose 4-phosphate, formaldehyde, glycolaldehyde (GoA), D-glyceraldehyde and many other aldehydes as acceptors (Schürmann and Sprenger, 2001; Schürmann et al., 2002; Sugiyama et al., 2007; Garrabou et al., 2009; Castillo et al., 2010; Sánchez-Moreno et al., 2012a; Yang et al., 2017a; Mao et al., 2021). Therefore, in *E. coli* the reversible cleavage of F6P might not necessarily be the physiological reaction of FSA.

In the present work (partly published by Guitart Font and Sprenger; 2020) it was investigated whether *in vitro* reactions catalysed by FSA (FSAA wt, FSAA A129S or FSAB) could take place *in vivo* in *E. coli*. For this purpose, mutant strains deficient in genes of the central carbon metabolism (Embden-Meyerhof-Parnas and pentose phosphate pathway) or anabolism (2-keto-3-deoxymanno-octulosonic acid synthesis pathway) were constructed by using a recombineering technique (Datsenko and Wanner, 2000) or CRISPR/Cas (Jiang et al., 2015). These mutant strains were characterised in combination with the expression of different FSA genes (*fsaA*, *fsaA^{A129S}* and/or *fsaB*). Furthermore, the LJ110 reporter strains P*~fsaA~*-*lacZYA* and P*~fsaB~*-*lacZYA* were constructed according to Trachtmann et al. (2016) to study the native promoters of the *fsaA* and *fsaB* genes (P*~fsaA~* and P*~fsaB~*).

One of the studied strains, GL3 (LJ110, Δ*zwf::*FRT Δ*pfkB::*FRT Δ*pfkA::*FRT), is deficient in phosphofructokinase and glucose 6-phosphate (G6P) dehydrogenase activities. As expected, the block on glycolysis and the pentose phosphate pathway (PPP) impaired growth of GL3 on C-sources that exclusively enter glycolysis above or at the level of F6P, such as glucose, mannitol, glucitol, xylose, maltose or galactose. Furthermore, growth on sugars that partially lead to an intracellular accumulation of sugar phosphates was either partially or totally

impaired. GL3 could deplete fructose probably by using the fructose PTS, instead of the mannose PTS (Kornberg, 2001; Luo et al., 2014).

In the presence of glucose as sole C-source, GL3 accumulated intracellular G6P and F6P (1.6 ± 0.6 mM and 1.1 ± 0.4 mM, respectively), whereas these metabolites were below the detection level in LJ110 (enzymatic quantification). Thus, impaired growth of GL3 on glucose could be a result of the accumulation of sugar phosphates and lack of further catabolism (Richards et al., 2013). Therefore, it was evaluated if FSA activities (F6P cleavage to DHA and G3P) from the expression of plasmid-borne genes (pJF119*fsaA* or pJF119 *fsaA*^{A129S}) might open a glycolytic bypass in GL3. Whereas the activity of FSAA wt was not sufficient to restore growth of GL3 on glucose, the activity of FSAA A129S enabled the triple mutant GL3 to deplete glucose with a growth rate of 0.12 ± 0.01 h^{-1} and a doubling time of 6 h (Guitart Font and Sprenger, 2020). FSAA A129S is a variant of FSAA wt (Schürmann, 2001) that has an increased catalytic efficiency (k_{cat}/K_M) for F6P when compared to FSAA wt (Schürmann, 2001; Castillo et al., 2010). Furthermore, proof that the activity of FSAA A129S was responsible in GL3 for the complementation of growth on glucose was gathered: retro-aldol activity in heat-treated enriched fractions, SDS-PAGE, and transient appearance of DHA in the supernatant. It was investigated if the growth defect of GL3 on glucose could also be removed by chromosomally integrating one copy of the *fsaA*^{A129S} gene under the control of the promoter P$_{tac}$ in the *lac*-operon instead of using a plasmid-based expression. For this purpose, GL4 (LJ110, $\Delta zwf::$FRT $\Delta pfkB::$FRT $\Delta pfkA::$FRT $\Delta lacZ::$P$_{tac}$-*fsaA*^{A129S}) was constructed. The lower overexpression of FSAA A129S could restore growth of GL4 on glucose as well (0.05 ± 0.00 h^{-1}). Furthermore, the transient appearance of DHA in the supernatant of GL4 is evidence of the activity of FSAA A129S. Transcripts levels for *dhaK* in GL4, a gene that codes for a subunit of the enzyme complex DHAKLM (responsible for the detoxification of DHA in the cell; Erni et al., 2006), were 50-fold higher than the transcript levels measured for *glpK*. Whereas in LJ110 the transcript levels for *dhaK* were below the detection level, and for *glpK* were similar to the levels determined for GL4.

To produce and accumulate more DHA, the chromosomal copy of *dhaKLM* was deleted in GL4, creating GL5 (LJ110, $\Delta zwf::$FRT $\Delta pfkB::$FRT $\Delta pfkA::$FRT $\Delta dhaKLM$ $\Delta lacZ::$P$_{tac}$-*fsaA*^{A129S}). A 6-fold higher DHA concentration (3.1 ± 0.3 mM) could be detected in the supernatant of GL5 during growth on glucose. This accumulation was only temporary. Thus, another possible enzyme candidate for the consumption of DHA, glycerol kinase GlpK, was identified. As a result, GL6 (LJ110, $\Delta zwf::$FRT $\Delta pfkB::$FRT $\Delta pfkA::$FRT $\Delta dhaKLM$ $\Delta lacZ::$P$_{tac}$-*fsaA*^{A129S} $\Delta glpK$) was constructed by deleting *glpK* from the chromosome of GL5. During growth on

glucose, GL6 was able to accumulate 8.8 ± 0.3 mM DHA in the medium over time and in the stationary phase glycerol (1.9 ± 0.2 mM) was detected as well. The prospect that 1 mole glycerol might be produced from 1 mole glucose via DHA by overproducing the *E. coli* glycerol dehydrogenase GldA (encoded by *gldA*) emerged with the detection of glycerol in the supernatant of GL6. For this purpose, GL7 (LJ110, Δzwf::FRT $\Delta pfkB$::FRT $\Delta pfkA$::FRT $\Delta dhaKLM$ $\Delta lacZ$::P*tac*-*fsaA*^{A129S} $\Delta glpK$ $\Delta rbsk$::P*tac*-*gldA*) was created by inserting the *gldA* gene under the control of the inducible promoter P*tac* in the ribose-operon of the GL6 chromosome. On glucose GL7 reached a maximal theoretical yield from glucose to DHA and glycerol of 84 % (3.5 ± 0.3 mM DHA and 21.8 ± 0.0 mM glycerol) with a significantly reduced growth rate (240 h until maximal OD$_{600\,nm}$). Due to the low growth rates on glucose of GL5, GL6 and GL7, these strains were subjected to growth rate selection pressure to examine if their fitness could be improved trough adaptive evolution (Feuer et al., 2012). An increase in growth rate was reached by the GL-evolved strains (GL-evolved strains: 0.08 - 0.12 h^{-1}; GL-strains: 0.02 -0.03 h^{-1}) without a trade-off in the production of DHA or glycerol. The most promising *E. coli* strain for the production of DHA in regards to conversion rate and growth rate was the evolved strain GL5***** (44 % of maximum theoretical yield from glucose), followed by GL6***** (43 %). GL7 achieved the highest molar yield of glucose to glycerol (72 %) with a low growth rate on glucose, while GL7***** reached a yield of 66 % with a higher growth rate (GL7***** 0.11 ± 0.01 h^{-1} vs. GL7 0.03 ± 0.00 h^{-1} and the maximal OD$_{600\,nm}$ reached after 48 h incubation instead of 240).

In *E. coli* the surface of the outer membrane (OM) to the exterior is covered by lipopolysaccharide (LPS). *E. coli* K-12 has a rough-LPS (without O-antigen; Liu and Reeves, 1994). LPS prevents the entry of hydrophobic compounds into the cell. The presence of two 2-keto-3-deoxymanno-octulosonic acid (KDO) molecules in the inner core of each LPS is necessary for *E. coli* to survive (Neidhardt et al., 1990; Schnaitman and Klena, 1993; Gronow and Brade, 2001; Raetz and Whitfield, 2002; Cipolla et al., 2010; Whitfield and Trent, 2014; Sperando et al., 2017). In *E. coli* the arabinose 5-phosphate isomerases (API) KdsD and GutQ are the only enzymes that supply arabinose 5-phosphate (A5P) to the KDO synthesis pathway. Therefore, if both KdsD and GutQ activities are missing, growth of *E. coli* is dependent on external A5P (Meredith and Woodard, 2005; Sperandeo et al., 2006). In this work, it was reported for the first time that FSAA A129S can catalyse the cleavage of A5P to G3P and GoA (K_M for A5P = 1.1 ± 0.2 mM; V_{max} = 5.3 ± 0.5 U/mg). Furthermore, the *in vitro* synthesis of A5P was performed with FSAA A129S achieving a yield of 32 % (63 ± 1 mM A5P from 200 mM GoA). Following this, an A5P auxotroph *E. coli* K-12 BW25113 strain was created

(BW25113 $\Delta gutQ$ $\Delta kdsD$::km) by the deletion of the genes $gutQ$ and $kdsD$ that code for the APIs GutQ and KdsD, respectively. A positive correlation was identified between the initial external A5P concentration available to the cells and the maximal $OD_{600\,nm}$ reached by the strain. The A5P auxotroph strain needed more than 60 µM external A5P to reach its maximal $OD_{600\,nm}$ on glucose, whereas 5 µM A5P were sufficient for this strain to survive. Furthermore, the external A5P concentration available had an impact on the integrity of the LPS produced. At concentrations of 50 µM A5P or above, the integrity of LPS was ensured. When 20 µM A5P or less were available, LPS partly lost its integrity. The expression of $fsaA$, $fsaA^{A129S}$ or $fsaB$ could restore growth of the A5P auxotroph strain on glucose + GoA as a result of the synthesis of A5P. Furthermore, one copy of the gene $fsaA^{A129S}$ in the chromosome (BW25113, $\Delta gutQ$::FRT $\Delta kdsD$::FRT $\Delta rbsK$::P_{tac}-$fsaA^{A129S}$) was sufficient to allow growth on glucose. Evidence for an unknown source of GoA was shown.

Finally, the strength of the native promoters of the genes $fsaA$ and $fsaB$ (P_{fsaA} and P_{fsaB}) was evaluated. According to the β-galactosidase activities measured with the LJ110 reporter strains P_{fsaA}-$lacZYA$ and P_{fsaB}-$lacZYA$, even though both fsa-promoters in comparison with P_{lac} are weak, P_{fsaA} is stronger than P_{fsaB} (3155 ± 117 $U/OD_{600\,nm}$ for P_{lac}, 76.7 ±10.4 $U/OD_{600\,nm}$ for P_{fsaA} and 5.3 ± 1.7 $U/OD_{600\,nm}$ for P_{fsaB}). Furthermore, these LJ110 reporter strains were put under lactose growth selection to study if spontaneous mutations in the sequence of the promoters P_{fsaA} and P_{fsaB} could enhance their strength. A deletion of six bases upstream of the -35 motif of P_{fsaB} (3'-AAAACA-5') enabled a 3-fold increase in β-galactosidase activity. Moreover, both $fsaB$ promoters (native and mutant) showed an 8 times increase in β-galactosidase activity in the presence of 15 mM HA.

In conclusion, in the present work a novel bypass pathway for the production of glycerol from glucose by using DHA as an intermediate was established. This pathway was functional as a result of the expression of genes ($gldA$, $fsaA$) already present in the $E.$ $coli$ chromosome under the control of the non-native promoter P_{tac}. Furthermore, the expression of the mutant $fsaA^{A129S}$ gene was required for this pathway to work. In addition, the fitness of the constructed strains was improved by adaptive laboratory evolution (ALE). Therefore, this is the first report of the production of DHA and glycerol from glucose in an $E.$ $coli$ strain by the homologous expression of its genes (Guitart Font and Sprenger, 2020). Furthermore, the present study is as well the first report that demonstrates the in $vivo$ synthesis of A5P from GoA and G3P catalysed by the FSA enzymes (FSAA wt, FSAA A129S and FSAB) through growth complementation of a BW25113 A5P auxotroph strain ($\Delta gutQ$ $\Delta kdsD$).

1.2 Zusammenfassung

In *Escherichia coli* (*E. coli*) K-12 gibt es nur zwei bekannte Gene, die für Enzyme mit Fructose-6-Phosphat-Aldolase (FSA)-Aktivitäten kodieren: *fsaA* kodiert für FSAA wt und *fsaB* für FSAB. Diese Isoenzyme gehören zu den Klasse-I-Aldolasen und können Dihydroxyaceton (DHA) anstelle von Dihydroxyaceton-3-phosphat (DHAP) als Donor-Substrat verwenden (Schürmann und Sprenger, 2001). Darüber hinaus ist die reversible Spaltung von Fructose-6-phosphat (F6P) zu DHA und Glycerinaldehyd-3-phosphat (G3P) ihre erste, aber nicht einzige bekannte *in vitro* Reaktion. Aufgrund der schwachen Expression der nativen Promotoren von *fsaA* und *fsaB* stammen die einzigen enzymatischen Daten, über die bisher berichtet wurde, von rekombinanten FSA. Des Weiteren wurde berichtet, dass FSAA wt und ihre Variante FSAA A129S ein breites Spektrum von Substraten wie DHA und Hydroxyaceton als Donoren und Erythrose-4-Phosphat, Formaldehyd, Glykolaldehyd (GoA), D-Glyceraldehyd und viele andere Aldehyde als Akzeptoren verwenden (Schürmann und Sprenger, 2001; Schürmann et al., 2002; Sugiyama et al., 2007; Garrabou et al., 2009; Castillo et al., 2010; Sánchez-Moreno et al., 2012a; Yang et al., 2017a; Mao et al., 2021). Daher muss die reversible Spaltung von F6P in *E. coli* nicht unbedingt die physiologische Reaktion von FSA sein.

In der vorliegenden Arbeit (teilweise veröffentlicht von Guitart Font und Sprenger, 2020) wurde untersucht, ob *in vitro* Reaktionen, die von FSA (FSAA wt, FSAA A129S oder FSAB) katalysiert werden, *in vivo* in *E. coli* stattfinden können. Zu diesem Zweck wurden Mutante-Stämme unter Verwendung der Rekombinationstechnik von Datsenko und Wanner (2000) oder CRISPR/Cas (Jiang et al., 2015) erzeugt, denen Gene des zentralen Kohlenstoffstoffwechselwegs (Embden Meyerhof Parnas und Pentosephosphatweg) oder des Anabolismus (KDO-Syntheseweg) fehlen. Diese Mutante-Stämme wurden in Kombination mit der Expression verschiedener FSA-Gene (*fsaA*, *fsaA*^{A129S} und/oder *fsaB*) charakterisiert. Weiterhin wurden die LJ110 Reporterstämme P$_{fsaA}$-*lacZYA* und P$_{fsaB}$-*lacZYA* nach Trachtmann et al. (2016) generiert, um die nativen Promotoren der *fsaA*- und *fsaB*-Gene (P$_{fsaA}$ und P$_{fsaB}$) zu untersuchen.

Einer der untersuchten Stämme, GL3 (LJ110, Δzwf::FRT $\Delta pfkB$::FRT $\Delta pfkA$::FRT), mangelt es an Phosphofructokinase- und Glucose-6-phosphat (G6P) Dehydrogenase-Aktivitäten. Wie erwartet beeinträchtigte die Blockierung der Glykolyse und des Pentosephosphatwegs (PPP) das Wachstum von GL3 auf C-Quellen, die ausschließlich oberhalb oder auf der Ebene von F6P in die Glykolyse eintreten, wie Glucose, Mannitol, Glucitol, Xylose, Maltose oder Galaktose. Darüber hinaus war das Wachstum auf Zuckern, die teilweise zu einer intrazellulären Akkumulation von Zuckerphosphaten führen, teilweise oder vollständig

beeinträchtigt. GL3 konnte Fructose abbauen, wahrscheinlich indem es das Fructose-PTS anstelle des Mannose-PTS verwendete (Kornberg, 2001; Luo et al., 2014). In Gegenwart von Glucose als einziger C-Quelle akkumulierte GL3 intrazelluläres G6P und F6P (1.6 ± 0.6 mM bzw. 1.1 ± 0.4 mM), während diese Metaboliten in LJ110 unter der Nachweisgrenze lagen (enzymatische Quantifizierung). Somit könnte das beeinträchtigte Wachstum von GL3 auf Glucose eine Folge der Akkumulation von Zuckerphosphaten sein, sowie des fehlenden weiteren Katabolismus (Richards et al., 2013). Daher wurde bewertet, ob FSA-Aktivitäten (Spaltung von F6P zu DHA und G3P) aus der Plasmid-basierten Expression von Genen (pJF119*fsaA* oder pJF119*fsaA^{A129S}*) einen glykolytischen Bypass in GL3 öffnen könnten. Während die Aktivität von FSAA wt nicht ausreichte, um das Wachstum von GL3 auf Glucose wiederherzustellen, wurde dies durch die Aktivität von FSAA A129S mit einer Wachstumsrate von 0.12 ± 0.01 h^{-1} und einer Verdopplungszeit von 6 Stunden ermöglicht (Guitart Font und Sprenger, 2020). FSAA A129S ist eine Variante von FSAA wt (Schürmann, 2001), die im Vergleich zu FSAA wt eine erhöhte katalytische Effektivität (k_{cat}/K_M) für F6P aufweist (Schürmann, 2001; Castillo et al., 2010). Darüber hinaus wurde der Nachweis geführt, dass die Aktivität von FSAA A129S verantwortlich für das Wachstum von GL3 auf Glucose ist: Retro-aldol-Aktivität in hitzebehandelten zellfreien Extrakten, SDS-PAGE und das vorübergehende Auftreten von DHA im Überstand. Es wurde untersucht, ob der Wachstumsdefekt von GL3 auf Glucose auch durch die chromosomale Integration einer Kopie des *fsaA^{A129S}*-Gens unter der Kontrolle des Promotors P$_{tac}$ in das *lac*-Operon beseitigt werden könnte. Zu diesem Zweck wurde GL4 (LJ110, Δzwf::FRT $\Delta pfkB$::FRT $\Delta pfkA$::FRT $\Delta lacZ$::P$_{tac}$-*fsaA^{A129S}*) konstruiert. Die niedrigere Überexpression von *fsaA^{A129S}* konnte das Wachstum von GL4 auf Glucose wiederherstellen (0.05 ± 0.00 h^{-1}). Darüber hinaus war das Auftreten von DHA im Überstand von GL4 nur vorübergehend. Das Transkriptlevel für *dhaK*, einem Gen, das für den Enzymkomplex DHAKLM (verantwortlich für die Entgiftung von DHA in der Zelle; Erni et al., 2006) kodiert, war in GL4 50-mal höher als das gemessenen Transkriptlevel für *glpK*. In LJ110 lag das Transkriptlevel für *dhaK* unterhalb der Nachweisgrenze und für *glpK* war der Wert vergleichbar zu dem ermittelten Wert in GL4.

Um mehr DHA zu produzieren und zu akkumulieren, wurde die chromosomale Kopie von *dhaKLM* in GL4 deletiert, wodurch GL5 entstand (LJ110, Δzwf::FRT $\Delta pfkB$::FRT $\Delta pfkA$::FRT $\Delta dhaKLM$ $\Delta lacZ$::P$_{tac}$-*fsaA^{A129S}*). Eine 6-fach höhere DHA-Konzentration (3.1 ± 0.3 mM) konnte im Überstand von GL5 nachgewiesen werden. Diese Akkumulation war nur vorübergehend. Somit wurde ein weiterer möglicher Enzymkandidat für den Verbrauch von DHA, Glycerinkinase GlpK, identifiziert. Als Folge der Deletion von *glpK* aus dem

Chromosom von GL5 wurde GL6 (LJ110, Δ*zwf*::FRT Δ*pfkB*::FRT Δ*pfkA*::FRT Δ*dhaKLM* Δ*lacZ*::P*tac*-*fsaA*^{A129S} Δ*glpK*) konstruiert. Während des Wachstums auf Glucose konnte GL6 im Laufe der Zeit 8.8 ± 0.3 mM DHA im Medium anreichern und in der stationären Phase konnte Glycerin (1.9 ± 0.2 mM) nachgewiesen werden. Mit dem Nachweis von Glycerin im Überstand von GL6 ergab sich die Aussicht, aus 1 Mol Glucose 1 Mol Glycerin über DHA herstellen zu können. Notwendig hierfür wäre die Überproduktion der *E. coli* Glycerindehydrogenase GldA (kodiert durch *gldA*). Zu diesem Zweck wurde, durch Insertion des *gldA*-Gens unter der Kontrolle des induzierbaren Promotors P*tac* in das Ribose-Operon des GL6-Chromosoms, GL7 (LJ110, Δ*zwf*::FRT Δ*pfkB*::FRT Δ*pfkA*::FRT Δ*dhaKLM* Δ*lacZ*::P*tac*-*fsaA*^{A129S} Δ*glpK* Δ*rbsk*::P*tac*-*gldA*) erzeugt. Auf Glucose erreichte GL7 eine maximale theoretische Ausbeute von Glucose zu DHA und Glycerin von 84 % (3.5 ± 0.3 mM DHA und 21.8 ± 0.0 mM Glycerin) mit einer deutlich reduzierten Wachstumsrate (240 h bis zur maximalen OD$_{600\,nm}$). Aufgrund der niedrigen Wachstumsraten auf Glucose von GL5, GL6 und GL7 wurden diese Stämme einem Selektionsdruck hinsichtlich der Wachstumsrate ausgesetzt, um zu untersuchen, ob ihre Fitness durch adaptive Evolution verbessert werden könnte (Feuer et al., 2012). Eine Steigerung der Wachstumsrate wurde durch die GL-evolvierte Stämme, ohne eine Reduzierung der Produktion von DHA oder Glycerin, erreicht (GL-evolvierte Stämme: 0.08 - 0.12 h^{-1}; GL-Stämme: 0.02 - 0.03 h^{-1}). Der vielversprechendste *E. coli*-Stamm für die Produktion von DHA in Hinsicht auf die Umwandlungs- und Wachstumsrate war der evolvierte Stamm GL5* (44 % der maximalen theoretischen Ausbeute an Glucose), gefolgt von GL6* (43 %). GL7 erzielte die höchste molare Ausbeute von Glucose zu Glycerin (72 %) bei einer niedrigen Wachstumsrate auf Glukose, während GL7* eine Ausbeute von 66 % erreichte bei einer höheren Wachstumsrate (GL7* 0.11 ± 0.01 h^{-1} vs. GL7 0.03 ± 0.0 h^{-1} und die maximale OD$_{600\,nm}$ wurde nach 48 h Inkubation anstelle von 240 h erreicht).

Bei *E. coli* ist die Oberfläche der äußeren Membran (OM) nach außen von Lipopolysaccharid (LPS) bedeckt. *E. coli* K-12 hat LPS ohne O-antigen (Liu und Reeves; 1994). LPS verhindert das Eindringen von hydrophoben Verbindungen in die Zelle. Im inneren Kern des LPS müssen zwei 2-Keto-3-desoxyoctonsäure (KDO)-Moleküle vorhanden sein um das Überleben von *E. coli* zu sichern (Neidhardt et al., 1990; Schnaitman und Klena, 1993; Gronow und Brade, 2001; Raetz und Whitfield, 2002; Cipolla et al., 2010; Whitfield und Trent, 2014; Sperando et al., 2017). In *E. coli* sind die Arabinose-5-phosphat-Isomerasen (API) KdsD und GutQ die einzigen Enzyme, die Arabinose-5-phosphat (A5P) an den KDO-Syntheseweg liefern. Fehlen also sowohl die KdsD- als auch die GutQ-Aktivitäten, ist das Wachstum von *E. coli* abhängig von externem A5P (Meredith und Woodard, 2005; Sperandeo et al., 2006). In dieser Arbeit

7

wurde erstmals berichtet, dass FSAA A129S die Spaltung von A5P zu G3P und GoA katalysieren kann (K_M für A5P = 1.1 ± 0.2 mM; V_{max} = 5.3 ± 0.5 U/mg). Darüber hinaus wurde die *in vitro* Synthese von A5P mit FSAA A129S durchgeführt, wobei eine Ausbeute von 32 % (63 ± 1 mM A5P aus 200 mM GoA) erzielt wurde. Anschließend wurde ein A5P-auxotropher *E. coli* K-12 BW25113-Stamm (BW25113 Δ*gutQ* Δ*kdsD*::*km*) durch die Deletion der Gene *gutQ* und *kdsD*, die für die APIs GutQ bzw. KdsD kodieren, geschaffen. Es wurde eine positive Korrelation zwischen der initialen externen A5P-Konzentration, die den Zellen zur Verfügung stand, und der maximalen $OD_{600\,nm}$, die vom Stamm erreicht wurde, identifiziert. Der A5P-auxotrophe Stamm benötigte mehr als 60 µM externes A5P, um seine maximale $OD_{600\,nm}$ auf Glucose zu erreichen, während 5 µM A5P für das Überleben des Stammes ausreichte. Weiterhin hatte die verfügbare externe A5P-Konzentration einen Einfluss auf die Integrität des produzierten LPS. Bei Konzentrationen von 50 µM A5P oder darüber war die Integrität von LPS sichergestellt. Wenn 20 µM A5P oder weniger verfügbar waren, war die Integrität von LPS teilweise verloren. Die Expression von *fsaA*, *fsaA*^{A129S} oder *fsaB* konnte das Wachstum des A5P-auxotrophen Stamms auf Glucose + GoA als Folge der Synthese von A5P wiederherstellen. Außerdem war eine Kopie des Gens *fsaA*^{A129S} im Chromosom (BW25113, Δ*gutQ*::FRT Δ*kdsD*::FRT Δ*rbsK*::P$_{tac}$-*fsaA*^{A129S}) ausreichend, um ein Wachstum auf Glucose zu ermöglichen. Es wurden Beweise für eine unbekannte GoA-Quelle vorgelegt.

Abschließend wurde die Stärke der nativen Promotoren der Gene *fsaA* und *fsaB* (P$_{fsaA}$ und P$_{fsaB}$) untersucht. Gemäß der β-Galactosidase-Aktivitäten, die mit den LJ110-Reporterstämmen P$_{fsaA}$-*lacZYA* und P$_{fsaB}$-*lacZYA* gemessenen wurden, ist P$_{fsaA}$ stärker als P$_{fsaB}$, obwohl beide *fsa*-Promotoren im Vergleich zu P$_{lac}$ schwach sind (3155 ± 117 U/$OD_{600\,nm}$ für P$_{lac}$, 76.7 ± 10.4 U/$OD_{600\,nm}$ für P$_{fsaA}$ und 5.3 ± 1.7 U/$OD_{600\,nm}$ für P$_{fsaB}$). Darüber hinaus wurden diese LJ110-Reporterstämme einer Laktose-Wachstumsselektion unterzogen, um zu untersuchen, ob spontane Mutationen in den Promotoren-Sequenzen von P$_{fsaA}$ und P$_{fsaB}$ ihre Stärke erhöhen konnten. Eine Deletion von sechs Basen stromaufwärts des - 35-Motivs von P$_{fsaB}$ (3'-AAAACA-5') ermöglichte eine 3-fache Erhöhung der β-Galactosidase-Aktivität. Des Weiteren zeigten beide *fsaB*-Promotoren (nativ und mutant) in Gegenwart von 15 mM HA eine 8-fache Erhöhung der β-Galactosidase-Aktivität.

Zusammenfassend wurde in der vorliegenden Arbeit ein neuartiger glycolytischer Bypass für die Produktion von Glycerin aus Glucose unter Verwendung von DHA als Zwischenprodukt etabliert. Dieser Weg war durch die Expression von Genen (*gldA*, *fsaA*), die bereits im *E. coli*-Chromosom vorhanden sind, unter der Kontrolle des nicht-nativen Promotors P$_{tac}$, funktionsfähig. Zusätzlich war die Expression des mutierten *fsaA*^{A129S}-Gens erforderlich. Die

Fitness der konstruierten Stämme konnte durch adaptive Evolution verbessert werden. Daher ist dies der erste Bericht über die Produktion von DHA und Glycerin aus Glucose in einem *E. coli*-Stamm durch die homologe Expression seiner Gene (Guitart Font und Sprenger, 2020). Darüber hinaus ist die vorliegende Studie auch der erste Bericht der *in vivo* Synthese von A5P aus GoA und G3P, die das Wachstum eines A5P-auxotrophen Stamms (BW25113 Δ*gutQ* Δ*kdsD*) ohne die Zugabe von externe A5P ermöglicht hat. Diese Reaktion wurde durch die FSA-Enzyme (FSAA wt, FSAA A129S und FSAB) katalysiert.

2 Introduction

2.1 *Escherichia coli*

Escherichia coli (*E. coli*) is a facultative anaerobe, rod-shaped gram-negative bacterium and is widely studied. It grows optimally in moderate temperatures (mesophile) and at external pH values between 6.0 and 8.0 (neutrophile). It is a chemoheterotrophic microorganism. A further characteristic is its motility, that can be described as flagella-mediated chemotaxis. Chemotaxis is key for the survival of *E. coli* in unfavourable environments, by allowing the cells to locate nutrients, such as sugars (Deutscher et al., 2006), and move towards them, or to avoid environments where toxic compounds are present (Neidhardt et al., 1990).

In its outer membrane (OM) there are porin-forming channels that allow the transport of solutes into the periplasm. Some of these solutes are sugars. *E. coli* uses numerous transport systems. Depending on the solute, its transport through the inner membrane (IM) to the cytoplasm takes place passively (simple diffusion or facilitated diffusion) or actively (ion-coupled transport, ABC transporters, or group translocation; Neidhardt et al., 1990; Swanson et al., 2016).

E. coli central metabolism consists of the Embden-Meyerhof-Parnas (EMP) pathway (commonly known as glycolysis), the tricarboxylic acid (TCA) cycle and the pentose phosphate pathway (PPP). Glycolysis is reversibly linked to PPP and TCA. Together, these three pathways provide the cell with thirteen precursor metabolites, energy (adenosine triphosphate, proton motive force) and reducing power (NADPH). These thirteen precursor metabolites are: acetyl-CoA, erythrose 4-phosphate (E4P), fructose 6-phosphate (F6P), glucose 6-phosphate (G6P), α-ketoglutarate, oxaloacetate, phosphoenolpyruvate (PEP), 3-phosphoglycerate, pyruvate, ribose 5-phosphate (R5P), sedoheptulose 7-phosphate (S7P), succinyl-CoA, and triose phosphate. Together with NADPH, ATP, nitrogen (in its reduced form ammonium) and sulphur (as hydrogen sulphide), these precursors metabolites are the starting point for the biosynthesis of approximately 75 building blocks, such as amino acids, fatty acids, nucleotides and sugars. These building blocks are then polymerised to macromolecules (glycogen, lipid, lipopolysaccharide, murein, proteins, DNA or RNA, among others). By assembling these macromolecules, the following cell structures can be formed: cytosol, envelope, flagella, pili, nucleoid and ribosomes (Neidhart et al., 1990; Swanson et al., 2016).

There are two types of cellular activities in *E. coli*, the ones that are growth-dependent and the growth-independent. Both types have the same importance regarding the survival of *E. coli*. Growth-independent cellular activities consist of activities that maintain metabolite pools,

turgor pressure and cellular pH. Activities related to chemotaxis, motility, secretion, repair and communication also belong to this type of cellular activities. (Swanson et al., 2016).

2.2 Glucose metabolism

E. coli can transport external glucose and metabolise it to obtain energy and produce biomass. If glucose is present in the medium in concentrations greater than 0.2 mM, it is transported through the outer membrane by the non-specific channel proteins OmpC and OmpF (Gosset, 2005; Luo et al., 2014). Whereas, if glucose is present below this concentration (glucose limitation), *lamB* is expressed. *lamB* codes for the porin LamB (also known as maltoporin; Fuchs, 2007), which is the main responsible for the transport of glucose through the outer membrane (Gosset, 2005). Once in the periplasm, glucose can be transported into the cytoplasm by five different proteins/systems: the glucose phosphoenolpyruvate transport system (PTS^{Glc}; for more information see Chapter 2.2.1); the mannose PTS (PTS^{Man}); the *N*-acetyl-glucosamine PTS (PTS^{Nag}); galactose permease (GalP); and the MglBAC ABC transporter (see Figure 2-2). PTS^{Glc} is the transport system that exhibits the highest affinity for glucose with a K_M for glucose of 3 to 20 µM, followed by MglBAC with 10 µM and PTS^{Man} (15 µM). On the other hand, GalP is one of the transport systems with less affinity for glucose and PTS^{Nag} shows the lowest affinity (Jahreis et al., 2008). During translocation into the cytoplasm by one of the PTS transport systems, glucose is transformed to glucose 6-phosphate (G6P; see Chapter 2.2.1). In contrast, after the transport of glucose into the cell by the transporters MglBAC or GalP, the additional phosphorylation of glucose is required to prevent its transport back to the medium. This phosphorylation reaction is performed by glucokinase and the product of this reaction is G6P (Gosset, 2005; Jahreis et al., 2008). In both cases, once glucose is present in the *E. coli* cytoplasm as G6P, up to 70 % of G6P is metabolised in the Embden-Meyerhof-Parnas (EMP) pathway, also known as glycolysis, and the remaining G6P in the oxidative branch of the pentose phosphate pathway (PPP) (Neidhardt et al., 1990).

In glycolysis (see Figure 2-1), G6P is isomerised to the intermediate metabolite fructose 6-phosphate (F6P) by phosphoglucose isomerase (encoded by *pgi*). On the one hand, F6P can enter the non-oxidative branch of PPP. On the other hand, F6P can be further metabolised in glycolysis, where it is phosphorylated to fructose 1,6-bisphosphate (F,16BP) under the consumption of an ATP molecule by a phosphofructokinase. *E. coli* possesses two isoenzymes with phosphofructokinase activity: PfkA and PfkB (encoded by *pfkA* and *pfkB*, respectively). 90 % of the phosphofructokinase activity in the cell is carried out by PfkA, while PfkB is responsible for the remaining 10 %. PfkA interacts cooperatively with F6P, is activated

by ADP and inhibited by PEP (Blangy et al., 1968). Moreover, PfkB can interact with F6P, G6P and ATP, and its activity is inhibited by ADP, citrate, F1,6BP, GTP, or PEP (Babul, 1978; Campos et al., 1984; Piazza et al., 2018). The concentration levels of these two isoenzymes are under the regulation of Cra and CsrA (Romeo and Snoep, 2013). Following the formation of F1,6BP, this intermediate is cleaved to dihydroxyacetone phosphate (DHAP) and glyceraldehyde 3-phosphate (G3P) by fructose 1,6-bisphosphate aldolase. In *E. coli* there are two different fructose 1,6-bisphosphate aldolases present: FbaA and FbaB. FbaA (encoded by *fbaA*) is the main isoenzyme during glycolysis, while FbaB is predominant during gluconeogenesis. Then, DHAP can be isomerised to G3P by triose phosphate isomerase (TPI, encoded by *tpiA*). Afterwards, G3P is phosphorylated to 1,3-bisphosphoglycerate by glyceraldehyde 3-phosphate dehydrogenase (encoded by *gapA*). In this reaction the cofactor used is NAD^+. Then, a phosphoryl group is transferred by phosphoglycerate kinase (Pgk, encoded by *pgk*) from 1,3-bisphosphoglycerate to ADP forming 3-phosphoglycerate and ATP. The phosphoglycerate mutases GpmM and GpmA convert 3-phosphoglycerate to 2-phosphoglycerate. The latter metabolite is dehydrated by enolase to phosphoenolpyruvate (PEP). Finally, a phosphoryl group is transferred by pyruvate kinase (PykF or PykA, encoded by *pykF* and *pykA*, respectively) from PEP to ADP producing pyruvate and ATP. Furthermore, PEP can also be used by the PTS to transport sugars into the cell (see Chapter 2.2.1), in the KDO biosynthesis (see Chapter 2.5), or it can be converted to oxaloacetate by PEP carboxylase (Romeo and Snoep, 2013). Pyruvate is further metabolised in the TCA cycle. Even though ATP is needed in upper glycolysis, the EMP pathway has a positive balance of NADH and ATP molecules. These two cofactors are important for other relevant cellular processes, such as ABC transport systems. From all the glycolysis enzymes mentioned above, there are only four that are encoded by essential genes: *fbaA*, *gapA*, *pgk*, and *eno* (Nakahigashi et al., 2009).

When G6P enters into the oxidative branch of the PPP, it does so as 6-phosphogluconolactone (6PGluconolactone; see Figure 2-1). This reaction is irreversible and is catalysed by glucose 6-phosphate dehydrogenase (encoded by *zwf*). 6-phosphogluconolactone is then converted to 6-phosphogluconate by 6-phosphogluconolactonase (Pgl, encoded by *pgl*). The conversion of ribulose 5-phosphate (Ru5P) from 6-phosphogluconate is catalysed by 6-phosphogluconate dehydrogenase (Gnd, encoded by *gnd*). Furthermore, the oxidative branch of the PPP has a net production of two NADPH molecules. This is possible due to the two dehydrogenase reactions, which are the main sources of NADPH in the cell during growth on glucose (Sauer et al., 2004; Riemer et al., 2013).
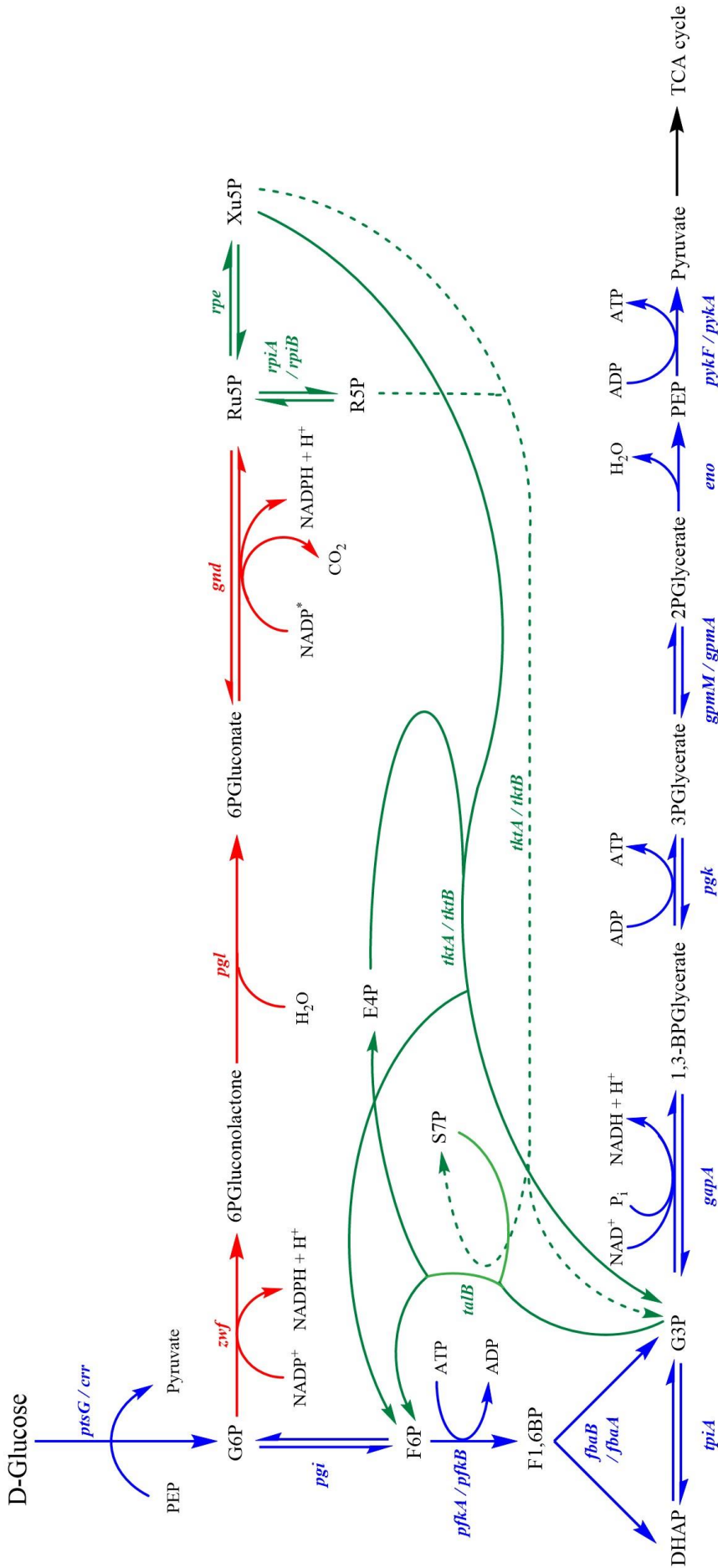
Figure 2-1. Glucose metabolism in *E. coli*. Glycolysis in blue, oxidative branch of PPP in red and non-oxidative branch of PPP in green. Enzymes activities are encoded by the genes *crr* (EIIA^{Glc}), *eno* (enolase), *fbaA*/*fbaB* (fructose 1,6-bisphosphate aldolase), *gapA* (glyceraldehyde 3-phosphate dehydrogenase), *gnd* (6-phosphogluconate dehydrogenase), *gpmM*/*gpmA* (phosphoglycerate mutase), *pfkA*/*pfkB* (phosphofructokinase), *pgi* (phosphoglucose isomerase), *pgk* (phosphoglycerate kinase), *pgl* (6-phosphogluconolactonase), *ptsG* (EIICB^{Glc}), *pykF*/*pykA* (pyruvate kinase), *rpe* (ribulose-phosphate 3-epimerase), *rpiA*/*rpiB* (ribose 5-phosphate isomerase), *talB* (transaldolase B), *tktA*/*tktB* (transketolase), *tpiA* (triose-phosphate isomerase), *zwf* (glucose 6-phosphate dehydrogenase), DHAP (dihydroxyacetone phosphate), E4P (erythrose 4-phosphate), F1,6BP (fructose 1,6-bisphosphate), F6P (fructose 6-phosphate), G3P (glyceraldehyde 3-phosphate), G6P (glucose 6-phosphate), PEP (phosphoenolpyruvate), R5P (ribose 5-phosphate), Ru5P (ribulose 5-phosphate), S7P (sedoheptulose 7-phosphate), Xu5P (xylulose 5-phosphate). Figure modified after Fuchs (2007) and Stincone et al. (2015).

The non-oxidative branch of the PPP uses F6P, G3P and sedoheptulose 7-phosphate (S7P) in reversible reactions forming erythrose 4-phosphate (E4P), ribose 5-phosphate (R5P) and xylulose 5-phosphate (Xu5P; see Figure 2-1). R5P can be further metabolised by the cell for the synthesis of nucleotides and E4P for the synthesis of amino acids. These interconversions are catalysed by transaldolases (S7P + G3P ↔ F6P + E4P; Sprenger et al., 1995b) and transketolases (F6P + G3P ↔ E4P + Xu5P; Sprenger et al., 1995a) and connect glycolysis with the PPP. The metabolites provided by the PPP are important for the survival of the cell. These include the cofactor NADPH, sugar phosphates, such as Ru5P, for the synthesis of vitamins (riboflavin) and LPS (isomerisation to A5P; see Chapter 2.5), and precursors for the synthesis of amino acids and nucleotides (Sprenger, 1995; Stincone et al., 2015).

2.2.1   Glucose phosphoenolpyruvate transport system (PTS^{Glc})

Many sugars, such as glucose, fructose, mannose and mannitol, are transported into the cell and phosphorylated by the PEP transport system (PTS), a group translocation (see Figure 2-2). Enzyme I (EI) and HPr (encoded by *ptsI* and *ptsH*, respectively) are soluble proteins present in the cytoplasm. These two proteins are non-specific due to their use in nearly all PTS systems. First, EI autophosphorylates by using PEP and, afterwards, transfers the phosphoryl group to HPr forming P~HPr. Then, P~HPr transfers the phosphoryl group to Enzyme II (EII) A. EIIA and EIIB are sugar-specific and responsible for the transfer of the phosphoryl group to the sugar being transported into the cytoplasm. Both enzymes are hydrophilic and together with EIIC (integral membrane domain) form the EII complex. In the glucose PTS, EIIB^{Glc} domain is covalently linked to EIIC^{Glc} domain, forming EIICB^{Glc}. EIIB^{Glc} is found on the cytoplasmic side, while EIIC^{Glc} is located within the inner membrane. EIIA^{Glc} is encoded by *crr* and EIICB^{Glc} by *ptsG*. The glucose uptake from the periplasmic space to the cytoplasm and its phosphorylation is carried out by the three domains of the EII complex. When the phosphoryl group of P~HPr is accepted by EIIA^{Glc}, P~EIIA^{Glc} is formed. Then, P~EIIA^{Glc} can transfer its phosphoryl group to EIIB^{Glc}, forming P~EIIB^{Glc}. After the translocation of glucose through the membrane by EIIC^{Glc}, glucose receives the phosphoryl group from P~EIIB^{Glc}. The phosphorylation of glucose yields G6P (Neidhardt et al., 1990; Tchleu et al., 2001; Mayer and Boos, 2005; Deutscher et al., 2006; Gabor et al., 2011; Deutscher et al., 2014).
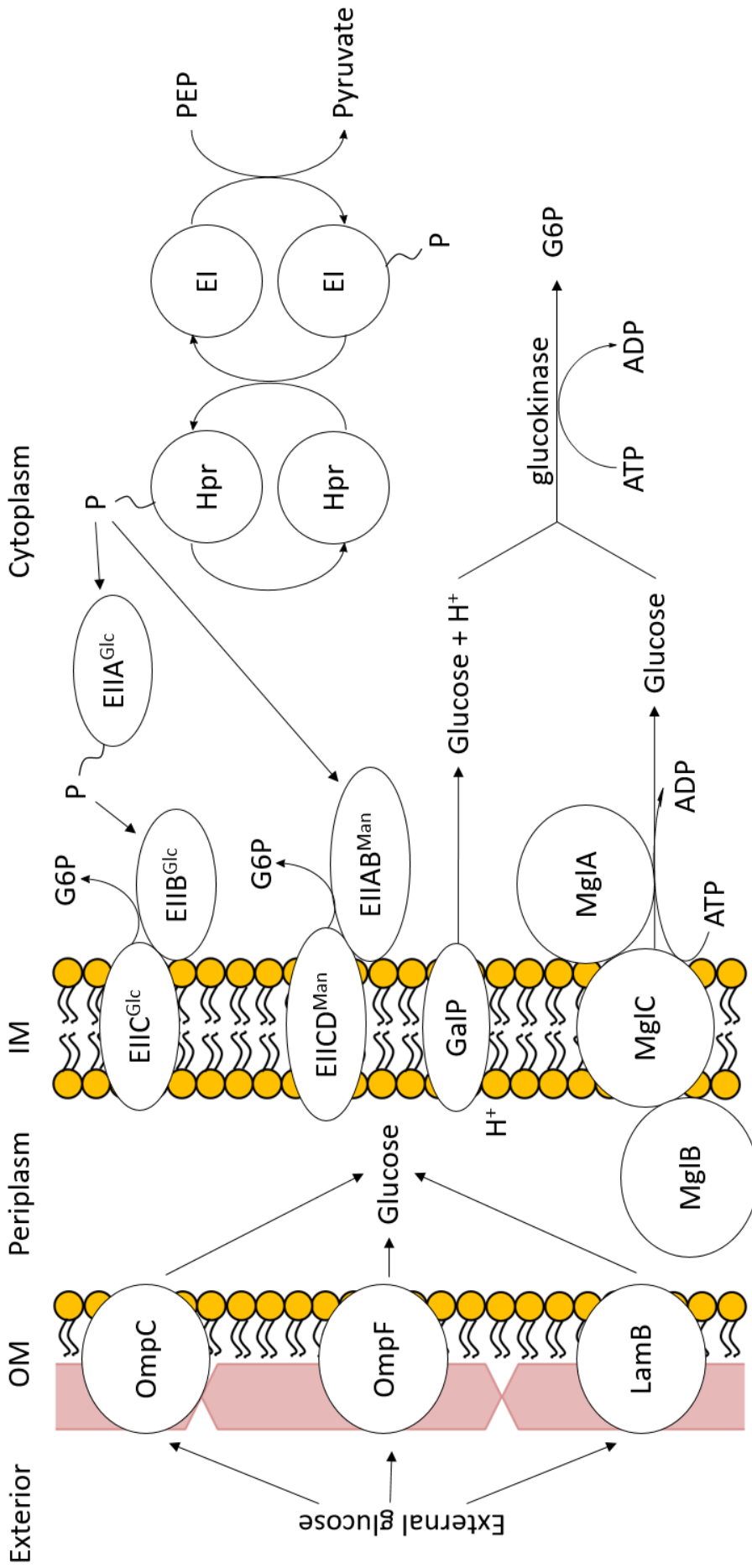
Figure 2-2. Transport of external glucose into the cell. First glucose is transported through the outer membrane (OM) by the porins OmpC, OmpF, or LamB. Once in the periplasm, glucose can be transported to the cytoplasm by the PTS systems for glucose (PTS^{Glc}) or for mannose (PTS^{Man}), the galactose permease (GalP) or the ABC transporter MglBAC. The transport by GalP and MglBAC requires the subsequent phosphorylation of glucose by glucokinase in the cytoplasm. For more details see Chapters 2.2 and 2.2.1. Figure modified after Gosset (2005).

The PTS is also a signal transduction system involved in regulatory mechanisms such as carbon catabolite repression (CCR) and chemotaxis. The phosphorylation state of components of the PTS changes depending on the presence of PTS substrates in the medium and the metabolism of the cells at that moment, giving each regulatory mechanism information. CCR acts by repressing the expression of genes belonging to the uptake and metabolism of other C-sources and/or the activity of its enzymes (Deutscher et al., 2006). The formation of cAMP from ATP by the adenylate cyclase is controlled by the phosphorylation state of EIIA^{Glc}. In the presence of P~EIIA^{Glc}, the activity of adenylate cyclase is activated. As a result, more cAMP is present in the cell. cAMP interacts with the global regulator cAMP receptor protein (CRP). Depending on the CRP/cAMP levels present in the cell, expression of determined genes, such as *ptsG*, will be up- or downregulated. On the other hand, when EIIA^{Glc} is dephosphorylated, it regulates the activity of some non-PTS sugars enzymes, such as permeases and glycerol kinase (GlpK), via the regulation mechanism known as inducer exclusion. These enzymes are only regulated when their substrate is present. Additionally, the dephosphorylated EIIB^{Glc} and the cytoplasmic protein MtfA (Mlc titration factor A) can both, independently from each other, bind to the transcription factor Mlc, inactivating it. This prevents the inhibition of the expression of a few genes, such as *malT*, *manXY*, *mlc*, *ptsG*, *ptsHI-crr* and *sgrS*, by Mlc (Mayer and Boos, 2005; Becker et al., 2006; Deutscher et al., 2006; Jahreis et al., 2008; Gabor et al., 2011; Deutscher et al., 2014; Luo et al., 2014). When there is a deficiency in nutrients, the expression of *ptsG* is suppressed by RpoS (Deutscher et al., 2006).

2.2.2   Sugar phosphate stress

Many reviews about the sugar phosphate stress and SgrS (sugar transport-related sRNA) have been published (see Vogel and Luisi, 2011; Bobrovskyy and Vanderpool, 2014; Deutscher et al., 2014; Gimpel and Brantl, 2016). SgrS is the only sRNA with at least two functions found in gram-negative bacteria: regulation of the translation of target mRNAs (*ptsG*, *manXYZ* and *yigL*) and production of the repressor SgrT (Gimpel and Brantl, 2016; see Figure 2-3). When G6P accumulates in the cell, SgrR activates *sgrS* expression (Vanderpool and Gottesman, 2004) and represses its own transcription by binding to the *sgrR-sgrS* intergenic region (Vanderpool and Gottesman, 2007). SgrS can inhibit the translation of different mRNAs by base-pairing to them. One of these mRNAs is *ptsG* mRNA, which in normal conditions is translated as the glucose transporter protein (PtsG or also known as EII^{Glc}). The base-pairing of SgrS to *ptsG* mRNA is stimulated significantly by Hfq (Kawamoto et al., 2006). However, Hfq is not responsible for its translational inhibition, only SgrS is (Maki et al., 2008). Only four bases in

SgrS and *ptsG* mRNA are essential for the translational repression through complementation of *ptsG* mRNA (Maki et al., 2010). Depending on the glycolytic flux, the degradation of *ptsG* mRNA is controlled through the activity of RNase E, the main ribonuclease for the degradation of mRNA (Kimata et al., 2001). SgrS can also bind to *manXYZ* mRNA (Rice and Vanderpool, 2011). The base-pairing at both the *manX* and within the intergenic region *manX* and *manY* is necessary for the degradation of *manXYZ* mRNA by RNase E (Rice et al., 2012).
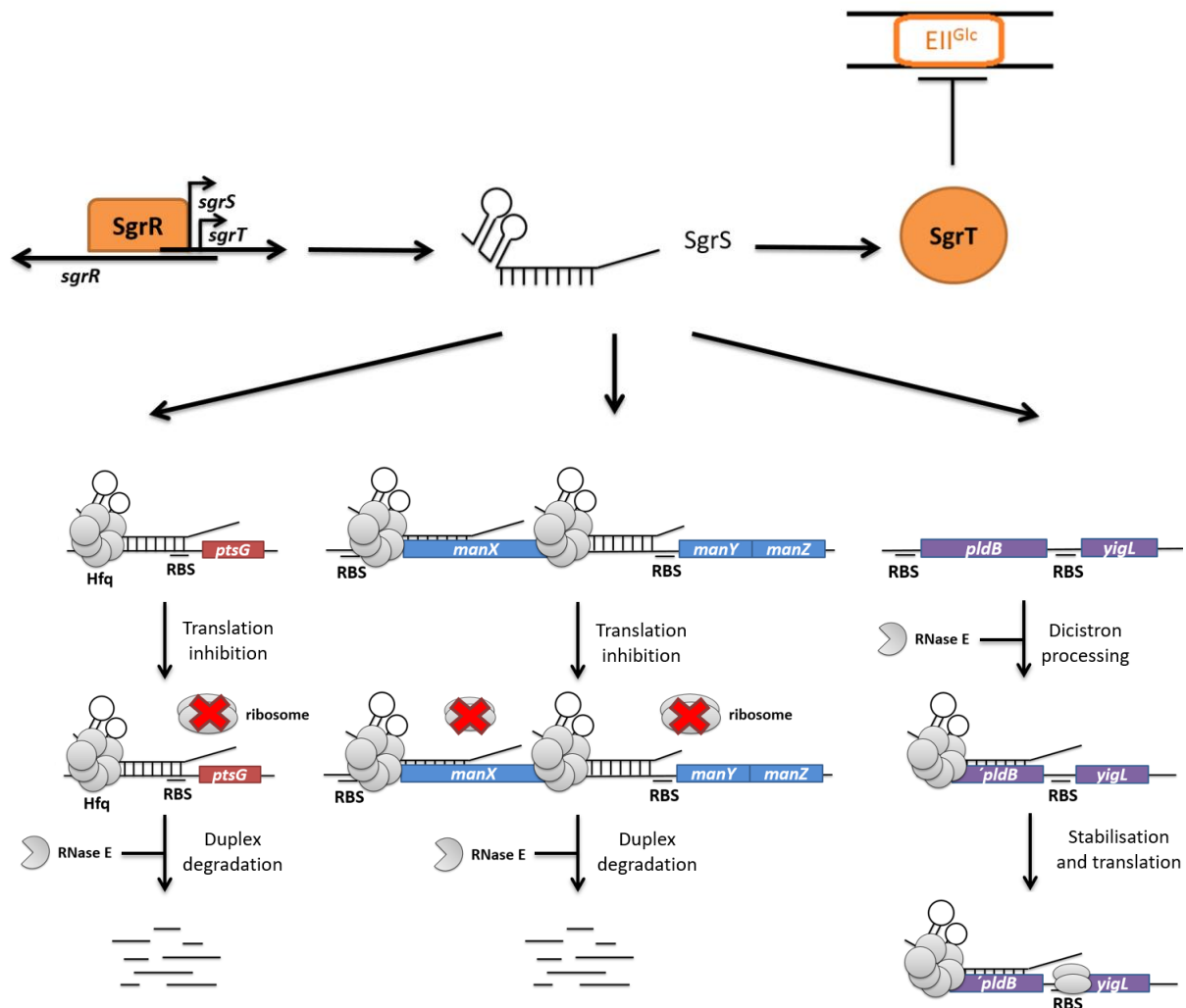
Figure 2-3. Sugar phosphate stress response. Activation of the expression of *sgrS* by SgrR (above, left). Production of SgrT from the *sgrS* gene and the transport inhibition of glucose through SgrT (above, right). Translation inhibition of the *ptsG* and *manXYZ* mRNAs by the base-pairing activity of SgrS and the posterior degradation of these mRNAs by RNase E (below, left and centre, respectively). Stabilisation of ʻ*pldB-yigL* mRNA as a result of the base-pairing activity of SgrS, which allows for an increase of the translation levels of this mRNA (below, right). Figure modified after Bobrovskyy and Vanderpool (2014).

The *sgrT* gene is found within the sequence of the *sgrS* gene and is expressed under glucose-phosphate stress conditions, but in contrast to SgrS, SgrT does not regulate the translation of

ptsG mRNA (Wadler and Vanderpool, 2007). SgrT interacts with PtsG, but not with ManXYZ. The interaction with the EIIC^{Glc} domain of PtsG allows SgrT to block the transport of glucose into the cell. As a result, phosphorylated EIIA^{Glc} accumulates easing inducer exclusion and, therefore, allowing the use of carbon sources other than glucose and decreasing the concentration of intracellular G6P (Raina and Storz, 2017; Lloyd et al., 2017). SgrS can also stabilise *'pldB-yigL* mRNA. This allows an increase of the translation levels of *'pldB-yigL* mRNA (Papenfort et al., 2013). The product of this mRNA is the haloacid dehalogenase phosphatase YigL, which dephosphorylates the accumulated sugar phosphates and, thus, is involved in the response to the sugar phosphate stress.

2.3   Aldolases

In *E. coli* metabolism, aldolases play a key role in the formation and cleavage of amino acids and carbohydrates. Aldolases catalyse the asymmetric aldol addition of a nucleophile (donor substrate) to an electrophile (acceptor substrate). This reaction is reversible and stereoselective. There are two classes of aldolases: class I and class II. Class I aldolases distinct themselves from class II aldolases by forming a Schiff base intermediate and by not requiring a cofactor. The Schiff base intermediate is formed between a conserved lysine residue present in the active site of the aldolase and the donor substrate. By activation of the donor substrate by the Schiff base intermediate, the acceptor substrate acquires its stereoselectivity (Samland and Sprenger, 2006; Clapés et al., 2010; Samland and Sprenger, 2014; Tittmann, 2014). Besides the classification between class I and class II, aldolases can also be differentiated regarding their donor substrate. In this aspect, there are five different aldolase groups: DHA and DHAP aldolases, PEP-dependent aldolases, pyruvate/2-oxobutyrate aldolases, glycine/alanine aldolases, and acetaldehyde aldolases (Samland and Sprenger, 2006; Clapés et al., 2010; Hélaine et al., 2022). The main advantage of DHA aldolases, in comparison with DHAP aldolases, is the use of nonphosphorylated donors for the aldol addition reaction instead of using the expensive and unstable phosphorylated donors (Hélaine et al., 2022).

2.4   Fructose 6-phosphate aldolase (FSA)

fsaA and *fsaB* are the only two known genes in *E. coli* K-12 that code for enzymes with fructose 6-phosphate aldolase (FSA) activities (Schürmann and Sprenger, 2001). The products of their expression are the isoenzymes fructose 6-phosphate aldolase A (FSAA) and fructose 6-phosphate aldolase B (FSAB), respectively. Furthermore, the name FSA originates from the

first known reaction *in vitro* of these enzymes. This reaction is the reversible cleavage of fructose 6-phosphate (F6P) to dihydroxyacetone (DHA) and glyceraldehyde 3-phosphate (G3P) (see Figure 2-4; Schürmann and Sprenger, 2001). However, because only data of the enzymatic activity from recombinant FSA have been reported, the reversible cleavage of F6P might not be necessarily the physiological reaction of FSA in *E. coli*. Therefore, the true physiological function of FSA in *E. coli* is still unknown (Samland and Sprenger, 2014).

FSAA and FSAB belong to the class I aldolases and can use DHA and not DHAP as donor substrate (Schürmann and Sprenger, 2001). Therefore, both isoenzymes are known DHA aldolases and belong to the 5th subfamily of transaldolases (Samland and Sprenger, 2009). DHA aldolases are not exclusively found in *E. coli* (Guérard-Hélaine et al., 2015). Other γ-proteobacteria, *Clostridia* species and lower plants have genes with similar sequences to *fsaA* and *fsaB* (Samland and Sprenger, 2014).

fructose 6-phosphate   dihydroxyacetone   glyceraldehyde 3-phosphate
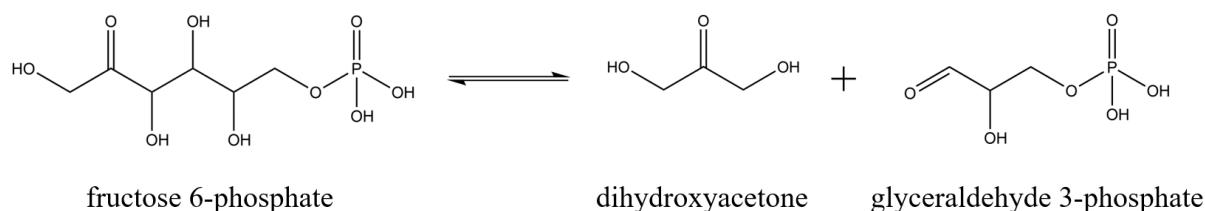
Figure 2-4. First known reaction catalysed by FSAA wt: the reversible cleavage of F6P to DHA and G3P (Schürmann and Sprenger, 2001).

2.4.1   FSAA wt

FSAA wt is the first reported enzyme that is able to cleave F6P into DHA and G3P (Schürmann and Sprenger, 2001). A maximal velocity (V_{max}) of 7 U/mg and a Michaelis-Menten constant (K_M) of 9 mM F6P was determined for the cleavage reaction of F6P by the purified enzyme and a V_{max} of 45 U/mg and a K_M of 35 mM DHA and of 0.8 mM G3P for the aldol formation (see Table 2-2). FSAA wt is a robust enzyme that retains its activity at pH between 6.0 and 12.0 and at temperatures between 20 and 75 °C. Each subunit has 24 kDa (Schürmann and Sprenger, 2001). According to Thorell et al. (2002), FSAA wt consists of ten identical subunits that are tightly packed and are organised in two pentamers, each of which exhibits a ring form. The active sites present in both pentamers face each other giving FSAA wt the form of a doughnut (for the quaternary structure of FSAA wt refer to Thorell et al., 2002). The lysine residue 85, present in the active site, is essential for the Schiff base formation typical for class I aldolases (Schürmann and Sprenger, 2001) and the tyrosine residue in the position 131 acts as an acid/base catalyst (Sautner et al, 2015; Stellmacher et al., 2015). The enzymatic activity of

FSAA wt can be inhibited by P_i, which could play an important role in the regulation of FSAA wt in the cell (Schürmann, 2001), and D-lactaldehyde (Rale et al., 2011).

By using a broad range of donors and acceptors, FSAA wt forms products with the stereoconfiguration 3*S*,4*R* (Schürmann et al., 2002). In Table 2-1 an overview of the most relevant reactions is given. The most studied donors are DHA, glycolaldehyde (GoA) and hydroxyacetone (HA). By the aldol addition of HA to different aldehydes, FSAA wt can form rare sugars, such as 1-deoxy-sugars (Schürmann et al., 2002). FSAA wt can also use acceptors, such as *N*-Cbz-protected amino aldehydes (Castillo et al., 2006), 4-nitrobutanal (Castillo et al., 2010), propanal (Rale et al., 2011), ribose 5-phosphate (Guérard-Hélaine et al., 2014), L-G3P (Hélaine et al., 2015), D-threose, 2-phenylethanal and 2-benzyloxyethanal (Concia et al., 2009). By using these acceptors with different donors, FSAA wt can form a considerable number of products. Unusual substrates such as pentanal (Guérard-Hélaine et al., 2015) and L-sorbose (Sánchez-Moreno et al., 2012b) can also be used by FSAA wt.

Table 2-1. Overview of the most relevant donors and acceptors of FSAA wt with the formed product. A5P (arabinose 5-phosphate), DHA (dihydroxyacetone), E4P (erythrose 4-phosphate), F6P (fructose 6-phosphate), FA (formaldehyde), G3P (glyceraldehyde 3-phosphate), GA (glyceraldehyde), GoA (glycolaldehyde), HA (hydroxyacetone), HB (1-hydroxy-2-butanone), S7P (sedoheptulose 7-phosphate).

Donor	Acceptor	Product	Reference
DHA	D-G3P	D-F6P	Schürmann and Sprenger (2001)
DHA	GoA	D-xylulose	Schürmann et al. (2002)
DHA	D-erythrose	D-sedoheptulose	Schürmann et al. (2002)
DHA	E4P	S7P	Schürmann et al. (2002)
GoA	FA	L-GA	Yang et al. (2017a)
GoA	GoA	D-threose	Garrabou et al. (2009)
GoA	D,L-G3P	D-A5P	Garrabou et al. (2009)
GoA	E4P	D-altrose 6-phosphate	Mao et al., 2021
HA	GoA	1-deoxyxylulose	Schürmann et al. (2002)
HA	D,L-G3P	1-deoxyfructose 6-phosphate	Schürmann et al. (2002)
HA	D-GA	1-deoxyfructose	Schürmann et al. (2002)
HA	D-erythrose	1-deoxysedoheptulose	Schürmann et al. (2002)
HB	D-G3P	D-1,2-dideoxy-arabino-hept-3-ulose-7-phosphate	Sugiyama et al. (2007) Sánchez-Moreno et al. (2012a)

FSAA wt is used in industrial applications, such as the production of D-fagomine (Castillo et al., 2006), iminocyclitols (Sugiyama et al., 2007), and furaneol (Schuermann et al., 2008). D-fagomine can be used as a food additive for patients with type II diabetes due to its anti-hyperglycaemic effect (Samland and Sprenger, 2006). Among other diseases, iminocyclitols are drug candidates for cancer, diabetes, lysosomal storage diseases and viral infections. Whereas furaneol has a sweet strawberry aroma that is used in the flavour and perfume industry (Samland et al., 2011).

Since the discovery of FSAA wt, many FSAA variants have been engineered, which are especially variable in positions found in the hydrophobic pocket of FSAA, for example L107, A129 or L163 (Schürmann, 2001; Hernández et al., 2018). All FSAA variants usually perform the reactions listed in Table 2-1 with better catalytic affinities than FSAA wt and are able to catalyse novel reactions (Schürmann, 2001; Castillo et al., 2010; Szekrenyi et al., 2014; Schmidt et al., 2016; Roldán et al., 2017; Yang et al., 2017b). Also, a variant of transaldolase B from *E. coli*, TalB F178Y, was discovered to show specific FSA activity with a V_{max} of 0.4 U/mg and a K_M of 1.5 mM F6P for the F6P cleavage reaction (Schneider et al., 2008). Garrabou et al. (2011) reported that the DHAP aldolase L-rhamnulose 1-phosphate aldolase can also add DHA to aldehydes, but the products of these reactions have another stereoconfiguration (3*R*,4*S*) than the products formed by FSAA wt.

2.4.2   FSAA A129S

The best studied FSAA variant has an amino acid exchange in the position 129, where instead of an alanine a serine is found. This variant is named FSAA A129S (Schürmann, 2001). FSAA A129S has an increased catalytic efficiency (k_{cat}/K_M) for DHA, F6P and G3P than FSAA wt (Schürmann, 2001; Castillo et al., 2010). The improved affinity for DHA could be due to the interaction between DHA and Ser129 through a hydrogen bond (Inoue, 2006). When DHA acts as the donor, formaldehyde can be used as an acceptor by FSAA A129S forming L-erythrulose (Castillo et al., 2010). Different *in vitro* cascade reactions make use of the catalytic properties of FSAA A129S. One of these reactions is the production of a precursor of D-fagomine from the addition of DHA to *N*-Cbz-3-aminopropanal (Sudar et al., 2013 and 2015).

Table 2-2. Kinetic parameters for the most relevant aldol formation and cleavage reactions catalysed by FSAA wt and FSAA A129S. Note that the values reported in this table were not determined under the same assay conditions. n.r. = not reported.

Substrate	FSAA wt		FSAA A129S	
	K_M (mM)	V_{max} (U/mg)	K_M (mM)	V_{max} (U/mg)
DHA	35[a]	45[a]	6.3[b]	104[b]
F6P	9[a]	7[a]	1.4[b]	22[b]
G3P	0.8[a]	45[a]	0.9[b]	99[b]
GoA donor	0.2[c]	0.22[c]	0.2[d]	0.02[d]
GoA acceptor	63[c]	0.22[c]	12[d]	0.44[d]
D-A5P	0.6[c]	0.3[c]	n.r.	n.r.

(a) Schürmann and Sprenger (2001)

(b) Schürmann (2001)

(c) Garrabou et al. (2009)

(d) Castillo et al. (2010)

2.4.3 FSAB

For the first decade after the discovery of both FSA isoenzymes, the main focus was put on FSAA wt. The only report regarding the characterisation of FSAB was published in 2012 by Sánchez-Moreno et al. (2012b). They showed that FSAB achieves its optimal activity at pH 8.5 and that, contrary to FSAA wt, FSAB is not thermostable at temperatures above 60 °C. In the reactions catalysed by FSAB, DHA, HA and GoA also act as donor substrates. FSAA wt and FSAB share 70 % of their amino acid sequence, their active sites are significantly alike and they both form decamers. Therefore, small differences in the enzymatic characteristics of FSAB compared to FSAA wt were expected (Sánchez-Moreno et al., 2012b).

2.5 Outer membrane and lipopolysaccharide

The outer membrane (OM) of gram-negative bacteria is asymmetrical and mainly self-assembled. It consists of lipopolysaccharide (LPS), phospholipids, murein lipoprotein, OmpA protein, porins, and proteins involved in specific diffusion processes. Furthermore, the composition of the OM gives gram-negative bacteria the necessary protection against toxic components, such as lysozyme, antibiotics and detergents (Nikaido and Vaara, 1985; Fuchs, 2007). LPS is a macromolecule present in the OM that covers 75 % of the surface of the outer leaflet. It prevents the entry of hydrophobic compounds through the OM by being an efficient

barrier, allows the cell to survive in severe environments, and is key to the resistance of *E. coli* against bile (Begley et al., 2005). In each *E. coli* cell, around 9×10^6 LPS molecules are present (Neidhardt et al., 1990; Swanson et al., 2016), adding up to 10 % of the cell dry weight (Fuchs, 2007). LPS typically consists of four different regions: lipid A, the inner core, the outer core and the O-antigen (see Figure 2-5). *E. coli* K-12 has a rough-LPS due to the missing O-antigen (Liu and Reeves, 1994). The inner core is a hydrophobic domain that consists of L-glycero-D-mannoheptose (Hep) and the acidic monosaccharide 2-keto-3-deoxymanno-octulosonic acid (KDO). It binds to lipid A, which is anchored to the OM. The negative charges supplied by KDO and the phosphate groups form divalent cations that are able to link LPS molecules. The outer core of LPS is formed by different sugars, mainly hexoses, that are nonrepeating. The O-antigen is a significant variable region that gives each strain an antigenic specificity. It is composed of mono- or oligosaccharides that are organised in repeating units (Neidhardt et al., 1990; Schnaitman and Klena, 1993; Gronow and Brade, 2001; Raetz and Whitfield, 2002; Cipolla et al., 2010; Whitfield and Trent, 2014; Sperandeo et al., 2017).

The biosynthesis pathway of KDO is conserved in most gram-negative bacteria (Smyth and Marchant, 2013). Two KDO molecules are the minimum requirement in LPS for *E. coli* survival. In *E. coli* the first reaction of the KDO synthesis pathway is the isomerisation of ribulose 5-phosphate (Ru5P) to arabinose 5-phosphate (A5P) catalysed by KdsD and GutQ, two A5P isomerases. This reaction takes place mainly in the direction of A5P formation (75 % A5P and 25 % Ru5P at equilibrium; Lim and Cohen, 1966). The A5P isomerases KdsD and GutQ are the only enzymes providing the *E. coli* K-12 cell with intracellular A5P. Therefore, individually they are non-essential, but if both activities are missing, growth of *E. coli* is dependent on external A5P (Meredith and Woodard, 2005; Sperandeo et al., 2006). After yielding A5P, it is condensed together with PEP to form KDO 8-phosphate by KdsA. Then, KDO 8-phosphate is metabolised to KDO by KdsC, which is further activated as a cytidine monophosphate (CMP) derivative by KdsB. Two CMP-KDO molecules are then covalently linked by WaaA to the precursor of lipid A (lipid IV$_A$) forming the KDO$_2$-lipid IV$_A$ moiety. LpxL and LpxM add the secondary acyl chains to the KDO$_2$-lipid IV$_A$ moiety resulting in hexa-acylated KDO$_2$-lipid A. Afterwards, two Hep molecules are transferred to the inner KDO molecule of the KDO$_2$-lipid IV$_A$ complex. With the addition of the sugars of the outer core by specific glycosyltransferases, the core-lipid A is complete. The core-lipid A, which is synthesised in the cytoplasmic side of the inner membrane, is flipped by MsbA (an ATP-binding cassette transporter) to the periplasmic side of the inner membrane (Mi et al.,

2017). In the periplasmic side of the inner membrane, O-antigen is attached to the core-lipid A forming the mature LPS. The Lpt complex is responsible to transport the mature LPS molecule from the inner membrane to the OM. The minimal LPS assembly that *E. coli* needs to survive is the synthesis of the KDO_2-lipid A, the transporter protein MsbA and the Lpt complex (Neidhardt et al., 1990; Schnaitman and Klena, 1993; Gronow and Brade, 2001; Raetz and Whitfield, 2002; Cipolla et al., 2010; Whitfield and Trent, 2014; Sperandeo et al., 2017).
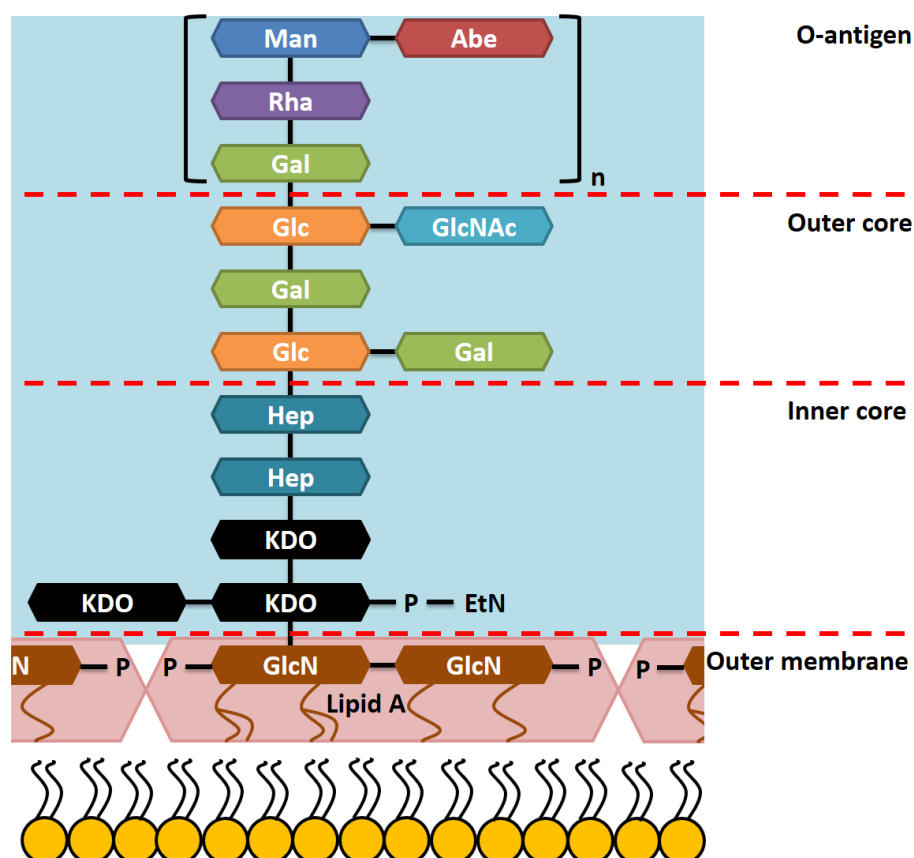
Figure 2-5. Display of the outer membrane of *E. coli*. *E. coli* K-12 LPS does not possess an O-antigen (rough-LPS; Liu and Reeves, 1994). Abe (Abequose), EtN (ethanolamine), Gal (galactose), Glc (glucose), GlcN (glucoseamine), GlcNAc (N-acetylglucosamine), Hep (L-glycero-D-mannoheptose), KDO (2-keto-3-deoxymanno-octulosonic acid), LPS (lipopolysaccharide), Man (mannose), P (phosphate), Rha (rhamnose). Figure modified after Yoo et al. (2017) and Fuchs (2007).

2.6   Dihydroxyacetone

As mentioned in Chapter 2.3, the cleavage of F6P by FSA yields dihydroxyacetone (DHA) and glyceraldehyde 3-phosphate (G3P). DHA is a monosaccharide consisting of three carbon molecules (a triose) and a ketone group (see Figure 2-6). It is a fine chemical of interest due to its application in the cosmetic industry, especially in tanning lotions. DHA reacts with proteins and free amino acids (specially arginine, glycine, lysine and histidine) present on the human

skin forming a colour ranging from yellow to dark brown (Wittgenstein and Berry, 1960; Levy, 1992).
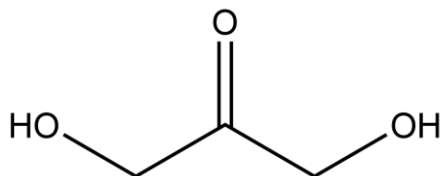
Figure 2-6. The chemical structure of dihydroxyacetone.

DHA can be produced chemically or microbiologically. Chemically, a DHA molecule can be synthesised from the self-condensation of three molecules of formaldehyde by thiazolium salts (Matsumoto et al., 1984; Deng et al., 2013). Furthermore, glycerol can be electrochemically oxidated to DHA, but the reported yield (25 % after 20 h) is significantly lower than the yields reached by the microbial production of DHA (Ciriminna et al., 2006). The microbial production of DHA has been mainly reported in yeast, such as *Saccharomyces cerevisiae*, or gram-negative bacteria, such as *Gluconobacter oxydans*. Under osmotic stress (addition of 0.7 M NaCl to the medium), *S. cerevisiae* is known to produce glycerol, which can be used as an intermediate for the production of DHA. With glucose as only carbon source (C-source) and the presence of a NAD^+-dependent glycerol dehydrogenase from *Hansenula polymorpha*, *S. cerevisiae* was reported to produce 1.1 mM DHA. With the additional deletion of the genes encoding for the DHA kinases (*S. cerevisiae* Δ*dak1* Δ*dak2*), the DHA formation increased by a factor of 7 (7.8 mM), but, even then, the yield of 7 % was too low (Nguyen and Nevoigt, 2009). Another yeast used to produce DHA from glycerol was *Pichia membranifaciens* with a reported maximal DHA concentration of 0.15 M and a yield of 35 % (Liu et al., 2008). Equally important, a study with gram-negative bacteria demonstrated that immobilised cells of a *Gluconobacter oxydans* strain formed 278 mM DHA from glycerol due to the presence of a pyrroloquinoline quinone-dependent membrane-bound glycerol dehydrogenase. The theoretical maximal yield reached was 87 % (Stasiak-Rózanska and Blazejak, 2012). Furthermore, conversion yields from glycerol to DHA of around 90 % and DHA concentrations between 0.96 M and 1.8 M were reported with *G. oxydans* mutant strains (Ma et al., 2010; Hu et al., 2010). Moreover, a recombinant *E. coli* strain produced DHA by increasing the intracellular levels of NAD^+ available to GldA with the NAD^+ oxidase from *Enterococcus faecalis* (Zhou et al., 2013). With the expression of a plasmid-borne heterologous gene (*cghdpA*) that codes for the DHAP dephosphorylase from *Corynebacterium glutamicum*, another *E. coli* strain (Δ*tpiA* Δ*mgsA* Δ*gldA*) reached a DHA concentration of 73.3 mM (87 % of the theoretical maximal yield) with glucose as sole C-source (Jain et al., 2016). Besides, it

has been shown that a computationally designed enzyme named formolase can produce DHA from three formaldehyde molecules *in vitro* (Siegel et al., 2015). Furthermore, DHA can be used to microbiologically produce other compounds, such as glycerol (see Chapter 2.7).

2.7 Glycerol

Glycerol is an alcohol composed of three carbons each of them bound to a hydroxyl group (see Figure 2-7). It is a clear, viscous, odourless and colourless compound. Glycerol is important for cells because of its presence in lipids and fats, forming part of membranes and being a source of carbon and energy. Due to its full miscibility with other substances, it is used in many applications, such as cosmetics, lubricants, pharmaceuticals, soaps and antifreeze solutions. Glycerol can either chemically or microbiologically be converted to different products, such as. aromatic amino acids, DHA, ethanol, fuel additive, fumarate, hydrogen, HA, 3-hydroxypropionic acid, lactate, lipids, malate, methanol, polyhydroxylalkanoates, 1,2-propanediol, 1,3-propanediol, or succinate (Chotani et al., 2000; Pagliaro et al., 2007; Wendisch et al., 2011; Quispe et al., 2013; Tan et al., 2013; Chen and Liu, 2016; Luo et al., 2016; Sprenger, 2017; Aroua and Cognet, 2020; Semkiv et al., 2020). The conversion of glycerol to HA, 3-hydroxypropionic acid or 1,2-propanediol has been reported in *E. coli* (Yao et al., 2015; Lim et al., 2016; Gonzalez et al., 2008). Whereas the production of 1,3-propanediol from glycerol as the sole C-source or as an intermediate has been reported in different microorganisms, such as *Citrobacter freundii* (Boenigk et al., 1993), *E. coli* (Nakamura and Whited, 2003), or *Corynebacterium glutamicum* (Li et al., 2022).
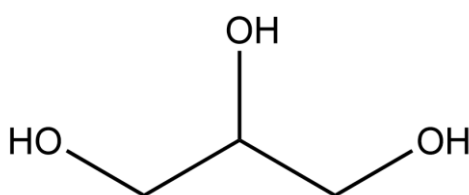
Figure 2-7. The chemical structure of glycerol.

Currently, the glycerol used for most of the above mentioned applications is refined glycerol. Refined glycerol is obtained from technical glycerol, which is purified from crude glycerol. The latter is obtained as a by-product of the production of biodiesel. From 1 ton of biodiesel, 100 kg of crude glycerol are formed. Crude glycerol consists of more than 80 % glycerol, but it is a low quality glycerol because of the presence of impurities, such as methanol, salts, water and non-glycerol organic material. Due to the low glycerol purity, crude glycerol has to be purified to reach the necessary glycerol purity for its transformation in the products mentioned above. Even though the amount of crude glycerol in the market is large, its purification costs are

significant. Therefore, there is still room in the market for refined glycerol from sources other than crude glycerol (Chotani et al., 2000; Pagliaro et al., 2007; Wendisch et al., 2011; Quispe et al., 2013; Tan et al., 2013; Chen and Liu, 2016; Luo et al., 2016; Sprenger, 2017; Aroua and Cognet, 2020; Semkiv et al., 2020). The forecast for the glycerol market in 2024 is around 5 billion US$ (Semkiv et al., 2020).

During World War I, industrial production of glycerol from glucose with the addition of steering agents in the yeast *Saccharomyces cerevisiae* (Neuberg fermentation), such as bisulphite ions, was developed (Semkiv et al., 2020). One of the first reports about the microbial production of glycerol was published in 1919. In this report Connstein and Lüdecke described the production of glycerol from sugars in yeast with a yield between 20-25 %. After that, more studies about the microbial production of glycerol were performed in various organisms. Some of them are listed below:

- In *Pichia farinosa* a yield of 59 % mole glycerol/mole glucose was obtained (Vijaikishore and Karanth, 1987);

- Under aerobic conditions, an engineered *S. cerevisiae* strain reached a yield of 83 % (mole glycerol/mole glucose). After adaptive evolution, the evolved *S. cerevisiae* strain obtained a 100 % yield (Overkamp et al., 2002);

- A molar yield of 100 % (mole glycerol/mole glucose) was achieved with an evolved *E. coli* mutant strain containing a plasmid with the genes of the *S. cerevisiae* glycerol pathway (Salles et al., 2007);

- Another *E. coli* mutant strain expressing the *S. cerevisiae* glycerol synthesis pathway was reported to produce under anaerobic conditions glycerol from glucose with a 86 % molar yield (mole glycerol/mole glucose). With the additional deletion of *glpK*, the yield was improved to 89 % (Balagurunathan et al., 2017);

- An engineered *Corynebacterium glutamicum* was reported to produce glycerol from glucose with a molar yield of 86 % (mole glycerol/mole glucose; Li et al., 2022).

Microalgae have also been studied for the production of glycerol by using carbon dioxide as the C-source. They produce glycerol in the chloroplast via the intermediate DHAP. A summary of the microalgae glycerol production can be found in Semkiv et al. (2020).

3   Scientific problem and aims of this study

Fructose 6-phosphate aldolase (FSA) enzymes are known to catalyse aldol and retroaldol reactions. These reactions have been shown *in vitro* by Schürmann and Sprenger (2001), Schürmann et al. (2002), Garrabou et al. (2009), Castillo et al. (2010), Sánchez-Moreno et al. (2012a and 2012b), among other groups. However, it is unclear whether these reactions would be possible *in vivo*.

Since the discovery of FSA, encoded by the genes *fsaA* and *fsaB* in the *Escherichia coli* chromosome in 2001 (Schürmann and Sprenger, 2001), its true physiological function has not been reported yet (Samland and Sprenger, 2014). Due to the weak expression of the native promoters of *fsaA* and *fsaB*, the only enzymatic data reported so far are from recombinant FSA. FSAA wt and FSAB were named after their first known reaction, the cleavage of fructose 6-phosphate (F6P) to dihydroxyacetone (DHA) and glyceraldehyde 3-phosphate (G3P). FSAA wt has a K_M for F6P of 9 mM (Schürmann and Sprenger, 2001), 6-fold larger than the reported K_M of the mutant FSAA A129S (Schürmann, 2001). That is a significant improvement in the K_M value due to an amino acid exchange.

To evaluate whether the reactions catalysed *in vitro* by FSA can also be performed *in vivo*, *E. coli* mutant strains should be constructed. These mutant strains should have blockades in central carbon metabolism or anabolism. Afterwards, it should be examined if the activity of recombinant FSA in these mutant strains can restore deficiencies in growth.

In Introduction Table 2-1 the metabolites for *E. coli* that could be relevant are listed, e.g. fructose 6-phosphate (F6P), arabinose 5-phosphate (A5P), 1-deoxyxylulose. These metabolites are of particular interest due to their role in key pathways, F6P in glycolysis, A5P in the synthesis of 2-keto-3-deoxymanno-octulosonic acid (KDO), and 1-deoxyxylulose in the synthesis of isoprenoids. Therefore, these three pathways were chosen to examine the corresponding reactions of FSA *in vivo*. Cleavage of F6P in glycolysis and formation of A5P and 1-deoxyxylulose in the synthesis of KDO and isoprenoid, respectively (see Figure 3-1). During the course of this study, the pathway with 1-deoxyxylulose was reported *in vivo* by another group (King et al., 2017). Thus, this pathway was not further pursued.

To be able to show the reactions of FSA *in vivo*, numerous mutations in metabolic pathways should be performed. Thus, it should be taken into account that these mutations might impact pleiotropic genes. Most probably there will be changes in metabolic fluxes which might have a significant impact on growth. Therefore, it will be a challenging task to keep these mutant strains alive in the laboratory.

1. Glucose $\longrightarrow$ Fructose 6-phosphate $\big\langle$ FSA

    Dihydroxyacetone $\longrightarrow$?

    Glyceraldehyde 3-phosphate $\longrightarrow$ Glycolysis

2. Glycerol $\longrightarrow$ Dihydroxyacetone
    +
    Glyceraldehyde 3-phosphate

    $\xrightarrow{\text{FSA}}$ Fructose 6-phosphate $\longrightarrow$ Glycolysis

3. Glycolaldehyde + Glyceraldehyde 3-phosphate $\xrightarrow{\text{FSA}}$ Arabinose 5-phosphate $\longrightarrow \longrightarrow$ KDO

4. Hydroxyacetone + Glycolaldehyde $\xrightarrow{\text{FSA}}$ 1-deoxyxylulose

Figure 3-1. Possible reactions of FSA *in vivo*.

With the reactions catalysed by FSA, the blocked pathways will not be restored, but new artificial pathways might emerge. Through the introduction of these new metabolic pathways in the cell, there is the possibility that new products can be synthesised. It is expected, that through the F6P bypass a new route for the production of dihydroxyacetone (DHA) will be opened and maybe an access to the production of glycerol as well. Furthermore, a new approach for the provision of A5P might be established. If these new artificial pathways are functional in *E. coli*, they could help make a statement about the possible physiological role of FSA in *E. coli*.

4   Materials and methods

4.1   Oligonucleotides, plasmids and bacterial strains

4.1.1   Oligonucleotides

All oligonucleotides were synthesized by biomers.net (Hohenbrunn, Germany). Oligonucleotides generated for gene deletions are listed in Table 4-1 and Table 4-2, for gene integrations in Table 4-3 and for screening of gene deletions and gene integrations in Table 4-5. Oligonucleotides for the construction of pTarget are enumerated in Table 4-4. In Table 4-6 the oligonucleotides employed in qPCR are annotated.

Table 4-1. Oligonucleotides used for gene deletions (recombineering technique, Datsenko and Wanner, 2000). The sequences homologous to pCO1-cat are underlined.

Name	Sequence (5'→ 3')
zwf-del5'	GTTAGTTAACTTAAGGAGAATGACATGGCGGTAACGCAAA<u>TTGTGTAGGCTGGAGCTGCTTCG</u>
zwf-del3'	ATTACTCAAACTCATTCCAGGAACGACCATCACGGGTAATCAT<u>CATATGAATATCCTCCTTAGTTC</u>
pfkB-del5'	TATACGTTGACACTTGCGCCCTCTCTCGATAGCGCAACAATTA<u>TTGTGTAGGCTGGAGCTGCTTCG</u>
pfkB-del3'	AATGCTGGGGGAATGTTTTTGTTAGCGGGAAAGGTAAGCGTAAA<u>CATATGAATATCCTCCTTAGTTC</u>
pfkA-del5'	CAGATTTCATTTTGCATTCCAAAGTTCAGAGGTAGTCATGAT<u>TTGTGTAGGCTGGAGCTGCTTCG</u>
pfkA-del3'	TTCCGAAATCATTAATACAGTTTTTTCGCGCAGTCCAGCCAG<u>CATATGAATATCCTCCTTAGTTC</u>
kdsD-del5'	ATGTCGCACGTAGAGTTACAACCGGGTTTTGACTTTCAGCAA<u>TTGTGTAGGCTGGAGCTGCTTCG</u>
kdsD-del3'	CGCAGTAAATCATGCATATGTAACACACCGAGTAAATGGT<u>CATATGAATATCCTCCTTAGTTC</u>

Table 4-2. Oligonucleotides used for gene deletions (CRISPR/Cas, Jiang et al., 2015). The inserted restriction sites are underlined (A$_r$ oligonucleotides contained the restriction site for Bgl*II* and C$_f$ for BamH*I*).

Name	Sequence (5'→ 3')
A$_f$-dhaKLM-5'	ATATTCCCAGGCATCTTCCAGCGCAG
A$_r$-dhaKLM-3'	TTTT<u>AGATCT</u>AGCAATTACGGTAGGGCATGGATG
C$_f$-dhaKLM-5'	TTTT<u>GGATCC</u>TTCGGATGGCATCGTTCTGATGTC
C$_r$-dhaKLM-3'	AATAAAATATCAGGCGGCTGTGGTGTTAC
A$_f$-glpK-5'	AAAGTGTTGATCTGGCTGGCACTTTC
A$_r$-glpK-3'	TTTT<u>AGATCT</u>AGCTTTTTGTTCTGAAGGAGTTGTG
C$_f$-glpK-5'	TTTT<u>GGATCC</u>TACTGCTTAGAGTTTGCTATGAGAC
C$_r$-glpK-3'	TTCAGATCAATGGTGCCTTTGGCTC

Table 4-3. Oligonucleotides used for gene integrations. The inserted restriction sites are underlined. P$_{tac}$-fsaA^{A129S} and P$_{tac}$-gldA were amplified from pJF119*fsaA*^{A129S} and pJF119ΔEP$_{tac}$*gldA*, respectively, by using the I$_f$-Ptac-gene (BstB*I*) and the I$_r$-Ptac-gene (Pst*I*) oligonucleotides. These fragments could be combined with either the A and C fragments of *lacZ* or the ones of *rbsK*.

Name	Sequence (5'→ 3')
A$_f$-lacZ-5' (EcoR*I*)	TTTT<u>GAATTC</u>TTCACACAGGAAACAGCTATGACC
A$_r$-lacZ-3' (BstB*I*)	TTTT<u>TTCGAA</u>AGCGAGTAACAACCCGTCGGATTC
C$_f$-lacZ-5' (Pst*I*)	TTTT<u>CTGCAG</u>ATGGCGATTACCGTTGATGTTGAAG
C$_r$-lacZ-3' (Hind*III*)	TTTT<u>AAGCTT</u>GCTCCAGGAGTCGTCGCCACCAATC
A$_f$-rbsK-5' (EcoR*I*)	TTTT<u>GAATTC</u>AATGCAGAACCTGTTGACCGCTCATC
A$_r$-rbsK-3' (BstB*I*)	TTTT<u>TTCGAA</u>TAAAATGCGCCACCGTGTTAGGGTG

Table 4-3. (Continuation)

Name	Sequence (5'→ 3')
C$_f$-rbsK-5' (Pst*I*)	TTTT<u>CTGCAG</u>TCAATAAAGATCGCTTCGTCAGTG
C$_r$-rbsK-3' (Hind*III*)	TTTT<u>AAGCTT</u>AATAAGATCGCTGTCGCCATCGAAC
I$_f$-Ptac-gene-5' (BstB*I*)	TTTT<u>TTCGAA</u>TGGTATGGCTGTGCAGGTCGTAAATC
I$_r$-Ptac-gene-3' (Pst*I*)	TTTT<u>CTGCAG</u>TTTTATCAGACCGCTTCTGCGTTC

Table 4-4. Oligonucleotides used for the construction of pTarget. For the amplification of each pTarget with a specific sgRNA, the "Universal pTarget" oligonucleotide was used in combination with the oligonucleotide containing the corresponding sgRNA (CRISPR). The sgRNA sequence is underlined.

Name	Sequence (5'→ 3')
Universal pTarget	ACTAGTATTATACCTAGGACTGAGCTAGC
dhaKLM (CRISPR)	<u>TTGTGGATCGTCAATTCCCG</u>GTTTTAGAGCTAGAAATAGCAAGTTAAAAT AAGGCTAG
glpK (CRISPR)	<u>GCACAACTGACCAAACAGCG</u>GTTTTAGAGCTAGAAATAGCAAGTTAAAA TAAGGCTAG
lacZ (CRISPR)	<u>TCACCGCCGTAAGCCGACCAC</u>GTTTTAGAGCTAGAAATAGCAAGTTAAA ATAAGGCTAG
rbsK (CRISPR)	<u>GCTGCCATCACACTTTCGAG</u>GTTTTAGAGCTAGAAATAGCAAGTTAAAAT AAGGCTAG

Table 4-5. Oligonucleotides used for screening of gene deletions and gene integrations in the chromosome with the expected amplicon length.

Name	Sequence (5'→ 3')	Amplicon length	
		Wild-type	**Mutant**
Test-zwf-5'	CGCGCTTTTCCCGTAATCGCACG	1.8 kb	0.5 kb
Test-zwf-3'	TGAGTTGTCAGAGCAGGATGATTCAC		
Test-pfkB-5'	AAGGATCAAAGATTAGCGTCCCTGGAA AG	1.6 kb	0.8 kb
Test-pfkB-3'	TCTGTTGCTATTCCATTCCTCCCAGGTC		
Test-pfkA-5'	GAAGCTGAATATCCTTTGCCATAAC	1.6 kb	0.8 kb
Test-pfkA-3'	TATTTTACGGCGTTTTCCGGGATCG		
A$_f$-dhaKLM-5'	ATATTCCCAGGCATCTTCCAGCGCAG	3.6 kb	0.8 kb
C$_r$-dhaKLM-3'	AATAAAATATCAGGCGGCTGTGGTGTT AC		
Test-lacZ-5'	AAAAACCACCCTGGCGCCCAATAC	3.3 kb	2 kb (P$_{tac}$-fsaA^{A129S})
Test-lacZ-3'	AGACCAACTGGTAATGGTAGCGAC		
A$_f$-glpK-5'	AAAGTGTTGATCTGGCTGGCACTTTC	2.5 kb	0.8 kb
C$_r$-glpK-3'	TTCAGATCAATGGTGCCTTTGGCTC		
A$_f$-rbsK-5'	TTTTGAATTCAATGCAGAACCTGTTGA CCGCTCATC	3 kb (LJ110, insD)	2.5 kb (P$_{tac}$-gldA)
C$_r$-rbsK-3'	TTTTAAGCTTAATAAGATCGCTGTCGC CATCGAAC	1.8 kb* (BW25113)	1.3 kb; 0.6 kb* (P$_{tac}$-fsaA^{A129S})
Test-gutQ-5'	TTCCAGCGTGAAACTATTCGTCAGG	1.3 kb	0.6 kb
Test-gutQ-3'	ATAAATTGTTTATGGGCACCGACGGC		

*Results after PCR with oligonucleotides for screening, followed by cleaning of amplified DNA and restriction with EcoR*I*.

Table 4-5. (Continuation)

Name	Sequence (5'→ 3')	Amplicon length	
		Wild-type	**Mutant**
Test-kdsD-5'	GCAATAGCGGGGGGTTCGCAAAGG	1.5 kb	0.7 kb
Test-kdsD-3'	TGAGCGCACAACGAATGCCATAACC		
Test-lacZα-5'	TTTTAAGCTTATGACCATGATTACGGA TTCACTG	0.7 kb (P*fsaA/fsaB-lacZYA*)	No fragment (ΔP*lac-lacZ*α)
Test-lacZα-3'	GCGAGTGGCAACATGGAAATCGCTG		
Test-Cm-PlacZα-5'	ATCTCGGTAGTGGGATACGACGATAC	2 kb (P*fsaA/fsaB-lacZYA*)	No fragment (ΔP*lac-lacZ*α)
Test-Cm-PlacZα-3'	GCGATTAAGTTGGGTAACGCCAGGG		

Table 4-6. Oligonucleotides used for qPCR with the amplicon length and the location of the amplicon in the gene (beginning, middle or end).

Name	Sequence (5'→ 3')	Amplicon length	Location
dhaK-5'-cDNA	AGACTGGAGCGGTTGTTTGG	207 bp	Middle
dhaK-3'-cDNA	CCTGGCGGATAATGAGATGG		
fsaA-5'-cDNA	GTAGCGGCATTCAGACTGTG	215 bp	End
fsaA-3'-cDNA	GCCAGTCCTGCTCAAACTTC		
fsaB-5'-cDNA	CGTTGCTCCGTATGTTAACC	197 bp	End
fsaB-3'-cDNA	TGTTGCGCTACATCTAAGGG		
ftsZ-5'-cDNA	TGCATTTGCTTCCGACAACG	111 bp	End
ftsZ-3'-cDNA	ACGTTTGTCCATGCCGATAC		
gapA-5'-cDNA	GACTATCAAAGTAGGTATCAACGGTTTT	148 bp	Beginning
gapA-3'-cDNA	GAGTGGAGTCATATTTCAGCATGTAT		

Table 4-6. (Continuation)

Name	Sequence (5'→ 3')	Amplicon length	Location
gldA-5'-cDNA	AAATTGCGCCGTTTGGCGGTG	450 bp	Middle
gldA-3'-cDNA	AGGGTGTTGTAGCACAGTTC		
glpK-5'-cDNA	GGCCGTGTCCATGTGACCGATTAC	194 bp	Middle
glpK-3'-cDNA	GGAGATTGGAATACGCGTGCCGCC		
lacI-5'-cDNA	ACGGCGGGATATAACATGAG	338 bp	Middle
lacI-3'-cDNA	ATCTGGTCGCATTGGGTCAC		
lacZ-5'-cDNA	CGAGTGGCAACATGGAAATC	295 bp	End
lacZ-3'-cDNA	TGAAAGCTGGCTACAGGAAG		
pfkA-5'-cDNA	TACGCTGGTGAGAAGAAGAG	263 bp	Middle
pfkA-3'-cDNA	AATTCCGCGACGAGAACATC		
pfkB-5'-cDNA	AGTTCTGGCGAAGCGTTAAG	303 bp	End
pfkB-3'-cDNA	CTGCCAGTTTCAGTGTCATC		
pgi-5'-cDNA	GGCGAAATTACAGGATCTGG	278 bp	Beginning
pgi-3'-cDNA	CCGATCCCGATGTTCACTAC		
ptsG-5'-cDNA	TTTGTGCCGATCATTTCTGGCCTG	241 bp	Middle
ptsG-3'-cDNA	ACCTGACCTGCTGCGTTGGTGTATTC		
sgrS-5'-cDNA	TGCCCCATGCGTCAGTTTTATCAGCAC	191 bp	Middle
sgrS-3'-cDNA	ATCTGCTGGCGGGTGATTTTACAC		

Table 4-6. (Continuation)

Name	Sequence (5'→ 3')	Amplicon length	Location
zwf-5'-cDNA	CAGCAGCAAACGTTCATAGG	256 bp	Beginning
zwf-3'-cDNA	GCCGACCAAATGTTCTGAAG		

4.1.2 Plasmids

All plasmids required to perform this work are listed in Table 4-7.

Table 4-7. Plasmids used during this work.

Plasmid	Characteristics	Reference
pJF119EH	P_{tac}, $lacI^q$, RBS, Amp^R	Fürste et al. (1986)
pJF119*fsaA*	*fsaA* gene cloned into pJF119EH (Xba*I*/Hind*III*)	Inoue (2006)
pJF119*fsaA*^{A129S}	*fsaA*^{A129S} gene cloned into pJF119EH (Xba*I*/Hind*III*)	Inoue (2006)
pJF119*fsaB*	*fsaB* gene cloned into pJF119EH (Eco*RI*/Hind*III*)	Sprenger (unpublished)
pJF119ΔEP$_{tac}$*gldA*	P_{tac}*gldA*, $lacI^q$, ΔEcoRI, ΔNdeI, optimized RBS, Amp^R	Riemer (2010)
pJF119*talB*^{F178Y}	*talB*^{F178Y} gene with N-term. 6xHis cloned into pJF119EH	Schneider et al. (2008)
pJF119*xfp*	*xfp* gene cloned into pJF119EH (EcoR*I*/Hind*III*)	Sprenger (unpublished)
pET22b	P_{T7}, *lacI*, His-tag, Amp^R	Novagen (Schwalbach, Germany)
pET22b*fsaA*	*fsaA* gene with N-term. 6xHis cloned into pET22b	Sánchez-Moreno et al. (2012b)
pET22b*fsaA*^{A129S}	*fsaA*^{A129S} gene with N-term. 6xHis cloned into pET22b	Stellmacher et al. (2016)
pKD46	*repA101* (Ts), *araC*, P_{araB}-ϒ-β-exo (red recombinase), Amp^R	Datsenko and Wanner (2000)
pCO1-cat	P_{tac}-*aroC*-*aroA*, oriR6' (first 36 bp), FRT-*cat*-FRT, $lacI^q$, Amp^R, Cm^R	Trachtmann et al. (2016)

Table 4-7. (Continuation)

Plasmid	Characteristics	Reference
pCO1-kan	P$_{tac}$-*aroC-aroA*, oriR6' (first 36 bp), FRT-*kan*-FRT, *lacI*^{q}, Amp^R, Cm^R	Trachtmann et al. (2016)
pCP20	FLP$^+$, λ cl857$^+$, λ p$_R$ Rep^{ts}, Amp^R, Cm^R	Cherepanov and Wackernagel (1995)
pCas	*repA101* (Ts), P$_{cas}$-*cas9*, P$_{araB}$-Υ-β-exo (red recombinase), *lacI*^{q}, P$_{trc}$-sgRNA-*pMB1*, Km^R	Jiang et al. (2015)
pTarget with sgRNAs	with (T) or without (F) donor DNA	
pTargetF-*dhaKLM*	*pMB1*, sgRNA-*dhaKLM*, Spc^R	Guitart Font and Sprenger (2020)
pTargetF-Cm-*glpK*	*pMB1*, sgRNA-*glpK*, Cm^R	Guitart Font and Sprenger (2020)
pTargetT-Cm-Δ*lacZ*::P$_{tac}$-*fsaA*^{A129S}	*pMB1*, sgRNA-*lacZ*, Δ*lacZ*::P$_{tac}$-*fsaA*^{A129S}, Cm^R	Guitart Font and Sprenger (2020)
pTargetF-Cm-*rbsK*	*pMB1*, sgRNA-*rbsK*, Cm^R	Guitart Font and Sprenger (2020)
pJNTN-m-L	P$_{tac}$, *lacI*^{q}, Km^R	Trachtmann (unpublished)
pJNTN-m-L-*pfkA*	*pfkA* gene cloned into pJNTN-m-L (Sac*I*/BamH*I*)	Trachtmann (unpublished)
pJLIC	Amp^R, Cm^R	Trachtmann et al. (2016)
pJLIC-P$_{fsaA}$	P$_{fsaA}$, Amp^R, Cm^R	This study
pJLIC-P$_{fsaB}$	P$_{fsaB}$, Amp^R, Cm^R	This study

4.1.3 Bacterial strains

Table 4-8. Bacterial strains list. In this study only *E. coli* strains were used. Methods employed to create the strains: (a) Datsenko & Wanner (2000); and (b) CRISPR/Cas.

Strain	Genotype	Reference
***E. coli* K-12**		
DH5α	F−, Φ80d, *lacZ*ΔM15, Δ(*lacZYA-argF*) U169, *recA1*, *endA1*, *hsdR17* (r_K^-, m_K^+), *phoA*, *supE44*, λ−, *thi*-1, *gyrA96*, *relA1*	Hanahan (1983)
LJ110	W3110 *fnr*⁺, wild type	Zeppenfeld et al. (2000)
GL1	LJ110, Δ*zwf*::FRT	Guitart Font and Sprenger (2020)[a]
GL2	LJ110, Δ*zwf*::FRT Δ*pfkB*::FRT	Guitart Font and Sprenger (2020)[a]
GL3	LJ110, Δ*zwf*::FRT Δ*pfkB*::FRT Δ*pfkA*::FRT	Guitart Font and Sprenger (2020)[a]
GL4	LJ110, Δ*zwf*::FRT Δ*pfkB*::FRT Δ*pfkA*::FRT Δ*lacZ*::P_{tac}-*fsaA*^{A129S}	Guitart Font and Sprenger (2020)[b]
GL5	LJ110, Δ*zwf*::FRT Δ*pfkB*::FRT Δ*pfkA*::FRT Δ*dhaKLM* Δ*lacZ*::P_{tac}-*fsaA*^{A129S}	Guitart Font and Sprenger (2020)[b]
GL6	LJ110, Δ*zwf*::FRT Δ*pfkB*::FRT Δ*pfkA*::FRT Δ*dhaKLM* Δ*lacZ*::P_{tac}-*fsaA*^{A129S} Δ*glpK*	Guitart Font and Sprenger (2020)[b]
GL7	LJ110, Δ*zwf*::FRT Δ*pfkB*::FRT Δ*pfkA*::FRT Δ*dhaKLM* Δ*lacZ*::P_{tac}-*fsaA*^{A129S} Δ*glpK* Δ*rbsk*::P_{tac}-*gldA*	Guitart Font and Sprenger (2020)[b]
GL35	LJ110, Δ*zwf*::FRT Δ*pfkB*::FRT Δ*pfkA*::FRT Δ*dhaKLM*	This study[b]
LJ110 ΔP_{lac}-*lacZ*α::FRT-*kan*-FRT	LJ110, lacking the codons for the first 40 amino acid residues of the *lacZ* gene, Km^R	Trachtmann et al. (2016)
LJ110 FRT-*cat*-FRT-P_{fsaA}-*lacZYA*	LJ110, P_{fsaA}-*lacZYA*, Cm^R	This study[a]
LJ110 FRT-*cat*-FRT-P_{fsaB}-*lacZYA*	LJ110, P_{fsaB}-*lacZYA*, Cm^R	This study[a]
BW25113	*lacI*^{q} *rrnB*$_{T14}$ Δ*lacZ*$_{WJ16}$ *hsdR514* Δ*araBAD*$_{AH33}$ Δ*rhaBAD*$_{LD78}$	Datsenko and Wanner (2000)
BW25113 Δ*gutQ*	BW25113, Δ*gutQ*::FRT	Trachtmann (unpublished)
BW25113 Δ*gutQ* Δ*kdsD*::*kan*	BW25113, Δ*gutQ*::FRT Δ*kdsD*::FRT-*kan*-FRT	This study[a]
BW25113 Δ*gutQ* Δ*kdsD*	BW25113, Δ*gutQ*::FRT Δ*kdsD*::FRT	This study[a]
BW25113 Δ*gutQ* Δ*kdsD* Δ*rbsK*::P_{tac}-*fsaA*^{A129S}	BW25113, Δ*gutQ*::FRT Δ*kdsD*::FRT Δ*rbsK*::P_{tac}-*fsaA*^{A129S}	This study[b]
***E. coli* B**		
BL21(DE3) pLysS	F−, *ompT*, *hsdSB* (r_B^-, m_B^-), *gal*, *dcm* (DE3), pLysS (Cm^R)	Novagen (Schwalbach, Germany)

4.2   Chemicals and enzymes

If not otherwise specified, all chemicals had the highest market available purity.

BD	Bacto^{TM} Agar
(Heidelberg, Germany)	Difco^{TM} MacConkey Agar Base
Bio-Rad Laboratories, Inc.	Bio-Rad protein assay dye reagent
(München, Germany)	(Bradford reagent)
Biozym Scientific GmbH	Biozym Blue S'Green qPCR Mix
(Hessisch Olendorf, Germany)	
Carl Roth GmbH + Co. KG	2-Propanol
(Karlsruhe, Germany)	Acetic acid (HoAc)
	Agar
	Agarose
	Albumin fraction V
	Ammonium sulphate $((NH_4)_2SO_4)$
	Amp
	Boric acid (H_3BO_3)
	Bromophenol blue
	Calcium chloride dehydrate $(CaCl_2 \cdot 2H_2O)$
	Cm
	Hydrochloric acid (37 %) (HCl)
	Chloroform $(CHCl_3)$
	Cobalt chloride hexahydrate $(CoCl_2*6H_2O)$
	Copper (II) sulphate $(CuSO_4)$
	DTT
	EDTA
	Ethanol (EtOH)
	D-Galactose
	D-Glucose
	Glycerol
	Glycine
	Glycylglycine Pufferan®

Carl Roth GmbH + Co. KG   Imidazole

(Karlsruhe, Germany)   IPTG

Km

Potassium acetate (KOAc)

Potassium hydroxide (KOH)

Lactose

Lysozyme

Magnesium chloride ($MgCl_2$)

MOPS Pufferan®

ONPG

Potassium chloride (KCl)

Di-potassium hydrogen phosphate (K_2HPO_4)

Potassium dihydrogen phosphate (KH_2PO_4)

Rotiphorese® gel 30 (37.5:1)

SDS pellets

Di-sodium hydrogen phosphate (Na_2HPO_4)

Sodium chloride (NaCl)

Sodium dihydrogen phosphate monohydrate

($NaH_2PO_4 \cdot H_2O$)

Sodium hydroxide (NaOH)

D-Sorbitol

Succinate

TEMED

Thiamine

Tricine Pufferan®

TRIS Pufferan®

Tryptone

D-Xylose

Yeast extract

Genaxxon bioscience GmbH   dNTPs

(Ulm, Germany)   Taq Polymerase

GERBU Biotechnik GmbH   NADH

(Heidelberg, Germany) $NADP^+$

Honeywell Specialty Chemicals Seelze GmbH (Seelze, Germany)	Fluka:
	Ammonium chloride (NH_4Cl)
	Coomassie Brilliant Blue R-250
	D-Fructose
	HA
	D,L-Lactate
	Magnesium sulphate heptahydrate ($MgSO_4 \cdot 7H_2O$)
	Manganese(II) chloride ($MnCl_2$)
	D-Mannitol
	MercaptoEtOH
	Zinc chloride ($ZnCl_2$)
	Zinc sulphate ($ZnSO_4$)
	Riedel-de-Haen:
	Ethylacetate (EtOAc)
Merck KGaA (Darmstadt, Germany)	Ammonium molybdate ($(NH_4)Mo_7O_{24} \cdot 4H_2O$)
	Iron (II) sulphate heptahydrate ($FeSO_4 \cdot 7H_2O$)
	Maltose
	Potassium sulphate (K_2SO_4)
	Sulphuric acid (H_2SO_4)
New England Biolabs GmbH (Frankfurt am Main, Germany)	DNA Ladder
	DNA Loading Dye
	T4 DNA ligase
	T4 polynucleotide kinase
	Q5 Hi-Fi DNA polymerase
	Restriction enzymes
	RNase H
Nippon Genetics Europe (Düren, Germany)	Blue Star Prestained Protein Marker
PEQLAB Biotechnologie GmbH (Erlangen, Germany)	X-gal

41

Qiagen GmbH   Ni^{2+}-NTA agarose

(Hilden, Germany)

Roche Diagnostics GmbH   G6P DH

(Mannheim, Germany)   Pwo DNA polymerase

                                         <u>Boehringer Mannheim GmbH (now Roche):</u>

                                         G6P

SERVA Electrophoresis GmbH   APS

(Heidelberg, Germany)

Sigma-Aldrich Chemie GmbH   p-Anisaldehyde

(Taufkirchen, Germany)   L-Arabinose

                                         D-A5P

                                         Deoxycholic acid

                                         DNaseI

                                         DHA

                                         DHAP

                                         EtBr

                                         D-F6P

                                         D-Gluconate

                                         D,L-G3P

                                         Gly3P DH

                                         GoA

                                         PGI

                                         Spc

                                         D- and L-Threose

                                         TPI

                                         TPI/Gly3P DH

Thermo Fisher Scientific Inc.   DNA Ladder

(Waltham, USA)   DNA Loading Dye

                                         RevertAid reverse transcriptase

VWR International GmbH   Methanol (MeOH)

(Darmstadt, Germany)

4.3 Devices

Devices that are specific for a method are listed in the description of the corresponding method.

Centrifuges

Allegra 64R Centrifuge, Avanti JXN-26 Centrifuge and Microfuge® 22R Centrifuge

(Beckman Coulter GmbH, Krefeld, Germany)

Centrifuge 5430

(Eppendorf Vertrieb Deutschland GmbH, Wesseling-Berzdorf, Germany)

Magnetic stirrer

MR200

(Heidolph Instruments GmbH & Co. KG, Schwabach, Germany)

pH meter

SevenCompact

(Mettler Toledo, Gießen, Germany)

Scales

A200S and L2200S

(Sartorius AG, Göttingen, Germany)

Spectrophotometer with water bath

Cary 60 UV-Vis with CaryWinUV Version 5.0.0.999

(Agilent Technologies, Waldbronn, Germany)

Thermo/Haake D3 Series Immersion Circulator

(Gebrüder HAAKE GmbH, Karlsruhe, Germany)

Vortex

RS-VA 10

(Phoenix Instrument, Garbsen, Germany)

Water bath shaker

G76 Water Bath Shaker (New Brunswick Scientific, New Jersey, USA)

Water purifier

ELGA Maxima

(Veolia Water Technologies Deutschland GmbH, Celle, Germany)

4.4   Culture media, buffers and solutions

Buffers for enzyme activity assays

Glycylglycine buffer	50 mM	glycylglycine
	pH 8.5	adjusted with NaOH
Potassium phosphate buffer	100 mM	potassium phosphate
	pH 7.0	
Z-buffer stock solution	4.270 g	Na_2HPO_4
(Li et al., 2012)	2.750 g	NaH_2PO_4 x H_2O
	0.375 g	KCl
	0.125 g	$MgSO_4$ x $7H_2O$
	ad 500 mL	dH_2O
	pH 7.0	

Store at 4 °C.

Growth media

LB medium	10 g	tryptone
(Sambrook et al., 1989)	5 g	yeast extract
	10 g	NaCl
	ad 1 L	dH_2O
LB-agar	10 g	tryptone
	5 g	yeast extract
	10 g	NaCl
	18 g	agar
	ad 1 L	dH_2O
2x YT medium	16 g	tryptone
(Ausubel et al., 2001)	10 g	yeast extract
	5 g	NaCl
	ad 1 L	dH_2O

Solution A (10 x)	47.0 g	NaH_2PO_4 x H_2O
	115.0 g	K_2HPO_4
	26.4 g	$(NH_4)_2SO_4$
	ad 1 L	dH_2O
Solution B (100 x)	7.4 g	$MgSO_4$ x $7H_2O$
	147.0 mg	$CaCl_2$ x $2H_2O$
	13.5 mg	$ZnCl_2$
	28.0 mg	$FeSO_4$ x $7H_2O$
	1 mL	HCl (1 N)
	ad 1 L	dH_2O
Minimal medium	100 mL	Solution A
(Tanaka et al., 1967)	10 mL	Solution B
	20 μg/mL	thiamine
	ad 1 L	dH_2O
Minimal medium agar	100 mL	Solution A
(Tanaka et al., 1967)	10 mL	Solution B
	20 μg/mL	thiamine
	18 g	Bacto^{TM} Agar
	ad 1 L	dH_2O
Micronutrient stock	9 mg	$(NH_4)Mo_7O_{24}$ x $4H_2O$
	62 mg	H_3BO_3
	18 mg	$CoCl_2$
	6 mg	$CuSO_4$
	40 mg	$MnCl_2$
	7 mg	$ZnSO_4$
	ad 50 mL	dH_2O

MOPS mixture (10 x)

Mix:

83.72 g	MOPS
7.17 g	tricine
ad 440 mL	dH_2O
pH 7.4	adjusted with 10 M KOH

Add:

10 mL	$FeSO_4$ (0.01 M)
50 mL	NH_4Cl (1.9 M)
10 mL	K_2SO_4 (0.276 M)
0.25 mL	$CaCl_2$ x $2H_2O$ (0.02 M)
2.1 mL	$MgCl_2$ (2.5 M)
100 mL	NaCl (5 M)
0.2 mL	Micronutrient stock
ad 1 L	dH_2O

Steril filtrate (0.2 µm filter).

Store at - 20 °C

MOPS minimal medium	100 mL	MOPS mixture (10x)
(Neidhardt et al., 1974)	10 mL	K_2HPO_4 (0.132 M)
	20 µg/mL	thiamine
	ad 1 L	dH_2O

Production of competent cells

Transformation Buffer I (TFB I)	30 mM	KOAc
	50 mM	$MnCl_2$
	100 mM	KCl
	10 mM	$CaCl_2$
	15 %	glycerol (w/v)

Transformation Buffer II (TFB II)	10 mM	Na-MOPS pH 7.0
	10 mM	KCl
	75 mM	$CaCl_2$
	15 %	glycerol (w/v)

Purification of recombinant proteins

Lysis Buffer	10 mM	imidazole
	50 mM	NaH_2PO_4
	300 mM	NaCl
	pH 8.0	

Wash Buffer I	25 mM	imidazole
	50 mM	NaH_2PO_4
	300 mM	NaCl
	pH 8.0	

Wash Buffer II	50 mM	imidazole
	50 mM	NaH_2PO_4
	300 mM	NaCl
	pH 8.0	

Elution Buffer I	250 mM	imidazole
	50 mM	NaH_2PO_4
	300 mM	NaCl
	pH 8.0	

Elution Buffer II	500 mM	imidazole
	50 mM	NaH_2PO_4
	300 mM	NaCl
	pH 8.0	

SDS-PAGE

SDS-gel Loading Buffer (2 x)	200 mM	Tris-HCl (pH 6.8)
	400 mM	mercaptoEtOH
	4 %	SDS
	~ 0.01 %	bromophenol blue
	40 %	glycerol

SDS-Running Buffer (10 x)	30.2 g	Tris
	188 g	glycine
	10 g	SDS
	ad 1 L	dH$_2$O

SDS-gel staining solution	0.1 %	Coomassie Brilliant Blue R-250
	40 %	isopropanol
	10 %	HOAc
	49.9 %	dH$_2$O

SDS-gel destaining solution	20 %	EtOH
	10 %	HOAc
	70 %	dH$_2$O

Agarose gel electrophoresis

TAE Buffer (50x)	242.2 g	Tris
	57.12 mL	HOAc
	100 mL	EDTA (0.5 M)
	ad 1L	dH$_2$O

TLC

| Mobile phase | 5:1 | CHCl$_3$:MeOH |

| Mobile phase for separation of sugar-P | 5:2:1.4:0.4 | EtOAc:MeOH:H$_2$O:HOAc |

Colouring solution	83 mL	MeOH
	3 mL	H$_2$SO$_4$
	1 mL	p-anisaldehyde
	1 mL	HOAc

Antibiotics

	100 µg/mL	Amp
	50 µg/mL	Km
	50 µg/mL	Spc
	25 µg/mL	Cm (dissolved in 70 % EtOH)

4.5   Cultivation of *E. coli*

4.5.1   Culture conditions

To grow *E. coli* in shake flasks or on agar plates, the Luria-Bertani (LB)-medium (Sambrook et al., 1989) was generally used. The solid culture medium was obtained after adding 1.8 % agar into the medium. For specific methods, the minimal medium (MM; Tanaka et al., 1967) or the MOPS minimal medium (MOPS-MM, Neidhardt et al., 1974) were employed. If not mentioned otherwise, the liquid cultures were incubated in a shaker at 37 °C and 180 - 200 rpm (INFORS HT, Bottmingen, Switzerland). Test tubes with a maximal filling volume of 20 mL were used for volumes up to 5 mL. For higher volumes, shake flasks were employed by filling 10 % of their total volume. If necessary, the medium was supplied with the corresponding antibiotic.

For long term storage of strains, 750 µL of an overnight culture was mixed with 750 µL sterile glycerol (40 %, v/v) and stored at - 70 °C.

4.5.2   Growth curves

The growth of different strains on different media was monitored to characterise the growth behaviour of these strains. A single colony was inoculated from MM-agar plates with 28 mM fructose on 5 mL MM containing 28 mM fructose and 100 µM IPTG, antibiotic was added if necessary. D-fructose was used as a neutral C-source in preculture media to prevent long lag phases in growth experiments with other C-sources. The preculture was incubated overnight at 200 rpm and 37 °C. The next day, 2 mL of the preculture were centrifuged at 16,500$\times$ *g* for 1 min and washed twice with 1 mL MM containing the corresponding C-source (intended starting concentrations were 28 mM D-glucose; 33 mM D-xylose; 33 mM L-arabinose; or 28 mM D-galactose; after inoculation with cells, the real starting concentrations were determined by HPLC measurements of C-source depletion and product formation). After centrifuging again at 16,500$\times$ *g* for 1 min, the pellet was resuspended in 1 mL MM with the corresponding C-source. The main culture (50 mL MM containing the corresponding C-source, 100 µM IPTG and, if necessary, antibiotic in a 500 mL shake flask with a metal cap) was inoculated with the resuspended pellet with a start $OD_{600\,nm}$ of 0.05. The cultures were incubated at 200 rpm and 37 °C until the stationary phase was reached. When cultures needed a long time to reach the stationary phase, only pipette tips with filter and glass pipettes were used to avoid any kind of contamination. During growth, the $OD_{600\,nm}$ was monitored and at the same time 1 mL culture was withdrawn, centrifuged at 16,500$\times$ *g* for 5 min, and 500 µL of the supernatant

were stored at - 20 °C for HPLC analysis. After reaching the stationary phase, a volume equivalent to an $OD_{600\,nm}$ of 15 was centrifuged at 3,400× g for 10 min at 4 °C. The resulting pellet was washed in 2 mL glycylglycine buffer (50 mM, pH 8.5) and centrifuged again at 3,400× g for 10 min at 4 °C. The washed pellet was stored at - 20 °C until testing for the presence of enzyme and its activity.

The analysis of the growth behaviour of the strains on LB-medium, LB-medium with 100 µM IPTG, 2.5 mM deoxycholate, or 56 mM glucose, and on MM containing 28 mM fructose with or without 100 µM IPTG was performed in a main culture with a total volume of 25 mL in a 250 mL shake flask with a metal cap. In all cases, the media in the preculture and the main culture were the same one. Here, only $OD_{600\,nm}$ was monitored during growth.

All growth curves were performed with two independent biological replicates.

4.5.3 Growth characterisation on solid media

The growth behaviour of all generated strains on different C-sources was studied to better understand the consequences each gene deletion or integration had on cell growth depending on the C-source used as substrate. MM-agar and MacConkey-agar plates with diverse C-sources were used. In Figure 4-1 is explained how the cells were streaked on solid media to evaluate their growth behaviour.
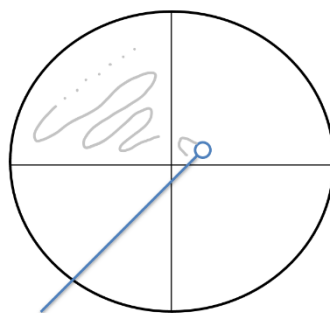
Figure 4-1. Schema of how growth behaviour was evaluated on solid media. The cell material was spread with an inoculation loop from the middle to the outer edge of the plate to obtain single colonies. Incubation days, cell size and colour of the colonies (MacConkey plates) were derived from those plates to evaluate the growth behaviour of LJ110, GL-strains and GL-evolved strains on different C-sources.

4.5.4 Dose-response curves

Different dose-response assays were performed on MOPS-MM containing 28 mM glucose with the D-arabinose 5-phosphate (A5P) auxotroph strains BW25113 Δ*gutQ* Δ*kdsD*::*kan* and BW25113 Δ*gutQ* Δ*kdsD* Δ*rbsK*::P*tac*-*fsaA*^{A129S}. BW25113 was always used as a control to

corroborate that the MOPS-MM containing 28 mM glucose enabled growth. This medium was chosen after testing which medium/C-source combination (MM vs. MOPS-MM / glucose vs. glycerol) was the best to avoid growth of BW25113 $\Delta gutQ$ $\Delta kdsD$::kan without the presence of A5P (see Appendix Chapter 9.9). The presence of external G6P in the medium was required for the induction of the active transport system for sugar phosphates UhpT (Neidhart, 1996; Meredith and Woodard, 2005).

Dose-response curves for A5P

The maximal $OD_{600\,nm}$ achieved by the A5P auxotroph strain BW25113 $\Delta gutQ$ $\Delta kdsD$::kan in the presence of different concentrations of A5P was measured to obtain a dose-response curve. A single colony, grown on MM-Agar with 28 mM glucose, 10 µM G6P, 50 µM A5P and 50 µg/mL Km, was inoculated on 10 mL MOPS-MM with 28 mM glucose, 10 µM G6P, 15 µM A5P and 50 µg/mL Km in a 100 mL shake flask and incubated overnight at 200 rpm and 37 °C. The next day, 2 mL of the preculture were centrifuged for 1 min at 16,500× g and washed twice with 1 mL MOPS-MM containing 28 mM glucose. The resulting pellet was resuspended again in 1 mL MOPS-MM with 28 mM glucose. The main culture consisted of 10 mL MOPS-MM with 28 mM glucose, 10 µM G6P, 50 µg/mL Km and different A5P concentrations (0 µM; 5 µM; 10 µM; 25 µM; 40 µM; 50 µM; 60 µM; 70 µM; 100 µM). It was inoculated with the washed cells with an initial $OD_{600\,nm}$ of 0.05 and was incubated at 200 rpm and 37 °C for 48 h. 48 h incubation were enough for BW25113 $\Delta gutQ$ $\Delta kdsD$::kan to reach its maximal $OD_{600\,nm}$ in the presence of different concentrations of A5P. After the 48 h incubation, the $OD_{600\,nm}$ was measured. The obtained $OD_{600\,nm}$ values were plotted against the different A5P concentrations to calculate the K_S (substrate concentration to reach half of the maximal $OD_{600\,nm}$) and the maximal $OD_{600\,nm}$ with the software "GraphPad Prism" version 6.01 from GraphPad Software, Inc. (San Diego, USA).

Dose-response curves for GoA

The maximal $OD_{600\,nm}$ was measured for the A5P auxotroph strain BW25113 $\Delta gutQ$ $\Delta kdsD$::kan carrying pJF119EH, pJF119$fsaA$ or pJF119$fsaA^{A129S}$, for BW25113 $\Delta gutQ$ $\Delta kdsD/$pJF119$fsaB$, and for BW2511 $\Delta gutQ$ $\Delta kdsD$ $\Delta rbsK$::P_{tac}-$fsaA^{A129S}$ on MOPS-MM containing 28 mM glucose, 100 µM IPTG and different concentrations of GoA to get dose-response curves. First, a single colony, grown on MM-agar with 28 mM glucose, 10 µM G6P, 50 µM A5P and, if needed, the corresponding antibiotics, was inoculated on 10 mL MOPS-MM with 28 mM glucose, 10 µM G6P, 15 µM A5P and the corresponding antibiotics

51

in a 100 mL shake flask and incubated overnight at 200 rpm and 37 °C. After the overnight incubation, 2 mL of the cell culture were centrifuged at $16,500 \times g$ for 1 min and washed two times with 1 mL MOPS-MM with 28 mM glucose. Then, the pellet was resuspended in 1 mL MOPS-MM with 28 mM glucose and inoculated with an initial $OD_{600\,nm}$ of 0.05 in the main culture, which contained 10 mL MOPS-MM with 28 mM glucose, 100 µM IPTG, the corresponding antibiotics and different GoA concentrations (0 µM; 10 µM; 25 µM; 40 µM; 50 µM; 90 µM; 100 µM; 125 µM). Directly afterwards, the cell culture was incubated at 200 rpm and 30 °C for 48 h. The $OD_{600\,nm}$ was measured when the incubation finished. The K_S and the maximal $OD_{600\,nm}$ values were determined as described in Chapter 4.5.4 for A5P.

4.5.5   Selection of faster-growing cells (GL*-strains and GL'-strains)

Two different approaches were carried out to select faster-growing *E. coli* cells. One selection was performed in liquid media and the other one in solid media. These resulted in two different types of evolved strains, *****-strains or '-strains, respectively. After the selection, the growth of these evolved strains was tested on MM containing glucose and 100 µM IPTG to confirm that they had an increased growth rate in comparison with their parent strains (for details see Chapter 4.5.2).

To obtain evolved GL5-, GL6 and GL7-strains, the corresponding GL-strain was first incubated on MM with 28 mM glucose and 100 µM IPTG (start $OD_{600\,nm}$ of 0.1 for GL5 and of 0.05 for GL6 and GL7) at 200 rpm and 37 °C until the culture reached the stationary phase. Then, the culture was transferred again to fresh MM with 28 mM glucose and 100 µM IPTG with the same start $OD_{600\,nm}$ as previously mentioned. When this second culture arrived at the stationary phase, 10 µL of the cell culture were stricken on MM-agar with 28 mM glucose to get single colonies of the evolved strains. After verifying by colony PCR and sequence comparison that these evolved strains had all the deletions and the integrations of the parent GL-strain, they were cryopreserved at - 70 °C.

To get GL'-strains, the GL-strain of interest was inoculated on 5 mL MM with 28 mM fructose and incubated overnight at 200 rpm and 37 °C. The next day, approximately 10^8 cells were spread on MM-agar with 28 mM glucose and incubated at 37 °C for many days until colonies with a considerable diameter would grow on a bacteria lawn. These larger colonies belong to the evolved strains. They were purified and their deletions and integrations were verified by colony PCR and sequence comparison. They were cryopreserved at - 70 °C.

4.5.6   Selection of a stronger P*fsaA* and P*fsaB*

To acquire changes in the promoter region which would allow its upregulation, LJ110 FRT-Cm-FRT-P*fsa**-*lacZYA* (P*fsa** being P*fsaA* or P*fsaB*) with a higher expression of the *lacZ* gene were selected. A single colony of each *lacZ*-reporter strain was inoculated on MM with 28 mM glucose and 25 µg/mL Cm and incubated overnight at 37 °C in a shaker. The next day, 10^8 cells were plated on MM-agar with 15 mM lactose and incubated at 37 °C for many days until colonies with a considerable diameter would grow on a bacteria lawn. These larger colonies belong to the evolved strains. A couple of these larger colonies were purified on MM-agar with 15 mM lactose and, their *β*-galactosidase activity was determined (see Chapter 4.7.9). The promoter region of the best evolved strain (highest *β*-galactosidase activity) was sequenced and this sequence was compared to the sequence of the parent promoter.

4.5.7   Microscopy

Cell cultures were always observed under the "Axioplan" microscope (Carl Zeiss, Jena, Germany) when they had reached the stationary phase to examine if they were homogenous or if they had morphological anomalies in comparison with the wild-type cells. First, 100 µL of hot agarose solution (1 %) was poured on the microscope slide and, immediately after, the cover slip was put on the poured agarose. When the agarose had turned solid, the cover slip was removed with a scalpel and a preparation consisting of 3 µL cell culture and 3 µL dH$_2$O was scattered on the solid agarose. When the preparation had dried, the cover slip was put on the agarose again and the cells were observed with the 100x oil-immersion objective. The microscope pictures were taken with the "CoolSNAPcf" camera (Photometrics, Tucson, USA) with the help of the "MetaVue" software version 6.0r1 (Molecular Devices, Sunnyvale, USA).

4.6   Molecular biological methods

4.6.1   Production of chemically competent *E. coli* cells (Mülhardt, 2009)

For the production of chemically competent *E. coli* cells, the desired strain was first inoculated on 5 mL LB medium and incubated at 180 rpm and 37 °C overnight. The next day, 1 mL of the overnight culture was transferred to 50 mL 2YT medium and incubated at 200 rpm and 30 °C until the OD$_{600 \, nm}$ reached 0.8. Then, 50 mL 2YT medium were added to the culture and the culture was further incubated at 200 rpm and 30 °C until the OD$_{600 \, nm}$ value was 0.8. Directly after, the whole culture was centrifuged at 2,800× *g* and 4 °C for 10 min and the resulting pellet was resuspended in 20 mL TFBI buffer. The suspension was incubated on ice for 10 min and

afterwards centrifuged (2800 xg, 10 min, 4 °C). Afterwards, the obtained pellet was resuspended in 5 mL TFBII buffer. Then, the resuspended cells were distributed in 100 µL aliquots, frozen with liquid nitrogen and stored at - 70 °C until further use.

4.6.2   Transformation of chemically competent *E. coli* cells

For the transformation, 100 µL of chemically competent *E. coli* cells were thawed on ice, mixed with approximately 100 µg plasmid DNA and kept on ice for 30 min. Then, they were submitted to a heat shock at 42 °C for 90 sec and, directly after, put shortly on ice. 1 mL LB medium (RT) was added to the mixture. Afterwards, the mixture was incubated at 180 rpm and 37 °C for 1 h, except if the plasmid was temperature-sensitive, in which case, the mixture was incubated at 95 rpm and 30 °C for 1 h. Finally, 100 µL of the mixture were plated on a LB-agar plate with the corresponding antibiotic. The plates were incubated overnight at 37 °C (or 30 °C for temperature-sensitive plasmids).

4.6.3   Production and transformation of electrocompetent *E. coli* cells (Dower et al., 1988)

A single colony was inoculated on 5 mL LB medium and incubated overnight at 180 rpm and 37 °C. The next day, 100 µL of the overnight culture were transferred to 5 mL LB medium and incubated at 180 rpm and 37 °C until an $OD_{600\,nm}$ between 0.6 and 0.8 was reached. Immediately, the tube containing the culture was put on ice. A 2 mL micro tube was filled with 2 mL culture and centrifuged at $21,000\times g$ and RT for 20 sec. The pellet was kept on ice at all times, washed twice with 1 mL glycerol (10 %, ice-cold) and centrifuged again at $21,000\times g$ and RT for 20 sec. The pellet was resuspended in 50 µL glycerol (10 %, ice-cold) and 1 µL (approximately 100 ng) plasmid DNA was added to the suspension. After mixing, the suspension was put in a 2 mm electroporation cuvette that was previously cooled down on ice. The electroporation took place at 2.3 kV and 25 µF between 4 and 5.2 msec. Directly afterwards, 1 mL LB medium (RT) was added to the shocked cells and incubated at 30 °C or 37 °C for 1 h, depending on the plasmid DNA type. After the incubation, 100 µL of the culture were plated on LB-agar with the corresponding antibiotic to select for cells that contain the plasmid DNA.

4.6.4   Polymerase chain reaction (Mullis and Faloona, 1987)

The polymerase chain reaction (Mullis and Faloona, 1987), also known as PCR, was used to amplify DNA from isolated DNA samples (PCR) or from cell material (colony PCR), or to quantify gene expression (quantitative real-time PCR, qPCR) from complementary DNA (cDNA). The PCR and the colony PCR were carried out in one of the following thermal cyclers: "Biometra® T Gradient Thermoblock" (Biomedizinische Analytik, Göttingen, Germany) or "Px2 Thermal Cycler" (Thermo Electron Corportation, Milford, USA). The PCR and the colony PCR products were separated by agarose gel electrophoresis (see Chapter 4.6.7) and, depending on their intended use, purified from the agarose gel (see Chapter 4.6.8). On the other hand, the qPCR was performed in the device "qTower 2.0" (Analytik Jena AG, Jena, Germany) using the software "qPCRsoft 3.4" from the same manufacturer. In this case, the qPCR products were not further used.

For PCR, Pwo DNA polymerase (Roche Diagnostics GmbH, Mannheim, Germany) and Q5 Hi-Fi DNA polymerase (NEB, Frankfurt am Main, Germany), both with proofreading activity, were used to amplify fragments using plasmid DNA or the product of a ligation as DNA matrix, respectively. Depending on the polymerase employed, different PCR programs were utilised (see below). For colony PCR, instead of using already isolated DNA as DNA matrix, a small quantity of cell material was picked with a sterile pipette tip and inserted in a PCR tube. The concentrations of the components used were the same ones listed in Table 4-9. Pwo DNA polymerase and Q5 Hi-Fi DNA polymerase were used to amplify fragments which would be used for cloning. Taq polymerase (Genaxxon bioscience GmbH, Ulm, Germany) was used for screening and for fragments that would be only sequenced. For the colony PCR performed by the Taq polymerase, the same composition as described for Pwo DNA polymerase in Table 4-9 was used. The colony PCR programs applied were the same ones as the ones for PCR with the exception that the initial denaturation lasted 10 min instead of 5 min. For the Taq polymerase, the program described for the Pwo DNA polymerase was used.

Table 4-9. Composition of a PCR sample.

Compound	Concentration
Plasmid DNA/ligation preparation	100 ng/2 µL
Polymerase buffer	1x
DMSO	6 %
Forward primer	2 µM
Reverse primer	2 µM
dNTPs	0.4 mM
Pwo DNA Polymerase/Q5 Hi-Fi DNA Polymerase	2.5 U/1 U
Sterile MQ H$_2$O	ad 25 µL

The PCR program sequence used for Pwo DNA polymerase was:

	1) 95 °C, 5 min	Initial denaturation
	2) 95 °C, 45 sec	Denaturation
30x	3) 53 °C, 10 sec	Annealing
	4) 72°C, 1 kb/min	Elongation
	5) 72 °C, 3 min	Final elongation

The PCR program sequence utilised for Q5 Hi-Fi DNA polymerase was:

	1) 98 °C, 5 min	Initial denaturation
	2) 98 °C, 10 sec	Denaturation
30x	3) 62 °C, 30 sec	Annealing
	4) 72°C, 2 kb/min	Elongation
	5) 72 °C, 2 min	Final elongation

The qPCR (Higuchi et al. 1992; Wittwer et al., 1997) was employed to confirm that the strains carried the desired deletions and integrations and to find out what differentiated the GL-strains from their evolved strains. The MIQE guidelines were followed (Bustin et al., 2009). First of all, the RNA sample isolated as described in Chapter 4.6.16 was reverse-transcribed to cDNA with the RevertAid reverse transcriptase (Thermo Fisher Scientific Inc., Waltham, USA). 400 ng isolated RNA were first mixed with 5 µM random hexamer primer and filled to 13 µL with H$_2$O (RNase free), and, then, 1x reaction buffer, 1 mM dNTPs and 200 U RevertAid reverse transcriptase were added to the mixture. This preparation was incubated for 10 min at 25 °C in one of the thermal cyclers mentioned above, followed by 60 min at 42 °C and, finally, for 10 min at 70 °C. Afterwards, the samples were further used or stored at - 20 °C. Because

there would still be the RNA template present in the samples, which could disturb the qPCR measurement, 2.5 U RNase H (NEB, Frankfurt am Main, Germany) were added to the sample and the mixture was incubated at 37 °C for 30 min to cleave the RNA. Then, the mixture was cleaned and concentrated in 15 µL sterile dH$_2$O (see Chapter 4.6.9). Afterwards, the concentration and purity of the cDNA was measured using the "NanoDrop 2000 Spectrophotometer" (Thermo Fisher Scientific Inc., Waltham, USA). The cDNA was stored at - 20 °C until its use in the qPCR. For the qPCR, a white 96 well plate with a colourless cap strip plate (Biozym Scientific GmbH, Hessisch Olendorf, Germany) was utilised. In each well, a reaction mixture containing 20 ng cDNA, 2 µM forward primer, 2 µM reverse primer, 1x Biozym Blue S'Green qPCR Mix and filled-up to 10 µL with sterile dH$_2$O was pipetted. For each sample and primer pair, three technical replicates per plate were analysed. A reference gene and a control gene were also quantified for each cDNA sample at each plate, and a negative control (without cDNA) was also carried out for each primer pair to rule out any false results.

The qPCR program sequence used was:

$$
\begin{array}{lll}
& \text{1) 95 °C, 2 min} & \text{Initial denaturation} \\
& \text{2) 95 °C, 5 sec} & \text{Denaturation} \\
\text{39x} & \text{3) 60 °C, 20 sec} & \text{Annealing/Elongation} \\
& \text{5) Melting temperature analysis} &
\end{array}
$$

The measured gene expression was normalised relative to the reference gene. *ftsZ* gene mRNA was used as the reference gene and *gapA* gene mRNA as a control to ensure that the reference gene was stably expressed in all samples. The tested genes were: *zwf* (pentose phosphate pathway), *pfkA*, *pfkB* (glycolysis), *lacZ*, *dhaK* and *glpK* to verify the gene deletions of the strains; *fsaA* and *gldA* to evaluate if the gene integrations in the chromosome were expressed; *sgrS* and *ptsG* (glucose transport into the cell); *fsaB* to examine if it was expressed at all; and *lacI* for a possible negative regulation of the P$_{tac}$. Furthermore, it was analysed if differences in the expression levels of the above mentioned genes exist between the GL-strains and their evolved strains.

4.6.5   Plasmid isolation

To obtain enough cells for plasmid isolation, a single colony was inoculated in 5 mL LB medium with the appropriate antibiotic and incubated at 180 rpm and 37 °C overnight. Plasmid DNA was purified with the kit "NucleoSpin Plasmid/Plasmid (NoLid):

Isolation of high-copy plasmid DNA from *E. coli*" (Macherey-Nagel GmbH & Co. KG, Düren, Germany) according to the manufacturer's instructions. 5 mL of the overnight culture were centrifuged and used as the starting material. For the clarification of the lysates, the sample was centrifuged for 10 min instead of 5 min. The wash step with the buffer AW was only carried out if a strain other than DH5α was used for the plasmid isolation. The elution was performed with 50 µL sterile dH_2O. To verify the success of the isolation, approximately 200 ng DNA were loaded in a 1 % (w/v) agarose gel (see Chapter 4.6.7).

4.6.6 DNA cleavage by restriction enzymes

The restriction enzymes were chosen with the software "Clone Manager 7" (Version 7.03) from Sci Ed Central (Denver, USA) based on the restriction sites present in the DNA sequence of interest. They were used following the instructions of the manufacturer (NEB, Frankfurt am Main, Germany). The DNA cleavage took place in a 20 µL preparation that contained approximately 1 µg DNA, 20 U of the restriction enzyme and 1x of the corresponding buffer. The preparation was incubated during 1 h at the optimal temperature of the restriction enzyme. The restriction results were examined in an agarose gel (see Chapter 4.6.7).

4.6.7 Agarose gel electrophoresis

DNA was separated and visualised in an agarose gel (1 % agarose in 1x TAE buffer with 0.5 µg/mL ethidium bromide solution). Prior to use, the samples were diluted with a 6x TrickTrack DNA Loading Dye from Thermo Fisher Scientific Inc. (Waltham, USA). The DNA Ladder from Thermo Fisher Scientific Inc. (Waltham, USA) or NEB (Frankfurt am Main, Germany) with a range from 100 bp to 10 kb was applied as a marker to determine the size of the DNA fragments in bp. The electrophoresis ran in 1x TAE buffer at 140 V until the first colour front reached ¾ of the agarose gel. Then, the DNA was visualised and documented using UV-light at 365 nm.

4.6.8 Extraction of DNA fragments from agarose gels

Before the DNA fragments were purified from the agarose gel, the DNA bands with the expected size were cut with a scalpel and removed from the rest of the agarose gel. Then, the "QIAquick® Gel Extraction Kit" (Qiagen, Hilden, Germany) was used to extract the DNA from the agarose gel by following the instructions of the manufacturer. At the end, the DNA fragments were eluted from the column with 30 µL ddH_2O.

4.6.9 Cleaning and concentration of DNA

To change the solvent in which the DNA sample was dissolved to water, the "DNA Clean & Concentrator™ – 5 – Uncapped Columns" kit from Zymo Research Europe GmbH (Freiburg, Germany) was utilised according to the instructions of the manufacturer.

4.6.10 Ligation of DNA fragments

The 20 µL reaction preparation consisted of previously cleaved fragments, 400 U T4 DNA ligase and the corresponding buffer. Approximately 3 nM of each cleaved fragment (insert) and a plasmid:insert molarity ratio of 1:3 were used. The reaction preparation was incubated for 1 h at RT. In the case of a plasmid ligation, 10 µL of the ligated plasmid preparation were transformed into 100 µL DH5α competent cells.

4.6.11 Construction of chromosomal P$_{fsaA}$-*lacZ* and P$_{fsaB}$-*lacZ* fusion reporter strains (Trachtmann et al., 2016)

The promoter regions of *fsaA* (225 bp) and *fsaB* (495 bp) were custom-synthesised (GeneArt™ Life Science Technology, Regensburg, Germany). These synthesised sequences were inserted in pJLIC using the restriction sites for Bgl*II* (5' end) and Hind*III* (3' end) as described by Trachtmann et al. (2016). In this plasmid, a chloramphenicol resistance cassette is found upstream of the inserted promoter region. It also contains flanking DNA regions upstream of the antibiotic resistance cassette and downstream of the promoter region corresponding to the 3' region of the *lacI* gene (*lacI'*) and the 5' region of the *lacZ* gene (*'lacZ*), respectively. The cassette is transcribed in the opposite direction of the inserted promoter. As pictured in Figure 4-2, the restriction of pJLIC-P$_{fsaA}$ and pJLIC-P$_{fsaB}$ took place with the restriction enzymes EcoR*V* and Zra*I* to obtain a fragment with the DNA flanking regions, the Cm resistance cassette and the promoter region. This fragment was purified through agarose gel electrophoresis and was homologously recombined in the chromosome of LJ110 ΔP$_{lac}$-*lacZ*α::FRT-*kan*-FRT using the recombineering technique of Datsenko and Wanner (2000) (see Chapter 4.6.12). LJ110 FRT-*cat*-FRT-P$_{fsaA}$-*lacZYA* and LJ110 FRT-*cat*-FRT-P$_{fsaB}$-*lacZYA* were the resulting strains. The insertion of the promoter region upstream of the intact *lacZ* gene was first verified on LB-agar with 25 µg/mL Cm and 0.008 % X-gal. Only clones that had an active promoter due to α-complementation would turn blue. Afterwards, the inserted sequence was validated by colony PCR and by sequencing.
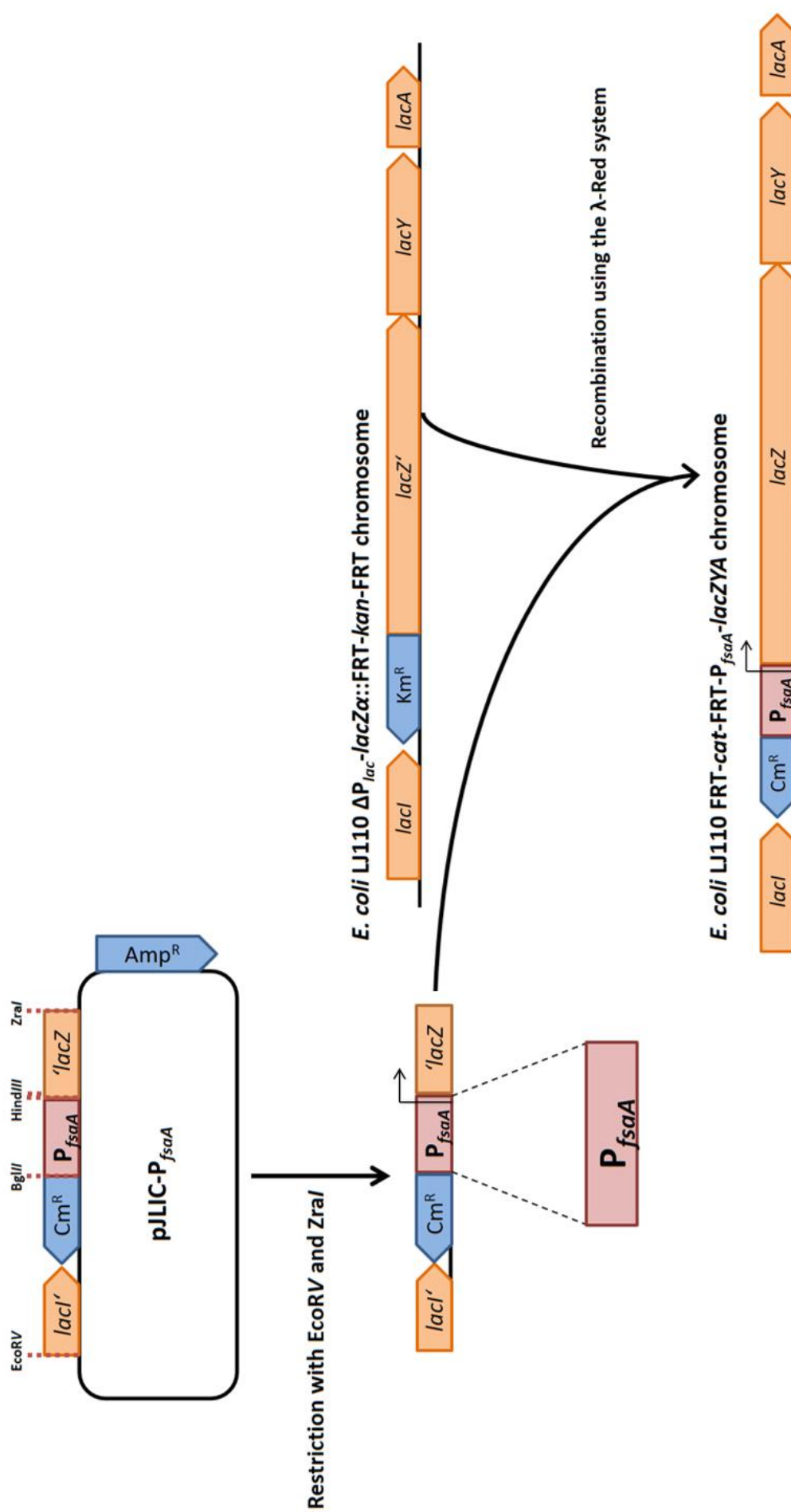
Figure 4-2. Construction of the P*fsaA*-*lacZ* fusion reporter strain. Figure modified after Trachtmann et al., 2016).

4.6.12 Chromosomal deletion of genes (knock-out mutagenesis) – Recombineering technique (Datsenko and Wanner, 2000)

Knock-out mutagenesis of the *zwf*, *pfkB* and *pfkA* genes in *E. coli* K-12 were performed as described by Datsenko and Wanner (2000). For the deletion of these genes, a fragment containing the flanking regions of the target gene and the FRT-*cat*-FRT cassette was amplified by PCR from the pCO1-cat plasmid in a 100 µL preparation. Then, 20 U Dpn*I* were added to eliminate the plasmid and the preparation was purified in an agarose gel.

E. coli K-12 bearing pKD46, which is a temperature-sensitive plasmid and contains the λ-Red system genes under the control of the arabinose promoter, was inoculated in LB medium with 100 µg/mL Amp overnight at 30 °C. The next day, 100 µL of the culture were transferred into 5 mL of fresh LB medium with 100 µg/mL Amp and induced with 20 mM L-arabinose at 95 rpm and 30 °C until the $OD_{600\,nm}$ of the culture reached 0.6-0.8 (approximately 5 h). Then, all cells were centrifuged at $21,000\times g$ and RT for 20 sec. The resulting pellet was further prepared for electroporation as described in Chapter 4.6.3 with the following modifications: after the washing step, the cells were resuspended in 100 µL glycerol (10 %, ice-cold) instead of 50 µL; 200 ng of the amplified DNA fragment for the disruption of the target gene were added to the electrocompetent cells; a 1 mm electroporation cuvette was used with 1.8 kV; after the electroshock, the cells were incubated in 1 mL LB medium at 37 °C for more than 2 h; and, at the end, four LB-agar plates with 25 µg/mL Cm were each spread with 250 µL cell culture and incubated overnight at 37 °C. The obtained Cm^R transformants were streaked on LB-agar with 25 µg/mL Cm and incubated overnight at 42 °C to remove the temperature-sensitive pKD46 plasmid. The next day, the obtained colonies were picked and streaked on LB-agar with 25 µg/mL Cm and on LB-agar with 100 µg/mL Amp to select for Cm^R Amp^S colonies. The Cm^R Amp^S colonies were electroporated with pCP20 (FLP helper plasmid) to eliminate the FRT-flanked *cat* gene. Amp^R transformants were then selected at 30°C. Afterwards, these were streaked on LB-agar and incubated at 42 °C to cure the pCP20 plasmid. The obtained colonies were then tested for the loss of all antibiotic resistances. Finally, the deletions were verified by colony PCR and by additionally sequencing the amplified fragments.

Also, the *kdsD* gene was deleted in *E. coli* K-12 as described above, but a FRT-*kan*-FRT cassette amplified from pCO1-kan was used and, accordingly, during the whole procedure Km was employed instead of Cm.

4.6.13 Chromosomal deletion of genes (knock-out mutagenesis) – CRISPR/Cas (Jiang et al., 2015)

Knock-out mutagenesis of the *dhaKLM* and *glpK* genes in *E. coli* K-12 were performed as described by Jiang et al. in 2015 (see Figure 4-3). For the deletion of these genes, the pTarget plasmid containing the sgRNA sequence specific for the gene to be deleted had to be constructed. A PCR was performed as described in Chapter 4.6.4 in a total volume of 100 µL containing the original pTarget, Pwo DNA Polymerase, the Universal pTarget primer and the primer containing the sgRNA sequence of the gene that had to be deleted. After the PCR, 10 U Dpn*I* were added to the sample to degrade the original pTarget. The DNA cleavage took place for 1 h at 37 °C. Afterwards, the amplified DNA was separated in an agarose gel as described in Chapter 4.6.7. The amplified fragment with the expected length was then extracted from the gel as described in Chapter 4.6.8 and eluted with 45 µL dH_2O. To recircularise the purified plasmid DNA, 50 U T4 Polynucleotide kinase from NEB (Frankfurt am Main, Germany) were added together with 1x T4 DNA Ligase buffer to the purified sample with a final volume of 55 µL. Then, the preparation was incubated for 1 h at 37 °C. After the incubation, 5 µL of the preparation were mixed with 280 U T4 DNA Ligase from NEB in a total volume of 50 µL for 1 h at RT. For the isolation of only one pTarget, 10 µL of the ligation preparation were transformed in 100 µL DH5α competent cells as described in Chapter 4.6.2. Plasmids were isolated from a couple of single colonies (see Chapter 4.6.5) and were sequenced (see Chapter 4.6.5). Furthermore, adjacent fragments to the desired gene deletion had to be amplified by colony PCR. Each adjacent fragment had around 400 bp. The X1 fragment was amplified by using the primers A_f and A_r and the X2 fragment by C_f and C_r as described in Chapter 4.6.4. The amplified fragments were separated as described in Chapter 4.6.7 and later extracted in 30 µL dH_2O (see Chapter 4.6.8). 20 ng of each extracted DNA fragment, X1 and X2, were mixed with 400 U T4 DNA Ligase from NEB with a total volume of 50 µL and incubated for 2 h at RT. Afterwards, to gain the necessary amount of the X1-X2 fragment, 2 µL of the ligation were amplified by PCR (see Chapter 4.6.4) by using the A_f and the C_r primers. The PCR sample was separated by agarose gel electrophoresis and the X1-X2 fragment, known as donor DNA, was extracted from the gel, eluted with 30 µL dH_2O and quantified by using the "NanoDrop 2000 Spectrophotometer" (Thermo Fisher Scientific Inc., Waltham, USA). Once the sgRNA sequence of the pTarget was verified and the donor DNA was purified and quantified, the chromosomal deletion of the specific gene was performed as pictured in Figure 4-3.
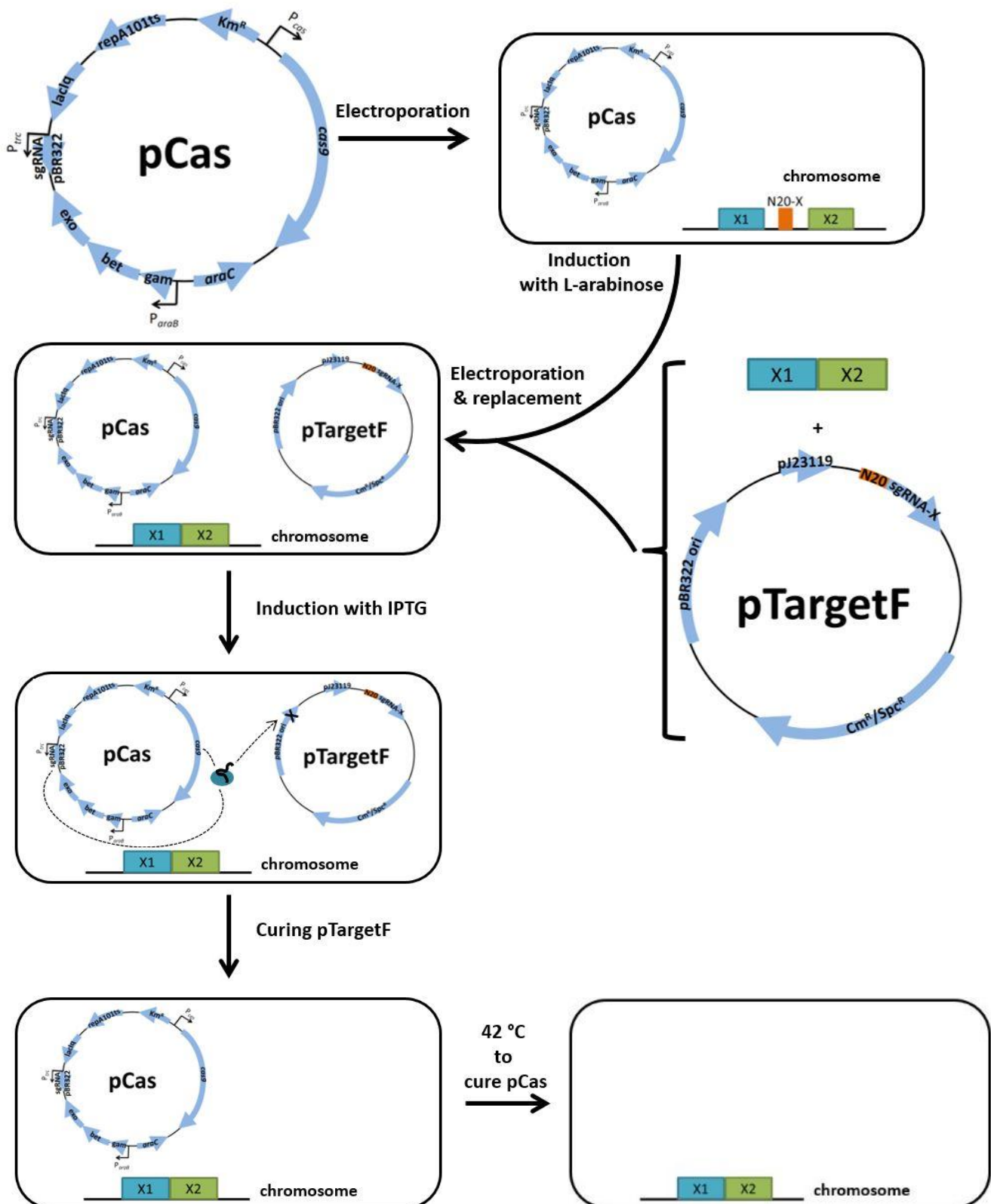
Figure 4-3. CRISPR/Cas genome editing method after Jiang et al. (2015). pCas comprises the *cas9* gene with a native promoter, an IPTG-inducible sgRNA that directs Cas9 to the pBR322 replicon of pTarget, a temperature-sensitive replicon (repA101ts) and the λ-Red recombination system. pTarget expresses the sgRNA of the target gene. pJ23119, synthetic promoter; N20, 20 bp region complementary to the targeting region; *araC*, arabinose-inducible transcription factor.

63

First, the strain, where the deletion had to be performed, was transformed with pCas, a temperature-sensitive plasmid, as described in Chapter 4.6.3. The cells containing the plasmid had to be incubated at temperatures not higher than 30 °C. After the transformation, a single colony was inoculated in 5 mL LB medium with 50 µg/mL Km and incubated at 95 rpm and 30 °C overnight. The next day, 200 µL of the overnight culture were transferred to 5 mL of fresh LB medium containing 50 µg/mL Km and 20 mM L-arabinose to induce the λ-Red system. The fresh inoculated culture was incubated at 95 rpm and 30 °C until the $OD_{600 \, nm}$ of the culture reached at least 0.6. Then, the whole culture was centrifuged at $21,000 \times g$ and RT for 20 sec. The resulting pellet was further prepared for electroporation as described in Chapter 4.6.3 with a small number of changes in the procedure: after the washing step, instead of using 50 µL glycerol (10 %, ice-cold) to resuspend the cells,100 µL glycerol (10 %, ice-cold) were employed; 400 ng of the donor DNA and 100 ng pTarget for the deletion of the target gene were added to the electrocompetent cells; a 1 mm electroporation cuvette was used with 1.8 kV; after the electroshock, the cells were incubated in 1 mL LB medium at 95 rpm and 30 °C for more than 4 h; and then, 250 µL cell culture were spread on four different LB-agar plates with 50 µg/mL Km and 25 µg/mL Cm or 50 µg/mL Spc, depending on the pTarget used, and the plates were incubated at 37 °C until single colonies were observed. Up to 20 colonies were picked and streaked on a LB-agar plate with 50 µg/mL Km and 25 µg/mL Cm or 50 µg/mL Spc. The picked colonies were also tested via colony PCR (see Chapter 4.6.4) to verify that they did not contain the target gene anymore. Once confirmed, one of the colonies was inoculated in 5 mL LB medium with 50 µg/mL Km and 0.5 mM IPTG and the culture was incubated overnight at 95 rpm and 30 °C to induce the loss of the pTarget. The next day, a small amount of the overnight culture was streaked on a LB-agar plate with 50 µg/mL Km to obtain single colonies. At least four of the obtained single colonies were picked and streaked on a LB-agar plate with 50 µg/mL Km and a LB-agar plate with 25 µg/mL Cm or 50 µg/mL Spc and incubated overnight at 30 °C to find out if the curation of pTarget had been a success. If the colonies were Km^R Cm^S/Spc^S, they were streaked on a LB-agar plate without antibiotics and were incubated overnight at 42 °C to obtain single colonies which had loss pCas. When the obtained strain was Km^S Cm^S/Spc^S, the gene deletion was verified by colony PCR and by additionally sequencing the amplified fragment.

4.6.14 Chromosomal integration of genes (knock-in mutagenesis) – CRISPR/Cas

To integrate genes in the chromosome of *E. coli* K-12, the same method was used as described in the knock-out mutagenesis by CRISPR/Cas (Jiang et al., 2015; see Chapter 4.6.13). The

desired gene for the integration under the control of P_{tac} was amplified from a pJF119 plasmid already containing the P_{tac}-gene by using the primers I_f-P_{tac}-gene (BstB*I*) and I_r-P_{tac}-gene (Pst*I*). The amplified fragment contained at the 5'-end of its sequence the same restriction site as the A (X1) fragment (BstB*I*), and at the 3'-end the same restriction site as the C (X2) fragment (Pst*I*). This way, the three fragments could be joined to form a sole fragment, which would be recombined at a specific region in the chromosome given by the X1 and X2 fragments and the sgRNA.

4.6.15 Sequence analysis

To analyse the sequences of DNA fragments or plasmid DNA, 30 µL of the DNA preparation with a concentration of approximately 50 ng/µL were sent to GATC Biotech AG (Konstanz, Germany) to be sequenced by the Sanger sequencing method. The resulting data were aligned with the original sequence with the software "ApE – A plasmid Edition" (Version 2.0.52; Utah, USA) to evaluate differences between both sequences.

4.6.16 RNA isolation

RNA was extracted from cells grown on MM containing 28 mM glucose and 100 µM IPTG during the mid-exponential phase ($OD_{600\,nm}$ 0.8-1.4) to investigate if there were considerable changes in the expression of certain genes between the GL-strains and their evolved strains. Two biological replicates per strain were performed. The RNA sample was obtained by centrifuging 1 mL of the culture at 18,000× g for 15 sec. After discarding the supernatant, the pellet was stored at - 70 °C for up to 4 weeks. On the day of the RNA isolation, the pellet was thawed on ice and resuspended in 350 µL RTL buffer containing 10 µL/mL β-mercaptoethanol from the "RNeasy Mini Kit" (Qiagen GmbH, Hilden, Germany). This mixture was then transferred into a 1.5 mL micro tube containing approximately 250 µg silica (0.1 mm diameter; Carl Roth GmbH, Karlsruhe, Germany) and strongly mixed in the device Silamat® S6 (Ivoclar Vivadent GmbH, Ellwangen, Germany) for 30 sec to lyse the cells. After centrifuging at 18,000× g for 15 sec, the supernatant was added to 250 µL EtOH (100%) present in another 1.5 mL micro tube and mixed by pipetting up and down. Then, up to 700 µL of the mixture were transferred to the RNeasy Mini spin column. From here, the instructions of the "Protocol 7: Purification of total RNA from bacterial lysate using the RNeasy Mini Kit" available in the "RNAprotect Bacteria Reagent Handbook" (Qiagen GmbH, Hilden, Germany) were followed, including the on-column DNase digestion ("Appendix B: Optional on-column DNase digestion using the RNase-free DNase set"). When the RNA was already isolated, 1 µL was used to

measure the RNA concentration and its purity with the "NanoDrop 2000 Spectrophotometer" (Thermo Scientific, Waltham, USA), 2 µL were loaded in an agarose gel containing 250 µL sodium hypochlorite to visualise the RNA integrity and rule out RNA degradation, 1 µL was mixed with 20 µL sterile dH_2O to assess DNA contamination, and the rest was stored at - 70 °C until further use.

To rule out any DNA contamination in the RNA sample, a PCR was performed as described in Chapter 4.6.4 in a total volume of 25 µL with 1 µL of the diluted RNA sample (1:21) and the primers pgi-5'-cDNA and pgi-3'-cDNA, which anneal on the *pgi* gene. If the presence of DNA was confirmed, the RNA sample was freed from DNA according to "Appendix E: DNase digestion of RNA before RNA cleanup" except that the incubation step took place for more than 1 h to guarantee that no DNA would be present anymore, and followed by the "Protocol: RNA cleanup", both from the "RNeasy Mini Handbook" (Qiagen, Hilden, Germany). Here again, the RNA concentration and its purity were quantified, and its integrity and the presence of DNA were analysed. The RNA sample was stored at - 70 °C.

4.7   Protein biochemical methods

4.7.1   Overproduction of recombinant proteins and cell harvesting

For the overproduction of a recombinant protein, the BL21(DE3) pLysS strain was transformed as described in Chapter 4.6.2 with a plasmid which contained the gene that encodes for the protein of interest. A single transformant was inoculated in 10 mL 2x YT medium and the corresponding antibiotics and incubated overnight at 180 rpm and 37 °C. The next day, the 10 mL overnight culture were transferred to a 1 L shake flask containing 200 mL 2x YT medium and the appropriate antibiotics and incubated at 200 rpm and 37 °C. When an $OD_{600\,nm}$ value of 0.6-0.8 was reached, 1 mM IPTG was added to the culture to induce expression of the gene of interest. The culture was further incubated at 200 rpm and 37 °C. After 4 h incubation, the whole cell culture was centrifuged at 6,400× *g* and 4 °C for 10 min. The supernatant was discarded and the pellet was resuspended in 10 mL lysis buffer and centrifuged at 3,400× *g* and 4 °C for 10 min. After discarding the supernatant, the pellet was stored at - 20 °C until further use.

4.7.2   Cell disruption and preparation of cell-free extracts

For the disruption of *E. coli* B cells, the pellets obtained as described in Chapter 4.7.1 were thawed on ice. Then, the pellet was resuspended in 2 mL lysis buffer with 40 Kunitz U/mL

DNase I per gram cell wet weight. DNase I was added to reduce the viscosity caused by DNA in the cell lysate. The mixture was incubated at 95 rpm and 30 °C for 30 min. Directly after, the mixture was kept on ice for 30 min to cool it down for cell disruption. The ultrasonic cell lysis was performed on ice using the ultrasonic homogeniser Bandelin Sonopolus HD200/UW200 (Bandelin electronic GmbH & Co. KG, Berlin, Germany) four times for 30 sec with a 50 % duty cycle. The cell lysate was centrifuged at $18,000 \times g$ and 4 °C for 1 h. The pellet and 40 µL cell-free extract (CE) were stored at 4 °C for further analysis and the rest of the CE was used for protein purification as described in Chapter 4.7.4.

E. coli K-12 cells were disrupted after reaching the stationary phase on LB or MM with a C-source to verify the presence of different proteins and quantify their specific activity. With the comparison of these values, differences might be found that explain different growth behaviours. The pellet obtained as described in Chapter 4.5.2 was resuspended in 500 µL glycylglycine buffer (50 mM; pH 8.5) containing 40 Kunitz U/mL DNase I and 200 U/mL lysozyme. The suspension was incubated at 95 rpm and 30 °C for 30 min, then, kept on ice for 30 min and centrifuged at $18,000 \times g$ and 4 °C for 1 h. 200 µL CE were kept at 4 °C and the rest of CE was treated with heat for the purification of FSAA (see Chapter 4.7.3).

4.7.3   Heat treatment of cell-free extracts

An accumulation of FSAA in the supernatant was desired, so that its presence could be verified by activity assays and SDS-PAGE. By taking advantage that FSAA is a known thermostable protein (Schürmann, 2001), FSAA could be enriched in the CE by heat treatment. The CE obtained as described for *E. coli* K-12 strains in Chapter 4.7.2 was incubated for 20 min at 75 °C in the device "Biometra TSC ThermoShaker" (Analityk Jena AG, Jena, Germany). At this temperature thermosensitive proteins would denaturalize and precipitate, and thermostable proteins would still be soluble. Afterwards, the mixtures were centrifuged at $18,000 \times g$ and 4 °C for 30 min and the resulting heat-treated enriched fractions (HT), which contained mostly FSAA, were stored at 4 °C.

4.7.4   Purification of recombinant proteins

All recombinant proteins overproduced as described in Chapter 4.7.1 were 6x His-tagged proteins. Therefore, these proteins were purified by Ni^{2+}-NTA affinity chromatography as explained below. First, 5 mL Lysis buffer were added to a 1 mL Ni^{2+}-NTA agarose column (Qiagen GmbH, Hilden, Germany) to equilibrate the column. Secondly, the CE obtained as described for *E. coli* B strains in Chapter 4.7.2 was loaded into the column and the flow-through

was collected for safety. Then, different column volumes (CV) were added into the column in the order shown in Table 4-10. Each fraction was collected in a new 1.5 mL micro tube. To find out which fractions contained the highest amount of the recombinant protein, 200 µL Bradford reagent and 10 µL fraction were mixed. The elution fractions with the strongest blue were selected and were all loaded in the same Amicon® Ultra-15 centrifugal filter units (10 kDa) from Merck Millipore Ltd. (Cork, Ireland) to increase the concentration of the recombinant protein by concentrating it and replacing the imidazole buffer by a more suitable buffer, such as the glycylglicine buffer. Therefore, the centrifugal filter unit was centrifuged at 4,000× g and 4 °C until approximately 200 µL – 500 µL were retained by the filter. Then, 4 mL glycylglycine buffer (50 mM; pH 8.5) with 1 mM DTT were added into the centrifugal filter unit and mixed with the retained volume. A centrifugation step took place again at 4,000× g and 4 °C until approximately 200 µL – 500 µL remained. This end volume contained the concentrated recombinant protein in an appropriate buffer. It was transferred to a new 1.5 mL micro tube and stored at 4 °C until further use.

Table 4-10. Buffer sequence for the purification of 6x His-tagged proteins.

Step	CV	Buffer
1)	5	Lysis buffer
2)	3	Wash buffer I
3)	1	Wash buffer II
4)	5	Elution buffer I
5)	5	Elution buffer II

4.7.5   Determination of protein concentration (Bradford, 1976)

A colorimetric assay (Bradford, 1976) was carried out to measure the concentration of total protein present in a sample. This method is based on the binding of proteins to the dye Coomassie® Brilliant Blue G-250. The formation of this complex gives a colour change, shifting the absorbance maximum of the dye from 465 nm to 595 nm. The higher the amount of proteins in the sample, the higher is the absorbance at 595 nm. Bovine Serum Albumin (BSA) was used as the standard protein from a concentration of 0.01 mg/mL to 0.5 mg/mL. By plotting the absorbance of the standards (y-axis) against their concentration (x-axis), a linear graph was acquired. Its equation was utilised to calculate the total protein concentration of the unknown samples. The assay was performed by mixing 1 mL Bradford reagent with 50 µL sample, incubating the mixture for 5 min at RT, and reading its absorbance at 595 nm with a spectrophotometer. All samples were assayed in duplicate.

4.7.6   SDS-polyacrylamide gel electrophoresis (Laemmli, 1970)

The cell-free extract (CE) and the heat-treated enriched fraction (HT) of each cell lysate were separated via SDS-PAGE by using 12 % SDS-gels. The composition of the SDS-gels is listed in Table 4-11. The SDS-gel consisted of two parts: the separating gel and the stacking gel. The separating gel was casted after adding APS and TEMED in the already prepared equipment. Directly afterwards, 1 mL isopropanol was added on the separating gel to obtain a straight completion. After the polymerisation of the gel, the isopropanol was removed and the stacking gel was casted. While the stacking gel was still liquid, a comb was used to give it the form of 15 wells. After its polymerisation, the comb was carefully removed and the gel was wrapped in a wet tissue and stored at 4 °C until further use.

Table 4-11. 12 % SDS-gel composition.

Solutions	Separating gel	Stacking gel
Rotiphorese® gel 30 (37.5:1)	8 mL	2.6 mL
0.5 M Tris-HCl (pH 6.8)	-	3.75 mL
1 M Tris-HCl (pH 8.8)	7.5 mL	-
10 % SDS (w/v)	200 µL	150 µL
dH$_2$O	4.2 mL	8.5 mL
10 % APS (w/v)	100 µL	110 µL
TEMED	10 µL	12 µL

The electrophoresis was performed inside a gel chamber. For this aim, the gels were assembled inside this chamber which was filled up with 1x SDS-running buffer. 5 µg protein from each sample (CE and HT) were analysed by mixing them with 2x SDS-loading buffer. Then, the mixtures were boiled for 10 min. Afterwards, they were left on ice for at least 5 sec, centrifuged at maximal speed for 3 sec and loaded in the wells of the gel. The marker used was the "Blue Start Prestained Protein Marker" (Nippon Genetics Europe, Düren, Germany). The electrophoresis was performed at 40 mA at RT until the green dye band from the marker nearly reached the end of the gel (a duration of approximately 2 h). The gel was stained by incubating it for 30 min in a solution with the dye Coomassie Brilliant Blue R-250. After, the gel was incubated several times for 30 min in fresh decolouring solution until the background colour was removed from the gel and the protein bands could be easily visualised.

4.7.7   Fructose 6-phosphate aldolase activity test

The fructose 6-phosphate aldolase activity test (FSA assay; see Figure 4-4) allowed the quantification of the specific FSA activity and was modified after Schürmann and Sprenger (2001). The purified His-tagged FSAA wt / FSAA A129S and the heat-treated enriched fractions (HT) were analysed for specific FSA activity. Each cuvette contained: 0.3 mM NADH; 40 U TPI and 4 U Gly3P DH as coupled enzymes; 10 µL protein sample (diluted to match the exact protein quantity needed); 7.5 mM/27 mM F6P depending if FSAA A129S or FSAA wt was studied; and 50 mM glycylglycine buffer (pH 8.5) with 1 mM DTT to reach a total volume of 1 mL. The reaction was always initiated by adding F6P, and was carried out at 30 °C. The NADH consumption was spectrophotometrically monitored at 340 nm. A negative control (without substrate addition) was performed for each sample to rule out any background activity. All samples were tested in duplicate.
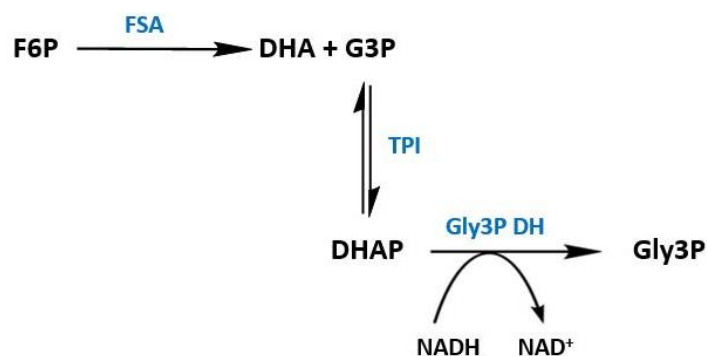
Figure 4-4. FSA assay with fructose 6-phosphate (F6P) as substrate, and triose-phosphate isomerase (TPI) and glycerol 3-phosphate dehydrogenase (Gly3P DH) as coupled enzymes (Schürmann and Sprenger, 2001). The assay took place at 30 °C and was monitored at 340 nm. DHA (dihydroxyacetone), DHAP (dihydroxyacetone phosphate), G3P (glyceraldehyde 3-phosphate), Gly3P (glycerol 3-phosphate), NAD⁺/NADH (nicotinamide adenine dinucleotide oxidised/reduced).

4.7.8   Glycerol dehydrogenase activity test

The glycerol dehydrogenase activity test (GldA assay; see Figure 4-5) enabled the determination of the specific GldA activity of the purified His-tagged GldA and the cell-free extract (CE) samples. The assay was modified after Subedi et al. (2008). Each 1 mL reaction mixture consisted of 0.3 mM NADH, 60 mM NH_4Cl, 10 µL protein sample (diluted to correspond the precise quantity of protein needed), 1 mM DHA, and 100 mM potassium phosphate buffer (pH 7.0). The reaction took place in a cuvette at 30 °C, always started with the addition of DHA, and the depletion of NADH was spectrophotometrically monitored at 340 nm. A negative control (without substrate addition) was carried out for each sample to exclude any background activity. All samples were tested in duplicate.
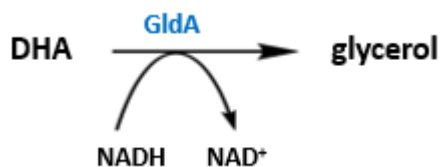
Figure 4-5. GldA assay with dihydroxyacetone (DHA) as substrate (Subedi et al., 2008). The assay was performed at 30 °C and monitored at 340 nm. NADH/NAD⁺ (nicotinamide adenine dinucleotide reduced/oxidised).

4.7.9 *β*-galactosidase assay to determine promoter strength

To study which substances upregulate or downregulate the promoters of the *fsaA* and *fsaB* genes, the *lacZ* reporter strains LJ110 FRT-*cat*-FRT-P$_{fsaA}$-*lacZYA* and LJ110 FRT-*cat*-FRT-P$_{fsaB}$-*lacZYA* were used (see Chapter 4.6.11). The *lacZ* gene encodes for the enzyme *β*-galactosidase. This enzyme cleaves lactose in glucose and galactose. Its activity can be determined by using chromogenic or fluorogenic substrate analogues of lactose (see Figure 4-6). O-nitrophenyl-*β*-D-galactopyranoside (ONPG) is a colourless substrate that is hydrolysed by *β*-galactosidase to o-nitrophenol (ONP) and galactose. ONP is a yellow chromophore, which can be quantified at a wavelength of 420 nm. The assay was modified after Li et al. (2012) and whole-cells were used.

Figure 4-6. *β*-galactosidase assay with o-nitrophenyl-*β*-D-galactopyranoside (ONPG) as substrate (Li et al., 2012). The assay was performed at 30 °C and monitored at 420 nm. ONP (o-nitrophenol).

First, a single LJ110 FRT-*cat*-FRT-P$_{fsaA}$-*lacZYA* or LJ110 FRT-*cat*-FRT-P$_{fsaB}$-*lacZYA* colony was inoculated in 20 mL MM containing 28 mM glucose and 25 µg/mL Cm. The culture was incubated overnight at 200 rpm and 37 °C. The next day, 20 mL of the preculture were centrifuged at 3,400× *g* and RT for 6 min, the supernatant was removed and the pellet was washed with 20 mL MM without the presence of a C-source. After centrifuging again, the resulting pellet was resuspended in 20 mL MM without a C-source. The preculture was inoculated in a 250 mL shake flask with a metal cap containing the main culture with a start OD$_{600\,nm}$ of 0.1. The main culture consisted of 50 mL MM containing 25 µg/mL Cm and one of the following components: 28 mM glucose; 28 mM glucose and 15 mM HA; 28 mM glucose and 5 mM DHA; 28 mM glucose and 4 mM GoA; 28 mM glucose and 5 mM GA; 28 mM glucose and 20 mM glycerol; 28 mM fructose; 33 mM L-arabinose; 28 mM mannitol; or 42 mM succinate (pH 7.0). The incubation took place at 200 rpm and 37 °C for 24 h. The OD$_{600\,nm}$ of the cultures was measured after 0 h, 6 h and 24 h incubation. After 24 h their

β-galactosidase activity was also determined. For the latter, 100 µL of the culture were added to a mixture containing 900 µL Z-buffer (which contained 2.8 µL mercaptoEtOH/mL Z-buffer), 10 µL SDS (0.1 %) and 20 µL chloroform. The cell preparation was vortexed for 15 sec and, directly afterwards, transferred to a glass cuvette and mixed to avoid SDS precipitation. After incubating the cuvettes for 5 min at 30 °C, the cell suspension was mixed again and 200 µL ONPG (4 mg/mL) were added into the cuvette. Immediately, the $OD_{420\,nm}$ was monitored for 10 min. For the blank measurement, 100 µL MM were used instead of cells.

$$\beta\text{-}galactosidase\ activity = \frac{1\ \mu mol\ ONP}{min}$$

$$specific\ activity = \frac{\frac{OD_{420\,nm}}{time} \cdot reaction\ volume \cdot 10^6}{\varepsilon_{ONP} \cdot cell\ volume \cdot OD_{600\,nm}}$$

The change given in $OD_{420\,nm}$/time is the change in the $OD_{420\,nm}$/minute; the reaction volume is equal to 1.2 mL; the ε_{ONP} at 420 nm is equivalent to 2238.1 $M^{-1}\,cm^{-1}$; and the cell volume corresponds to the 100 µL culture used in this assay.

4.7.10 Determination of K_M and V_{max}

To understand the growth behaviour of the GL-strains on glucose in the presence of FSAA wt or FSAA A129S, the K_M and V_{max} values for F6P of the purified His-tagged enzymes FSAA wt and FSAA A129S were determined. These values were also calculated for A5P because the cleavage of A5P catalysed by FSAA A129S has never been studied before.

The specific activity of these two purified His-tagged FSAA enzymes with 12 different concentrations of the substrate F6P (0 mM, 0.1 mM, 0.2 mM, 0.5 mM, 1 mM, 1.5 mM, 3 mM, 5 mM, 10 mM, 15 mM, 20 mM and 25 mM) was measured. The same assays conditions were used as in the FSA assay (Chapter 4.7.7) with two exceptions: the reaction was initiated by adding the purified enzyme and not with the substrate; and different concentrations of F6P were used.

To quantify the specific activity of the His-tagged FSAA A129S with nine different concentrations of the substrate A5P (0 mM, 0.05 mM, 0.1 mM, 0.15 mM, 0.2 mM, 0.5 mM, 1 mM, 2 mM and 3 mM), quartz cuvettes with a volume of 500 µL were used. A reduced volume of the reaction was desired due to the high price and the low availability of A5P. The reaction mixture consisted of: 0.3 mM NADH; 2.5 µL TPI/Gly3PDH (18-48 U and 1.8-4.8 U, respectively); different A5P concentrations; 5 µg purified FSAA A129S; and was filled up to a volume of 500 µL with glycylglycine buffer (50 mM; pH 8.5). The reaction temperature was

30 °C and was initiated by the addition of the purified enzyme. The NADH consumption was monitored spectrophotometrically at 340 nm. A schema of the reaction can be found in Chapter 4.8.3.

With the software "GraphPad Prism" version 6.01 from GraphPad Software, Inc. (San Diego, USA), the specific activities were plotted against the different substrate concentrations to calculate the K_M and V_{max} by using Michaelis-Menten enzyme kinetics.

4.7.11 *In vitro* synthesis of A5P

The *in vitro* synthesis of A5P has already been shown by Sánchez-Moreno et al. (2012a), where DHA and GoA were used as substrates for the one-pot synthesis. In this study, the DHA phosphorylation step was omitted and DHAP was used directly as shown in Figure 4-7. FSAA A129S catalysed the formation of A5P instead of FSAA wt.
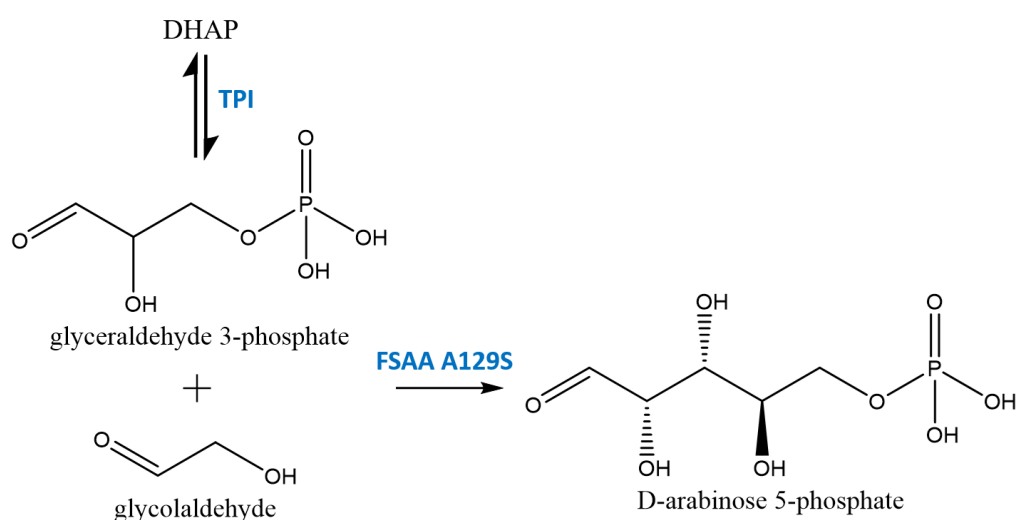
Figure 4-7. Possible *in vitro* synthesis of arabinose 5-phosphate from dihydroxyacetone phosphate (DHAP) and glycolaldehyde catalysed by triose-phosphate isomerase (TPI) and FSAA A129S.

Eleven mixtures were prepared on ice in 1.5 mL micro tubes. Ten of them were controls with a final volume of 20 µL and one of them was the synthesis mixture with a total volume of 1 mL filled-up with a 50 mM glycylglycine buffer (pH 8.5). The micro tubes were incubated at 95 rpm and 30 °C for 24 h in a INFORS HT shaker (Bottmingen, Switzerland). The composition of the mixtures is listed in Table 4-12. GoA was added in the synthesis mixture every 45 min in low concentrations to avoid large excess of this compound. At considerable GoA concentrations, FSAA A129S might catalyse the cross-aldol addition of GoA forming threose as product (Castillo et al., 2010). The formation of threose in the A5P synthesis would be an undesired by-product. After 24 h incubation, the synthesis mixture was filtrated in an "Amicon® Ultra-2 mL Centrifugal Filter Units - 10 K" from Merck KGaA (Darmstadt,

Germany) at 4 °C. The manufacturer's instructions to separate the protein from the product and the remaining substrates were followed. The product-containing filtrate was always stored on ice or at 4 °C. For the validation of the *in vitro* A5P synthesis refer to Chapter 4.8.2 (thin layer chromatography) and Chapter 4.8.3 (determination of the concentration of synthesised A5P).

Table 4-12. Composition and total volume of the mixtures for the *in vitro* synthesis of A5P.

Mixtures	Composition	Total volume
1.	50 mM A5P	
2.	250 mM DHAP	
3.	280 mM G3P	
4.	200 mM GoA	
5.	250 mM DHAP + 200 mM GoA	**Controls (20 µL)**
6.	250 mM DHAP + 40 U TPI	
7.	50 mM A5P + 1 U FSAA A129S	
8.	200 mM GoA + 0.5 U FSAA A129S	
9.	250 mM DHAP + 200 mM GoA + 40 U TPI	
10.	250 mM DHAP + 200 mM GoA + 0.5 U FSAA A129S	
11.	250 mM DHAP + 8 x 25 mM GoA (added every 45 min) + 2000 U TPI + 25 U FSAA A129S	**Synthesis (1 mL)**

4.7.12 LPS integrity test

An indirect LPS integrity test was carried out to find a correlation between the lack of A5P and the viability of the cell membrane. Normally, the outer membrane protects the cell from lysozyme hydrolysis, but without LPS, lysozyme might be able to lyse the cell.

A single BW25113 $\Delta gutQ$ $\Delta kdsD$::*kan* colony was inoculated in 25 mL MOPS-MM containing 28 mM glucose, 10 µM G6P, 15 µM A5P and 50 µg/mL Km in a 100 mL shake flask. This preculture was incubated overnight at 200 rpm and 37 °C. The next day, 2 mL of the overnight culture were centrifuged at $16,500\times g$ for 1 min and the pellets were washed twice with 1 mL MOPS-MM with 28 mM glucose. The resulting pellet was resuspended in 1 mL MOPS-MM with 28 mM glucose. The resuspended cells were inoculated with a start $OD_{600\,nm}$ of 0.05 in 25 mL MOPS-MM containing 28 mM glucose, 10 µM G6P, 50 µg/mL Km and various concentrations of A5P (0 µM; 5 µM; 10 µM; 20 µM; 30 µM; 50 µM; and 100 µM) in 250 mL shake flasks with metal caps. Each quantity of A5P should enable the biosynthesis of different amounts of LPS. The culture with 0 µM A5P was used as a negative growth control to ensure that the right strain was inoculated. The cultures were then incubated at 200 rpm and 37 °C for

48 h to be able to reach the maximal $OD_{600\,nm}$. Directly after the 48 h, five 1.5 mL micro tubes were filled with the volume of the culture corresponding to an $OD_{600\,nm}$ of 4. The samples were centrifuged at $18,000 \times g$ and 4 °C for 10 min. The pellets were then washed with 1 mL of glycylglycine buffer (50 mM; pH 8.5) and centrifuged again at $18,000 \times g$ and 4°C for 10 min. The resulting pellets were resuspended in 400 µL glycylglycine buffer (50 mM; pH 8.5). 40 Kunitz U/mL DNase I and different lysozyme units (0 U/mL; 100 U/mL; 200 U/mL; 1000 U/mL; and 2000 U/mL) were added to the cell suspensions. Then, the micro tubes were incubated at 90 rpm and 30 °C for 30 min. Immediately afterwards, the micro tubes were put on ice and centrifuged at $18,000 \times g$ and 4 °C for 30 min. The supernatant was transferred to a fresh 1.5 mL micro tube and the protein concentration of the supernatant was determined by mixing 50 µL of the supernatant with 1 mL Bradford reagent, incubating for 5 min at RT and measuring the $OD_{595\,nm}$. Two biological replicates, each with two technical replicates, were performed for each A5P concentration and each lysozyme unit.

4.8   Analytical methods

4.8.1   High Performance Liquid Chromatography (HPLC) analysis

The following separation system was used for the detection and determination of sugars, DHA and glycerol:

- HPLC system: 1100 series with a 1260 Infinity RID detector from Agilent Technologies (Waldbronn, Germany).
- Column: Organic Acid, 300 x 8 mm (Chromatographie-Service GmbH, Langerwehe, Germany).
- Column temperature: 5 - 30 °C. Due to the degradation of the column, the temperature had to be adjusted to avoid overlapping of peaks. These changes had no effect on the retention times.
- Injection volume: 5.00 µL
- Flow: 0.6 mL/min
- Mobile phase: 5 mM H_2SO_4
- Duration of elution: 20 min
- RID temperature: 35 °C
- RID polarity: positive

The concentration of sugars, DHA and glycerol was quantified after calibration with their respective standards. Each run was analysed with the Agilent software "ChemStation for LC 3D Systems" (software version: Rev. B.04.03 [16]).

4.8.2   Thin layer chromatography

Thin layer chromatography (TLC) was performed to detect different compounds, to check if the synthesis of A5P was successful and if any by-products were produced. For these analyses, the "TLC silica gel 60 F_{254}" from Merck KGaA (Darmstadt, Germany) was used as stationary phase and two different mobile phases were applied depending on the type of compounds that should be separated. The solvent system $CHCl_3$/MeOH (5:1) was employed for the separation of sugars. However, for the detection of A5P, the solvent mixture containing EtOAc:MeOH:H_2O:HOAc (5:2:1.4:0.4) was utilised (Wen et al., 2016). First of all, 1 µL of each mixture was spotted at 1 cm of the bottom of the TLC silica gel plate. After the spots had dried, the TLC plate was placed in a chamber containing one of the previously mentioned solvent mixtures (mobile phase). When the mobile phase reached approximately a height 1 cm from the top of the TLC plate, the chromatography was stopped by removing the TLC plate from the chamber and letting it dry. Then, the TLC plate was immersed in the staining solution composed of 83 mL MeOH, 3 mL H_2SO_4, 1 mL p-anisaldehyde and 1 mL HOAc. Finally, the TLC plate was dried with a hot-air gun to visualise the different compounds present in the spots, which would turn into different colours depending on the functional groups they had.

4.8.3   Determination of the concentration of synthesised A5P

The concentration of A5P present in the filtrate of the synthesis preparation (see Chapter 4.7.11 for A5P synthesis details) was determined enzymatically, together with the concentrations of G3P and DHAP still present in the filtrate (see Figure 4-8). All tests were performed at 30 °C and spectrophotometrically monitored at 340 nm. First, 10 µL of different dilutions of the filtrate were mixed with 0.3 mM NADH and ad 1 mL glycylglycine buffer (50 mM; pH 8.5). Then, the background activity of this mixture was measured to ensure that it did not influence the measurements. After 2 min of stabilisation of the curve in form of a horizontal line, 1.3 U Gly3P DH were added to measure how much DHAP was still present in the filtrate. The NADH consumption was monitored. When the absorbance value did not decrease anymore in 2 min, 8.6 U TPI were also supplemented to the mixture to determine the G3P present in the filtrate. Again, the NADH depletion was followed. When it stopped, 1.6 U FSAA A129S were added to quantify the concentration of the synthesised A5P in the filtrate (see Figure 4-9). Here again,

the decrease in NADH concentration was monitored until it ceased. Because 1 mole NADH stoichiometrically corresponds to 1 mole DHAP, 1 mole G3P or 1 mole A5P, it was possible to determine the concentration of these three compounds in the filtrate by calculating first the concentration of NADH consumed after each reaction.

The Lambert-Beer law is expressed as:

$$A = \varepsilon \cdot l \cdot c$$

where A is the absorbance, ε is the molar extinction coefficient at a specific wavelength, l is the path length of the cuvette, and c is the analyte concentration.

From the Lambert-Beer law it is possible to determine the concentration of NADH that has been consumed in each reaction:

$$c = \frac{A}{\varepsilon \cdot l}$$

where A corresponds to the difference in $OD_{340\ nm}$ between the value at the beginning of the reaction and at its end, the ε value for NADH at 340 nm is 6.3 $mmole^{-1} \cdot cm^{-1}$ (Bergmeyer, 1975), and the l is 1 cm.
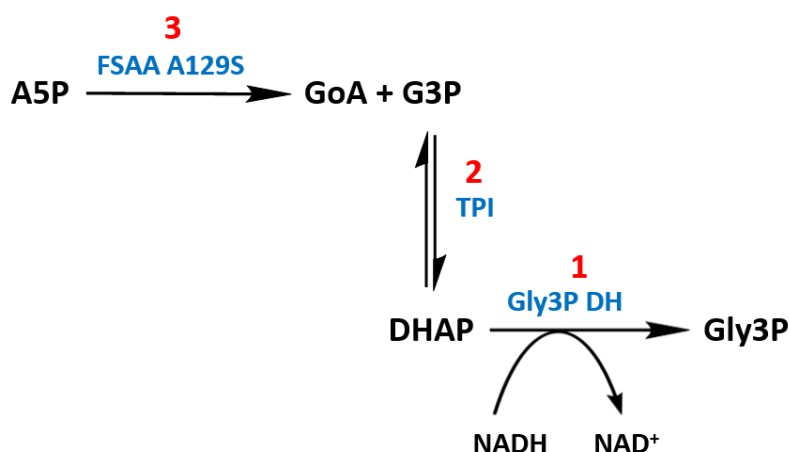
Figure 4-8. Cascade reaction to determine the concentration of A5P present in a mixture. First, Gly3P DH is added to consume any DHAP still present in the mixture. Secondly, TPI is supplemented to the mixture to deplete any G3P. At the end, FSAA A129S is added to quantify only the A5P present.

4.8.4   Determination of the cell dry weight of *E. coli* cells

For the quantification of the intracellular concentration of F6P and G6P as described in Chapter 4.8.5, it was necessary to determine the cell dry weight (CDW) of LJ110 and GL3. Given that the CDW is dependent on the strain used and the growth conditions, the relationship between CDW and $OD_{600\ nm}$ was calculated for each strain. The strains were inoculated in MM with 28 mM fructose and incubated overnight at 180 rpm and 37 °C. The overnight cultures were centrifuged at 3,400× *g* and RT for 5 min. The resulting pellet was washed with 1 mL MM

containing 28 mM glucose per 4 mL original culture and centrifuged again at 3,400× g and RT for 5 min. After discarding the supernatant, the pellet was resuspended in 1 mL MM with 28 mM glucose per 4 mL original culture and inoculated in the main culture (50 mL MM with 28 mM glucose in a 500 mL shake flask with a metal cap) with a start $OD_{600\,nm}$ of 0.5. The cultures were incubated at 200 rpm and 37 °C for 2 h. After the incubation, volumes corresponding to a total $OD_{600\,nm}$ of 2, 5, 10, 20 and 30 were filtered through a "Durapore® PVDF membrane 0.45 µm" from Merck Millipore Ltd. (Cork, Ireland), previously weighed, and left to dry in a 37 °C incubator for 2 days. Then, the weight was controlled again and annotated. A control, where only 50 mL MM with 28 mM glucose were filtered, was also carried out to be able to get the real CDW after subtracting the medium weight from the total weight of the cell culture samples. The CDW for each $OD_{600\,nm}$ and strain was calculated as follows:

$$\text{CDW} = m_{\text{after drying}} - m_{\text{before filtration took place}} - m_{\text{only MM filtered}}$$

m refers to the weight of the filter.

When the y-axis (CDW) was plotted against the x-axis ($OD_{600\,nm}$), a linear trendline was drawn and an equation that stated the relationship between $OD_{600\,nm}$ and CDW for each strain was displayed.

4.8.5   Determination of the intracellular concentration of G6P and F6P

The intracellular concentrations of G6P and F6P in LJ110 and GL3 were quantified in the presence of glucose. First, these strains were inoculated in 20 mL MM containing 28 mM fructose in a 100 mL shake flask with a cotton plug and incubated overnight at 180 rpm and 37 °C. The 20 mL of the overnight culture were centrifuged at 3,400× g and RT for 5 min. Immediately after, the supernatant was discarded and the pellet was washed in 5 mL MM with 28 mM glucose and centrifuged again at 3,400× g and RT for 5 min. The pellet was resuspended in 5 mL MM with 28 mM glucose. Then, the obtained cell suspension was inoculated into the main culture (50 mL MM with 28 mM glucose in 500 mL shake flask with a metal cap) with a start $OD_{600\,nm}$ of 0.5 and incubated at 200 rpm and 37 °C for 2 h. After the incubation, the volume equivalent to an $OD_{600\,nm}$ of 25 was centrifuged at 3,400× g and 4 °C for 5 min. No rapid quenching or sampling was required, because GL3 showed no growth to appreciate considerable differences in a few seconds or minutes. The following metabolite extraction was adapted from Teleki et al. (2015). The pellet was washed with 1 mL NaCl-solution (0.9%), transferred into a micro tube (1.5 mL) and centrifuged at 20,000× g and RT for 20 sec. 600 µL glycylglycine buffer (50 mM; pH 8.5) were added on the pellet and the micro tube was vortexed

for 5 sec. Then, it was incubated for 5 min at 100 °C (hot water bath) to extract the intracellular metabolites. Directly afterwards, the micro tube was chilled on ice for a short time and centrifuged at 20,000× g and 4 °C for 10 min. 500 µL of the supernatant were transferred into a new micro tube (1.5 mL) and kept on ice until further use. The concentration of G6P and F6P present in the obtained supernatant was determined enzymatically (see Figure 4-9). The tests were performed at 25 °C for 20 min/reaction in the 96 well cell culture plate Cellstar® from greiner bio-one (Frickenhausen, Germany) and the change in the optical density at 340 nm was followed using an "Eon^{TM} High Performance Microplate Spectrophotometer" and the software "Gen5^{TM}" (version 2.05.5) both from BioTek Instruments, Inc. (Bad Friedrichshall, Germany).

Each well contained:

        150 µL of the sample (extracted metabolites)

        0.3 mM NADP$^+$

        0.5 U G6P DH (added first to start the determination of G6P)

        0.5 U PGI (added at the end to start the determination of F6P)

        ad 200 µL glycylglycine buffer (50 mM; pH 8.5)
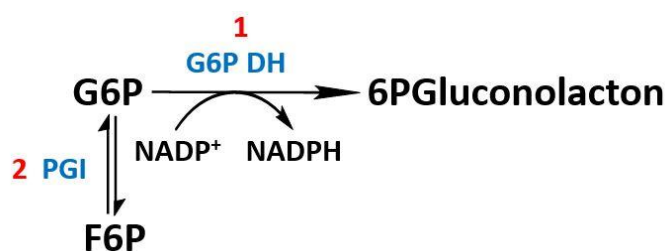
Figure 4-9. Enzymatic determination of the intracellular concentrations of G6P and F6P. First, G6P DH was added to measure G6P. Afterwards, the addition of PGI made it possible to determine F6P.

The average $OD_{340\,nm}$ values from 2 min before enzyme addition and 2 min after the reaction finished (20 min) were calculated. The first value was subtracted from the second one and, by means of a trend line produced with known concentrations of G6P and F6P, the concentrations of the G6P and F6P present in the samples were determined. Assuming that the cells have 2.7 µL cell water for each mg CDW (Winkler and Wilson, 1966) and after calculating the relationship of CDW to $OD_{600\,nm}$ of LJ110 and GL3, it was possible to determine the intracellular concentrations of G6P and F6P. Controls were performed to rule out that G6P and F6P were degraded during the hot water metabolite extraction and that the other intracellular components of the cells disturbed the measurements of the concentrations of G6P and F6P. A control mixture consisting of 0.1 mM G6P and 0.1 mM F6P was present in each plate to identify any problems with the NADP$^+$ and the enzymes used to quantify these sugar phosphates.

79

5 Results

5.1 Novel bypass for glucose degradation

The first FSA reaction to be performed *in vivo* was the cleavage of fructose 6-phosphate (F6P), an intermediate of glycolysis. To show that this reaction was also functional *in vivo*, numerous deletions in central carbon metabolism were required. Through this new glycolytic bypass in *E. coli*, new products were synthesised. Part of these results were published by Guitart Font and Sprenger (2020).

5.1.1 Construction and characterisation of the *E. coli* K-12 mutant strain GL3, which is deficient in glucose 6-phosphate dehydrogenase and in phosphofructokinase activities.

The genes *zwf*, *pfkB* and *pfkA* were consecutively deleted from the parent strain LJ110 generating the strain GL3 (see Chapter 4.6.12 for details of strain construction and Table 4-8 for genotypes of strains). The consumption of glucose in GL3 is disturbed as a consequence of the block in glycolysis due to the missing phosphofructokinase activity and of the non-functional bypass through the pentose phosphate pathway as a result of the missing glucose 6-phosphate dehydrogenase activity, (see Figure 5-1).
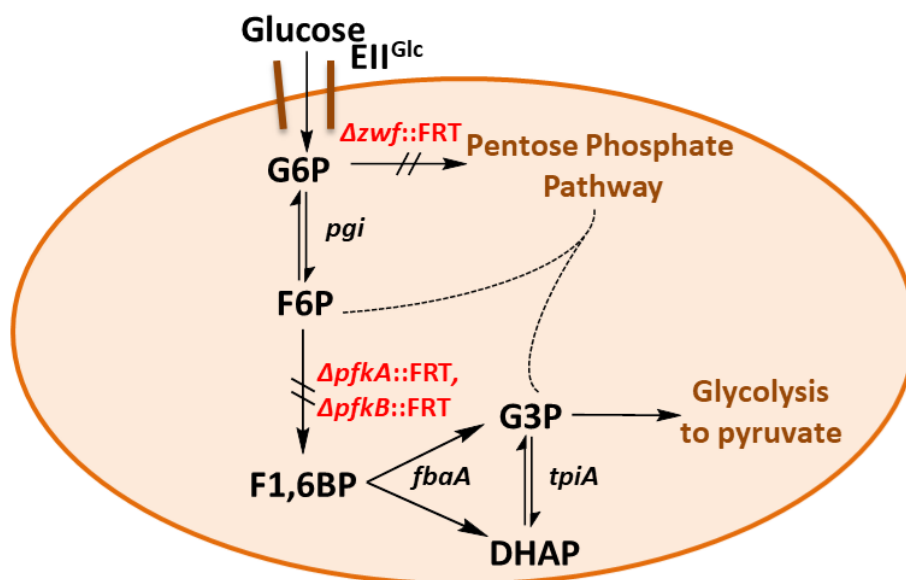
Figure 5-1. Schematic of the impaired glucose depletion pathway in GL3, a triple deletion strain. Relevant enzyme activities are encoded by the genes *fbaA* (fructose 1,6-bisphosphate aldolase A), *pfkA* (phosphofructokinase A), *pfkB* (phosphofructokinase B), *pgi* (phosphoglucose isomerase), *tpiA* (triosephosphate isomerase), *zwf* (glucose 6-phosphate dehydrogenase). EII^{Glc} (glucose-specific enzyme II of the PEP-dependent sugar:phosphotransferase system, PTS), FRT (FLP recognition site). Figure taken from Guitart Font and Sprenger (2020).

To understand how the deletions of *zwf*, *pfkB* and *pfkA* influence the growth behaviour of GL3 in comparison with LJ110, their growth was compared on several solid media (LB-agar, MM-agar, MacConkey-agar) with different single sugars and sugar alcohols as described in Chapter 4.5.3. The C-sources chosen for the characterisation of GL3 enter glycolysis above or below F6P. Results are displayed in Table 5-5 and Table 5-6 (Chapter 5.1.14). LJ110 grew well on all C-sources. However, no colony was formed by GL3 on MM-agar with the PTS substrates D-glucose, mannitol, or glucitol, nor with D-xylose, maltose, D-galactose, or lactose. D-fructose allowed GL3 to grow on MM-agar, but the colonies were smaller (diameter of ≤ 1 mm) and needed 2 days at 37°C to be visible with the naked eye. Therefore, the three missing activities in GL3 (G6P DH, PfkA and PfkB) led to impaired growth on sugars that enter glycolysis at the level of or above F6P (Guitart Font and Sprenger, 2020). GL3 also showed slower growth on D-gluconate, L-arabinose, and the gluconeogenic substrates glycerol, D- or L-lactate, and succinate. This might be a consequence of intracellular accumulation of sugar phosphates or of regulatory deficiencies (Guitart Font and Sprenger, 2020). Results on MacConkey-agar in the presence of the different sugars corroborated the results obtained on MM-agar (see Table 5-6).

Growth experiments were also performed in liquid MM (shake flasks) with D-fructose and D-glucose (for details see Chapter 4.5.2). As observed in Figure 5-2, LJ110 grew on both fructose and glucose as sole C-sources with similar growth rates (0.55 ± 0.04 h^{-1} and 0.59 ± 0.01 h^{-1}). In contrast, GL3 only showed growth on fructose with a reduced growth rate of 0.26 ± 0.01 h^{-1}, and did not grow on glucose, even after a prolonged time of incubation of 96 h (Guitart Font and Sprenger, 2020). It might be possible that GL3 did not grow on glucose because of the accumulation of sugar phosphates (see Figure 5-3), which is known to stress the cells (see Chapter 2.2.2). Thus, the intracellular concentrations of G6P and F6P in LJ110 and in GL3 were determined (see Chapter 4.8.5 for details on the method). In LJ110, both (G6P and F6P) intracellular concentrations were below the detection level (≤ 0.2 mM). However, GL3 accumulated 1.6 ± 0.6 mM G6P and 1.1 ± 0.4 mM F6P intracellularly, even though it did not grow on glucose after the 2 h incubation on MM containing glucose (see Figure 5-4). At each biological replicate of GL3, the intracellular G6P concentration was higher than F6P. In both biological replicates, the concentration of intracellular G6P was always 1.4-times higher than the intracellular concentration of F6P. These results are proof that the incapability of GL3 to degrade the sugar phosphates G6P and F6P through glycolysis (lack of phosphofructokinases) or the pentose phosphate pathway (missing G6P DH) leads to the impaired growth of GL3 on glucose (Guitart Font and Sprenger, 2020).

(a)
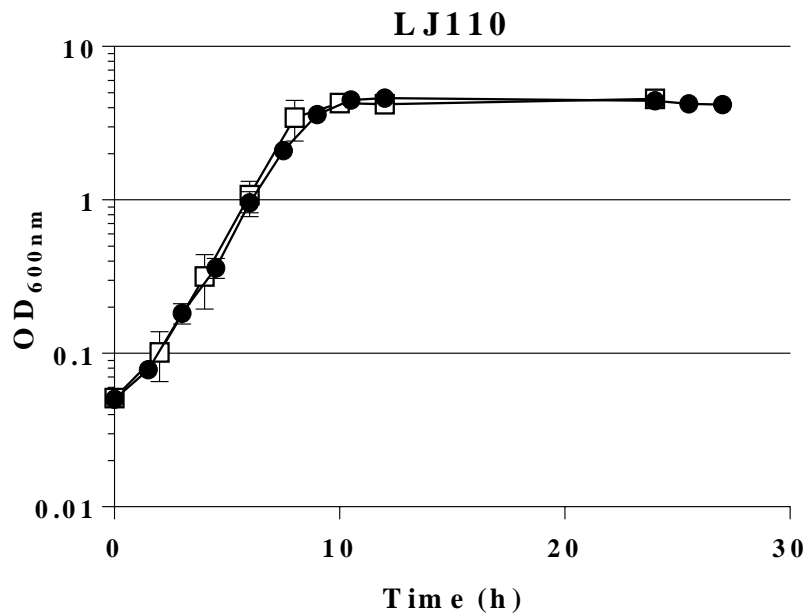
(b)
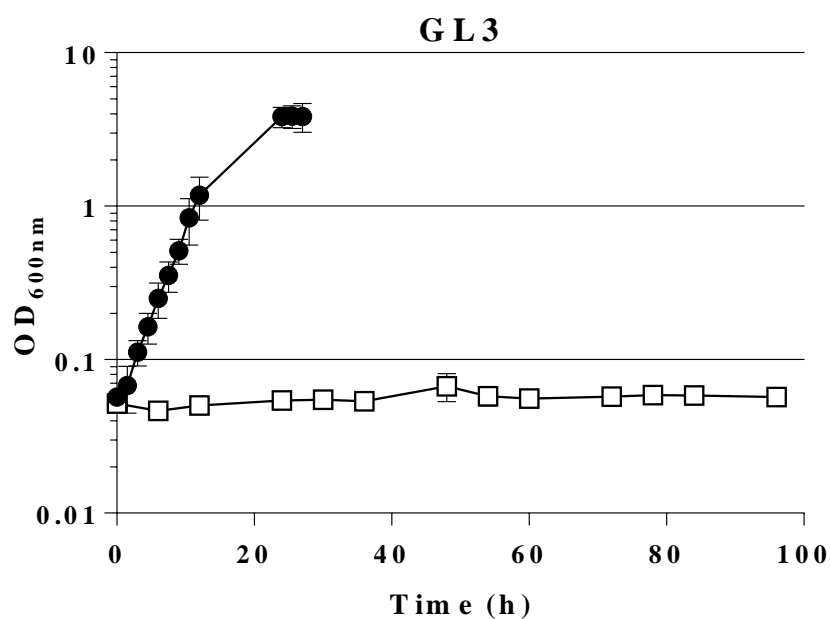
Figure 5-2. Growth behaviour of LJ110 (a) and GL3 (b) on MM with fructose and 100 μM IPTG (●) and on MM with glucose and 100 μM IPTG (□). At 37 °C and 200 rpm. Average values of two independent biological replicates. Inoculation of both strains took place from MM fructose with 100 μM IPTG overnight cultures. Note that the time axis is different for the two graphs. For details see Chapter 4.5.2. Figure taken from Guitart Font and Sprenger (2020).
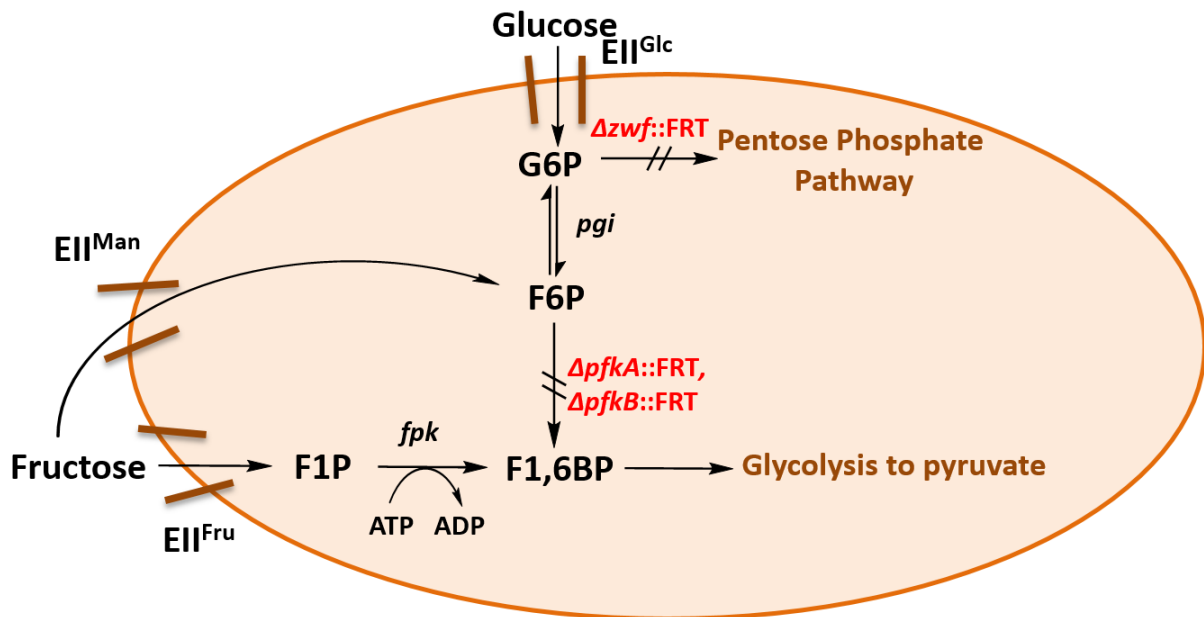
Figure 5-3. Schematic of the possible metabolic pathways of GL3 for glucose and fructose. Relevant enzyme activities are encoded by the genes *fsaA* (fructose 6-phosphate aldolase), *fpk* (fructose 1-phosphate kinase), *pfkA* (phosphofructokinase A), *pfkB* (phosphofructokinase B), *pgi* (phosphoglucose isomerase), *zwf* (glucose 6-phosphate dehydrogenase). EII^{Glc} (glucose-specific enzyme II of the PTS), EII^{Fru} (fructose-specific enzyme II of the PTS), EII^{Man} (mannose-specific enzyme II of the PTS), FRT (FLP recognition site).
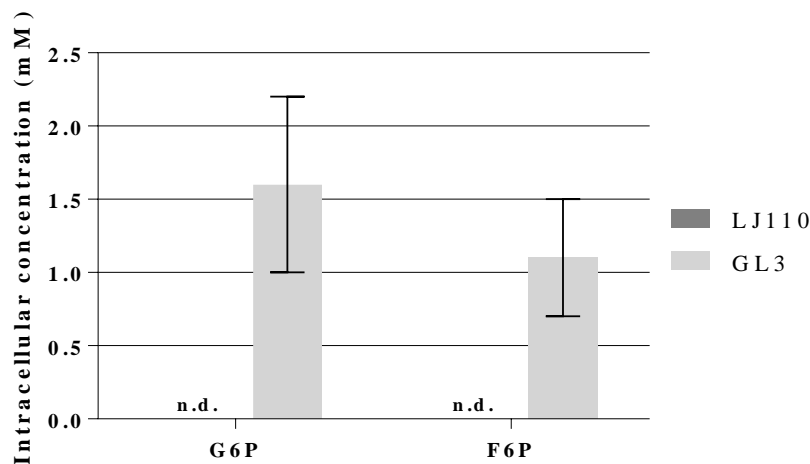
Figure 5-4. Intracellular concentrations of G6P and F6P in LJ110 and GL3 after 2 h incubation on MM with glucose. Average of two biological replicates, each with three technical replicates. n.d. = not detected (≤ 0.2 mM).

It was hypothesised that prolonged incubation of GL3 on MM-agar with glucose as sole C-source might yield mutants that would suppress the glucose-negative phenotype by activating the native chromosomal genes *fsaA* and/or *fsaB*. The product of these genes, the enzymes FSAA wt and FSAB, can both cleave of F6P to DHA and G3P (Schürmann and Sprenger, 2001; Sánchez-Moreno et al., 2012b). Nevertheless, no growth was observed after 3 weeks'

83

incubation (Guitart Font and Sprenger, 2020). The expression of the plasmid-borne *pfkA* gene (pJNTN-m-L-*pfkA*) in GL3 could however complement the growth defect on glucose (data not shown).

5.1.2 GL3 growth restoration on glucose by expression of a mutant gene of fructose 6-phosphate aldolase (*fsaA*^{A129S})

The plasmid-based expression of the *E. coli fsaA* gene or its mutant gene *fsaA*^{A129S} might open a bypass for glucose degradation at the F6P metabolic block in GL3, which would enable GL3 to grow on glucose as sole C-source. For this reason, GL3 was transformed with pJF119*fsaA* or pJF119*fsaA*^{A129S}; the empty plasmid pJF119EH was used as a control (see Table 4-7 for plasmid details). The growth behaviour of GL3/pJF119*fsaA* and GL3/pJF119*fsaA*^{A129S} was examined as described in Chapter 4.5.2.
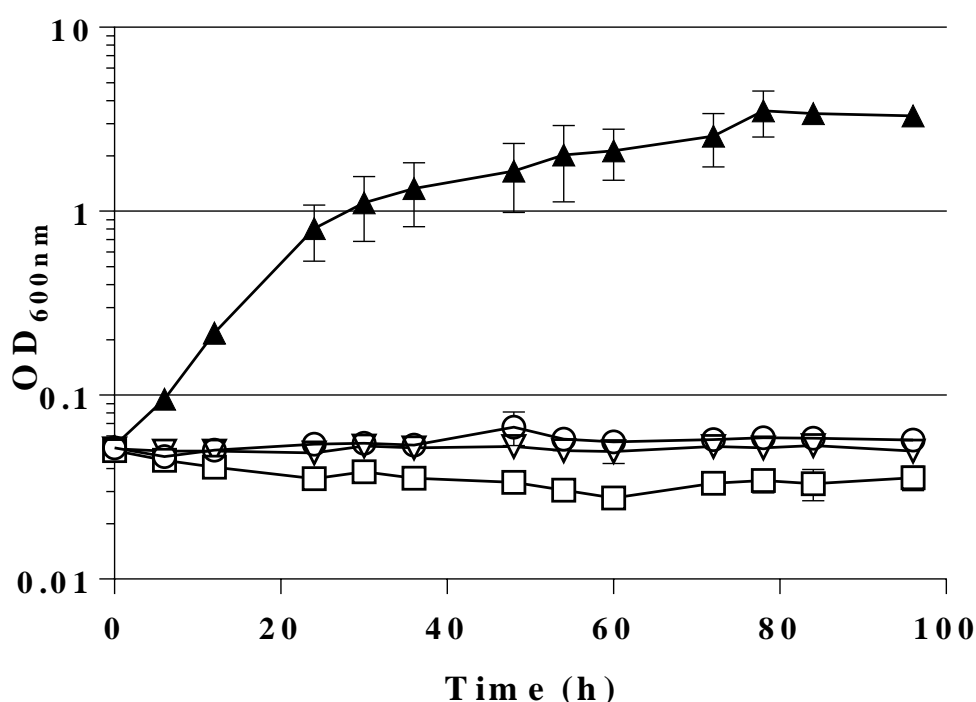
Figure 5-5. Growth behaviour of GL3 (○), GL3/pJF119EH (▽), GL3/pJF119*fsaA* (□), and GL3/pJF119*fsaA*^{A129S} (▲) on MM with glucose, 100 μM IPTG and, if necessary, 100 μg/mL Amp. At 37 °C and 200 rpm. Average values of two independent biological replicates. For comparison, data for GL3 are taken from Figure 5-2. Inoculation of all strains took place from MM fructose with 100 μM IPTG overnight cultures. For details see Chapter 4.5.2. Guitart Font and Sprenger (2020).

As observed in Figure 5-5, no growth could be detected when GL3 was carrying pJF119*fsaA* despite 96 h incubation. However, *fsaA* was expressed and the protein was active in the

preculture with a specific activity of 0.7 U/mg (MM with 28 mM fructose and 100 μM IPTG; Figure 5-6). On the contrary, *fsaA*^{A129S} expression restored growth on glucose without a noticeable lag-phase, with a growth rate of 0.12 ± 0.01 h^{-1} and a doubling time of 359 ± 52 min (Guitart Font and Sprenger, 2020). The growth of GL3/pJF119*fsaA*^{A129S} on glucose could be explained through the expression of *fsaA*^{A129S} and the activity of the protein coded by this gene. The following methods were used to verify this affirmation: retro-aldol specific activity of heat-treated enriched fractions (HT; FSAA is thermostable; see Method Chapter 4.7.7); presence of the protein confirmed by SDS-PAGE (see Chapter 4.7.6); and appearance of DHA in the supernatant using the HPLC (see Chapter 4.8.1). No specific FSA activity could be detected on LJ110 HT, while on GL3/pJF119*fsaA*^{A129S} HT a specific FSA activity of 4.9 ± 1.7 U/mg was measured. On the SDS-PAGE gel (see Figure 5-21) a prominent band just below 28 kDa could be observed in GL3/pJF119*fsaA*^{A129S} HT, but none in LJ110 HT.
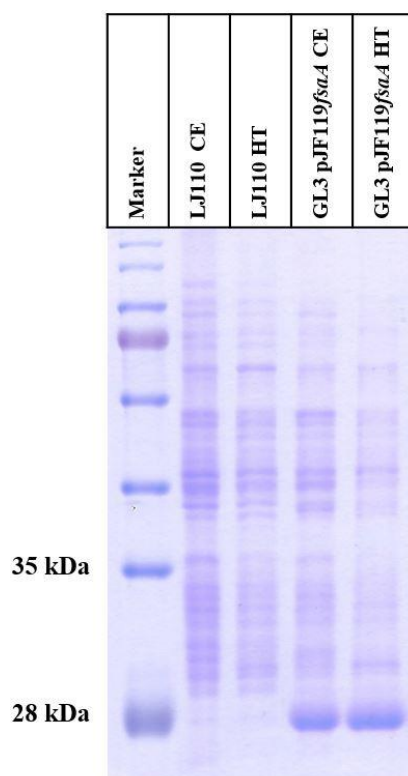
Figure 5-6. SDS-PAGE of cell-free extracts (CE) and heat-treated enriched fractions (HT) of LJ110 and GL3/pJF119*fsaA*. After overnight growth on MM with 28 mM fructose and 100 μM IPTG. The band at 24 kDa corresponds to FSAA wt. Note that to enable the separation of protein bands around 28 kDa, the SDS-PAGE was stopped after the lower bands of the protein marker had already left the SDS-gel on purpose. 5 μg protein were analysed per sample. Figure taken from Guitart Font and Sprenger, 2020.

To study why FSAA A129S, but not FSAA wt, allowed GL3 to grow on glucose as sole C-source, enzyme affinities for F6P were compared. Purified His-tagged FSAA A129S had an 8-fold higher V_{max} compared to purified His-tagged FSAA wt and the K_{M} value was about half the one for FSAA wt. Furthermore, the catalytic efficiency of FSAA A129S for F6P is 16-fold

85

higher than the catalytic efficiency measured for FSAA wt ($k_{cat}/K_M = 31$ s^{-1} mM^{-1} vs. 2 s^{-1} mM^{-1}; see Figure 5-7). This is in accordance with prior reported results by Castillo et al. (2010).

GL3 bearing pJF119$fsaA^{A129S}$ could be selected directly after transformation, either with the help of Amp or by growth on media with glucose. The transformation efficiency (colony forming units per µg DNA) on a MM-agar plate with 28 mM glucose and 100 µM IPTG was approximately the same as on LB-agar with 100 µg/mL Amp (Guitart Font and Sprenger, 2020).

GL3 was also able to grow on glucose as sole C-source after IPTG induction when carrying either pJF119$talB^{F178Y}$ (for details on TalB F178Y see Chapter 2.4.1) or pJF119xfp (for growth details see Table 5-4). xfp codes for X5P/F6P phosphoketolase, this enzyme uses inorganic phosphate to cleave F6P to acetyl phosphate, water and E4P (Suzuki et al., 2010).
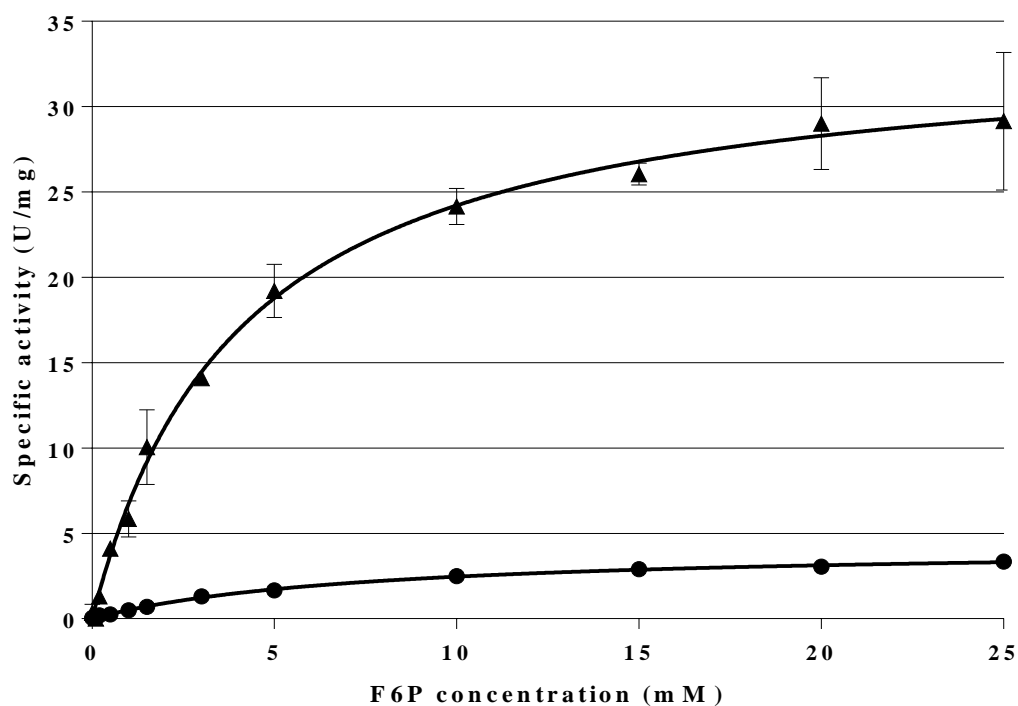
Figure 5-7. Dependence of initial specific activity (U/mg) of retro-aldol reaction of purified His-tagged FSAA wt and FSAA A129S on F6P concentration. FSAA wt (●) $K_M = 7.4 \pm 0.6$, $V_{max} = 4.3 \pm 0.1$, $k_{cat} = 17$ s^{-1}; $k_{cat}/K_M = 2$ s^{-1} mM^{-1}; FSAA A129S (▲) $K_M = 4.1 \pm 0.4$, $V_{max} = 34.0 \pm 1.1$, $k_{cat} = 129$ s^{-1}; $k_{cat}/K_M = 31$ s^{-1} mM^{-1}. K_M and V_{max} values were determined with the software "GraphPad Prism" version 6.01 from GraphPad Software, Inc. (San Diego, USA). k_{cat} values were calculated with the equation $k_{cat} = (V_{max}/V_{max\ F6P}) \times k_{cat\ F6P}$.

5.1.3 Temporary formation of DHA from glucose

To gather more evidence about the growth restoration on glucose of GL3/pJF119*fsaA*[*A129S*] due to the bypass reaction catalysed by FSAA A129S at the level of F6P (see Figure 5-9), the appearance of DHA in the supernatant was monitored by HPLC (see Chapter 4.8.1 for measurement details). As already explained in the Introduction Chapter 2.4, FSAA A129S catalyses the cleavage of 1 mole F6P to 1 mole DHA and 1 mole G3P. In *E. coli* G3P can be directly metabolised in glycolysis or enter the PPP via transketolase (see Chapter 2.2). On one hand DHA could be phosphorylated in *E. coli* by DHAKLM (Erni et al., 2006). On the other hand, it might also be excreted to the medium (Subedi et al., 2008). As can be seen from Figure 5-8, while the concentration of glucose in the medium rapidly decreased, the concentration of DHA increased steadily during the first 60 h incubation reaching a maximal concentration of 12 ± 4 mM. Afterwards, the DHA concentration in the medium also decreased until it could no longer be detected (Guitart Font and Sprenger, 2020).
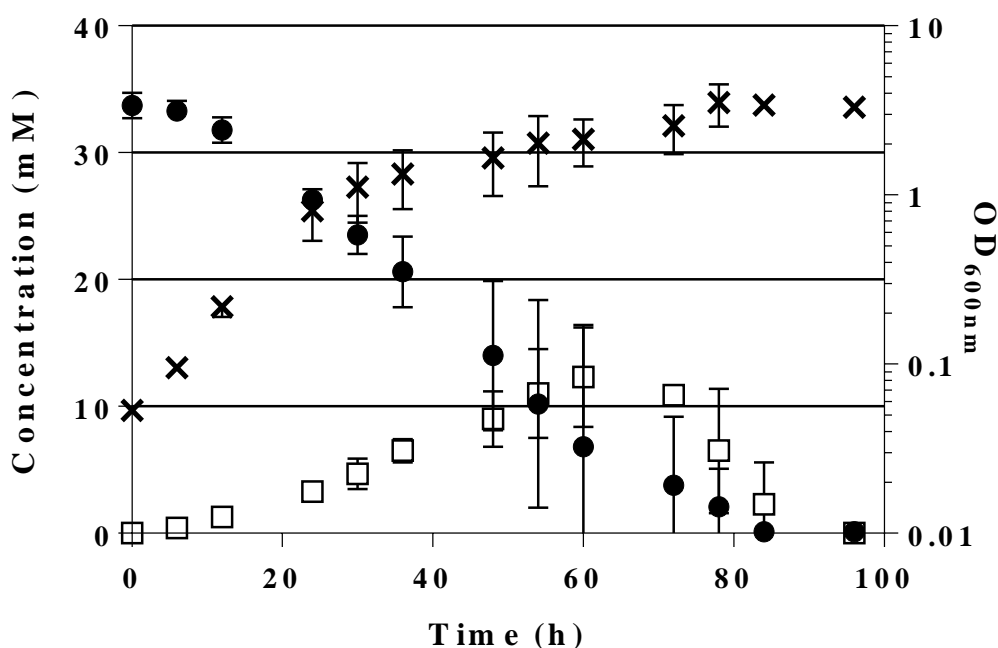
Figure 5-8. Progress over time of the concentrations of glucose (●) and DHA (□) in the culture supernatant of GL3/pJF119*fsaA*[*A129S*] during growth on MM glucose, 100 μM IPTG and 100 μg/mL Amp. At 37 °C and 200 rpm. OD$_{600\,nm}$ (✖). The glucose and DHA concentrations were determined by HPLC. Average values of two independent biological replicates and two technical replicates each (Guitart Font and Sprenger, 2020).

From the linear range displayed in Figure 5-8 the decrease of glucose and the increase of DHA over time in the medium can be estimated. Between 36 h and 60 h incubation there was a decrease of 0.58 mM/h glucose and an increase of 0.24 mM/h DHA. At 60 h incubation the

culture reached an $OD_{600\,nm}$ of 2.132. If it is assumed that the CDW of GL3/pJF119$fsaA^{A129S}$ is the same as GL3 (see Appendix Figure 9-4), then at an $OD_{600\,nm}$ value of 2.132 the CDW would correspond to 3.3 mg. Neidhardt et al. (1990) reported that in *E. coli* 55 % of the CDW is protein. Therefore, there would be 1.8 mg protein present in GL3/pJF119$fsaA^{A129S}$ after 60 h incubation. The percentage of FSAA A129S in a SDS-PAGE with GL3/pJF119$fsaA^{A129S}$ heat-treated enriched fraction (see Figure 5-21) was around 90 %. It was expected that a reduced percentage of FSAA A129S would be present in the cell-free extracts. Thus, it was assumed that FSAA A129S in cell-free extracts could be present between 1-90%. These correspond to 0.2-1.6 mg FSAA A129S. The main culture had 50 mL MM. Therefore, in this volume there would be an increase of DHA of 0.2 µmol/min. FSAA A129S catalyses the cleavage of 1 mole F6P to 1 mole DHA. As a result, a specific FSA activity between 0.1 and 1.1 U/mg was required in GL3/pJF119$fsaA^{A129S}$ to produce this amount of DHA from glucose.

The colour of the culture could also be an indicator of the presence of DHA (see Appendix Chapter 9.3). The complete disappearance of DHA in the medium after 96 h incubation might be explained by its uptake and further metabolism by the PEP-dependent DHAKLM system in the cells (encoded in the *dha* operon; Erni et al., 2006; Guitart Font and Sprenger, 2020). Furthermore, the presence of DHA is known to induce the expression of the *dha* operon (Bächler et al., 2005). The transient appearance of DHA in the medium is additional proof of the functionality of FSAA A129S in the bypass reaction that restores growth of GL3 on glucose (Guitart Font and Sprenger, 2020).

5.1.4   One copy of $fsaA^{A129S}$ in the chromosome is sufficient to restore growth of the triple mutant strain on glucose

Because the overexpression of the $fsaA^{A129S}$ gene from a multicopy plasmid suppressed the glucose-negative phenotype of GL3 (see Chapter 5.1.3), further studies were needed to elucidate how many copies of this gene would be sufficient to allow GL3 to grow on glucose. Therefore, the $fsaA^{A129S}$ gene under the control of the P$_{tac}$ was introduced in the *lac*-operon of GL3 as described in Chapter 4.6.14, generating GL4 (see Figure 5-9). As reported in Table 4-8 (strain details), GL4 contains only one copy of $fsaA^{A129S}$ in the chromosome.

As observed in Figure 5-10, one copy of the $fsaA^{A129S}$ gene was enough to restore growth of GL4 on glucose. Growth of GL4 was compared to growth of GL3/pJF119$fsaA^{A129S}$, where multiple copies of the $fsaA^{A129S}$ gene are available. GL3/pJF119$fsaA^{A129S}$ grew more than two times faster than GL4 on MM with glucose and 100 µM IPTG (0.12 ± 0.01 h^{-1} against 0.05 ± 0.00 h^{-1}, respectively). Only traces of DHA could be detected in the supernatant of GL4

(0.5 ± 0.0 mM after 30 h of incubation; see Table 5-3 in Chapter 5.1.12). The difference on the number of copies of the *fsaA^{A129S}* gene present in the cell (plasmid-borne or chromosomally) not only influenced the growth rate of these strains, but also the specific FSA activity of their heat-treated enriched fractions (HT). In these extracts GL3/pJF119*fsaA^{A129S}* showed a specific FSA activity of up to 5.0 U/mg and GL4 only 0.1 U/mg (see Chapter 5.1.10; Guitart Font and Sprenger, 2020).
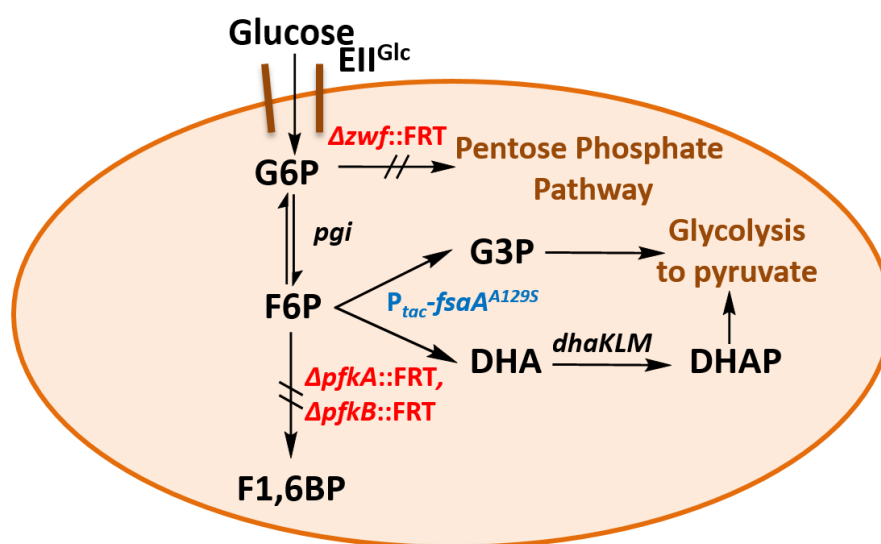
Figure 5-9. Schematic of the glucose bypass metabolism in GL3/pJF119*fsaA*^{A129S} and GL4 (Guitart Font and Sprenger, 2020). Genes: *dhaKLM* (dihydroxyacetone kinase), *fsaA*^{A129S} (fructose 6-phosphate aldolase), *pfkA* (phosphofructokinase A), *pfkB* (phosphofructokinase B), *pgi* (phosphoglucose isomerase), *zwf* (glucose 6-phosphate dehydrogenase). DHA (dihydroxyacetone), DHAP (dihydroxyacetone phosphate), F1,6BP (fructose 1,6-bisphosphate), F6P (fructose 6-phosphate), G3P (glyceraldehyde 3-phosphate), G6P (glucose 6-phosphate). EII^{Glc} (glucose-specific enzyme II of the PTS), FRT (FLP recognition site). P_{tac} (*tac* promoter).

It was assumed that the expression levels of certain genes in GL4 could give insight on how glucose is consumed and DHA metabolised in this strain. This knowledge might help improve the DHA formation from glucose on further strains. Thus, transcript levels of selected genes (see Method Chapter 4.6.4 for information regarding the choice of genes) were measured in GL4 by using qPCR (see Chapter 4.6.4 for more details) and compared to the expression levels in LJ110 (see Figure 5-11; Guitart Font and Sprenger, 2020). It was confirmed that GL4 does not express the genes that code for phosphofructokinase (*pfkA*, *pfkB*) and glucose 6-phosphate dehydrogenase activities (*zwf*), as these genes were deleted in GL4. Equally important, GL4 expressed *dhaK* in a higher amount than *glpK* and showed expression of *sgrS*. The expression of *ptsG* detected for LJ110 was nearly four times higher than for GL4. *fsaA* was strongly expressed in GL4, but only minute levels were measured in LJ110. It should be noted that it could not be distinguished between the transcript from the native *fsaA* gene and the mutant allele *fsaA^{A129S}* inserted in the *lac*-operon. No expression of *fsaB* was detected in GL4 or LJ110.

Because of IPTG presence in the medium, LJ110 expressed *lacZ*. However, the expression of *lacZ* was not detected in GL4 because of the integration of P*tac*-*fsaA*^A129S in the *lac*-operon. These results suggest a correlation between the transcript levels of *fsaA* and *dhaK* in GL4. Both genes showed a significantly increase in their expression rate in GL4 compared to LJ110. No differences were observed in the expression levels of the genes for glycerol metabolism, *gldA* and *glpK*. This indicates that DHA is further metabolised in GL4 through its phosphorylation to DHAP by the PEP-dependent DHAKLM and not through its reduction to glycerol by the action of GldA (Guitart Font and Sprenger, 2020).
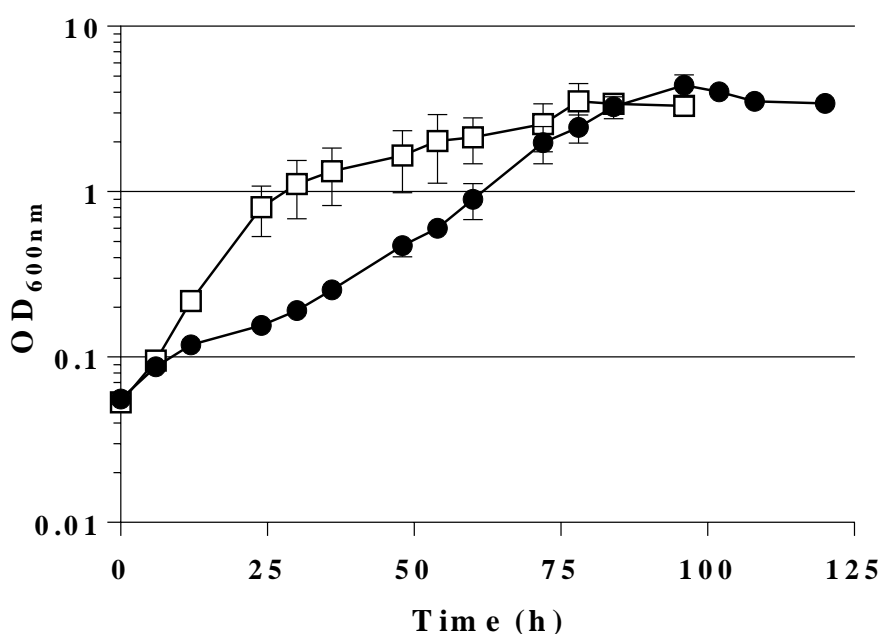
Figure 5-10. Growth behaviour of GL3/pJF119*fsaA*^A129S **(□) in comparison with GL4 (●) on MM with glucose, 100 μM IPTG and, if necessary, 100 μg/mL Amp. At 37 °C and 200 rpm. Average values of two independent biological replicates. For comparison, data for GL3/pJF119***fsaA*^A129S **are taken from Figure 5-5. Inoculation of both strains took place from MM fructose with 100 μM IPTG overnight cultures. For details see Chapter 4.5.2. Figure taken from Guitart Font and Sprenger (2020).**
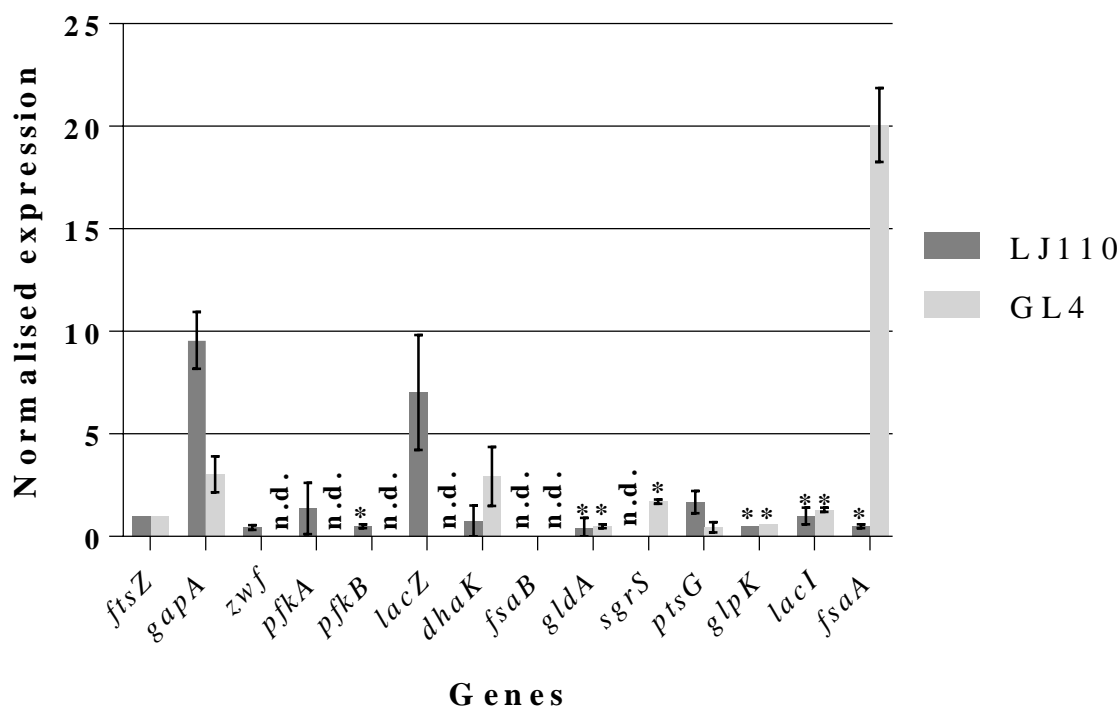
Figure 5-11. qPCR results of RNA samples harvested during the exponential phase of LJ110 and GL4 when grown on MM with glucose and 100 μM IPTG. Average values of two independent biological replicates, each with three technical replicates. *ftsZ* was used as a calibrator. n.d. = not detected; * denotes values multiplied by 10 for better visibility.

5.1.5   DHA production from glucose in *E. coli*

With GL4, a plasmid-free system was established in *E. coli* where 1 mole of glucose could be converted to 1 mole of DHA due to the cleavage of the glycolytic intermediate F6P by FSAA A129S. Yet, this strain was not able to accumulate DHA in the medium (see data from Chapter 5.1.4). It was hypothesised that the formation of glycerol from glucose could be possible via DHA (Guitart Font and Sprenger, 2020). But first, enough DHA should accumulate. Thus, the chromosomal copy of *dhaKLM* was deleted in GL3 and GL4, creating the strains GL35 and GL5, respectively (see Table 4-8 and Chapter 4.6.13 for strain construction details). It was expected that the missing DHA kinase activity would enhance DHA accumulation in GL5 and in GL35/pJF119*fsaA^{A129S}* (see Figure 5-12).

GL5 showed a decreased growth rate on glucose in comparison to its parent GL4 and, as GL4, this mutant strain produced DHA transiently. The maximal measured DHA concentration in the GL5 culture was 6-times higher than in the GL4 culture (see Table 5-3, page 113). The deletion of the *dhaKLM* genes might have helped GL5 accumulate more DHA in the medium for a

period of time, but it could not prevent the eventual consumption of DHA (Guitart Font and Sprenger, 2020).

A
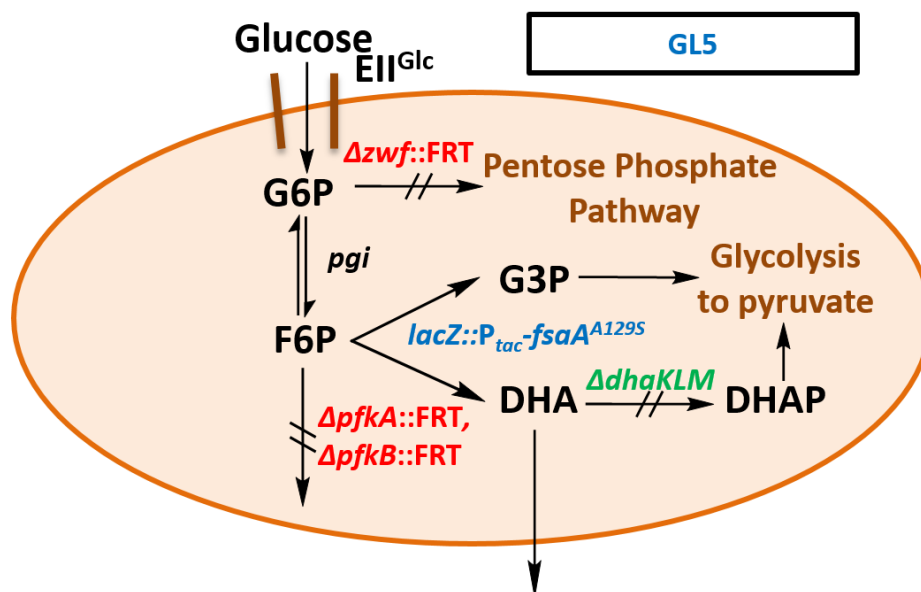
B
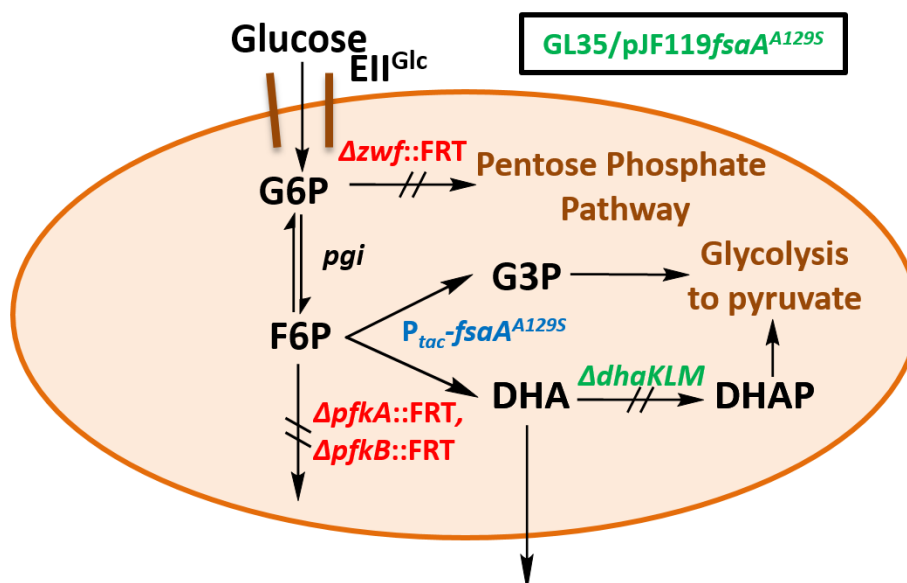
Figure 5-12. Schematic of the possible pathway to produce DHA from glucose and accumulate it. A. GL5; B. GL35/pJF119*fsaA^{A129S}*. Genes: *dhaKLM* **(dihydroxyacetone kinase),** *fsaA^{A129S}* **(fructose 6-phosphate aldolase),** *lacZ* **(β-galactosidase),** *pfkA* **(phosphofructokinase A),** *pfkB* **(phosphofructokinase B),** *pgi* **(phosphoglucose isomerase),** *zwf* **(glucose 6-phosphate dehydrogenase). DHA (dihydroxyacetone), DHAP (dihydroxyacetone phosphate), F1,6BP (fructose 1,6-bisphosphate), F6P (fructose 6-phosphate), G3P (glyceraldehyde 3-phosphate), G6P (glucose 6-phosphate). EII^{Glc} (glucose-specific enzyme II of the PTS), FRT (FLP recognition site). P_{tac} (*tac* promoter).**

Like its parent strain (GL3), GL35 was only able to grow on glucose as sole C-source when the plasmid-borne $fsaA^{A129S}$ gene was expressed (see Table 5-3 and Table 5-4 in Chapter 5.1.12). GL35/pJF119$fsaA^{A129S}$ excreted more DHA in the medium (maximal measured DHA concentrations: 5.9 ± 2.1 mM against 3.1 ± 0.3 mM by GL5). Furthermore, a 3-fold higher specific FSA activity than GL5 (0.26 ± 0.11 U/mg and 0.08 ± 0.02 U/mg, respectively) was determined for GL35/pJF119$fsaA^{A129S}$. It was assumed that the number of copies of the $fsaA^{A129S}$ gene in the cell could be the bottleneck in GL5. This may explain the difference in DHA concentrations between GL5 and GL35/pJF119$fsaA^{A129S}$. To confirm this assumption, GL5 was transformed with pJF119$fsaA^{A129S}$ to increase the number of copies of the $fsaA^{A129S}$ gene in the cell. The growth of GL5/pJF119$fsaA^{A129S}$ on glucose as sole C-source was then compared to the growth of GL5 (see Figure 5-13).
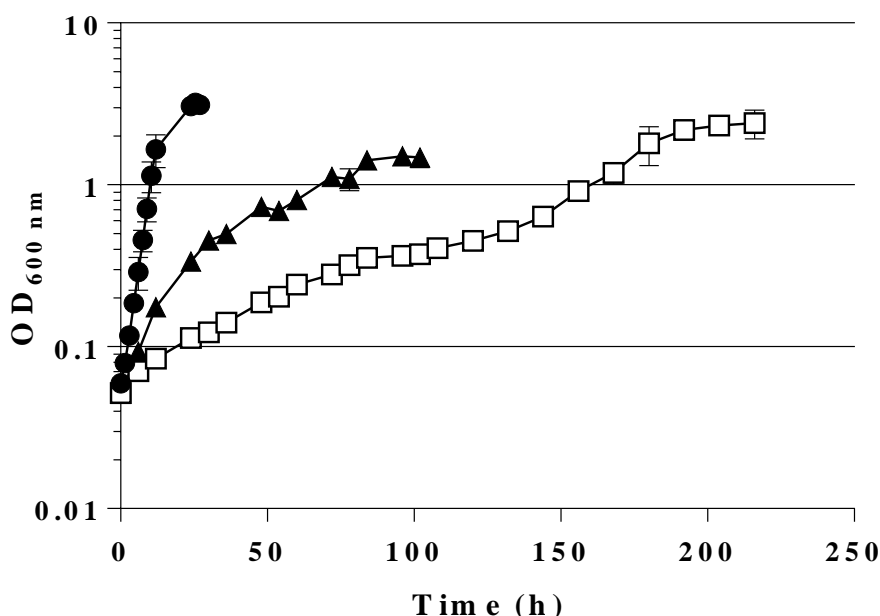
Figure 5-13. Growth behaviour of: GL5 (●) on MM with fructose and 100 μM IPTG; GL5 (□) and GL5/pJF119$fsaA^{A129S}$ (▲) on MM with glucose, 100 μM IPTG and, if necessary, 100 μg/mL ampicillin. At 37 °C and 200 rpm. Average of two independent biological replicates. Inoculation of all strains took place from MM fructose with 100 μM IPTG overnight cultures. For details see Method Chapter 4.5.2.

During growth on glucose, GL5 and GL5/pJF119$fsaA^{A129S}$ presented the characteristics of diauxic growth. GL5/pJF119$fsaA^{A129S}$ reached the maximal $OD_{600\,nm}$ after 96 h incubation, approximately half the time needed by GL5 (for more details see Table 5-3 and Table 5-4 in Chapter 5.1.12). GL5/pJF119$fsaA^{A129S}$ produced more DHA than GL5 over time, with a maximal concentration on the medium of 4.2 ± 0.7 mM. At the end of the incubation, DHA could only be detected in the supernatant of GL5/pJF119$fsaA^{A129S}$ with an end concentration of

3.5 ± 0.3 mM, whereas no DHA was detected in GL5. In GL5/pJF119$fsaA^{A129S}$ heat-treated enriched fractions (HT), a specific FSA activity up to 0.45 U/mg was measured, which was more than 5-fold higher than the one determined in GL5 HT and 11-fold lower than the specific FSA activity in GL3/pJF119$fsaA^{A129S}$.

As a result of the inability of GL5 to build up DHA (at the end of incubation the DHA concentration was below detection level, see Table 5-3), further enzymes that would favour DHA consumption in the cell were examined. Two candidates were the inherent *gldA* and *glpK* genes. The *gldA* gene codes for the glycerol dehydrogenase. This enzyme can reduce DHA to glycerol (Tang et al., 1979). Glycerol can then be phosphorylated by glycerol kinase (encoded by *glpK*) to glycerol 3-phosphate, which in turn can be used for glycolysis in the form of DHAP (Koch et al., 1964). Therefore, it was expected that a considerable increase in DHA concentration, and the formation and possible accumulation of glycerol in the medium could be feasible by deleting the *glpK* gene from the GL5 chromosome (Guitart Font and Sprenger, 2020).

5.1.6 A novel glycerol production pathway from glucose in *E. coli*

After successfully constructing GL6 (Δzwf::FRT $\Delta pfkB$::FRT $\Delta pfkA$::FRT $\Delta dhaKLM$ $\Delta lacZ$::P$_{tac}$-$fsaA^{A129S}$ $\Delta glpK$; see Chapter 4.6.13 for strain construction details), growth of GL6 on glucose as sole C-source was studied. GL6 needed 288 h to reach its maximal OD$_{600\,nm}$. Its growth rate with 0.03 ± 0.01 h^{-1} was also relatively low, but in comparison with GL5, DHA accumulated in the medium over time, reaching a maximal concentration of 8.8 ± 0.3 mM from 30.2 mM glucose. In the supernatant of GL6, the new product glycerol was detected with a maximal concentration of 1.9 ± 0.2 mM. Specific GldA activity was below detection level in the cell-free extracts (CE) of GL6 (see Table 5-2 in Chapter 5.1.10). GL6 HT exhibited a specific FSA activity of 0.12 ± 0.00 U/mg, 1.5-fold increase in activity compared to GL5 HT. With the deletion of the *glpK* gene, GL6 was unable to consume the DHA and glycerol that accumulated over time in the medium (see Appendix Figure 9-7).

The detection of glycerol in the supernatant of GL6 opened the possibility to produce glycerol from glucose via DHA in a 1:1 molar ratio. For this purpose, *gldA* under the control of P$_{tac}$ was chromosomally inserted in the ribose-operon of GL6 forming GL7 (see Table 4-8 for strain details and Chapter 4.6.13 for strain construction details; Guitart Font and Sprenger, 2020). This insertion should allow the overproduction of GldA in the cell (see Figure 5-14).

GL7 required 48 h less than GL6 to reach its maximal OD$_{600\,nm}$ on MM with glucose and 100 µM IPTG (240 h compared to 288 h). GL7 HT displayed 0.1 U/mg specific FSA activity

as did GL6 HT. GL7 was the first of the GL-strains where specific GldA activity could be detected in the CE (0.4 ± 0.1 U/mg; see Table 5-2). During growth on glucose a maximal DHA concentration of 3.5 ± 0.3 mM was detected in the supernatant of GL7, which indicated a decrease in DHA concentration compared to the supernatant of GL6. However, the concentration of glycerol increased by a factor of 11 to 21.8 ± 0.0 mM. Both products remained in the supernatant until the end of the incubation without a significant decrease in their maximal concentrations (see Appendix Figure 9-7; Guitart Font and Sprenger, 2020).
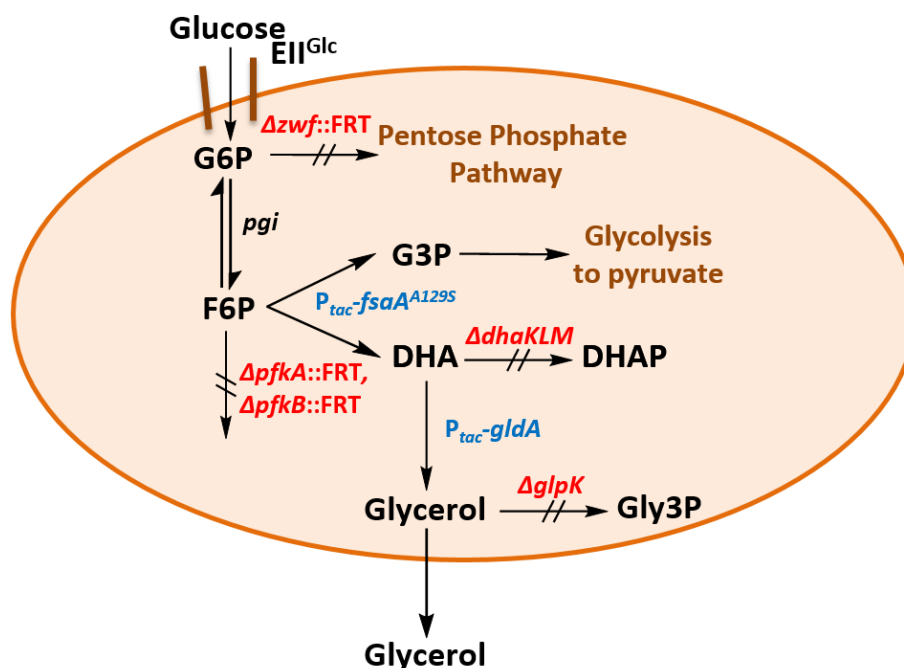
Figure 5-14. Schematic of the novel biosynthetic pathway from glucose to DHA and glycerol in GL7. Genes: *dhaKLM* (dihydroxyacetone kinase), *fsaA^{A129S}* (fructose 6-phosphate aldolase), *gldA* (glycerol dehydrogenase), *glpK* (glycerol kinase), *pfkA* (phosphofructokinase A), *pfkB* (phosphofructokinase B), *pgi* (phosphoglucose isomerase), *zwf* (glucose 6-phosphate dehydrogenase). DHA (dihydroxyacetone), DHAP (dihydroxyacetone phosphate), F6P (fructose 6-phosphate), G3P (glyceraldehyde 3-phosphate), G6P (glucose 6-phosphate), Gly3P (glycerol 3-phosphate). EII^{Glc} (glucose-specific enzyme II of the PTS), FRT (FLP recognition site). P_{tac} (*tac* promoter). Guitart Font and Sprenger, 2020.

It was also considered whether GL7 could use other sugars for glycerol production (Guitart Font and Sprenger, 2020). Hence, the hexose galactose and the pentoses xylose and L-arabinose were utilised as sole C-sources with the initial concentrations mentioned in Chapter 4.5.2. On galactose, GL7 needed half the time to reach the maximal $OD_{600\,nm}$ than on glucose (120 h against 240 h). A maximal glycerol concentration of 17.9 ± 1.4 mM was determined during growth on galactose. This is a difference of 4 mM glycerol compared to the maximal concentration reached on glucose. Whereas on xylose and on L-arabinose, GL7 reached its maximal $OD_{600\,nm}$ after only 48 h with a growth rate of 0.12 ± 0.01 h^{-1} with nearly half the

glycerol concentration achieved on glucose (13.3 ± 0.8 mM and 13.9 ± 0.9 mM, respectively). For all obtained data see Table 5-3.

5.1.7   Selection of faster-growing GL-strains

As seen in the data gathered for GL5, GL6 and GL7 during growth on glucose (see Chapter 5.1.5, Chapter 5.1.6 and Table 5-3 page 113), these plasmid-free strains can produce DHA and/or glycerol, but their growth rates are below 0.04 h^{-1} and they need more than 200 h to reach their maximal OD$_{600\ nm}$. Therefore, GL5, GL6 and GL7 were subject to growth rate selection pressure on MM with glucose and 100 µM IPTG with the aim to obtain strains with improved growth rates and, if possible, better DHA and/or glycerol yields. For this purpose, the two approaches described in Method Chapter 4.5.5 were applied (see Figure 5-15). At the end of both selection processes, only the colonies that showed an improved growth rate (for example, due to an increase in colony size) were isolated and characterised. These isolated strains were named GL* or GL', depending on the approach used for their selection.
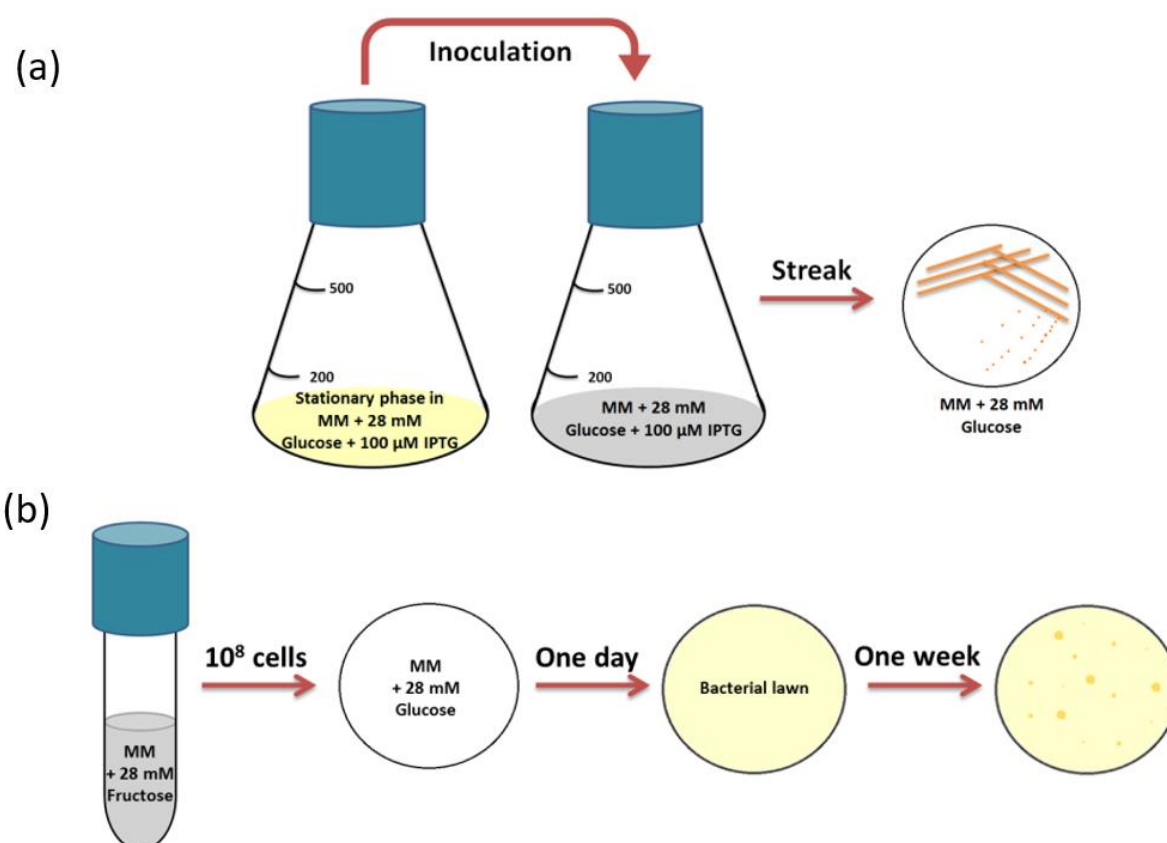
Figure 5-15. Selection approaches of GL evolved strains with better growth on MM with glucose. (a) Selection method for GL* strains; (b) Selection method for GL' strains.

5.1.8   Faster-growing GL-strains for the production of DHA

Next, the growth behaviour of GL5 and the evolved strains GL5* and GL5' on MM with glucose was compared. As observed in Figure 5-16, the strain with the highest growth rate was GL5* with 0.12 ± 0.00 h^{-1}, followed by GL5' with 0.08 ± 0.01 h^{-1}. Both evolved strains, did not only have increased growth rates compared to GL5, but they also reached the maximal OD$_{600\,nm}$ earlier (54 h for GL5* and 78 h for GL5'). They also showed higher DHA concentrations (13.6 ± 0.7 mM and 6.3 ± 0.2 mM) and had higher specific FSA activities (0.81 ± 0.03 U/mg and 0.17 ± 0.04 U/mg). In fact, GL5* had an increased growth rate, DHA concentration and specific FSA activity when compared to GL5/pJF119$fsaA^{A129S}$. For more details see Table 5-1 (page 102), Table 5-3 (page 113) and Table 5-4 (page 114). In both GL5-evolved strains, the produced DHA was consumed over time, a phenomenon which was also observed in GL5 (see Figure 5-17 for the progress of GL5* OD$_{600\,nm}$ and of the concentrations of glucose and DHA over time, the progress for GL5 and GL5' is shown in Appendix Figure 9-6).

GL6 produced 2.8-fold and 1.4-fold more DHA than GL5 and even GL5', respectively, and could accumulate DHA over time.
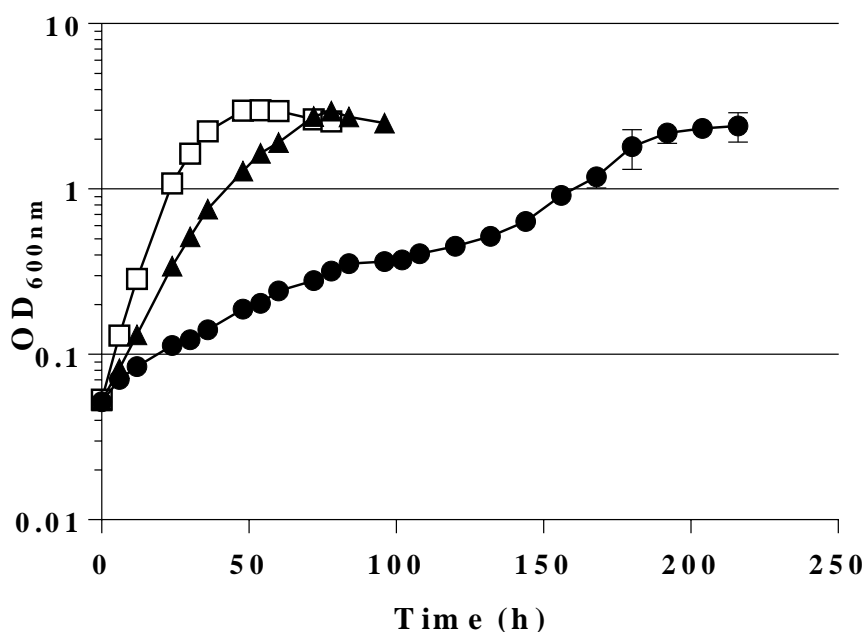
Figure 5-16. Growth behaviour on MM with glucose and 100 µM IPTG of GL5 (●), GL5* (□) and GL5' (▲). At 37 °C and 200 rpm. Monitoring of OD$_{600\,nm}$ took place until the cultures reached the stationary phase. Average of two independent biological replicates. For comparison, data for GL5 are taken from Figure 5-13. Inoculation of all strains took place from MM fructose with 100 µM IPTG overnight cultures. For details see Method Chapter 4.5.2.
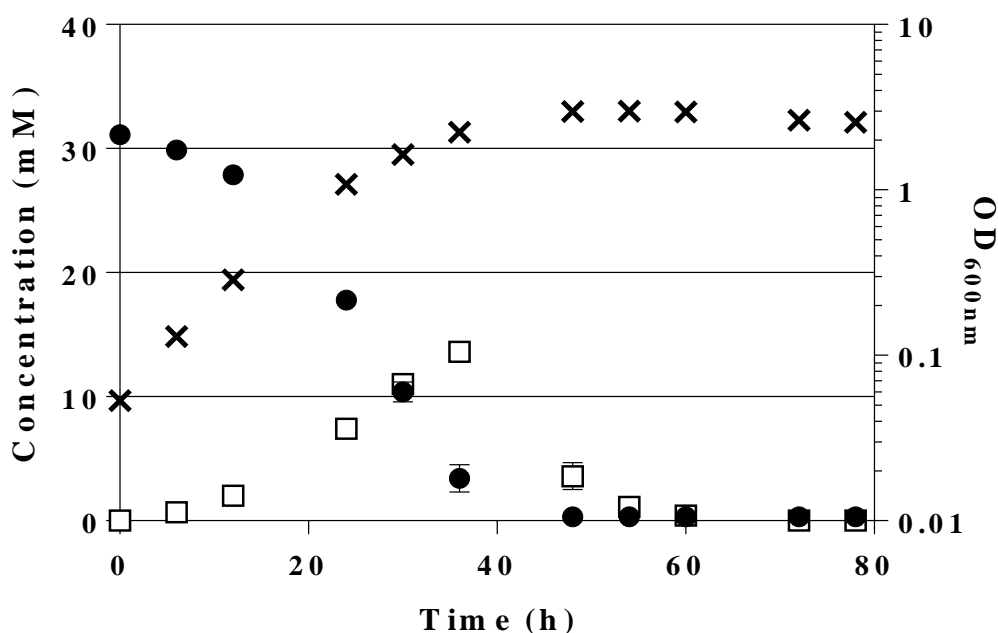
Figure 5-17. Progress over time of the concentrations of glucose (●) and DHA (□) when GL5* grew on MM with glucose and 100 µM IPTG. At 37 °C and 200 rpm. $OD_{600\ nm}$ (✖). Average of two independent biological replicates. Inoculation of all strains took place from MM fructose with 100 µM IPTG overnight cultures.

As mentioned above, one of the drawbacks that GL6 had, was its slow growth on glucose (see Table 5-3). To improve this, faster-growing GL6 strains were isolated (see Figure 5-15), characterised and compared to their parent strain. As shown in Figure 5-18, both GL6* and GL6' had a similar growth rate with $0.10 \pm 0.00\ h^{-1}$ and $0.08 \pm 0.01\ h^{-1}$, respectively, and reached their maximal $OD_{600\ nm}$ in just 84 h, 3-times faster than GL6. Compared to GL6, which showed a diauxic growth, the GL6-evolved strains displayed exponential growth. GL6* and GL6' presented an increase in the accumulation of DHA with $13.3 \pm 0.4\ mM$ and $11.2 \pm 1.4\ mM$, respectively, and yet, a slight decrease in glycerol formation was observed in both strains (maximal measured concentration for GL6* was $1.4 \pm 0.1\ mM$ and $1.5 \pm 0.0\ mM$ for GL6'; see Table 5-3). Like in GL6 cell-free extracts (CE), in GL6* CE and GL6' CE the specific GldA activity (DHA reduction to glycerol) was below detection level, but a slight increase in specific FSA activity was observed in GL6* HT ($0.18 \pm 0.02\ U/mg$) and GL6' HT ($0.16 \pm 0.00\ U/mg$) compared to GL6 HT (see Table 5-1 and Table 5-2).
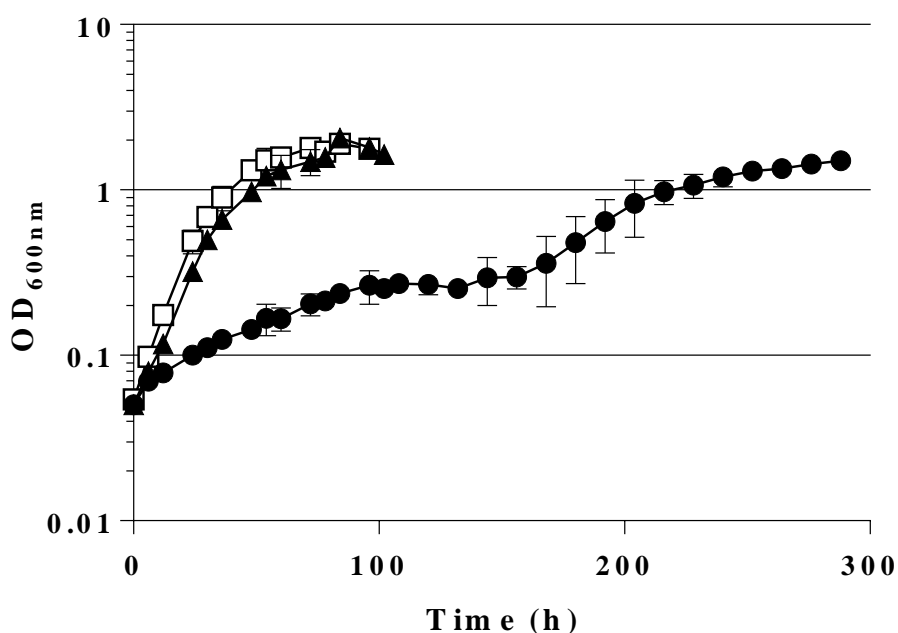
Figure 5-18. Growth behaviour of GL6 (●), GL6* (□) and GL6' (▲) on MM with glucose and 100 μM IPTG.
At 37 °C and 200 rpm. Average of two independent biological replicates. Inoculation of all strains took place
from MM fructose with 100 μM IPTG overnight cultures. For details see Method Chapter 4.5.2.

5.1.9   Faster-growing GL-strains for the production of glycerol

Two evolved strains were also obtained from GL7 and characterised on MM containing glucose
and 100 μM IPTG. GL7* and GL7' showed exponential growth on glucose, whereas GL7
presented a diauxic growth (see Figure 5-19). GL7* and GL7' had a similar growth rate with
0.11 ± 0.01 h^{-1} and 0.12 ± 0.02 h^{-1}, respectively, which meant a 4-times increase in comparison
with the growth rate of GL7. Both GL7-evolved strains achieved the maximal $OD_{600\,nm}$ in only
48 h incubation, 5 times faster than GL7. Furthermore, in the supernatants of GL7, GL7* and
GL7' similar concentrations of DHA (3.5 ± 0.3 mM; 4.5 ± 0.5 mM; and 4.9 ± 0.5 mM) and
glycerol (21.8 ± 0.0 mM; 21.8 ± 0.7 mM; and 20.7 ± 0.6 mM) were determined (see Table 5-3
and Appendix Figure 9-7). GL7* CE and GL7' CE had, both with 0.6 U/mg, a slightly improved
specific GldA activity compared to GL7 (see Table 5-2). In both GL7-evolved strains HT
specific FSA activity was detected. GL7* HT had 0.19 ± 0.01 U/mg and GL7' HT 0.22 ± 0.03
U/mg, which correspond to two times the specific FSA activity measured in GL7 HT (see Table
5-1 page 102).
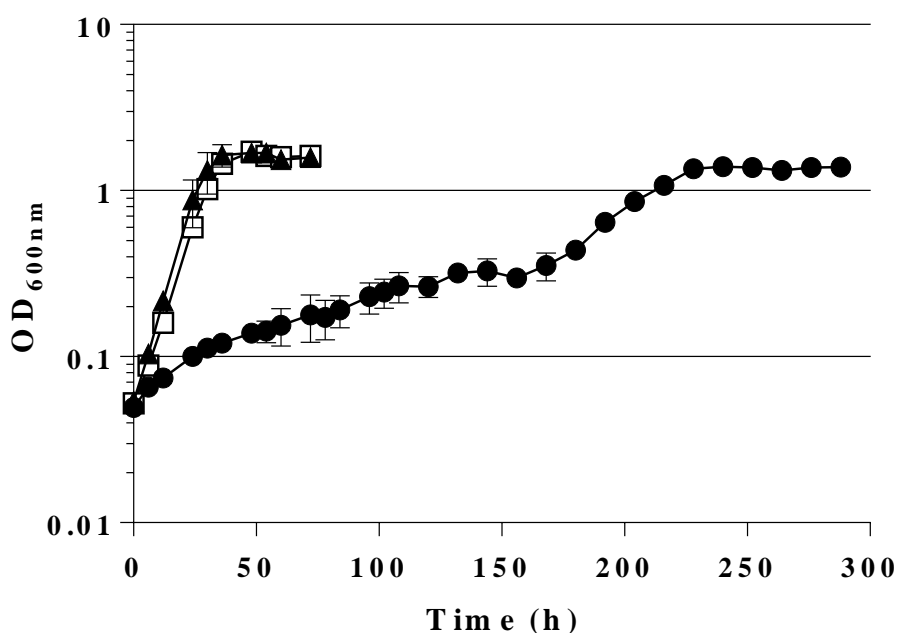
Figure 5-19. Growth behaviour of GL7 (●), GL7* (□) and GL7' (▲) on MM with glucose and 100 μM IPTG. At 37 °C and 200 rpm. Average of two independent biological replicates. Inoculation of all strains took place from MM fructose with 100 μM IPTG overnight cultures. For details see Chapter 4.5.2.

5.1.10 Evaluation of the presence and the specific activity of FSA and/or GldA

The presence or absence of FSA and/or GldA and their specific activity in the GL-strains/GL-evolved strains might help explain the different growth characteristics of these strains. Therefore, these two aspects were evaluated after growth on different media. All values belonging to the specific FSA and GldA activities of all strains with and without plasmids were compared. These values are listed in Table 5-1 and Table 5-2. A general representation of the specific activities after growth on MM containing glucose and 100 µM IPTG is found in Figure 5-20 and Figure 5-23. In addition, presence of FSA and GldA was verified by SDS-PAGE.

As observed in Figure 5-20, GL5* HT held with 0.81 ± 0.03 U/mg the highest specific FSA activity after growth on glucose as sole C-source. All other HTs exhibited just a fourth of it or even less. The only HT where the specific FSA activity was below detection level was LJ110 HT. In addition, when the GL-strains bore pJF119*fsaA* or pJF119*fsaA*^{A129S}, their HT presented a specific FSA activity between 0.26 and 0.45 U/mg with the exception of GL3/pJF119*fsaA*^{A129S} with up to 5 U/mg, more than 5 times the specific activity of GL5*.
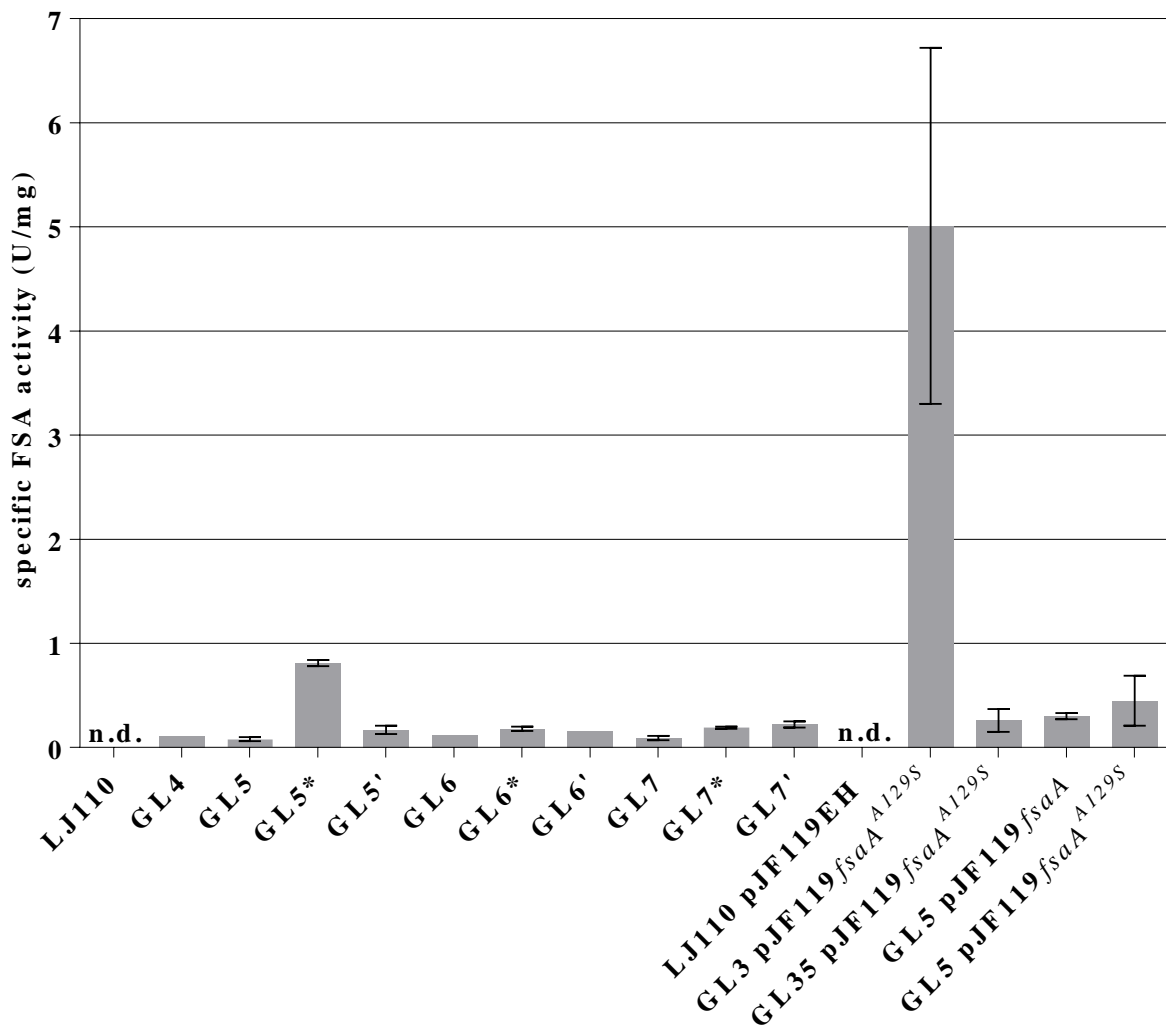
Figure 5-20. Specific FSA activities of heat-treated enriched fractions. Prior to analysis, the cells had reached the stationary phase on MM with glucose and 100 µM IPTG. n.d. = not detected. Average of two independent biological replicates, each with two technical replicates.

The specific FSA activity was also below the detection level in the HT of LJ110 after growth on MM with 100 µM IPTG containing xylose, L-arabinose, or galactose. Whereas, all GL7 HTs showed specific FSA activity: 0.04 U/mg (xylose); 0.05 U/mg (L-arabinose); and 0.08 U/mg (galactose).

Table 5-1. Compilation of specific FSA activities of heat-treated enriched fractions from different experiments. These activities were determined from cells that had reached the stationary phase on: MM with glucose and 100 µM IPTG; MM with fructose and 100 µM IPTG; and LB with 100 µM IPTG. n.d. = below the threshold of detection; n.a. = not analysed. Average of two independent biological replicates with two technical replicates each. Highlighted in grey is the highest specific FSA activity measured in each medium.

Strains	specific FSA activity (U/mg)		
	MM glucose + 100 µM IPTG	MM fructose + 100 µM IPTG	LB + 100 µM IPTG
LJ110	n.d.	n.d.	0.03 ± 0.01
GL3	no growth	n.d.	n.d.
GL4	0.11 ± 0.00	0.23 ± 0.14	0.32 ± 0.03
GL35	no growth	n.d.	n.d.
GL5	0.08 ± 0.02	0.13 ± 0.02	0.22 ± 0.04
GL5*	0.81 ± 0.03	**0.78 ± 0.30**	**1.13 ± 0.27**
GL5'	0.17 ± 0.04	0.20 ± 0.06	0.47 ± 0.05
GL6	0.12 ± 0.00	0.11 ± 0.05	0.15 ± 0.02
GL6*	0.18 ± 0.02	0.24 ± 0.10	0.24 ± 0.06
GL6'	0.16 ± 0.00	0.18 ± 0.11	0.17 ± 0.03
GL7	0.09 ± 0.02	0.15 ± 0.06	0.16 ± 0.04
GL7*	0.19 ± 0.01	0.21 ± 0.05	0.25 ± 0.10
GL7'	0.22 ± 0.03	0.20 ± 0.11	0.30 ± 0.10
LJ110/pJF119EH	n.d.	n.a.	n.a.
GL3/pJF119*fsaA*^{A129S}	**4.94 ± 1.71**	n.a.	n.a.
GL35/pJF119*fsaA*^{A129S}	0.26 ± 0.11	n.a.	n.a.
GL5/pJF119*fsaA*	0.30 ± 0.03	n.a.	n.a.
GL5/pJF119*fsaA*^{A129S}	0.45 ± 0.24	n.a.	n.a.

Not only was it corroborated by the FSA assay that the GL-strains could grow on glucose because of the presence of FSAA A129S, but its presence in the cell was also verified through SDS-PAGE (see Figure 5-21 and Figure 5-22). As outlined in Figure 5-21 with *****, the HT of GL3/pJF119*fsaA*^{A129S}, GL35/pJF119*fsaA*^{A129S}, GL5/pJF119*fsaA*^{A129S} and GL5***** possessed a protein band just below 28 kDa which was not present in LJ110 HT and that was hardly visible in GL5 HT. These marked protein bands corresponded to the size of FSA (24 kDa) when compared to the purified His-tag FSAA A129S. The higher the amount of FSA visible in the SDS-PAGE, the higher the specific FSA activity measured (see Table 5-1). From the 5 µg

protein analysed per SDS-PAGE sample, the 24 kDa protein band in GL3/pJF119*fsaA*^{A129S} HT contains approximately 3 times more protein than the 24 kDa protein band in GL5/pJF119*fsaA*^{A129S} HT. While the difference in specific FSA activity is approximately 10-fold higher in GL3/pJF119*fsaA*^{A129S} HT. In Figure 5-22 a protein band just below 28 kDa was observed in the HTs of GL4, GL5, GL5**, GL5', GL6, GL6**, GL6', GL7, GL7** and GL7' as well. Furthermore, DHA was detected in the supernatants of these GL-strains (see Chapter 5.1.12).
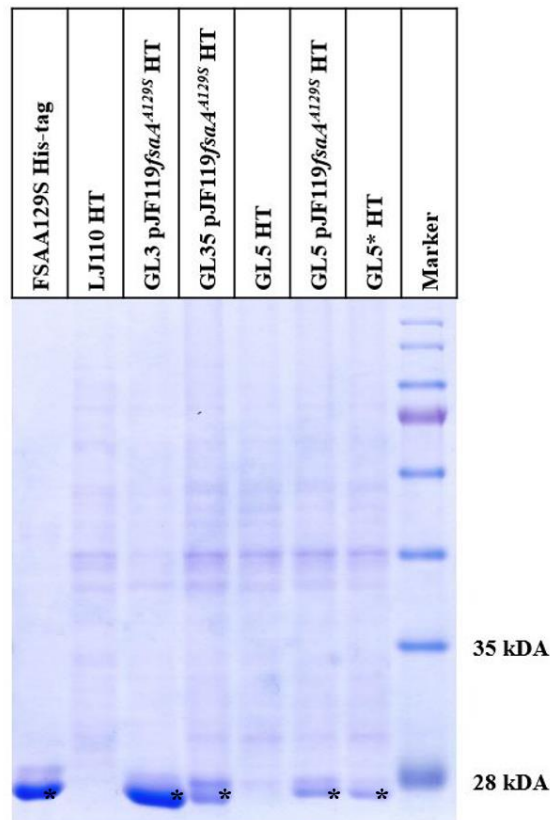
Figure 5-21. SDS-PAGE of heat-treated enriched fractions (HT) of LJ110, GL3/pJF119*fsaA*^{A129S}, GL35/pJF119*fsaA*^{A129S}, GL5, GL5/pJF119*fsaA*^{A129S} and GL5* after growth on MM with glucose and 100 µM IPTG. * denotes the protein bands corresponding to the size of FSA (24 kDa). Note that to enable the separation of protein bands around 28 kDa, the SDS-PAGE was stopped after the lower bands of the protein marker had already left the SDS-gel on purpose. 5 µg protein were analysed per sample. + 20 % contrast.
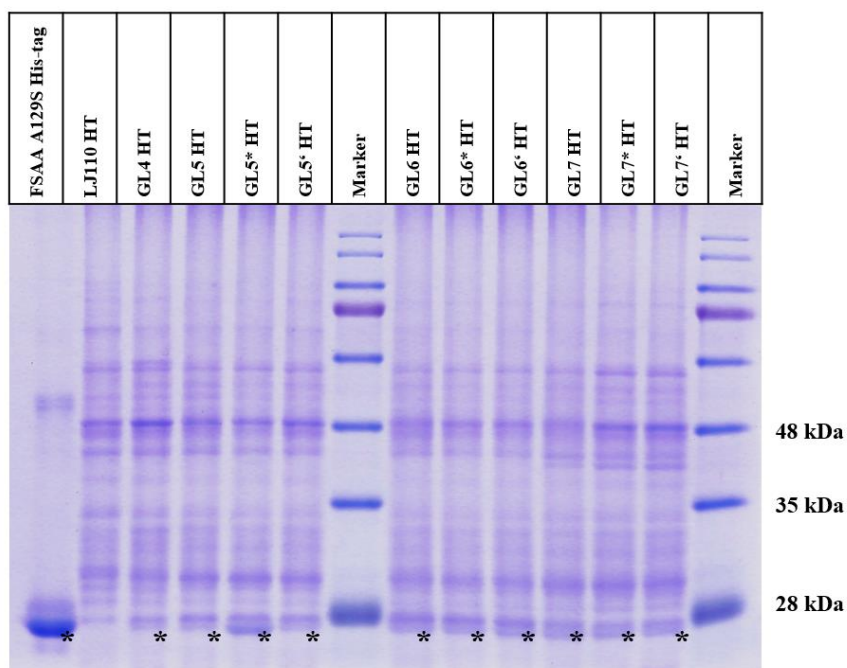
Figure 5-22. SDS-PAGE of heat-treated enriched fractions (HT) of LJ110, GL-strains and GL-evolved strains after growth on MM with glucose and 100 μM IPTG. * denotes the protein bands corresponding to the size of FSAA A129S (24 kDa). Note that to enable the separation of protein bands around 28 kDa, the SDS-PAGE was stopped after the lower bands of the protein marker had already left the SDS-gel on purpose. 5 μg protein were analysed per sample. - 20 % brightness and + 40 % contrast.

Specific GldA activities above 0.3 U/mg were only detected in the CEs belonging to GL7, GL7* and GL7' after growth on MM with glucose and 100 µM IPTG. No clear difference in the specific GldA activities could be observed between these three CEs, their values ranging from 0.4 U/mg to 0.6 U/mg (see Figure 5-23). In the CEs of LJ110 and all other GL-strains the specific GldA activity was below detection level. The specific GldA activity in the CE of LJ110 was also below the detection level after growth on MM containing 100 µM IPTG and xylose, L-arabinose, or galactose. In contrast, in the GL7 CEs the following specific GldA activities were measured: 0.3 U/mg (xylose and L-arabinose) and 0.5 U/mg (galactose).
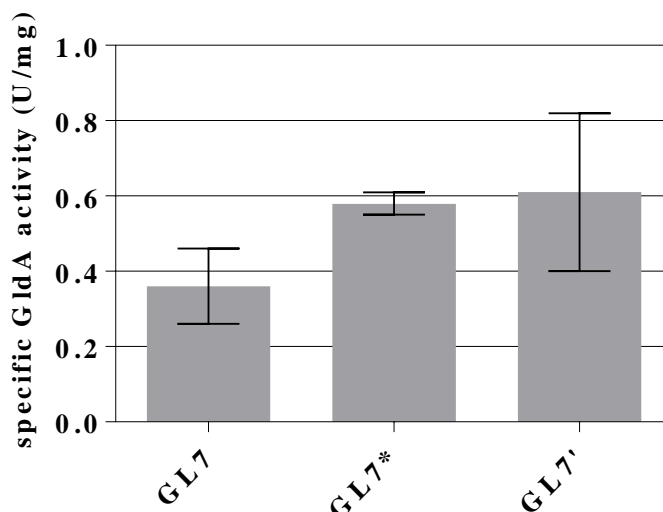
Figure 5-23. Specific GldA activities of cell-free extracts. Prior to analysis, the cells had reached the stationary phase on MM with glucose and 100 μM IPTG. LJ110, GL4, GL5, GL6 and their evolved strains are not displayed on this diagram because the specific GldA activity on their CE was below detection level. Average of two independent biological replicates, each with two technical replicates.

Table 5-2. Compilation of specific GldA activities of cell-free extracts from different experiments. These activities were determined from cells that had reached the stationary phase on: MM with glucose and 100 μM IPTG; MM with fructose and 100 μM IPTG; and LB with 100 μM IPTG. n.d. = below the threshold of detection. Highlighted in grey is the highest specific GldA activity measured in each medium.

Strains	specific GldA activity (U/mg)		
	MM glucose + 100 μM IPTG	MM fructose + 100 μM IPTG	LB + 100 μM IPTG
LJ110	n.d.	n.d.	n.d.
GL3	no growth	n.d.	n.d.
GL4	n.d.	n.d.	n.d.
GL35	no growth	n.d.	n.d.
GL5	n.d.	n.d.	n.d.
GL5*	n.d.	n.d.	n.d.
GL5'	n.d.	n.d.	n.d.
GL6	n.d.	n.d.	n.d.
GL6*	n.d.	n.d.	n.d.
GL6'	n.d.	n.d.	n.d.
GL7	0.4 ± 0.1	**0.8 ± 0.2**	**1.3 ± 0.1**
GL7*	**0.6 ± 0.0**	0.4 ± 0.1	0.8 ± 0.0
GL7'	**0.6 ± 0.2**	0.4 ± 0.1	0.9 ± 0.2

In Figure 5-24 the SDS-PAGE corresponding to the CEs samples of LJ110, GL-strains and GL-evolved strains after growth on MM with glucose and 100 µM IPTG is displayed. The visualisation of the CEs protein bands in a gel was important to confirm the existence of GldA in GL7 and its evolved strains. The protein band present in GL7 CE which should correspond to GldA was nearly imperceptible, but in GL7* CE and GL7' CE it was possible to distinguish an extra protein band also observed in the purified His-tag GldA. All other strains CEs showed no protein band with this size.

For the SDS-PAGEs after growth on MM with fructose and 100 µM IPTG and on LB with 100 µM IPTG see Appendix Chapter 9.8.
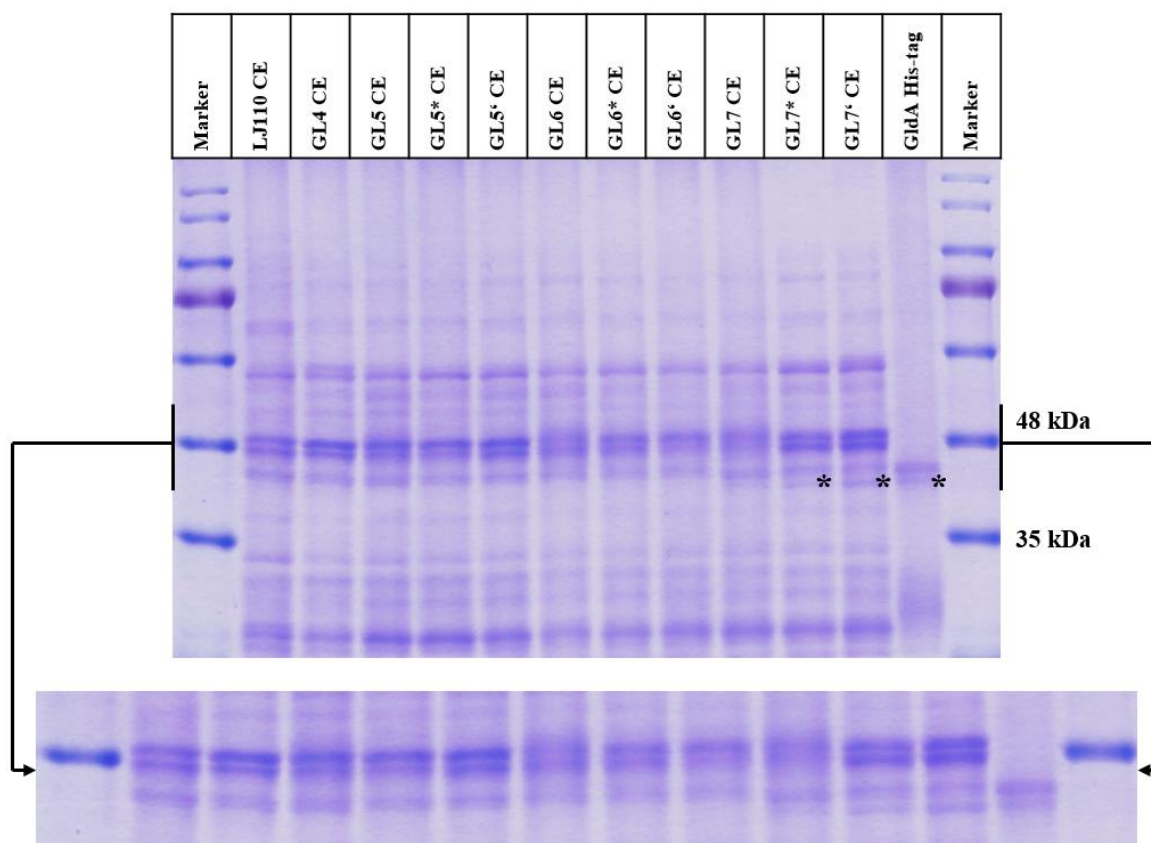
Figure 5-24. SDS-PAGE of cell-free extracts (CE) of LJ110, GL-strains and GL-evolved strains after growth on MM with glucose and 100 µM IPTG. Above the complete SDS-gel, below an enlargement of the SDS-gel at around 48 kDa. * denotes the protein bands corresponding to the size of GldA (39 kDa; Tang et al., 1979). Note that to enable the separation of protein bands between 35 kDa and 48 kDa, the SDS-PAGE was stopped after the lower bands of the protein marker had already left the SDS-gel on purpose. 5 µg protein were analysed per sample. - 20 % brightness and + 40 % contrast.

5.1.11 Comparison of mRNA levels of key genes between GL-strains and their evolved strains

It was investigated if the transcript levels of selected genes (see Method Chapter 4.6.4 for information regarding the choice of genes) in the GL-evolved strains was different to the expression of the same genes in the corresponding GL-parent strain. A difference in gene expression might be responsible for the considerable increase in the growth rate on glucose of the GL-evolved strains. Furthermore, the expression of specific genes might explain the concentrations of DHA and/or glycerol measured in their supernatants. For this purpose, qPCR of RNA samples harvested during the exponential phase of GL-strains and their GL-evolved strains when grown on MM containing glucose and 100 µM IPTG was performed as described in Chapter 4.6.4. It should be noted that it could not be distinguished between the transcript from the native *fsaA* gene and the mutant allele *fsaA^{A129S}* inserted in the *lac*-operon. In addition, the missing expression of the deleted genes in each strain was confirmed with the exception of the *glpK* gene (for more details see below).

The measured gene transcript levels for GL5, GL5* and GL5'are shown in Figure 5-25. The measured expression of *fsaA* in the GL5-evolved strains was significantly higher than in GL5. GL5 showed an approximately 10 times increase in expression of *glpK* compared to GL5* and GL5'. GL5* was the only strain where expression of *ptsG* was detected.
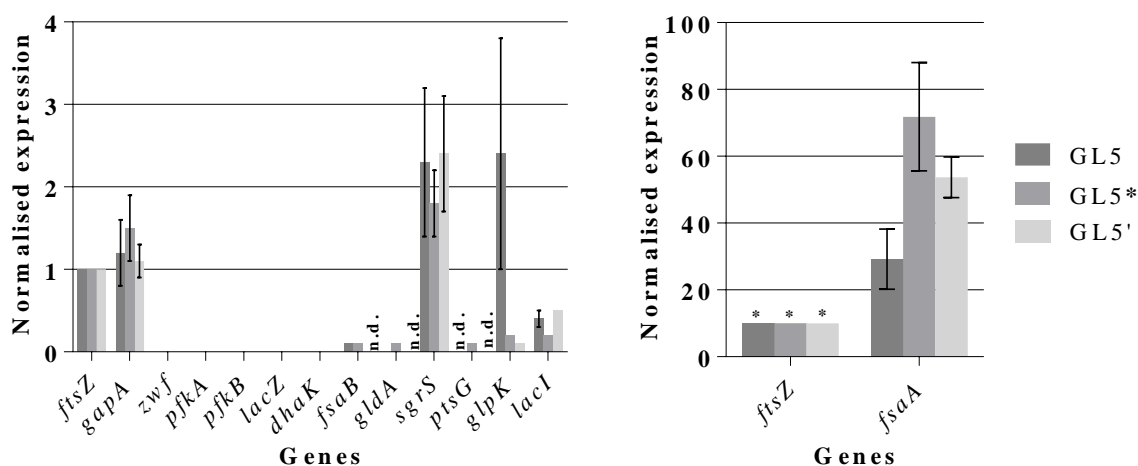
Figure 5-25. qPCR results of RNA samples harvested during the exponential phase of GL5, GL5* and GL5' when grown on MM with glucose and 100 µM IPTG. The expression of the genes *zwf*, *pfkA*, *pfkB*, *lacZ* and *dhaK* could not be detected in any of the strains. Average values of two biological replicates, each with three technical replicates. *ftsZ* was used as a calibrator. n.d. = not detected; * denotes values multiplied by 10 for better visibility. Standard deviations are higher than 10 %, because only two independent biological replicates each with three technical replicates were measured. Note that the normalised expression axis is different in the two graphs. See Method Chapter 4.6.4 for details.

In Figure 5-26 the gene transcript levels of GL6, GL6* and GL6' are displayed. The samples belonging to the GL6-evolved strains showed a more than 2-fold increase in the expression of *fsaA* compared to GL6. In addition, GL6' had a higher expression of *sgrS* than GL6. All other genes were expressed in similar quantities between GL6 and its evolved strains.

With the exception of the expression of *ptsG* between GL7 and GL7**,** no considerable differences between GL7, GL7* and GL7' could be stated in the transcript levels of the other tested genes (see Figure 5-27).

On the samples of GL6, GL7 and their evolved strains, extremely low levels of *glpK* transcripts were detected (normalised expression between 0.01 and 0.08), even though there is proof that the gene *glpK* is deleted in all these strains (see Appendix Chapter 9.1.1) and that they show no growth on glycerol (see Table 5-5). It is unclear if the primers chosen for the qPCR of this gene are not sensitive enough, or if there is another reason why such low transcript levels were measured for *glpK*.
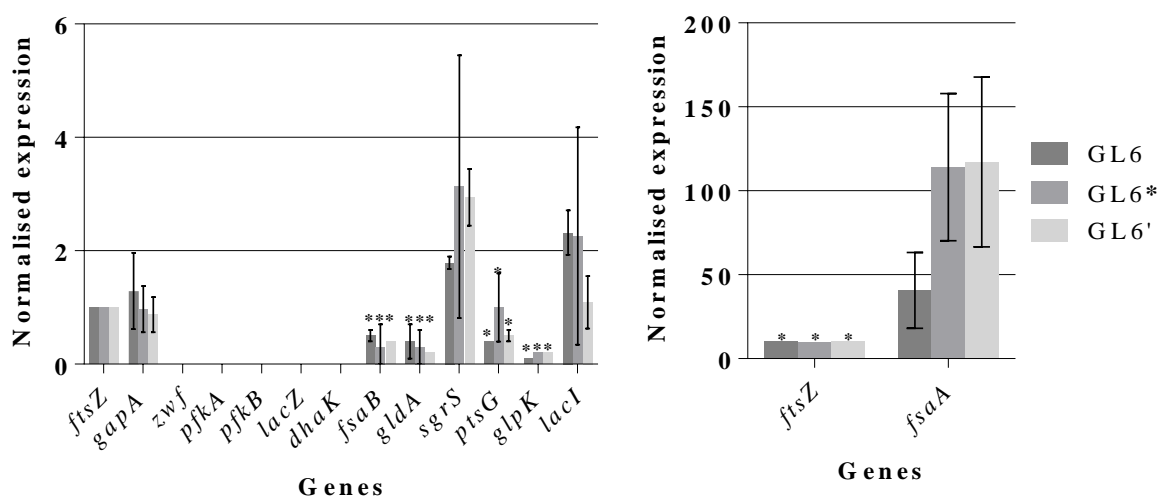
Figure 5-26. qPCR results of RNA samples harvested during the exponential phase of GL6, GL6* and GL6' when grown on MM with glucose and 100 μM IPTG. The expression of the genes *zwf*, *pfkA*, *pfkB*, *lacZ* and *dhaK* could not be detected on any of the strains. Average values of two biological replicates, each with three technical replicates. *ftsZ* was used as a calibrator. * denotes values multiplied by 10 for better visibility. Standard deviations are higher than 10 %, because only two independent biological replicates each with three technical replicates were measured. Note that the normalised expression axis is different in the two graphs. See Method Chapter 4.6.4 for details.

What the evolved strains from GL5 and GL6 have in common is that they produced an increased number of *fsaA* transcripts than their parent strains. If all these transcripts are translated to FSAA A129S that could explain their faster growth on glucose (see Chapter 5.1.4). But this assumption cannot be applied to the GL7-evolved strains. GL7* grew 4-times faster than GL7 most probably because of the nearly double expression of the *ptsG* gene. More *ptsG* transcripts

might mean more glucose transporters (EII^{Glc}) produced, which in turn allow the transport of more glucose into the cell that can be further metabolised through the glucose degradation pathway. But the reason for the increased growth rate of GL7' could not be elucidated alone with the gene transcript levels reported here and, thus, it remains unclear.
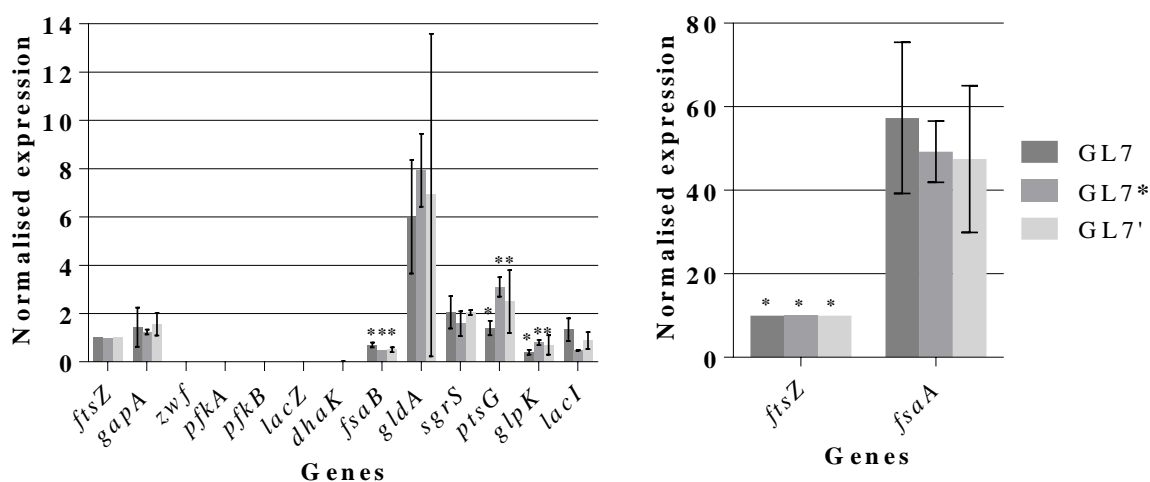
Figure 5-27. qPCR results of RNA samples harvested during the exponential phase of GL7, GL7* and GL7' when grown on MM with glucose and 100 μM IPTG. The expression of the genes *zwf*, *pfkA*, *pfkB*, *lacZ* and *dhaK* could not be detected on any of the strains. Average values of two biological replicates, each with three technical replicates. *ftsZ* was used as a calibrator. * denotes values multiplied by 10. Standard deviations are higher than 10 %, because only two independent biological replicates each with three technical replicates were measured. Note that the normalised expression axis is different in the two graphs. See Method Chapter 4.6.4 for details.

5.1.12 Comparison of the DHA concentrations reached by the GL-strains and the GL-evolved strains

DHA concentrations might show a relationship to the growth rate, the maximal OD$_{600\,nm}$ reached and the absence and/or the presence of enzyme activities in LJ110, GL-strains, GL-strains with plasmid-borne gene copies of *fsaA*, *fsaA*^{A129S}, *gldA*, *talB*^{F178Y} or *xfp*, and GL-evolved strains. Therefore, the maximal concentrations of DHA detected in their supernatants during growth on different media were compared.

As shown in Figure 5-28, the highest DHA concentrations were measured in the supernatants of GL3/pJF119*fsaA*^{A129S}, GL5*, GL6* and GL6' when grown on glucose. In all these cases, the DHA concentration was between 11 mM and 14 mM from 30 mM to 34 mM glucose. Furthermore, the concentration of DHA was below the threshold level in a) the supernatants of LJ110 cultures regardless of the C-source present in the medium, b) the supernatants of

GL4/pJF119*fsaA* and GL4/pJF119ΔEP$_{tac}$*gldA*, c) the supernatants of GL3/pJF119*xfp* and GL35/pJF119*xfp*. For more details see Table 5-3 and Table 5-4. No strains with plasmid-borne genes other than GL3/pJF119*fsaA*^{A129S}, GL4/pJF119*fsaA*^{A129S}, GL5/pJF119*fsaA* and GL5/pJF119*fsaA*^{A129S} obtained an increase in DHA concentration compared to the plasmid-free GL-strain. GL6/pJF119*fsaA* or GL6/pJF119*fsaA*^{A129S} reached a lower DHA concentration when compared to the concentration obtained with GL6. When GL3 or GL35 bore pJF119*talB*^{F178Y}, the presence of TalB F178Y allowed GL3 and GL35 to grow on glucose, but it did not improve the DHA concentration in comparison with GL3/pJF119*fsaA*^{A129S} and GL35/pJF119*fsaA*^{A129S}. Interestingly, GL7 produced a similar amount of DHA independently of the C-source available in the medium. No reliable data could be gathered with GL7 bearing any plasmids, because the results of growth on glucose were not reproducible.
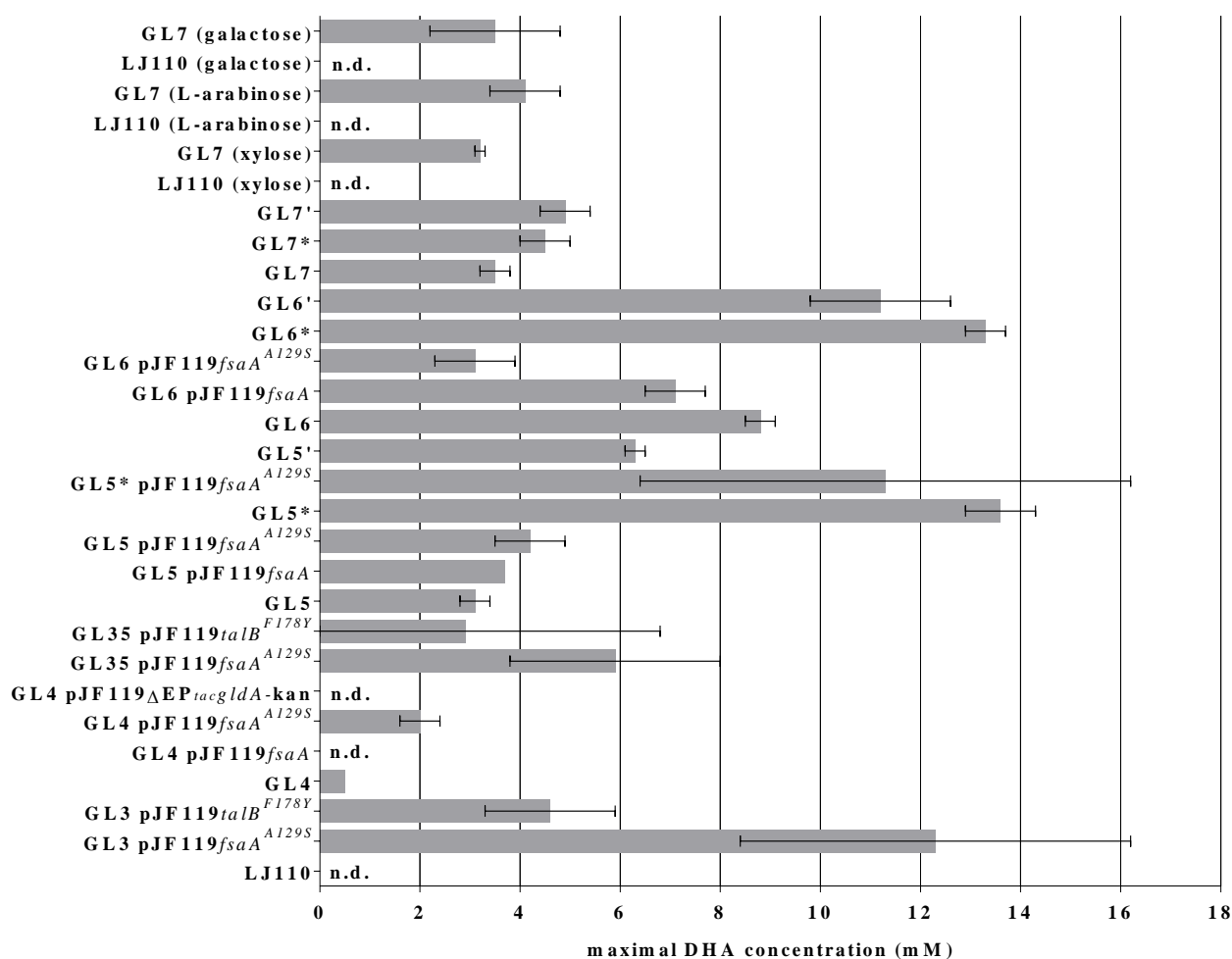
Figure 5-28. Maximal DHA concentrations measured in the supernatants of LJ110, GL-strains and GL-evolved strains in the absence or presence of plasmids during growth on different C-sources. At 37 °C and 200 rpm. If not otherwise indicated, growth took place on MM with glucose, 100 μM IPTG and, if necessary, 100 μg/mL Amp. LJ110 and GL7 grew also on MM with 100 μM IPTG and xylose/L-arabinose/galactose. n.d. = not detected. Average of two independent biological replicates.

5.1.13 Comparison of the glycerol concentrations reached by the GL-strains and the GL-evolved strains

As well as the DHA concentrations, the amount of glycerol determined in the supernatants of the GL-strains and their evolved strains might show a relationship to the growth rate, the maximal $OD_{600\,nm}$ reached and the absence and/or the presence of enzyme activities in these strains. Therefore, the maximal concentrations of glycerol detected in their supernatants during growth on different media were compared.
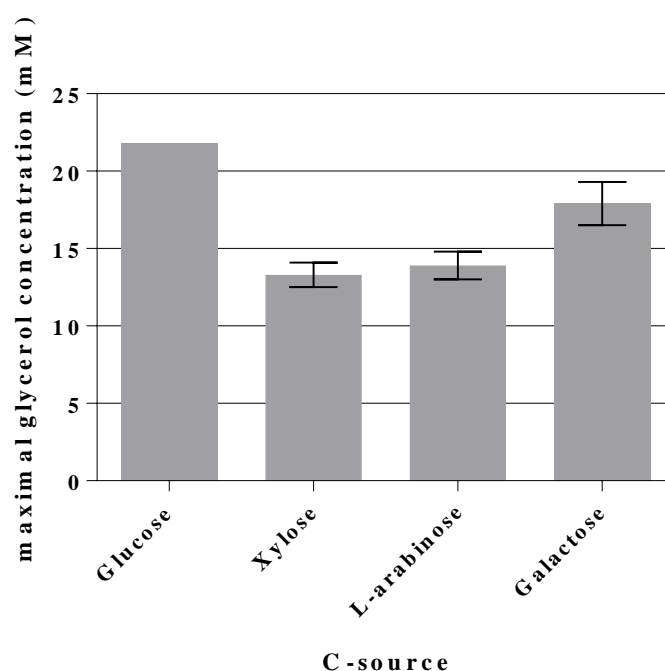
Figure 5-29. Maximal glycerol concentrations achieved by GL7 during growth on MM with different C-sources and 100 μM IPTG. Glucose and galactose (hexoses) had an intended initial concentration of approximately 28 mM, L-arabinose and xylose (pentoses) of approximately 33 mM. Actual starting concentrations were determined by HPLC and differed from the intended initial concentrations. Average of two independent biological replicates. For more details see Chapter 4.5.2. Guitart Font and Sprenger (2020).

Glycerol was detected in the supernatants of GL6, GL7, GL6- and GL7-evolved strains. The production of glycerol in GL7 and their evolved strains was expected due to the integration of the *gldA* gene under the control of the promoter P_{tac} in the ribose-operon. In the supernatants of GL3, GL4, GL5, their evolved strains and LJ110, the concentration of glycerol was below the detection level. As well as, when GL3, GL4, GL5 and GL35 expressed plasmid-borne genes. For more information see Table 5-3 and Table 5-4. As shown in Figure 5-29, the most significant conversion of substrate to glycerol in GL7 was monitored during growth on glucose, followed by growth on galactose. In terms of C atom molarity, approximately 72 % of the

theoretical maximal value was reached on glucose against 63 % on galactose). On L-arabinose and on xylose, GL7 achieved a similar conversion of substrate to glycerol, but lower than on galactose. On both pentoses (L-arabinose and xylose), the theoretical maximal value reached was approximately 40 % (Guitart Font and Sprenger, 2020).

Table 5-3. Compilation of data sets: formation of DHA and/or glycerol, and growth parameters of LJ110, GL-strains and GL-evolved strains in shake flasks. All cultivations contained MM and 100 µM IPTG. The values in the left column are the approximately set concentrations of the C-sources. Due to inevitable technical limitations in media preparations, not all shake flasks had the same initial C-source concentration. Starting C-source concentrations were measured directly after inoculation of cells and monitored throughout the cultivation by HPLC measurements. n.a., not applicable; n.g, no growth; Res*, residual DHA or glycerol at the end of cultivation; G_t, generation time determined during logarithmic growth phase. [a] Results from Guitart Font and Sprenger (2020).

C-source	Strain	Time (h) until max. $OD_{600\,nm}$	max. $OD_{600\,nm}$	C-source consumed (mM)	max.$OD_{600\,nm}$ / [C-source]	DHA max. concentration (mM)	DHA Res*	Glycerol max. concentration (mM)	Glycerol Res*	Yellow culture	μ (h^{-1})	G_t (min)
28 mM glucose	LJ110[a]	24	4.562 ± 0.003	33.8	0.13	0.0 ± 0.0	No	0.0 ± 0.0	No	No	0.59 ± 0.01	71 ± 1
	GL3[a]	n.g.	n.g.	n.a.	n.a.	n.a.	n.a.	n.a.	n.a.	n.a.	n.a.	n.a.
	GL4[a]	96	4.399 ± 0.675	32.2	0.14	0.5 ± 0.0	No	0.0 ± 0.0	No	No	0.05 ± 0.00	808 ± 11
	GL35	n.g.	n.g.	n.a.	n.a.	n.a.	n.a.	n.a.	n.a.	n.a.	n.a.	n.a.
	GL5[a]	216	2.410 ± 0.489	30.2	0.08	3.1 ± 0.3	No	0.0 ± 0.0	No	Yes	0.02 ± 0.00	2293 ± 85
	GL5*	54	2.993 ± 0.111	30.8	0.10	13.6 ± 0.7	No	0.0 ± 0.0-	No	Yes	0.12 ± 0.00	354 ± 9
	GL5'	78	2.968 ± 0.313	30.7	0.10	6.3 ± 0.2	No	0.0 ± 0.0	No	Yes	0.08 ± 0.01	554 ± 35
	GL6[a]	288	1.497 ± 0.033	30.6	0.05	8.8 ± 0.3	Yes	1.9 ± 0.2	Yes	Yes	0.03 ± 0.01	1655 ± 103
	GL6*	84	1.902 ± 0.171	30.9	0.06	13.3 ± 0.4	Yes	1.4 ± 0.1	Yes	Yes	0.10 ± 0.00	427 ± 5
	GL6'	84	2.061 ± 0.257	29.7	0.07	11.2 ± 1.4	Yes	1.5 ± 0.0	Yes	Yes	0.08 ± 0.01	540 ± 22
	GL7[a]	240	1.395 ± 0.165	30.2	0.05	3.5 ± 0.3	Yes	21.8 ± 0.0	Yes	No	0.03 ± 0.00	1526 ± 49
	GL7*	48	1.717 ± 0.137	32.8	0.05	4.5 ± 0.5	Yes	21.8 ± 0.7	Yes	No	0.11 ± 0.01	403 ± 26
	GL7'	48	1.683 ± 0.154	32.4	0.05	4.9 ± 0.5	Yes	20.7 ± 0.6	Yes	No	0.12 ± 0.02	360 ± 59
33 mM xylose	LJ110[a]	24	4.492 ± 0.011	32.7	0.14	0.0 ± 0.0	No	0.0 ± 0.0	No	No	0.55 ± 0.01	76 ± 1
	GL7[a]	48	4.431 ± 0.187	32.9	0.13	3.2 ± 0.1	Yes	13.3 ± 0.8	Yes	No	0.12 ± 0.01	361 ± 8
33 mM L-arabinose	LJ110[a]	24	1.991 ± 0.107	34.5	0.06	0.0 ± 0.0	No	0.0 ± 0.0	No	No	0.53 ± 0.01	79 ± 4
	GL7[a]	48	2.024 ± 0.061	35.0	0.06	4.1 ± 0.7	Yes	13.9 ± 0.9	Yes	No	0.12 ± 0.01	360 ± 21
28 mM galactose	LJ110[a]	28	4.133 ± 0.160	28.0	0.15	0.0 ± 0.0	No	0.0 ± 0.0	No	No	0.19 ± 0.01	222 ± 21
	GL7[a]	120	1.264 ± 0.001	28.2	0.05	3.5 ± 1.3	Yes	17.9 ± 1.4	Yes	No	0.04 ± 0.01	1266 ± 143

Table 5-4. Compilation of data sets: formation of DHA and glycerol, and growth parameters of GL-strains bearing plasmids in shake flasks cultivations. All cultivations contained MM with glucose, 100 µM IPTG and the corresponding antibiotic. The glucose concentration value in the left column is set approximately. Due to inevitable technical limitations in media preparations, not all shake flasks had the same initial glucose concentration. Initial glucose concentrations were measured directly after inoculation and monitored throughout the cultivation by HPLC measurements. n.a., not applicable; n.g., no growth; Res*, residual DHA or glycerol at the end of cultivation; G_t, generation time determined during logarithmic growth phase.

Strains	Time (h) until max. $OD_{600 nm}$	max. $OD_{600 nm}$	max. $OD_{600 nm}$ / [C-source]	C source consumed (mM)	DHA max. concentration (mM)	DHA Res*	Glycerol max. concentration (mM)	Glycerol Res*	Yellow culture	μ (h^{-1})	G_t (min)
GL3 pJF119$fsaA$	n.g.	n.g.	n.a.	n.a.	n.a.	n.a.	n.a.	n.a.	n.a.	n.a.	n.a.
GL3 pJF119$fsaA^{A129S}$	78	3.517 ± 0.984	0.10	33.6	12.3 ± 3.9	No	0.0 ± 0.0	No	Yes	0.12 ± 0.01	359 ± 52
GL3 pJF119$talB^{F178Y}$	120	4.002 ± 0.468	0.12	32.6	4.6 ± 1.3	No	0.0 ± 0.0	No	Yes	0.05 ± 0.00	769 ± 1
GL3 pJF119xfp	48	3.965 ± 0.226	0.13	31.2	0.0 ± 0.0	No	0.0 ± 0.0	No	No	0.15 ± 0.03	290 ± 57
GL4 pJF119$fsaA$	108	4.169 ± 0.006	0.13	32.2	0.0 ± 0.0	No	0.0 ± 0.0	No	Yes	0.06 ± 0.00	677 ± 40
GL4 pJF119$fsaA^{A129S}$	78	3.946 ± 0.276	0.12	32.1	2.0 ± 0.4	No	0.0 ± 0.0	No	Yes	0.07 ± 0.01	674 ± 85
GL4 pJF119$\Delta EP_{uac}gldA$	84	3.982 ± 0.359	0.12	31.7	0.0 ± 0.0	No	0.0 ± 0.0	No	No	0.12 ± 0.00	340 ± 2
GL35 pJF119$fsaA$	n.g.	n.g.	n.a.	n.a.	n.a.	n.a.	n.a.	n.a.	n.a.	n.a.	n.a.
GL35 pJF119$fsaA^{A129S}$	120	2.257 ± 0.401	0.07	31.6	5.9 ± 2.1	Yes	0.0 ± 0.0	No	Yes	0.02 ± 0.00	2143 ± 52
GL35 pJF119$talB^{F178Y}$	216	2.166 ± 0.391	0.07	31.8	2.9 ± 3.9	No	0.0 ± 0.0	No	Yes	0.07 ± 0.01	682 ± 78
GL35 pJF119xfp	30	3.556 ± 0.007	0.11	32.6	0.0 ± 0.0	No	0.0 ± 0.0	No	No	0.16 ± 0.01	262 ± 24
GL5 pJF119$fsaA$	172	2.388 ± 0.397	0.07	30.6	3.7 ± 0.0	Yes	0.0 ± 0.0	No	Yes	0.03 ± 0.01	1735 ± 245
GL5 pJF119$fsaA^{A129S}$	96	1.501 ± 0.044	0.04	25.0	4.2 ± 0.7	Yes	0.0 ± 0.0	No	Yes	0.02 ± 0.00	1811 ± 110
GL6 pJF119$fsaA$	336	1.622 ± 0.042	0.05	31.9	7.1 ± 0.6	Yes	2.8 ± 0.5	Yes	Yes	0.02 ± 0.00	1956 ± 33
GL6 pJF119$fsaA^{A129S}$	102	0.622 ± 0.042	0.02	13.7	3.1 ± 0.8	Yes	0.4 ± 0.0	No	Yes	0.06 ± 0.01	786 ± 69
GL5* pJF119$fsaA^{A129S}$	54	3.250 ± 0.038	0.11	30.0	11.3 ± 4.9	No	0.0 ± 0.0	No	Yes	0.11 ± 0.00	393 ± 6

C-source	28 mM glucose

5.1.14 Growth characterisation of the GL-strains and the GL-evolved strains on solid media

Changes in the chromosome of *E. coli*, such as deletions or integrations of genes, might have an impact on metabolic pathways. Furthermore, new roles of the enzymes encoded within these genes might be discovered. To evaluate which impact the chromosome changes in the GL-strains and their evolved strains have, the growth behaviour of these strains on different C-sources was studied on solid media (see Table 5-5, Table 5-6 and Table 5-7). MM-agar was used to identify if these strains can metabolise these C-sources. In addition, MacConkey-agar was utilised to determine if the consumption of a specific C-source took place in a fast or a slow rate. If a zone of acid precipitated bile is observed (pink colonies), the strain is able to metabolise the C-source with a fast rate (overflow metabolism). However, if the colonies are colourless, the strain either cannot metabolise the C-source or it metabolises it in a slow rate. In Figure 5-30 examples of MM-agar and MacConkey-agar plates are shown.

It was expected that the blockades in glycolysis ($\Delta pfkA$ $\Delta pfkB$) and the PPP (Δzwf) would impair the consumption of C-sources that enter above or at the level of F6P (see Discussion Figure 6-1). Fructose can enter glycolysis at two different levels, as F6P or as F1,6BP. Therefore, it was expected that all constructed strains would be able to metabolise fructose, but not at wild-type levels due to the accumulation of F6P.

On MM-agar, all strains could utilise fructose, succinate (pH 7.0) and D,L-lactate (pH 7.0). gluconate (pH 7.0) and L-arabinose as sole C-source. None of the GL-strains could grow on lactose. Lactose is cleaved to glucose and galactose. Because both GL3 and GL35 showed no growth on glucose nor on galactose, it was expected that these strains could not grow on lactose either. On the other hand, GL4, GL5, GL6, GL7 and all GL-evolved strains have an integration (P_{tac}-$fsaA^{A129S}$) in the *lac*-operon. Thus, the *lac*-operon of these strains is not functional, preventing the metabolism of lactose. GL4, GL5, GL6, GL7 and all of GL-evolved strains carry a copy of the $fsaA^{A129S}$ gene in the chromosome. Therefore, it was expected that they could deplete glucose. As observed in Table 5-5, all these strains could use glucose as sole C-source, even though at a very low rate. GL3 and GL4 showed no growth on mannitol or galactose, whereas GL4 could use glucitol and xylose for growth. Both strains could grow on glycerol. GL5 and GL5-evolved strains showed growth on galactose, glycerol and xylose as sole C-source. While GL5 could not utilise mannitol or glucitol, the GL5-evolved strains did. GL6, GL6* and GL6' could not grow on galactose, but showed growth on xylose. GL6-evolved strains showed weak growth on mannitol and on glucitol, whereas GL6 could not use any of these two C-sources for growth. It was not possible for the strains missing the *glpK* gene to

grow on glycerol (GL6, GL7 and their evolved strains). Galactose could barely be used for growth by GL7, while GL7* and GL7' showed no growth. GL7 and GL7-evolved strains grew on xylose. No growth was visible on MM-agar without any C-source for any of the listed strains.
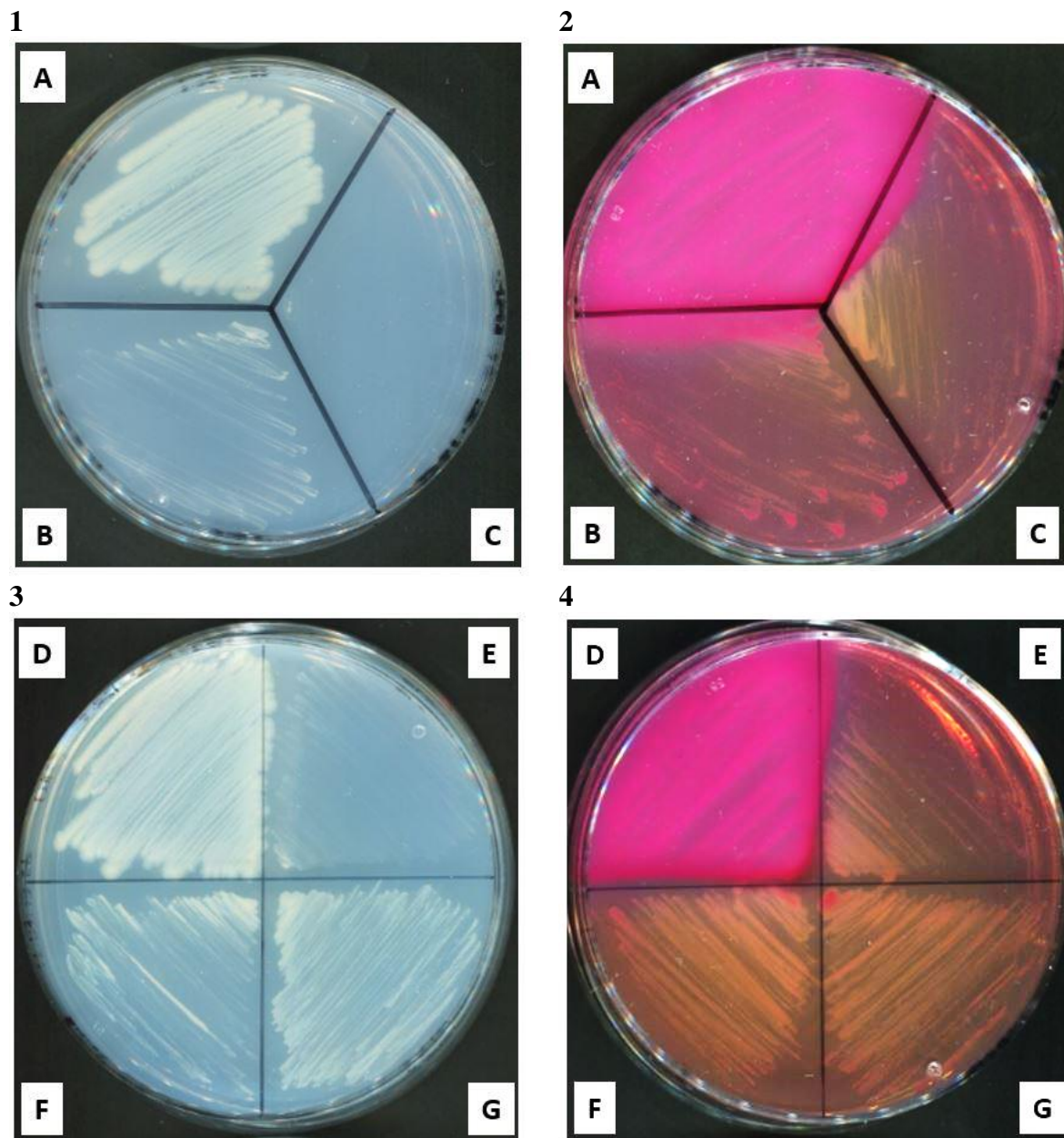
Figure 5-30. Examples of MM-agar plates and MacConkey-agar plates. 1) MM-agar plate containing 0.5 % glucose (w/v), 100 μM IPTG and 100 μg/mL Amp; 2) MacConkey-agar plate containing 1 % glucose (w/v), 100 μM IPTG and 100 μg/mL Amp; 3) MM-agar plate containing 0.5 % glucose (w/v); 4) MacConkey-agar plate containing 1 % glucose (w/v). A = LJ110/pJF119EH; B = GL3/pJF119*fsaA*^{A129S}; C = GL3/pJF119EH; D = LJ110; E = GL5; F = GL5'; G = GL5*. MacConkey-agar plates with + 20 % brightness and + 40 % contrast.

Similar results to the growth on MM were observed on MacConkey. On fructose and L-arabinose, a zone of acid precipitated bile was visible in different quantities in all strains. Lactose, maltose and mannitol did not allow any of the GL-strains to produce a zone of acid

precipitated bile. GL3 showed no visible acid production on galactose nor on xylose. GL35 colonies were colourless on galactose. GL4 colonies were light red during growth on glucose and on glucitol. GL5* and GL5' colonies were light red during growth on glucose, but only GL5* colonies were also light red in the presence of glucitol. GL4, GL5, GL6, GL7 and all GL-evolved strains displayed small amounts of acid production in the presence of galactose and xylose. On glycerol, GL6, GL6*, GL6', GL7, GL7* and GL7' showed no acid formation, while all other strains displayed acid production in the presence of glycerol. No acid was detected on MacConkey-agar without any C-source by any of the strains.

The growth of LJ110/pJF119EH, GL3/pJF119EH and GL3/pJF119$fsaA^{A129S}$ on solid media was compared (data are summarised in Table 5-7). LJ110/pJF119EH could grow on all C-sources (MM-agar) and produced acid in the presence of all of them (MacConkey-agar). In contrast, on MM-agar GL3/pJF119EH could only grow on glycerol and D,L-lactate (pH 7.0) and had difficulties to grow on fructose, succinate (pH 7.0) and gluconate (pH 7.0). Acid production on MacConkey-agar was observed during growth of GL3/pJF119EH in the presence of fructose and glycerol. As for GL3 bearing pJF119$fsaA^{A129S}$, it could grow on MM-agar containing all C-sources except on maltose and displayed a decreased growth on glucitol, xylose, galactose, gluconate (pH 7.0) and L-arabinose. GL3/pJF119$fsaA^{A129S}$ showed acid formation on MacConkey-agar in the presence of all C-sources with the exception of maltose. Evidence of a considerable amount of acid was observed during growth on fructose, followed by a normal amount on glucose and galactose. On all other C-sources, the amount of acid formed was small. None of these strains showed growth on MM-agar without any C-source and no acid production was visible on MacConkey-agar without any C-source.

Table 5-5. Growth phenotypes of LJ110, GL-strains and GL-evolved strains on: LB-agar; and MM-agar with 0.5 % C-source (w/v). All sugars were of D-configuration unless otherwise specified. normal = single colonies with a diameter of ≥ 1 mm; small = single colonies with a diameter ≤ 1 mm; (1) = colonies evaluation after 1 day of incubation at 37 °C; (2) = colonies evaluation after 2 day of incubation at 37 °C; highlighted in grey = barely visible; - = no growth; * = presence of papillae; ** = lactose-minus due to gene insertion. Average of at least three independent biological replicates. [a] Results from Guitart Font and Sprenger (2020).

Strain	LJ110[a]	GL3[a]	GL4[a]	GL35	GL5	GL6	GL7	GL5*	GL5'	GL6*	GL6'	GL7*	GL7'
LB	normal (1)	normal (1)	normal (1)	normal (1)	normal (1)	normal (1)	normal (1)	normal (1)	normal (1)	normal (1)	normal (1)	normal (1)	normal (1)
MM-agar + 0.5 % C-source (w/v)													
without C-source	-	-	-	-	-	-	-	-	-	-	-	-	-
Fructose	normal (1)	small (2)	small (2) *	small (2)	small (2)	small (2)	small (2)	small (2)	small (2)	small (2)	small (2)	small (2)	small (2)
Glucose	normal (1)	-	small (2)	-	small (2)	small (2)	small (2)	small (2)	small (2)	small (2)	small (2)	small (2)	small (2)
Glycerol	normal (1)	small (1)	small (1)	small (1)	normal (2)	-	-	normal (2)	normal (2)	-	-	-	-
D,L-Lactate (pH 7.0)	small (1)	small (1)	small (1)	small (1)	small (1)	small (1)	small (1)	normal (2)	normal (2)	small (1)	normal (2)	normal (2)	small (1)
Mannitol	normal (1)	-	-	-	-	-	-	small (2)	small (2)	small (2)	small (2)	small (2)	small (2)
Succinate (pH 7.0)	small (1)	small (1)	small (1)	small (1)	small (1)	small (1)	small (1)	small (1)	small (1)	small (1)	small (1)	small (1)	small (1)
Glucitol	normal (1)	-	small (2) *	-	-	-	-	small (2)	small (2)	small (2)	small (2)	small (2) *	small (2)
Xylose	small (1)	-	small (2)	-	small (2)	small (2)	small (2)	small (2)	small (2)	small (2)	small (2)	small (2)	small (2)
Maltose	normal (1)	-	-	-	-	-	-	-	-	-	-	-	-
Galactose	small (1)	-	-	-	small (2)	-	small (2)	small (2)	small (2)	-	-	-	-
Gluconate (pH 7.0)	normal (1)	small (2)	small (1)	small (1)	small (2)*	small (2)	small (2)	small (2)	small (2)	small (2)	small (2)	small (2)	small (2)
L-Arabinose	normal (1)	small (2)	small (2)	small (2)	small (1)	small (2)	small (2)	small (2)	small (2)	small (1)	small (1)	small (2)	small (2)
Lactose	normal (1)	-	**	-	**	**	**	**	**	**	**	**	**

Table 5-6. Growth phenotypes of LJ110, GL-strains and GL-evolved strains on MacConkey-agar with 1 % C-source (w/v). All sugars were of D-configuration unless otherwise specified. normal = single colonies with a diameter of ≥ 1 mm; small = single colonies with a diameter ≤ 1 mm; (1) = colonies evaluation after 1 day of incubation at 37 °C; (2) = colonies evaluation after 2 day of incubation at 37 °C; in light red = small amounts of acid production; in red = acid production; in dark red = considerable amounts of acid production. Average of at least three independent biological replicates.

	Strain	LJ110	GL3	GL4	GL35	GL5	GL6	GL7	GL5*	GL5'	GL6*	GL6'	GL7*	GL7'
	without C-source	normal (1)	small (1)	normal (1)	small (1)	small (1)	small (1)	normal (1)	normal (1)	normal (1)	normal (1)	normal (1)	normal (1)	normal (1)
MacConkey-agar + 1 % C-source (w/v)	Fructose	normal (1)	small (1)	normal (1)	small (1)	normal (1)	small (1)	normal (1)	normal (1)	normal (1)	normal (1)	small (1)	normal (1)	normal (1)
	Glucose	normal (1)	small (1)	small (1)	small (1)	small (1)	small (1)	small (1)	small (1)	small (1)	small (1)	normal (1)	normal (1)	normal (1)
	Glycerol	normal (1)	small (1)	small (1)	small (1)	small (1)	small (1)	small (1)	normal (1)	normal (1)	small (1)	normal (1)	normal (1)	normal (1)
	Maltose	normal (1)	small (1)	small (1)	small (1)	normal (1)	small (1)	small (1)	normal (1)	normal (1)	normal (1)	normal (1)	normal (1)	normal (1)
	Mannitol	normal (1)	small (1)	small (1)	small (1)	small (1)	small (1)	small (1)	small (1)	small (1)	small (1)	small (1)	small (1)	small (1)
	Xylose	normal (1)	small (1)	small (1)	small (1)	small (1)	small (1)	small (1)	normal (1)	normal (1)	normal (1)	normal (1)	normal (1)	normal (1)
	Lactose	normal (1)	small (1)	small (1)	small (1)	small (1)	small (1)	small (1)	small (1)	small (1)	small (1)	small (1)	small (1)	small (1)
	Galactose	normal (1)	small (1)	small (1)	small (1)	small (1)	small (1)	small (1)	small (1)	small (1)	small (1)	small (1)	small (1)	small (1)
	Glucitol	normal (1)	small (1)	small (1)	small (1)	small (1)	small (1)	small (1)	normal (1)	small (1)	small (1)	small (1)	normal (1)	normal (1)
	L-Arabinose	normal (1)	small (1)	small (1)	small (1)	small (1)	small (1)	small (1)	small (1)	small (1)	small (1)	small (1)	small (1)	small (1)

Table 5-7. Growth phenotypes of LJ110/pJF119EH, GL3/pJF119EH and GL3/pJF119*fsaA*^{A129S}. Growth on: LB-agar; MM-agar with 5 % C-source (w/v), 100 μM IPTG and 100 μg/mL Amp; and MacConkey-agar with 1 % C-source (w/v), 100 μM IPTG and 100 μg/mL Amp. All sugars were of D-configuration unless otherwise specified. normal = single colonies with a diameter of ≥ 1 mm; small = colonies with a diameter ≤ 1 mm; (1) = colonies evaluation after 1 day of incubation at 37 °C; (2) = colonies evaluation after 2 day of incubation at 37 °C; in grey= barely visible; - = no growth; in light red = small amounts of acid production; in red = acid production; in dark red = considerable amounts of acid production; * = presence of papillae. Average of at least three independent biological replicates.

Strain		LJ110/pJF119EH	GL3/pJF119EH	GL3/pJF119*fsaA*^{A129S}
LB-agar		normal (1)	small (1)	small (1)
MM-agar + 0.5 % C-source (w/v) + 100 μM IPTG + 100 μg/mL Amp	**without C-source**	-	-	-
	Fructose	small (1)	small (1)	small (2)
	Glucose	normal (1)	-	small (2)*
	Glycerol	small (1)	normal (2)	normal (2)
	D,L-Lactate (pH 7.0)	small (1)	small (2)	small (2)
	Mannitol	normal (1)	-	small (2)*
	Succinate (pH 7.0)	small (1)	small (1)	normal (2)
	Glucitol	small (1)	-	small (2)
	Xylose	small (1)	-	small (2)
	Maltose	small (1)	-	-
	Galactose	small (1)	-	small (2)
	Gluconate (pH 7.0)	normal (1)	small (1)	small (2)
	L-Arabinose	normal (1)	-	small (2)
MacConkey-agar + 1 % C-source (w/v) + 100 μM IPTG + 100 μg/mL Amp	**without C-source**	normal (1)	small (1)	small (1)
	Fructose	normal (1)	small (1)	small (1)
	Glucose	small (1)	small (1)	normal (2)
	Glycerol	normal (1)	small (1)	small (1)
	Maltose	small (1)	small (1)	small (1)
	Mannitol	normal (1)	small (1)	small (1)*
	Xylose	small (1)	small (1)	small (1)
	Lactose	normal (1)	small (1)	small (1)
	Galactose	normal (1)	small (1)	small (1)
	Glucitol	normal (1)	small (1)	small (1)
	L-Arabinose	normal (1)	small (1)	small (1)*

5.2 New arabinose 5-phosphate synthesis pathway

In vitro, FSAA wt can catalyse the retro-aldol cleavage of A5P to GoA and G3P (Garrabou et al., 2009; Lachaux et al., 2019) and also the reverse reaction, the aldol addition of GoA to G3P forming A5P (Sánchez-Moreno et al., 2012a). *In vivo*, cleavage of A5P by FSAA wt has also been reported (Lachaux et al., 2019). Therefore, in *E. coli* FSA could play a role in the synthesis of A5P, the precursor of KDO (for more details about KDO see Introduction Chapter 2.5). This assumption was tested *in vivo* (see Chapters below).

5.2.1 *in vitro* assays with FSAA A129S

First of all, it was of interest to calculate the K_M and V_{max} values for A5P-cleavage of purified His-tagged FSAA A129S. Then, until this point, only data for FSAA wt had been reported (Garrabou et al., 2009; Lachaux et al., 2019).

The K_M and V_{max} values were determined as described in Chapter 4.7.10. Nearly all specific activity values had standard deviations greater than 10 %, due to the low total volume in the cuvette which increased the pipette error. The specific activity (y-axis) was plotted in respect to the corresponding substrate concentration used in the assay (x-axis) (see Figure 5-31).The generated curve allowed the calculation of the K_M and V_{max} values by using the Michaelis-Menten equation.
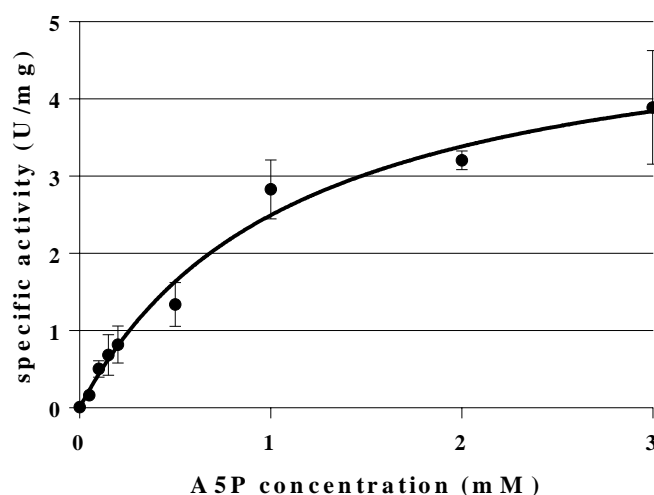
Figure 5-31. Dependence of FSAA A129S initial velocity on A5P concentration. $K_M = 1.1 \pm 0.2$ **mM;** $V_{max} = 5.3 \pm 0.5$ **U/mg;** $k_{cat} = 20$ **s^{-1};** $k_{cat}/K_M = 18$ **s^{-1} mM^{-1}.** K_M **and** V_{max} **values were determined with the software "GraphPad Prism" version 6.01 from GraphPad Software, Inc. (San Diego, USA).** k_{cat} **value was calculated with the equation** $k_{cat} = (V_{max}/V_{max\ F6P}) \times k_{cat\ F6P}$**.**

The majority of the data shown is found under 1 U/mg and, with the highest tested A5P concentration (3 mM), the maximal velocity was nearly reached. Purified His-tagged FSAA A129S had a K_M for A5P of 1.1 ± 0.2 mM and a V_{max} of 5.3 ± 0.5 U/mg. For a comparison of these values with the values reported by other for FSAA wt see Discussion Chapter 6.2.1.

These results demonstrate that FSAA A129S, as already reported for FSAA wt (Garrabou et al., 2009; Lachaux et al., 2019), can also catalyse the cleavage of A5P. Due to the reversibility of the reactions catalyse by FSA (formation and cleavage), it is expected that FSAA A129S can form A5P from the addition of GoA to G3P as well (see Chapter 5.2.2).

5.2.2   *In vitro* synthesis of A5P

To show that FSAA A129S can synthesise A5P from G3P and GoA *in vitro*, the A5P synthesis reaction was performed as explained in Chapter 4.7.11 with two independent runs. The initial DHAP concentration was of 250 mM and a total concentration of 200 mM GoA was added to the mixture. Both times, the end concentrations of A5P, DHAP and G3P were determined (see Chapter 4.8.3 for more details): 63 ± 1 mM A5P; 2 ± 0 mM DHAP; and 32 ± 1 mM G3P. The synthesis yield reached was 32 %. This low yield could be explained by the loss of GoA due to its cross-aldol addition to threose (see Appendix Chapter 9.10). The presence of A5P was also confirmed by TLC as described in Chapter 4.8.2. When compared to the A5P standards, the synthesised A5P sample had around 50 mM A5P (see Figure 5-32), which corresponded to the same magnitude as the concentration determined enzymatically.
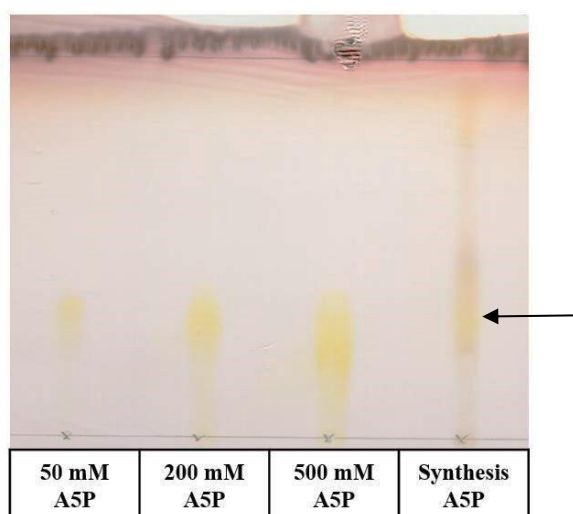
Figure 5-32. Thin layer chromatography with A5P standards and the synthesised A5P. Solvent mixture: EtOAc/MeOH/H$_2$O/HOAc (5:2:1.4:0.4) (Wen et al., 2016). 1 µl was spotted per sample. - 40 % contrast.

5.2.3   Construction of BW25113 Δ*gutQ* Δ*kdsD*::*kan*

After successfully synthesising A5P *in vitro* with FSAA A129S (see Chapter 5.2.2), a strain auxotroph for A5P needed to be constructed. With an A5P auxotroph strain, it might be possible to show that the synthesis of A5P with FSAA A129S also works *in vivo*. Meredith and Woodard (2005) reported an *E. coli* strain missing the genes that code for the A5P isomerases (API), *gutQ* and *kdsD*, to be A5P auxotroph. Therefore, the *E. coli* strain BW25113 Δ*gutQ* Δ*kdsD*::*kan* was constructed for the present work (see Table 4-8 for strain details and Chapter 4.6.12 for construction details). Selection took place on LB-agar with 100 µM A5P and 10 µM G6P (G6P is required to induce UhpT). As displayed in Figure 5-33, this double mutant strain should need external A5P to produce its KDO and be able to grow on LB or MOPS-MM with 28 mM glucose, This was examined in Chapter 5.2.4.
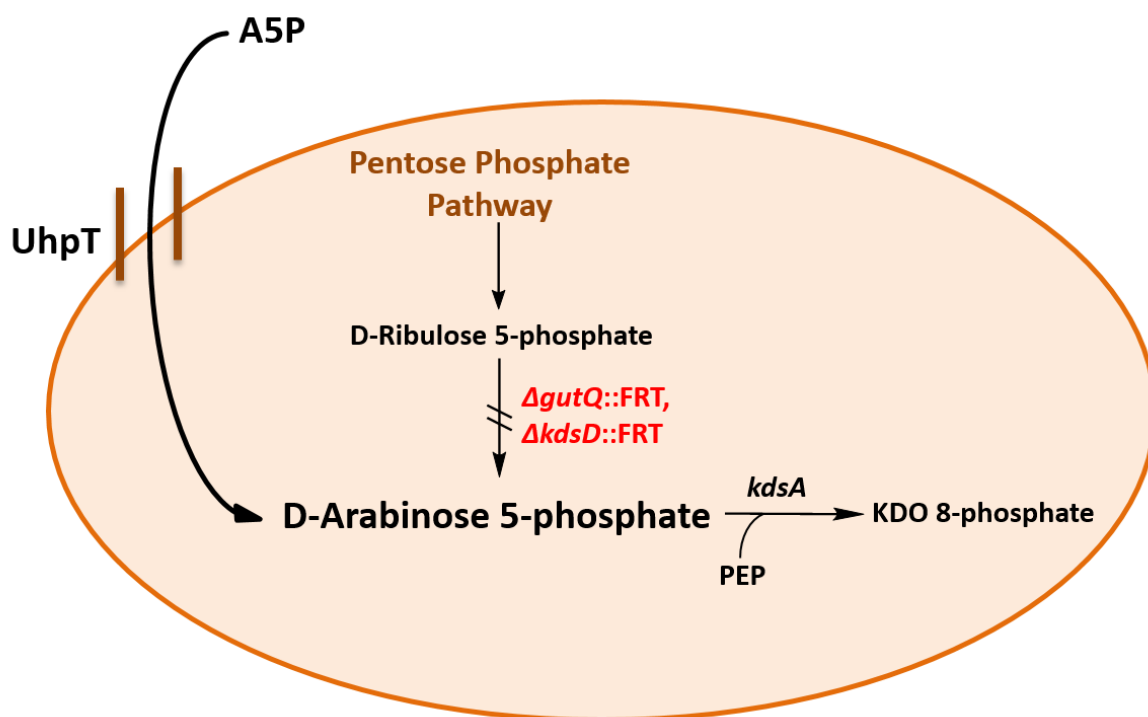
Figure 5-33. Schematic of the A5P auxotroph strain BW25113 Δ*gutQ* Δ*kdsD*, a strain deficient in A5P isomerases (KdsD and GutQ). KDO (2-keto-3-deoxymanno-octulosonic acid), PEP (phosphoenolpyruvate), UhpT (hexose phosphate transporter), *kdsA* (KDO 8-phosphate synthetase), FRT (FLP recognition site).

5.2.4   "Bioassay" with external A5P

A "Bioassay" was carried out to evaluate to which extent the constructed BW25113 Δ*gutQ* Δ*kdsD*::*kan* strain (see Chapter 5.2.4) was dependent on extracellular A5P.

In this "bioassay" it could also be assessed which A5P concentration this mutant strain needs to grow and achieve its maximal $OD_{600\,nm}$ on MOPS-MM with 28 mM glucose. The assay was performed as described in Chapter 4.5.4.

As can be seen in Figure 5-34, as little as 5 µM A5P enabled BW25113 $\Delta gutQ$ $\Delta kdsD$::*kan* to grow on MOPS-MM containing 28 mM glucose, while no addition of A5P in the medium did not lead to growth (see Appendix Chapter 9.9). A positive correlation was found between the initial concentration of A5P available in the medium and the maximal $OD_{600\,nm}$ reached by BW25113 $\Delta gutQ$ $\Delta kdsD$::*kan* in this medium. With increasing initial A5P concentrations, the maximal $OD_{600\,nm}$ increased as well. BW25113 $\Delta gutQ$ $\Delta kdsD$::*kan* reached its maximal $OD_{600\,nm}$ (3.4 ± 0.3) at low concentrations of A5P (≥ 60 µM). Furthermore, it seems that the absence or presence of external A5P has an impact on cell length (see Appendix Chapter 9.6).
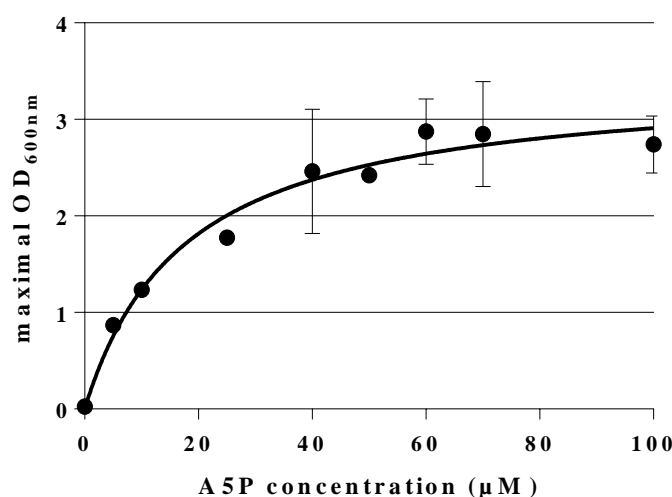
Figure 5-34. Correlation between the maximal $OD_{600\,nm}$ reached by BW25113 $\Delta gutQ$ $\Delta kdsD$::*kan* on different A5P concentrations. Growth took place on MOPS-MM with 28 mM glucose and at 37 °C and 200 rpm. $K_S = 17.7 \pm 4.5$ µM; max. $OD_{600\,nm} = 3.4 \pm 0.3$ determined with the software "GraphPad Prism" version 6.01 from GraphPad Software, Inc. (San Diego, USA). For details see Chapter 4.5.4.

5.2.5   Study of LPS integrity

Normally, the outer membrane protects the cell against lysozyme hydrolysis (see Discussion), but with less or without LPS, lysozyme might be able to lyse the cell more easily (Nikaido and Vaara, 1985) and liberate internal proteins. A correlation between the external concentration of A5P available to the BW25113 $\Delta gutQ$ $\Delta kdsD$::*kan* cells and the integrity of their LPS might explain why BW25113 $\Delta gutQ$ $\Delta kdsD$::*kan* needs more than 60 µM external A5P to reach its maximal $OD_{600\,nm}$ (see Figure 5-34 and Appendix Figure 9-9). Therefore, the indirect LPS

integrity test described in Chapter 4.7.12 was performed with BW25113 Δ*gutQ* Δ*kdsD*::*kan* cells to study if the shortage of A5P can endanger the integrity of the cell membrane.

As shown in Figure 5-35, when lower A5P concentrations were available during growth of BW25113 Δ*gutQ* Δ*kdsD*::*kan*, the relative protein concentration in the supernatant after treatment with lysozyme was higher than in the presence of higher A5P concentrations. Similarly, when the lysozyme activity used for treatment was higher, the relative protein concentration measured in the supernatant also increased. The difference was more significant when the mutant strain grew in the presence of lower external A5P concentrations (up to 20 µM A5P).
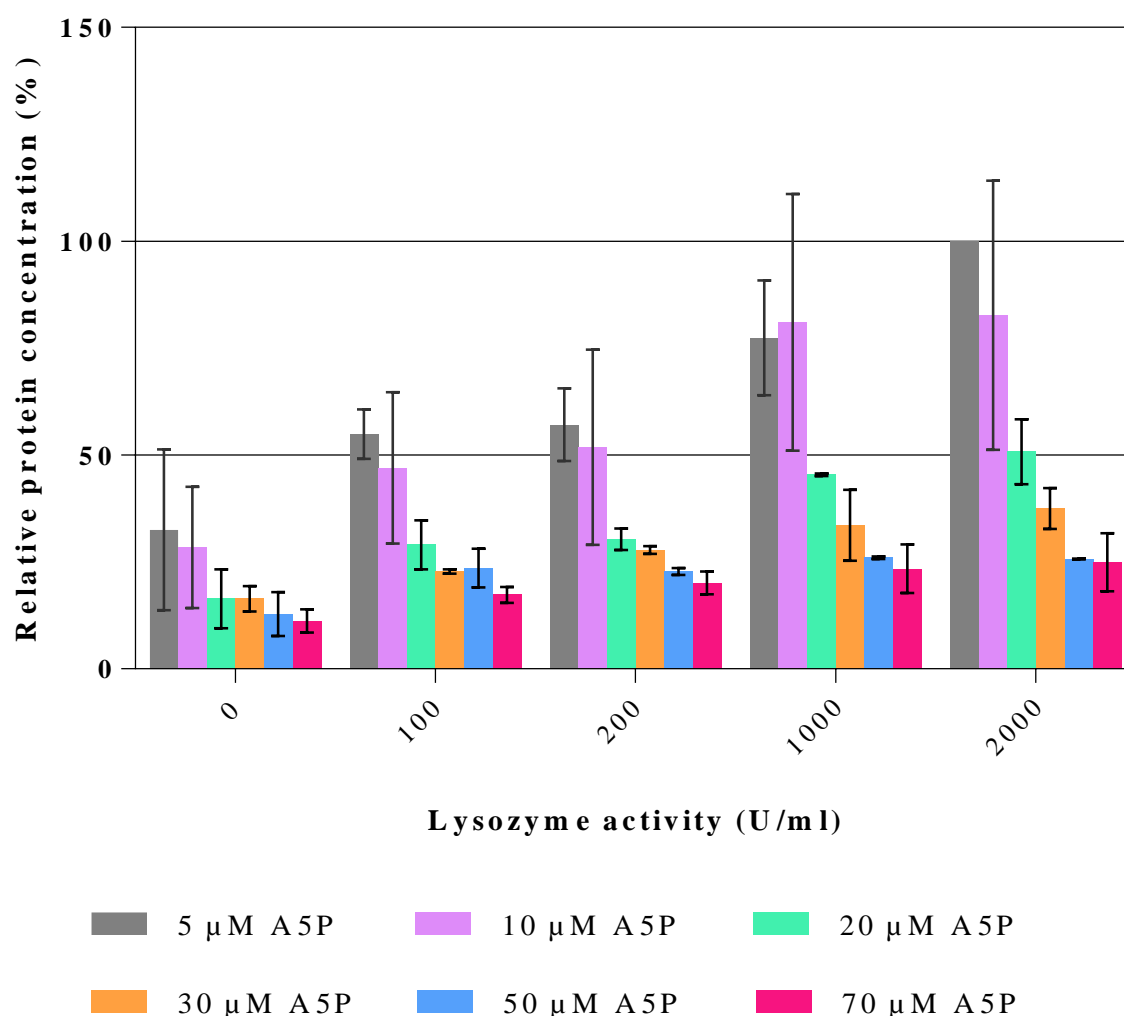
Figure 5-35. Correlation between A5P concentration (µM), lysozyme concentration (U/mL) and relative protein concentration (%) in the supernatant of BW25113 Δ*gutQ* Δ*kdsD*::*kan*. Averages of two independent biological replicates, each with two technical replicates.

5.2.6   *In vivo* synthesis of A5P

As previously reported, FSAA wt can cleave A5P *in vitro* (Garrabou et al., 2009) and *in vivo* (Lachaux et al., 2019), and form A5P from glyceraldehyde 3-phosphate (G3P) and glycolaldehyde (GoA) *in vitro* (Sánchez-Moreno et al., 2012a). FSAA A129S can also catalyse both reactions *in vitro* (see Chapters 5.2.1 and 5.2.2). Therefore, it was studied, if a plasmid-based expression of the *fsaA* or *fsaA^A129S* genes might establish a bypass reaction for the formation of A5P from intracellular G3P (from cell metabolism) and external GoA in the API-deficient strain BW25113 Δ*gutQ* Δ*kdsD*::*kan*, as displayed in Figure 5-36. The medium chosen for growth was MOPS-MM containing 28 mM glucose (see Appendix Chapter 9.9), 100 µM IPTG and, if necessary, 100 µg/mL Amp and/or 50 µg/mL Kan. External GoA was added to the medium to provide FSAA wt and FSAA A129S with a donor. The acceptor G3P was assumed to be provided by the cell from glycolysis. The plasmid-borne *fsaA* and *fsaA^A129S* genes were under the control of the P*tac* promoter (IPTG-inducible) and recombinantly expressed from pJF119*fsaA* and pJF119*fsaA^A129S* in BW25113 Δ*gutQ* Δ*kdsD*::*kan* (for more details on the plasmids see Table 4-7). A positive control, BW25113 (wild type), and two negative controls, BW25113 Δ*gutQ* Δ*kdsD*::*kan* and BW25113 Δ*gutQ* Δ*kdsD*::*kan*/pJF119EH, were carried out.
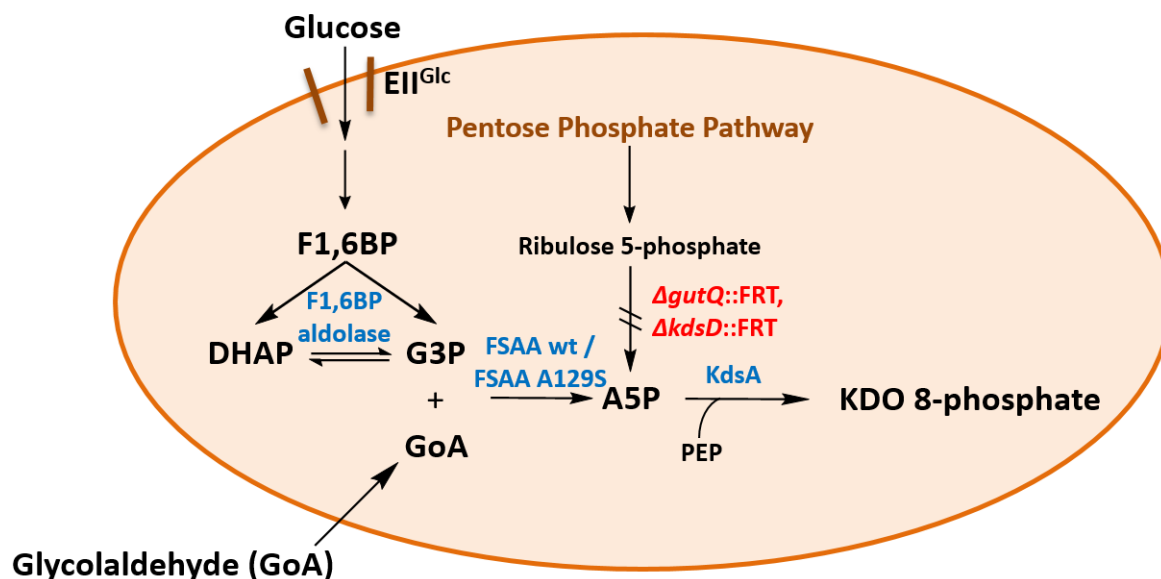
Figure 5-36. Schematic of the pathway for the *in vivo* synthesis of A5P in BW25113 Δ*gutQ* Δ*kdsD*::*kan*. It has to be noted that FSAA wt and FSAA A129S can catalyse a second reaction in this pathway: the cleavage of F6P to DHA and G3P. Therefore, not all F6P might be phosphorylated to F1,6BP. A5P (arabinose 5-phosphate), DHAP (dihydroxyacetone phosphate), EII^Glc (glucose-specific enzyme II of the PTS), F1,6BP (fructose 1,6-bisphosphate), FSA (fructose 6-phosphate aldolase), G3P (glyceraldehyde 3-phosphate), GoA (glycolaldehyde), KDO (2-keto-3-deoxymanno-octulosonic acid), KdsA (KDO 8-phosphate synthetase), PEP (phosphoenolpyruvate).

Addition of various concentrations of GoA into the medium allowed BW25113 $\Delta gutQ$ $\Delta kdsD$::*kan* carrying either pJF119*fsaA* or pJF119*fsaA^{A129S}* to grow (see Figure 5-37). However, in the presence of GoA, but without the external addition of A5P, growth of BW25113 $\Delta gutQ$ $\Delta kdsD$::*kan* and BW25113 $\Delta gutQ$ $\Delta kdsD$::*kan*/pJF119EH on MOPS-MM with glucose was completely impaired.

It was taken into consideration that the expression of only one copy of the *fsaA^{A129S}* gene in the chromosome could be sufficient to complement the APIs deficient strain BW25113 $\Delta gutQ$ $\Delta kdsD$::*kan*. The antibiotic resistance cassette was removed from this strain to allow the integration of *fsaA^{A129S}* under the control of P*tac* in the ribose-operon. The constructed strain, BW25113 $\Delta gutQ$ $\Delta kdsD$ $\Delta rbsK$::P*tac*-*fsaA^{A129S}*, also showed growth in the presence of GoA and without the external addition of A5P.

It was also considered that the other FSA protein encoded in the *E. coli* chromosome, FSAB (see Chapter 2.4.3), might also catalyse the aldol addition from GoA to G3P to form A5P. This reaction has never been reported so far for FSAB *in* vitro nor *in vivo*. BW25113 $\Delta gutQ$ $\Delta kdsD$ cells were transformed with pJF119*fsaB* (see Table 4-7 for plasmid details). BW25113 $\Delta gutQ$ $\Delta kdsD$/pJF119*fsaB* was able to grow with the external addition of GoA into the medium.

As displayed in Figure 5-37, BW25113 deficient in APIs (*gutQ*, *kdsD*) could grow on MOPS-MM containing 28 mM glucose, 100 µM IPTG and different concentrations of GoA when bearing pJF119*fsaA*, pJF119*fsaA^{A129S}*, pJF119*fsaB*, or a chromosomally integrated P*tac*-*fsaA^{A129S}* in the ribose-operon. In all four cases, the same positive correlation was shown between the GoA concentration present in the medium and the maximal $OD_{600\,nm}$ reached by these strains. It should be noted that even without GoA, a maximal $OD_{600\,nm}$ value above one was reached by all of them (see Discussion Chapter 6.2.3).

Thus, it was shown that FSA can be used to provide a novel route to A5P *in vivo*.

(a)

(b)

(c)

(d)
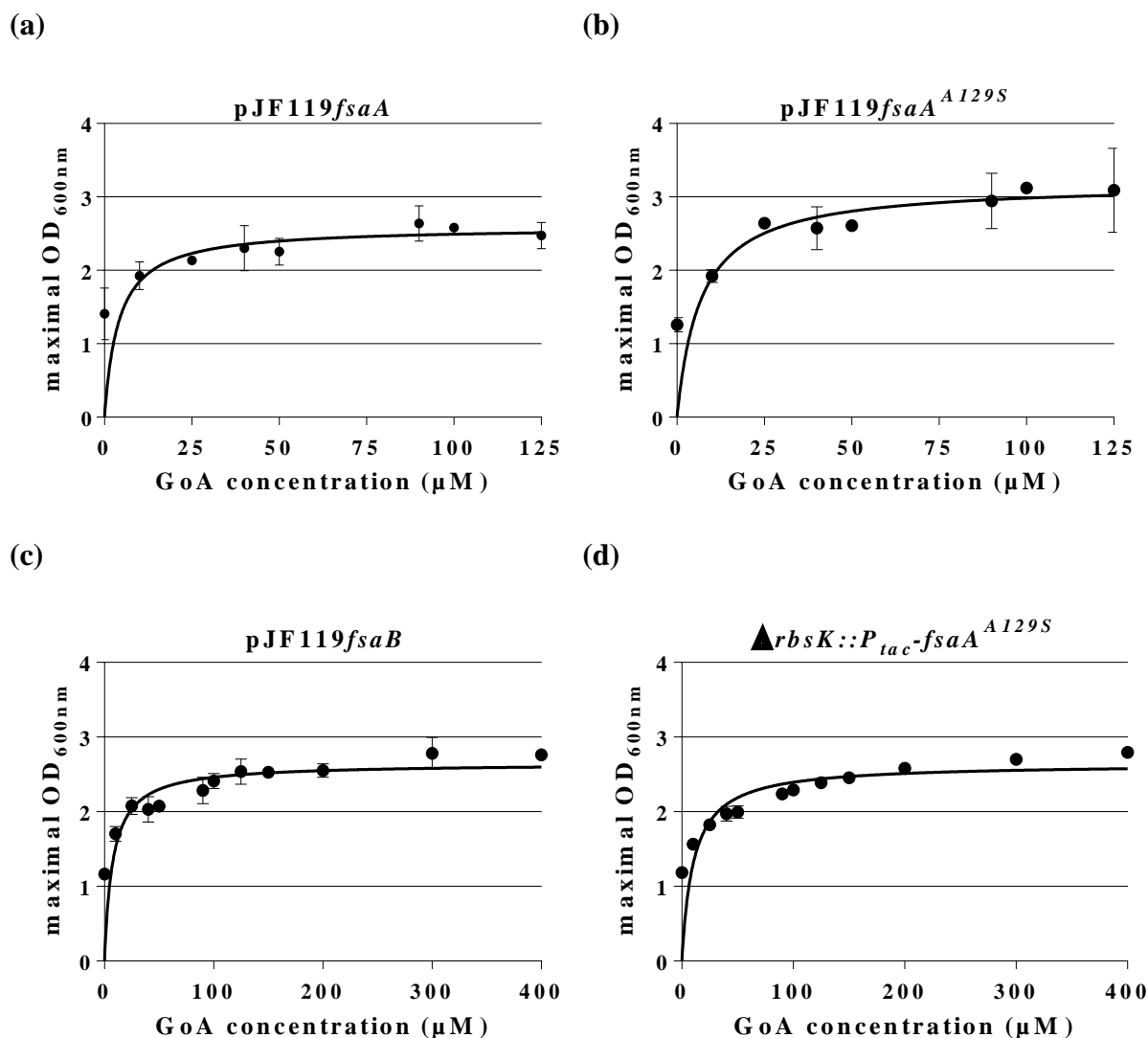
Figure 5-37. Dose-response curves for GoA. Growth on MOPS-MM containing 28 mM glucose, 100 μM IPTG and, if necessary, 50 μg/mL Kan or/and 100 μg/mL Amp. (a) BW25113 Δ*gutQ* Δ*kdsD*::*kan*/pJF119*fsaA* (K_S = 4.1 ± 3.6; max. $OD_{600 nm}$ = 2.6 ± 0.3). (b) BW25113 Δ*gutQ* Δ*kdsD*::*kan*/pJF119*fsaA*[A129S] (K_S = 6.8 ± 3.8; max. $OD_{600 nm}$ = 3.2 ± 0.3). (c) BW25113 Δ*gutQ* Δ*kdsD*/pJF119*fsaB* (K_S = 7.5 ± 3.0; max. $OD_{600 nm}$ = 2.6 ± 0.1). (d) BW25113 Δ*gutQ* Δ*kdsD* Δ*rbsK*::P$_{tac}$-*fsaA*[A129S] (K_S = 10.4 ± 3.8; $OD_{600nm max,}$ = 2.6 ± 0.1). At 37 °C and 200 rpm. Average of two independent biological replicates. Note that the GoA concentration axis from the graphs above is different than the one from the graphs below. For details see Chapter 4.5.4.

5.3   Study of the native promoters of the genes *fsaA* and *fsaB* (P*fsaA* and P*fsaB*)

5.3.1   Strength analysis of the promoters

It has not yet been reported under which conditions and/or in the presence of which molecules, the promoters of the *fsaA* and *fsaB* genes (P*fsaA* and P*fsaB*) are activated. This information might help to find the physiological function of FSA in *E. coli*. Therefore, the *E. coli* LJ110 reporter

strains P_{fsaA}-*lacZYA* and P_{fsaB}-*lacZYA* (see Table 4-8) were constructed to test the strength of the promoters of P_{fsaA} and P_{fsaB} under different conditions by measuring β-galactosidase activities. If the promoter is active, β-galactosidase activity can be detected.

The integration of P_{fsaA}-*lacZYA* and P_{fsaB}-*lacZYA* in LJ110 ΔP_{lac}-*lacZα*::FRT-*kan*-FRT was performed as described in Chapter 4.6.11. The integrations were verified by colony PCR and by sequence analysis of the integrated region (see Chapters 4.6.4 and 4.6.15). Both strains were also streaked on LB-agar with 0.008 % X-gal to screen for expression of *lacZ*. Two controls were performed: LJ110, which has a LacZ$^+$ phenotype; and LJ110 ΔP_{lac}-*lacZα*::FRT-*kan*-FRT, which is LacZ$^-$. As seen in Figure 5-38, the LJ110 reporter strains with P_{fsaA}-*lacZYA* and P_{fsaB}-*lacZYA* had both an active promoter (blue colonies), and P_{fsaA}-*lacZYA* showed a slightly stronger intensity than P_{fsaB}-*lacZYA*.

For the strength analysis of the promoters, the reporter strains were grown on MM containing different C-sources (0.5 % w/v) and in the presence of four different substrates for FSA (HA, DHA, GoA and GA). After 24 h incubation at 200 rpm and 37 °C, the β-galactosidase assay was performed as described in Chapter 4.7.9.

None of these reporter strains could grow during the first 10 h incubation when 10 mM DHA were present in MM with 28 mM glucose. In the presence of 15 mM DHA they were not able to grow at all. Furthermore, their growth was also inhibited when 5 mM GoA or more were available in the MM containing also 28 mM glucose.

As expected, the β-galactosidase activity measured for both promoters on glucose (see Figure 5-39) is significantly low compared to the activity measured for P_{lac} (3155 ± 117 U/OD$_{600\,nm}$ at an OD$_{600\,nm}$ of 0.4 in the presence of 1 mM IPTG; Trachtmann, personal communication). Especially P_{fsaB} with 5.3 ± 1.7 U/OD$_{600\,nm}$ can be considered a weak promoter. On glucose, P_{fsaA} is with 76.7 ± 10.4 U/OD$_{600\,nm}$ 15 times more active than P_{fsaB}.
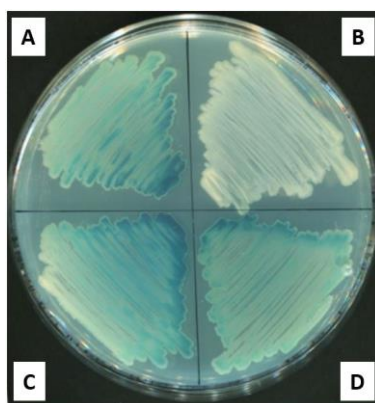
Figure 5-38. Screen of the expression of *lacZ* in different reporter strains. A. LJ110; B. LJ110 ΔP$_{lac}$-*lacZα*::FRT-*kan*-FRT, C. LJ110 FRT-*cat*-FRT-P$_{fsaA}$-*lacZYA*, D. LJ110 FRT-*cat*-FRT-P$_{fsaB}$-*lacZYA*. LB-agar plate with 0.008 % X-gal.
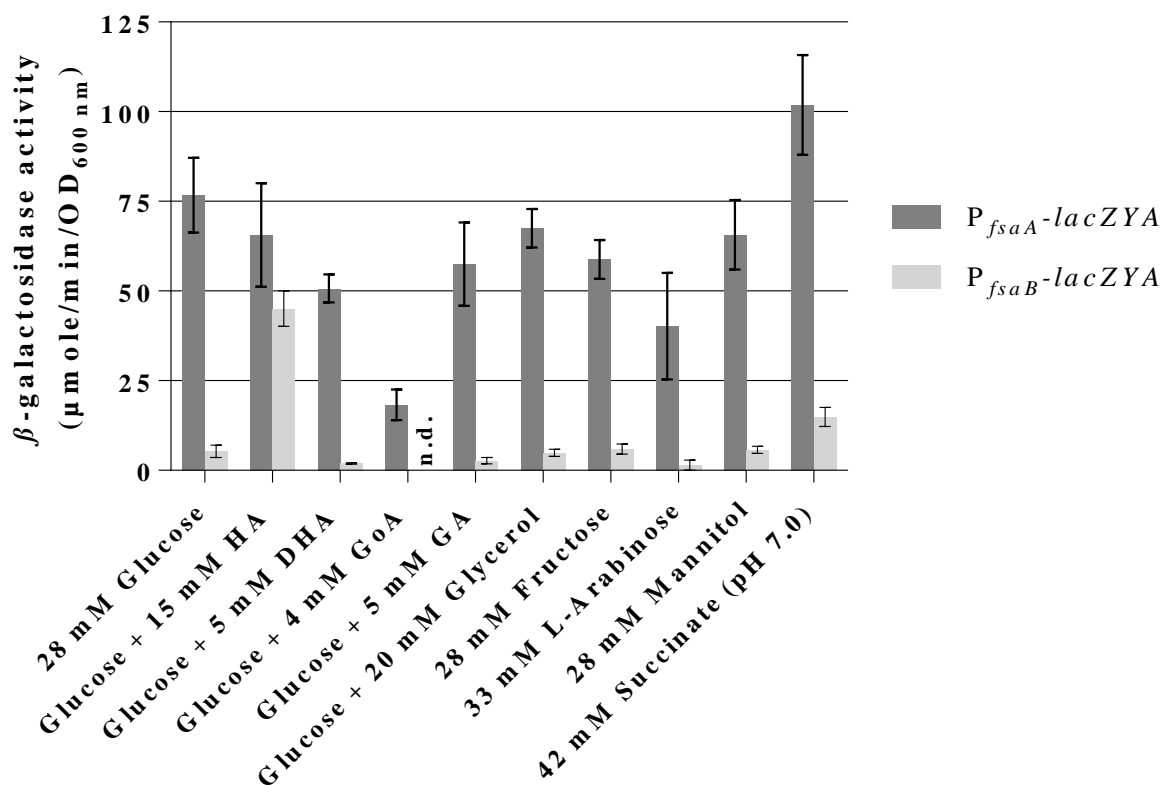
Figure 5-39. *β*-galactosidase activity (µmole/min/OD$_{600\ nm}$) in LJ110 reporter strains with a P$_{fsa*}$-*lac*ZYA fusion after growth on different C-sources. Average of three independent biological replicates, each with three technical replicates. n.d. = not detected.

As observed in Figure 5-39, the P$_{fsaA}$-*lacZYA* reporter strain showed a 1.5-fold, 4.2-fold and 1.9-fold lower *β*-galactosidase activity in the presence of DHA, GoA or L-arabinose, respectively, in comparison with only growth on glucose. On the other hand, in the presence of succinate (pH 7.0) the *β*-galactosidase activity increased by a factor of 1.3. The *β*-galactosidase activity in the P$_{fsaB}$-*lacZYA* reporter strain was enhanced by 8.5 and 2.8-fold in the presence of HA or succinate (pH 7.0), respectively, compared to the activity measured in the presence of only glucose. In the presence of all other C-sources, no differences were observed in the strength of neither of the promoters. In general, P$_{fsaA}$ showed a higher *β*-galactosidase activity than P$_{fsaB}$. These results indicate that if FSAA or FSAB are produced in *E. coli* LJ110 due to the activation of P$_{fsaA}$ or P$_{fsaB}$, their concentration might be so low, that their activity in the cell could be considered insignificant (see Discussion).

5.3.2   Mutant P$_{fsaB}$-*lacZ* fusion reporter strain

To evaluate if any mutation in the sequence of the promoters P$_{fsaA}$ and P$_{fsaB}$ could improve their strength, the P$_{fsa*}$-*lacZYA* reporter strains (P$_{fsaA}$-*lacZYA* and P$_{fsaB}$-*lacZYA*) were subject to

growth selection pressure (see Figure 5-40) and the colonies with the best growth (significant *lacZ* expression resulting in growth on lactose) were selected as described in Chapter 4.5.6 and analysed.
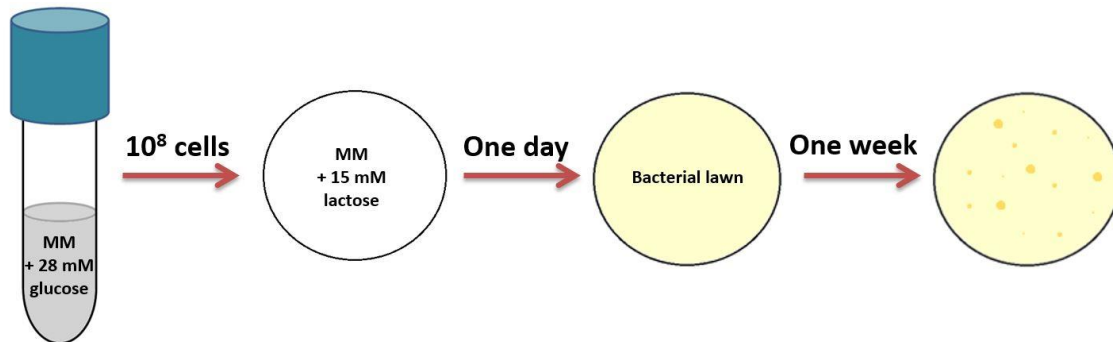
Figure 5-40. Selection approach of evolved P*fsa**-*lacZYA* strains with a better *β*-galactosidase activity as their parent strains.

It was not possible to isolate a P*fsaA*-*lacZYA* mutant reporter strain with a better expression of *lacZ*. However, it was possible to isolate a mutant reporter strain from P*fsaB*-*lacZYA* with an increased expression of *lacZ*. Two tests were performed to verify that the mutant reporter strain had a stronger promoter than the P*fsaB*-*lacZYA* reporter strain: hydrolysis of X-gal and *β*-galactosidase assay. On LB-agar containing 0.008 % X-gal, the P*fsaB'(mutant)*-*lacZYA* reporter strain presented a stronger intensity than the P*fsaB*-*lacZYA* reporter strain (see Figure 5-41). A difference in the *β*-galactosidase activity of approximately 3-fold between P*fsaB* and P*fsaB'(mutant)* was measured, and a nearly 8-fold increase in activity was achieved in both promoters with the addition of 15 mM HA to the MM containing 28 mM glucose (see Figure 5-42).
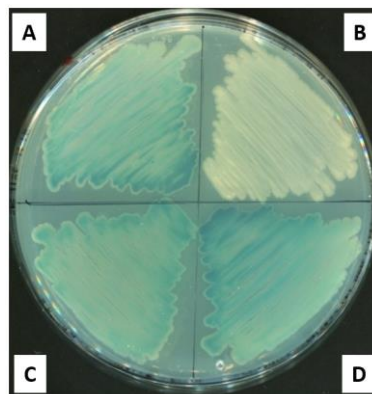
Figure 5-41. Screen of the expression of *lacZ* after adaptive laboratory evolution. A. LJ110; B. LJ110 ΔP*lac*-*lacZα*::FRT-*kan*-FRT,   C. LJ110 FRT-*cat*-FRT-P*fsaB*-*lacZYA*,   D. LJ110 FRT-*cat*-FRT-P*fsaB'(mutant)*-*lacZYA*. LB-agar plate with 0.008 % X-gal.

The promoter regions of P$_{fsaB}$-*lacZYA* and P$_{fsaB'(mutant)}$-*lacZYA* were sequenced. Both sequences were aligned with the software "ApE – A plasmid Edition" (Version 2.0.52; Utah, USA) (see Appendix Chapter 9.1.2). In the sequence of P$_{fsaB'(mutant)}$, six bases were missing upstream of the promoter compared to the sequence of P$_{fsaB}$ (see Appendix Figure 9-3).

To study which consequences this change in the promoter region had, the growth behaviour of the mutant reporter strain was analysed on MM containing 15 mM lactose in the presence or absence of 15 mM HA and compared to the parent strain (two independent biological replicates). A control was performed with the strain LJ110 ΔP$_{lac}$-*lacZα*::FRT-*kan*-FRT. Only when HA was present, it was possible for the P$_{fsaB}$-*lacZYA* reporter strain to grow on lactose $(0.29 \pm 0.01 \text{ h}^{-1})$. On the other hand, the P$_{fsaB'(mutant)}$-*lacZYA* reporter strain did not require HA to grow on lactose $(0.13 \pm 0.04 \text{ h}^{-1})$. However, with HA in the medium, the P$_{fsaB'(mutant)}$-*lacZYA* reporter strain had an increased growth rate on lactose $(0.43 \pm 0.01 \text{ h}^{-1})$. As expected, the control strain LJ110 ΔP$_{lac}$-*lacZα*::FRT-*kan*-FRT showed no growth on lactose. These results indicate that the P$_{fsaB'(mutant)}$ is able to express enough *lacZ* to support growth on lactose, even without the presence of HA.
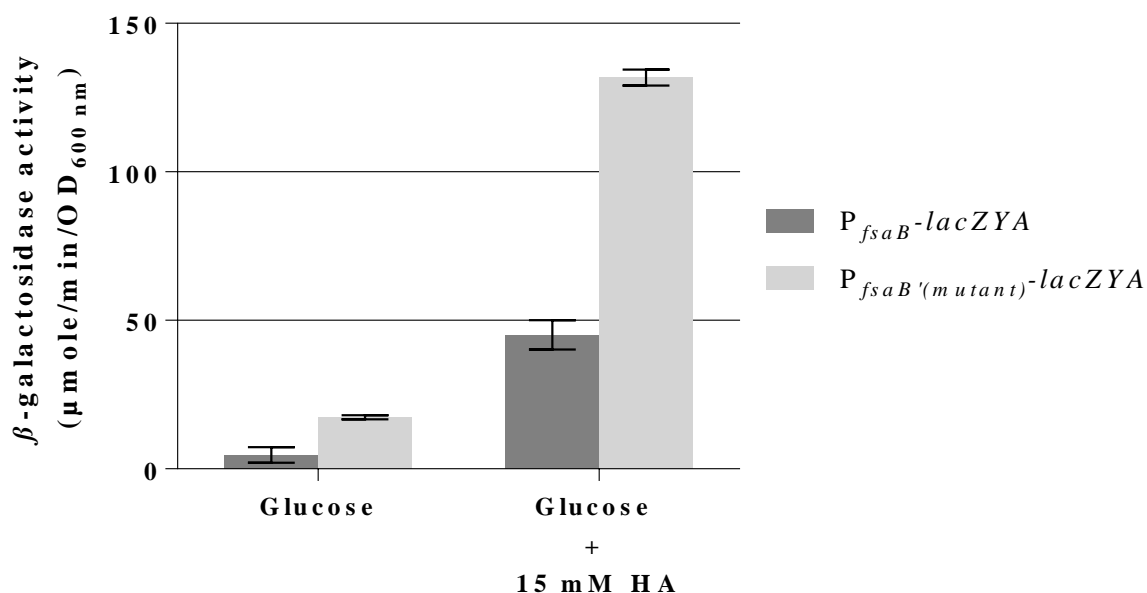
Figure 5-42. *β*-galactosidase activity (µmole/min/OD$_{600 \text{ nm}}$) in the reporter strains P$_{fsaB}$-*lacZYA* and P$_{fsaB'(mutant)}$-*lacZYA*. 100 µL overnight culture after growth on MM containing 28 mM glucose and in the absence or the presence of 15 mM HA. Average of two independent biological replicates, each with three technical replicates.

6   Discussion

6.1   Novel bypass for glucose degradation

6.1.1   Characterisation of an *Escherichia coli* triple mutant (*Δzwf ΔpfkB ΔpfkA*)

In this work, the genes *zwf*, *pfkB* and *pfkA* were successively deleted from an *E. coli* K-12 strain (Guitart Font and Sprenger, 2020). Therefore, this glucose-negative *E. coli* mutant strain, GL3, had a disrupted glucose depletion pathway as a result of the missing phosphofructokinase enzymes, PfkA and PfkB, in glycolysis and glucose 6-phosphate dehydrogenase (G6P DH) in the pentose phosphate pathway (PPP). Similar triple mutants to GL3 have been reported by other groups. Gleizer et al. (2019) deleted the *zwf*, *pfkA* and *pfkB* genes in the *E. coli* strain BW25113. In this mutant strain growth on xylose was impaired, but it could grow on glycerol and pyruvate. No information on glucose as sole C-source was provided for this strain. After the publication in 2020 of most of the results presented here (Guitart Font and Sprenger, 2020), Wang et al. (2022) claimed that the triple mutant *E. coli* strain MG1655(DE3) *Δzwf ΔpfkA ΔpfkB* was able to grow on glucose as sole C-source. Their justification for such a phenotype was that it might only be possible due to the presence of λ DE3. λ DE3 can modify the regulation and, therefore, also the expression of the genes of the host. Therefore, this observation is not applicable to GL3. Satanowski et al. (2020) also published information about an *E. coli* mutant strain missing the genes *zwf*, *pfkA* and *pfkB*, and also *fsaA*, *fsaB*, and *fruK*. But growth of this strain was only tested on xylose, which was negative, as it was shown for GL3 (see Table 5-5). It is known that the deletion of the *zwf* gene in *E. coli* minimally impacts growth on glucose (Fraenkel, 1968; Fischer and Sauer, 2003; Zhao et al., 2004). However, the deletion of the *pfkA* gene significantly affects the consumption of glucose as sole C-source due to a longer lag-phase and a diminished growth rate compared to the wild type cell (Roehl and Vinopal, 1976; Fischer and Sauer, 2003; Hollinshead et al., 2016). The additional deletion of *pfkB* to a *pfkA* mutant strain completely impairs its growth on glucose (Daldal, 1983; Lovingshimer et al., 2006; Wang et al., 2013), whereas the growth of a *Δzwf ΔpfkB* mutant strain is only slightly reduced (Brockman and Prather, 2015). Roehl and Vinopal (1976) reported that a *pfkA* deficient strain also shows impaired growth on sugars entering glycolysis at or above F6P, such as galactose, and transported in the cell by the PTS, such as mannitol. However, growth on sugars entering below F6P, such as fructose and glycerol, was not affected. These were also reported for a strain completely deficient in phosphofructokinase activity (Daldal, 1983).
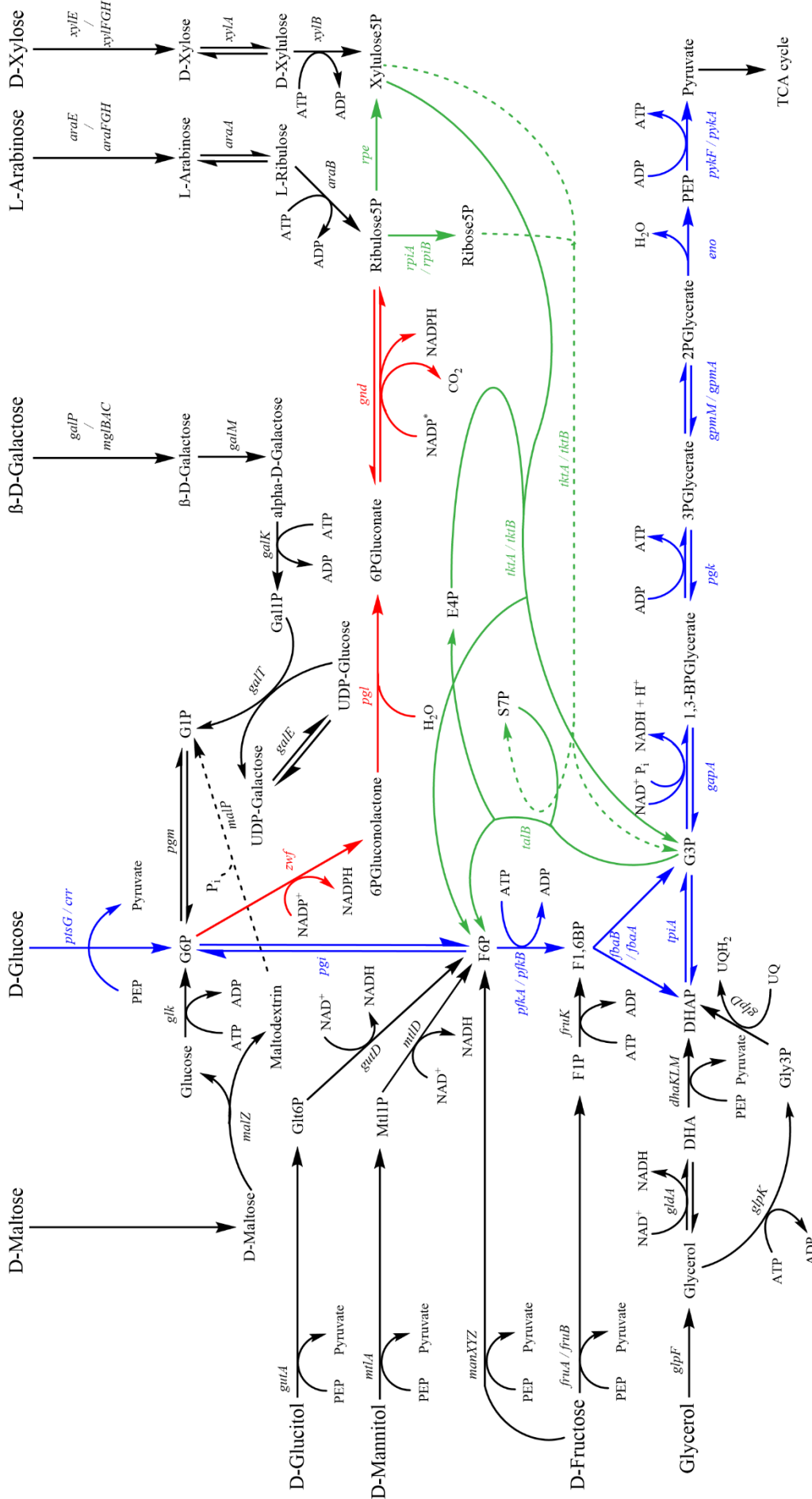
Figure 6-1. Metabolism of different C-sources in *E. coli*. Glycolysis in blue, oxidative branch of PPP in red and non-oxidative branch of PPP in green. Transport with the transporters MglBAC, AraFGH and XylFGH encoded by *mglBAC*, *araFGH* and *xylFGH*, respectively, requires 1 molecule of ATP. Figure modified after Weickert and Adhya (1993), Neidhardt (1996), Kornberg (2001), Mayer and Boos (2005), Fuchs (2007), Luo et al. (2014), Stincone et al. (2015).

As expected, growth of GL3 on C-sources that exclusively enter glycolysis above or at the level of fructose 6-phosphate (F6P), such as glucose, mannitol, glucitol, xylose, maltose or galactose, was impaired (see Figure 6-1). Growth of GL3 on sugars that can lead to an intracellular accumulation of sugar phosphates was partially or totally impaired. Growth on glycerol was possible because of the formation of dihydroxyacetone phosphate (DHAP) and its further isomerisation to glyceraldehyde 3-phosphate (G3P).

Fructose was determined as a good substrate for GL3. *E. coli* can transport and metabolise fructose through two pathways: using the fructose PTS (FruAB) to yield F1P, which enters glycolysis at F1,6BP; or using the mannose PTS (ManXYZ) to enter at F6P (Kornberg, 2001; Luo et al., 2014). Therefore, GL3 could grow on fructose probably by using the fructose PTS pathway, instead of the mannose PTS (see Figure 5-3). An *E. coli* deficient in both PfkA and G6P DH activities was reported to grew on fructose at the same rate than the wild type strain, but its growth on glucose, G6P and F6P was impaired (Kornberg and Smith, 1970). However, GL3 has a doubling time 2-fold higher than LJ110 (see Appendix Table 9-1). This might be a result of the missing PfkB activity in GL3. Pfk deficient strains are known to increase the induction of *uspA* gene, which codes for UspA, a universal stress protein (Persson et al, 2007). Richards et al. (2013) claimed that accumulation of intracellular G6P may cause growth arrest as a response to sugar phosphate stress or depletion of glycolytic intermediates. In their opinion accumulation of sugar phosphates is non-toxic for *E.* coli, but the decrease of glycolytic intermediates is the reason for the glucose-phosphate stress. This would correlate with the report from Shiue et al. (2015) that showed that a block in glycolysis (Δ*pgi*) and PPP (Δ*zwf*) completely inhibited the growth of *E. coli* on glucose. Under glucose-phosphate stress conditions, the sRNA SgrS is transcribed (Vanderpool and Gottesman, 2004) and the protein SgrT is produced (Wadler and Vanderpool, 2007). While SgrS inhibits the translation of *ptsG* mRNA (Maki et al., 2008) and *manXYZ* mRNA (Rice and Vanderpool, 2011), SgrT inhibits the glucose transport by interacting with PtsG (Raina and Storz, 2017; see Introduction Chapter 2.2.2). Accumulation of intracellular G6P and F6P was confirmed in GL3 in the presence of glucose as sole C-source, while none of these metabolites could be detected in LJ110 (see Figure 5-4 in Chapter 5.1.1) due to the low sensitivity of the method used (enzymatic quantification). The lowest detectable concentration for G6P and F6P was 0.2 mM. Despite the low precision of the method used, it can be concluded that the impaired growth of GL3 on glucose might be a consequence of the accumulation of these two sugar phosphates.

6.1.2 Expression of the genes *fsaA* and *fsaA^{A129S}* in GL3

It was hypothesised that the expression of the latent genes *fsaA* or *fsaB* that encode for FSA might be activated in GL3 and, as a consequence, growth on glucose might be restored (Guitart Font and Sprenger, 2020). This would not be the first example of microbial cells that activate other native pathways to overcome disturbances of the central metabolism pathways (Fong et al., 2006; Shimizu and Matsuoka, 2019). Depending on the need of the cell for a specific protein activity and the metabolic burden that the production of this protein will have on the cell, the expression level of each protein can vary (Li et al., 2014). Through a flux balance analysis, the FSAA wt bypass was already identified by Riemer et al. (2013) as a pathway in which high fluxes might be possible and the production of DHA takes place in considerable rates. Yet, no glucose-positive GL3 mutants were detected after prolonged incubation on MM-agar with glucose as sole C-source (Guitart Font and Sprenger, 2020). Thus, to evaluate if FSA would be sufficient to open a glycolytic bypass in GL3, the plasmid-based expression of the *E. coli fsaA* gene and its mutant allele *fsaA^{A129S}* were tested in GL3. While FSAA wt was produced as it could be seen by SDS-PAGE and was catalytically active in activity assays, its presence in GL3 did not restore growth on glucose, even after an extended incubation time of 96 h. GL3 only overcame the block on glycolysis and grew on glucose, when *fsaA^{A129S}* was expressed. These results might be explained by the increased affinity, catalytic efficiency and specific activity that FSAA A129S has for F6P when compared to FSAA wt (Schürmann, 2001; Castillo et al., 2010). According to Bennett et al. (2009) and Park et al. (2016), the substrate concentration in central carbon metabolism and the K_M values of these substrates for most enzymes are in the same range. Therefore, it would be expected that the intracellular concentration of F6P in GL3 would be between 1.4-4.1 mM ($K_{M\,F6P}$ for FSAA A129S determined in this work and by Schürmann, 2001) and 7.4-9 mM ($K_{M\,F6P}$ for FSAA wt determined in this work and by Schürmann and Sprenger, 2001). The measured intracellular concentrations of G6P and F6P in GL3 were 1.6 mM and 1.1 mM, respectively (see Results Chapter 5.1.1). These concentrations are considerably lower than the concentrations reported for exponentially growing *E. coli* cells (Benett et al., 2009; Park et al., 2016), but as mentioned before, the method used in the present work was not as accurate as the methods used in other reports. With a concentration of 1.1 mM F6P FSAA A129S shows a specific activity of 6 U/mg and FSAA wt 0.5 U/mg (see Results Chapter 5.1.2). In spite of this low sensitivity, the intracellular F6P concentration of 1.1 mM measured for GL3 can be used as evidence that this concentration could be more saturating for FSAA A129S than for FSAA wt (Schürmann, 2001; Schürmann and Sprenger, 2001; Guitart Font and Sprenger, 2020). Additionally, it has to be taken into account that the N-terminal

histidine tag (pET plasmid) reduces the activity of FSAA wt by 50 %, even though it does not prevent its quaternary structure (Inoue, 2006).

The plasmid-based expression of $fsaA^{A129S}$ opened a glycolytic bypass in GL3 by restoring growth on glucose with a growth rate of 0.12 h^{-1} and a doubling time of 6 h. Whereas the growth rate and doubling times determined for LJ110 on glucose, 0.59 h^{-1} and 71 min, respectively, showed an improved fitness in comparison with GL3 (Guitart Font and Sprenger, 2020). Doubling times of 23 min have been reported for *E. coli* so far, but these were determined in rich medium (Neidhardt et al., 1990). Evidence that the expression of $fsaA^{A129S}$ was responsible for the growth of GL3/pJF119$fsaA^{A129S}$ on glucose could be gathered. The retro-aldol activity of the protein encoded by this gene (FSAA A129S) was determined in heat-treated enriched fractions, its presence was confirmed by SDS-PAGE, and the transient appearance of DHA was detected in the supernatant. In fact, none of these could be detected in LJ110.

Furthermore, the expression of plasmid-borne genes *xfp* (from *Bifidobacterium* species) and $talB^{F178Y}$ in GL3 also complemented growth on glucose. Whereas His-tagged purified TalB F178Y has a V_{max} 10-times lower than the V_{max} determined for FSAA wt, its K_M for F6P with 1.5 mM F6P is similar to the value reported for FSAA A129S and its k_{cat}/K_M value of 0.15 s^{-1}mM^{-1} is lower than the values for both FSAAs (Schneider et al., 2008). Apparently, the K_M value for F6P is the kinetic parameter that determines if the enzyme will allow GL3 to grow on glucose or not. But if the kinetic parameters of X5P/F6P phosphoketolase (Xfp) from *Bifidobacterium* species are evaluated (specific activity of 4.3-14.5 U/mg and K_M for F6P of 10 mM; Meile et al., 2001 and Suzuki et al., 2010), then the former assumption cannot be applied to this enzyme due to the similar K_M value between Xfp and FSAA wt. However, it has to be noted that the Xfp reaction is irreversible.

The 5-fold difference in growth rate between GL3/pJF119$fsaA^{A129S}$ and LJ110 suggests that FSAA A129S cannot merely substitute the missing Pfk activity in GL3. The reasons for this large difference in growth rate could be numerous. These include shortage of NADPH and PEP, toxicity of the new intermediate DHA and inadequate enzyme activities (Guitart Font and Sprenger, 2020). As suggested by Noor et al. (2010) and Bar-Even et al. (2012) all steps of glycolysis are the minimum requirement to meet cellular demands. Therefore, this pathway has evolved to be as efficient as possible in terms of thermodynamics, availability of enzymes and the physicochemical characteristics of its metabolites. Even though, no extra reaction steps are required from F6P to G3P in the glycolysis bypass with FSAA A129S in comparison with glycolysis, some constraints were identified.

Maybe the phosphorylation of DHA to DHAP is not fast enough in GL3/pJF119$fsaA^{A129S}$ (Guitart Font and Sprenger, 2020). Wang et al. (2018) discovered that the activity of the PEP-dependent DHAK is not significant enough to support growth on DHA, which could mean that the phosphorylation of DHA to DHAP does not take place at the same or at a higher rate than the cleavage of F1,6BP by F1,6BP aldolase in wild-type cells. Further, intracellular DHA can easily leak out of the cell due to its significant permeability (Bar-Even et al., 2012). This possible leak would decrease the intracellular concentration of DHA available to the cell, decreasing the rate in which DHA is phosphorylated to DHA at the same time. It was observed that solely the cultures of strains that accumulate DHA in large quantities became yellow (Guitart Font and Sprenger, 2020), while the strains that could convert DHA to glycerol remained white (see Appendix Figure 9-5). A similar observation was made by Lindner et al. (2020) and by Wang et al. (2018) with cultures that also accumulated or contained DHA, respectively.

With lethal concentrations of 14 mM (LC_{10}), 28 mM (LC_{50}), and 48 mM (LC_{90}), it can be concluded that DHA is toxic for *E. coli* cells (Subedi et al., 2008). This toxicity has an effect on cell metabolism by being detrimental and it can also cause genetic instability. DHA toxicity is known to affect other organisms, such as the yeast *Saccharomyces cerevisiae* (Molin et al., 2003). DHA toxicity in yeast and bacteria relies mainly on the formation of methylglyoxal (MG) from DHA (Nomura et al., 2018). MG inhibits growth of *E. coli* by affecting protein synthesis and initiation of DNA replication (Fraval and McBrien, 1980). Riddle and Lorenz (1968) found out that in tissues under physiological conditions DHA is converted to MG as a result of reactions with phosphate, G6P, F6P among other molecules. The same group of researchers observed in 1973 that even in Ringer's phosphate suspensions of avian spermatozoa DHA and/or glycerol are responsible for the increase of the concentration of MG to levels that can be lethal (Riddle and Lorenz, 1973). Moreover, it was suggested that the detrimental effect of DHA in *S. cerevisiae* might be connected to the consumption of glutathione and formaldehyde (Molin and Blomberg, 2006). Furthermore, DHA is responsible for DNA damage in human cells (Petersen et al., 2004). Mutagenesis in *E. coli* caused by DHA is a consequence of an increase on the mutation rates of cells (Pischetsrieder et al., 1999; Benov and Beema, 2003). To counteract the negative effects that the toxicity of DHA can have in *E. coli*, this organism uses the enzyme complex DHAKLM, a PTS for the phosphorylation of DHA. DHA kinases are known to play an essential role in the detoxification of DHA (Molin et al., 2003; Erni et al., 2006). In *E. coli* DHAKLM is encoded within the *dha* operon. The expression of the *dha* operon is induced in the presence of DHA (Bächler et al., 2005). The increased transcript

levels of the *dhaK* gene in strain GL4 (Δzwf $\Delta pfkB$ $\Delta pfkA$ $\Delta lacZ$::P_{tac}-*fsaA*^{A129S}) during growth on glucose is proof of the importance of the DHAKLM in the detoxification of DHA formed in the glycolytic bypass through FSAA A129S.

G3P produced by the glycolytic bypass opened by FSAA A129S can be used in the lower glycolysis to form PEP and pyruvate. Furthermore, together with F6P, G3P can enter the non-oxidative branch of the PPP by the action of transketolase as erythrose 4-phosphate (E4P) and xylulose 5-phosphate (Xu5P) (Sprenger et al., 1995a). As mentioned in the Introduction (see Chapter 2.4.1), FSAA wt can also catalyse the addition of DHA to E4P, forming S7P (Schürmann et al., 2002). Therefore, the conversion rate of glucose to glycerol in strain GL7 was expected to be less than 1 (Guitart Font and Sprenger, 2020).

The missing Pfk activity in GL3 is responsible for the sugar phosphate stress caused by the accumulation of G6P and F6P. When G6P accumulates in the cell, SgrR activates the expression of the *sgrS* gene (Vanderpool and Gottesman, 2004). SgrS can base-pair with *ptsG* mRNA or *manXYZ* mRNA inhibiting their translation (Maki et al., 2008) This would lead to a decrease in the uptake rate of glucose due to the low translation levels of the glucose transporters PtsG and ManXYZ. Moreover, SgrS supports the translation of ´*pldB-yigL* mRNA, yielding the haloacid dehalogenase phosphatase YigL (Papenfort et al., 2013). YigL is responsible for the dephosphorylation of the accumulated sugar phosphates. Another protein, SgrT, encoded by the *sgrT* gene, is also important during sugar phosphate stress (Wadler and Vanderpool, 2007). SgrT interacts with PtsG blocking the transport of glucose *in vivo* (Raina and Storz, 2017; Lloyd et al., 2017). Richards et al. (2013) showed that accumulation of F6P in a *pfkA* mutant strain caused sugar phosphate stress, but the degradation of *ptsG* mRNA could be prevented with the addition of F1,6BP (a glycolytic downstream metabolite). It was reported that growth of *Salmonella* mutant strains was impaired in the presence of the C-source that led to accumulation of sugar phosphates and that only sugar phosphate build-up caused toxicity (Boulanger et al., 2022). Hence, even though FSAA A129S reduces the concentration of F6P accumulated in GL3 by its cleavage to DHA and G3P, the reaction rate might not be large enough to completely avoid sugar phosphate stress. Therefore, the decrease in the glucose uptake rate in GL3/pJF119*fsaA*^{A129S}, when compared to LJ110, might be a consequence of the expression of *sgrS* and *sgrT*. A lower glucose uptake rate results in the decrease of the growth rate (see Results Figure 5-8; Guitart Font and Sprenger, 2020). Slow growth rates result in a larger concentration of P~EIIA^{Glc}. This directly and positively influences the amount of cAMP produced (Deutscher et al., 2006).

No mRNA analysis was performed for GL3/pJF119*fsaA*^{A129S}, but data were generated for GL4, strain which has the *fsaA*^{A129S} gene integrated in its chromosome. In fact, *sgrS* transcripts were detected in GL4, but none in LJ110. The expression of *sgrS* in GL4 correlates with the decrease in expression of *ptsG* when compared to LJ110 (see Results Figure 5-11). Even though, the gene expression of *yigL* was not measured, it might be possible, that its expression was activated in GL4 due to the presence of SgrS (Papenfort et al., 2013). YigL can catalyse the dephosphorylation of G6P/F6P to glucose and fructose, respectively, which can then be exported back to the medium. Therefore, PEP used for transport would not be utilised effectively and would become a metabolic burden for the cell (Papenfort et al., 2013).

In *E. coli* NADPH is always nearly present in saturating concentrations (Park et al., 2016) because it is vital to keep the redox balance in the cell and prevent oxidative stress (Romeo and Snoep, 2013; Stincone et al., 2015). NADPH is used in fatty acid biosynthesis, sulphur assimilation, and biosynthesis of deoxyribonucleotides and phospholipids. Additionally, NADPH is required for the conversion of DHAP to glycerol 3-phosphate (Gly3P) by a glycerol 3-phosphate dehydrogenase (encoded by *gpsA*). Gly3P is essential for the production of phospholipids that form the cytoplasmic membrane. Furthermore, four molecules of NADPH are necessary in the last reduction step of one molecule of sulphate by sulphite reductase (Neidhardt et al., 1990). The intracellular NADPH concentration present in the cell is dependent on the ratio of F6P that is metabolised through glycolysis or PPP (Wang et al., 2013). During growth on glucose *E. coli* has an intracellular concentration of 120 µM NADPH (Bennett et al., 2009) that is mainly maintained constant through the regeneration of NADPH in the oxidative branch of the PPP (Riemer et al., 2013). All the reactions of the oxidative branch of the PPP are unidirectional (Stincone et al., 2015), with the exception of the reaction catalysed by Gnd (reversible under elevated CO_2 concentrations; Satanowski et al., 2020). Because of this and the missing G6P DH activity in GL3/pJF119*fsaA*^{A129S} and the other GL-strains, these strains do not have a functional oxidative branch. Therefore, not enough NADPH might be available to the cells since the glycolytic bypass opened by FSAA A129S does not provide additional NADPH (Guitart Font and Sprenger, 2020). As a consequence, the GL-strains depend mainly on the activity of transhydrogenase and isocitrate dehydrogenase for the regeneration of NADPH, and secondarily on malic enzyme (Sauer et al., 2004; Zhao et al., 2004). The proton-translocating transhydrogenase PntAB of *E. coli* can reduce $NADP^+$ to NADPH by oxidising NADH to NAD^+. Although this reaction can provide the same amount of NADPH to the cell as by the PPP during growth on glucose (Sauer et al., 2004), this does not correspond with the slower growth rate observed for GL3/pJF119*fsaA*^{A129S}.

Growth of GL3 on fructose was slower than in LJ110 (see Results Table 5-5). If fructose is additionally transported into the cell by the mannose PTS, it will enter glycolysis not only as F1,6BP (fructose PTS) but also as F6P (see Figure 6-1; Kornberg, 2001; Luo et al., 2014). Due to the missing Pfk and G6P DH activities in GL3, F6P could end up accumulating in the cell and/or be isomerised to G6P. Accumulation of sugar phosphates would result in a depletion of glycolytic intermediates (Richards et al., 2013), thereby reducing the growth rate of GL3 on fructose. Other than in GL3, the glycolytic bypass present in GL3/pJF119$fsaA^{A129S}$ and in GL4 allows the partial restoration of growth on other C-sources that enter glycolysis as F6P, such as glucitol or mannitol, or that are first metabolised to F6P in the non-oxidative branch of the PPP, such as xylose.

Another growth limitation of the glycolytic bypass presented here might be the supply of PEP (Guitart Font and Sprenger, 2020). PEP is mainly produced by the enolase reaction (Riemer et al., 2013). PEP together with E4P are two of the precursor metabolites mentioned in the Introduction (see Chapter 2.1). They are required for the synthesis of the amino acids phenylalanine, tryptophan and tyrosine. Whereas pyruvate is necessary for the synthesis of alanine, leucine and valine (Neidhardt et al., 1990). Furthermore, PEP is one of the most important metabolites in the control of glycolysis (Reznik et al., 2017). The intracellular concentrations of PEP and pyruvate, the phosphorylation state of EIIA^{Glc}, and the activity of adenylate cyclase regulate the expression of genes that code for enzymes involved in the uptake of sugars (Deutscher et al., 2006; Deutscher et al., 2014). Especially, the ratio of PEP to pyruvate, which changes in accordance with the glycolytic flux (Hogema et al., 1998), seems to be decisive for *E. coli* during sugar phosphate stress (Richards et al., 2013). The concentrations of glucose and the PEP to pyruvate ratio influence the phosphorylation state of EIIA^{Glc}. With the reduction of the PEP to pyruvate ratio, the amount of EIIA^{Glc} in a dephosphorylated state increases (Hogema et al., 1998). Equally important, the dephosphorylated state of EI is affected by the concentration of PEP. The lower the PEP concentration, due to e.g. the uptake of glucose, the larger the concentration of dephosphorylated EI. The interaction between dephosphorylated EI and CheA (a kinase of the regulatory mechanism chemotaxis) represses the autophosphorylation activity of the latter, thereby supporting the smooth swimming of *E. coli* towards glucose (see Chapter 2.2.1; Deutscher et al., 2006; Deutscher et al., 2014).

GL3/pJF119$fsaA^{A129S}$ and GL4 require two moles of PEP for the consumption of 1 mole of glucose: one mole for the transport into the cell by PTS^{Glc} and another mole for the phosphorylation of DHA to DHAP by DHAKLM (see Figure 6-2). Because both strains

produce 2 moles of PEP in glycolysis, there will be no net formation of PEP. Therefore, there might be a competition between glucose uptake, biomass formation, ATP production, production of aromatic amino acids (e.g. Phe, Tyr, Trp) and cell wall biosynthesis. The production of aromatic amino acids is key for the synthesis of many proteins. Each *E. coli* cell has 5.2×10^{-10} mg proteins. To produce this amount of proteins, 4.8×10^{-9} µmol amino acids are required (Neidhardt et al., 1990). Consequently, the low availability of PEP could jeopardise the production of aromatic amino acids, which in turn could limit growth of GL3/pJF*fsaA*^{A129S}, GL4 and GL7. Furthermore, PEP is also required by pyruvate kinase for the production of ATP. A PEP shortage would affect ATP synthesis, as well as, the next step in the TCA cycle, the production of acetyl-CoA. Acetyl-CoA is the main precursor of acetate. Therefore, due to the low availability of PEP and the slower metabolism of glucose in GL3/pJF*fsaA*^{A129S}, GL4 and GL7, less acetyl-CoA is produced. As a result, acetate might be formed in these strains at a lower rate than in LJ110 and less overflow metabolism might take place (see MacConkey-agar Results Table 5-6). Therefore, growth of GL3/pJF119*fsaA*^{A129S}, GL4 and GL7 on glucose is in theory more efficient than growth of LJ110 because less resources are wasted on by-products, such as acetate.

The provision of PEP might be improved in the GL-strains by inactivating the synthesis of some of the genes that use PEP as substrate. For instance, Li et al. (2022) reported a significant conversion rate from glucose to 1,3-propanediol with a *Corynebacterium glutamicum* strain missing the Pyk and Ppc activities (PEP-using enzymes). Whereas in *E. coli*, the removal of the glucose PTS and the expression of the *glk* and *galP* genes instead (encoding for glucokinase and galactose permease, respectively), was reported to increase the availability of PEP for biomass and the formation of aromatic amino acids (Flores et al., 2007; Meza et al., 2012).

Another issue that might be responsible for the slow growth of GL-strains is the concentration of F1,6BP. It was reported that when *E. coli* grows on glucose as sole C-source, F1,6BP is one of the intracellular metabolites with the largest concentration making 5 % of the total intracellular metabolite pool (Bennett et al. 2009). Contradicting previously published results (Kochanowski et al., 2013; Kochanowski et al., 2017), Folly et al. (2018) demonstrated that in *E. coli* F1,6BP does not interact with Cra and, thus, is not one of its regulators. Only F1P binds to Cra, thereby reducing the affinity of Cra for its operator. Even though in *E. coli* F1P does not belong to central metabolism, it is present in the cell during growth on fructose, but also under other growth conditions acting as a second messenger (Folly et al., 2018). A similar observation was already reported for *Pseudomonas putida* by Chavarría et al. (2014).
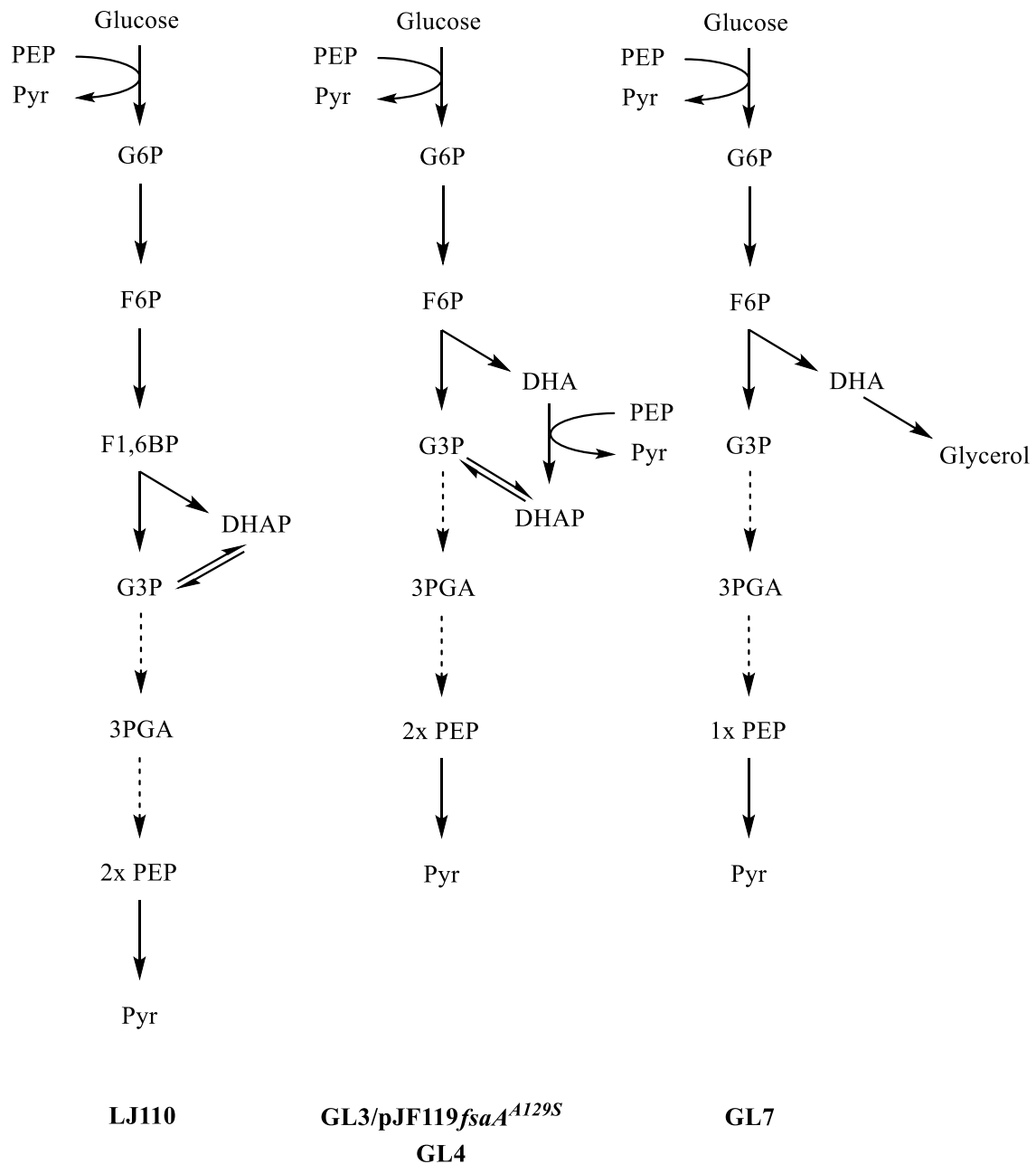
Figure 6-2. Schematic of the different pathways that form and consume PEP in strains LJ110, GL4 or GL3/pJF$fsaA^{A129S}$**, and GL7. DHA (dihydroxyacetone), DHAP (dihydroxyacetone phosphate), F6P (fructose 6-phosphate), F1,6BP (fructose 1,6-bisphosphate), G3P (glyceraldehyde 3-phosphate), G6P (glucose 6-phosphate), 3PGA (3-phosphoglycerate), PEP (phosphoenolpyruvate), Pyr (pyruvate). Figure taken from Guitart Font and Sprenger (2020)**

Cra controls mainly the expression levels of genes that encode for enzymes belonging to glycolysis, the TCA cycle or the aerobic respiration, by either repressing their expression or activating it. Some of these genes are *pfkA*, *ppc*, *pykF*, *sgrS* and *zwf*. In addition, Cra regulates the expression of genes that encode for 33 transcription factors, which result in the indirect regulation of many other genes (Shimada et al., 2011; Folly et al., 2018). Although, F1,6BP does not regulate Cra, this glycolytic intermediate is still important in *E. coli* by regulating the

activity of glycolytic enzymes (see Figure 6-3). F1,6BP, acetyl-CoA and GTP activate together PEP carboxylase (encoded by the *ppc* gene), increasing by 15-fold its maximal velocity. F1,6BP activates this enzyme only in the presence of acetyl-CoA (Izui et al., 1981). The removal of glucose and, therefore, the absence of F1,6BP results in the repression of the PEP carboxylase activity (more than 99 % decrease; Xu et al., 2012). Furthermore, it was reported that a *ppc* deficient *E. coli* strain showed a reduced glucose uptake and a lower growth rate on glucose (Peng et al., 2004). Therefore, not enough PEP carboxylase might be produced in GL3/pJF119*fsaA^{A129S}* due to its low intracellular F1,6BP concentration. This in turn reduces the growth rate of GL3/pJF119*fsaA^{A129S}* on glucose.

As mentioned above, the expression of *pykF* (codes for the pyruvate kinase) is known to be repressed by Cra. This repression is eased in the presence of glycolytic substrates, such as glucose and fructose (Bledig et al., 1996). Additionally, pyruvate kinase is activated by F1,6BP, which binds at an allosteric site different than the site for the substrate PEP (Waygood et al., 1976; Boiteux et al., 1983). Activation of pyruvate kinase reduces the PEP to pyruvate ratio, decreasing the amount of EIIA^{Glc} molecules which are phosphorylated. This in turn reduces the availability of cAMP and activates CsrD, a protein of the carbon storage regulator (Csr) system. CsrD increases the degradation of CsrB and CsrC, both small non-coding RNAs. The presence of less CsrB and CsrC decreases the inhibition of CsrA activity, allowing for the activation of the expression of glycolytic genes, such as *pykF*, by CsrA (Shimizu and Matsuoka, 2019). Therefore, the increase on pyruvate kinase results in an increased growth rate due to an increased glycolytic flux. However, if there is not enough F1,6BP available, pyruvate kinase activity will be reduced and the glycolytic flux will decrease. The missing activities of both pyruvate kinase isoenzymes affect the reactions where PEP and/or pyruvate are involved (Sauer et al., 1999). Another enzyme that needs F1,6BP, as well as F6P, 3-phosphoglycerate and pyruvate, for its activation is ADP-glucose pyrophosphorylase. This enzyme is responsible for the accumulation of glycogen in the cell (Preiss, 1984). Moreover, F1,6BP interacts with the twofold enzyme, kinase/phosphatase, PpsR by inhibiting the phosphorylation and activating the dephosphorylation of PEP synthetase (PpsA) (Piazza et al., 2018). F1,6BP can also act as an inhibitory molecule. It is known that in *E. coli* F1,6BP represses the activities of 6-phosphogluconate dehydrogenase (encoded by *gnd*; Wolf and Shea, 1979), transaldolase (Ogawa et al., 2016), and GlpK (de Boer et al., 1986).

As a consequence of the missing Pfk activities and the fact that the novel FSA-bypass does not produce F1,6BP, GL-strains most probably have a reduced intracellular F1,6BP pool when grown on glucose. F1,6BP might still be produced from the aldol addition of DHAP and G3P

during gluconeogenesis. Therefore, pyruvate kinase and PEP carboxylase might be less active resulting in a slower growth rate of GL-strains on glucose and any other C-source that enter glycolysis above or at the level of F6P (see Figure 6-1). Another problem that can arise due to the absence of PfkA in the GL-strains is that other activities performed by PfkA might be missing as well. One of these activities is the ATP-dependent phosphorylation of S7P to sedoheptulose 1,7-bisphosphate (Nakahigashi et al., 2009). Furthermore, the missing PfkA activity can lead to a reduced expression of EIICB^{Glc} due to an increase in the degradation rate of *ptsG* mRNA (Kimata et al., 2001). Thus, in a *pfkA* deficient strain not enough PtsG might be produced, hampering the sufficient transport of glucose into the cell. Besides, the K_M value for F6P of FSAA A129S is 100-fold higher than the values of PfkA and PfkB (Blangy et al., 1968; Babul, 1978; Schürmann, 2001). This can have a negative impact on the glycolytic flux and, as a result, the growth rate of the GL-strains might decrease.
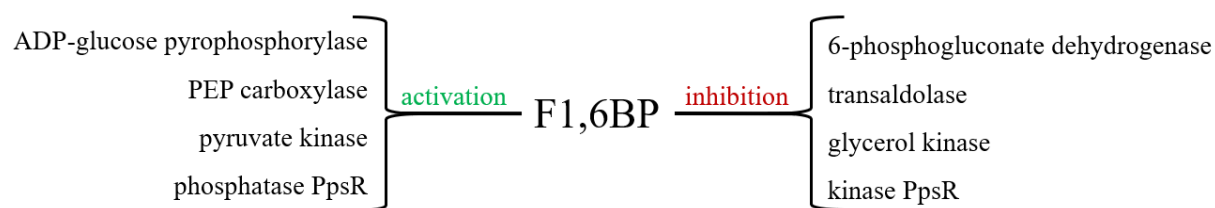
Figure 6-3. Role of fructose 1,6-bisphosphate (F1,6BP) in *E. coli*.

Plasmids are known to distinctly impact the expression of different endogenous genes (Ricci and Hernández, 2000). Because the plasmid-borne expression of *fsaA*^{A129S} in GL3 could partially restore growth on glucose, it was examined if a copy of *fsaA*^{A129S} would be sufficient to allow the mutant strain to grow. The number of copies of *fsaA*^{A129S} was reduced in GL3 by chromosomally integrating one copy of this gene under the control of the promoter P$_{tac}$ in the *lac*-operon, generating the plasmid-free GL4 (Guitart Font and Sprenger, 2020). GL4 showed approximately half the growth rate of GL3/pJF119*fsaA*^{A129S} on glucose (0.05 ± 0.00 h^{-1}; see Results Figure 5-10). Furthermore, GL4 heat-treated enriched fractions (HT) showed only a specific FSA activity of 0.1 U/mg, a 50 times lower activity than the largest specific FSA activity determined for GL3/pJF119*fsaA*^{A129S} (Guitart Font and Sprenger, 2020) Thus, it seems that the metabolic burden caused by the overexpression of FSAA A129S is low compared to the benefits that FSAA A129S provides to the cell. As already observed for GL3/pJF119*fsaA*^{A129S}, DHA could be transiently detected in the supernatant of GL4 (0.5 ± 0.0 mM DHA after 30 h incubation). This could be explained by the transcript levels determined in RNA samples of GL4 (see Results Figure 5-11). In GL4, the transcript levels for *dhaK* were 50-fold higher than the transcript levels measured for *glpK*. In RNA samples of

LJ110 a similar transcript level for *glpK* was determined, whereas no *dhaK* expression was detected. Therefore, the formation of DHA in GL4 due to the cleavage of F6P by FSAA A129S induced the expression of *dhaKLM* (Bächler et al., 2005), which codes for the DHA kinase DHAKLM. DHAKLM catalyses the phosphorylation of DHA to DHAP. Furthermore, the K_M for DHA is 10 times lower in DHAKLM (0.05 mM; Gutknecht et al., 2001) than in GlpK (0.5 mM; Hayashi and Lin, 1967). It can be concluded that GL4 prefers to convert DHA to DHAP with DHAKLM instead of via glycerol and Gly3P by using GlpK. The expression of *dhaKLM* and the activity of its encoded enzyme might be the main reasons of the transient appearance of DHA in the medium.

6.1.3   A novel glycerol production pathway from glucose in *E. coli*

It was hypothesised that the DHA produced from glucose could be used for the formation of glycerol. But before this could be tested, more DHA should be produced and accumulated. To achieve this, the chromosomal copy of *dhaKLM* was deleted in GL4, creating GL5. After growth on glucose GL4 and GL5 showed a similar specific FSA activity (0.1 U/mg) and the extracellular DHA concentration detected in GL5 (3.1 ± 0.3 mM) was 6-times larger than in GL4. The missing DHA kinase activity in GL5 could not prevent that the accumulation of DHA in the medium was only temporary (Guitart Font and Sprenger, 2020). It was reported by Deutscher et al. (2006) that growth on DHA and its phosphorylation can be prevented in *E. coli*, as a result of mutations in the *dhaKLM* operon. Whereas in GL4, DHAKLM does not seem to be the sole responsible for the consumption of DHA. Jin and Lin (1984) suggested that excreted DHA in the medium could be imported again into the cytoplasm. Furthermore, DHA is a poor substrate for *E. coli* because it can precipitate in MM due to the presence of larger amount of phosphate (main salt in MM after Tanaka; see Discussion Chapter 6.2) and it may contribute to the formation of biofilm, thereby reducing the growth rate (Peiro et al., 2019). Moreover, DHA can be transported into the cell by the glycerol facilitator GlpF (Wang et al., 2018). Therefore, it could be possible that the expression of the *glpF* gene is upregulated in all GL-strains that do not accumulate DHA in the medium. In this case, glycerol kinase GlpK might substitute the role of DHAKLM in the cell by phosphorylating DHA to DHAP. That this replacement is possible, was already observed in *Klebsiella pneumoniae* (Jin et al., 1982). As shown in Results Figure 5-25, the expression of the *glpK* gene is significant in GL5 (normalised expression of more than 2), which could correlate with an increase on the number of GlpK molecules present in the cell. The possible low concentration of F1,6BP in GL5 might prevent the inhibition of GlpK (de Boer et al., 1986; Holtman et al., 2001). As a consequence, DHA could be either

directly phosphorylated to DHAP by GlpK. Alternatively, it could be reduced (NADH-dependent) to glycerol by GldA (Tang et al., 1979; Guitart Font and Sprenger, 2020). Glycerol could then be phosphorylated to Gly3P by GlpK (Hayashi et al., 1967). Both DHAP and Gly3P can be further consumed in glycolysis. Interestingly, GL5 colonies had a larger diameter than the colonies of GL3 or GL4 when grown on MM-agar with glycerol (see Results Table 5-5). This might be explained by the missing inhibition of GlpK due to low F1,6BP concentrations (Zwaig et al., 1970). GL5 showed a nearly 3-fold slower growth on glucose than GL4 (see Results Table 5-3) with the characteristics of a diauxic growth (see Results Figure 5-13). Diauxic growth can take place when the CRP/cAMP levels are low and, as a result, the expression of the genes that metabolise the second substrate is also low due to inducer exclusion (see Chapter 2.2.1; Deutscher et al., 2006). But for GL5 this does not seem to apply (see Appendix Figure 9-6). During the second growth phase of GL5 on glucose, glucose is still present with a concentration of approximately 20 mM. In a classical diauxic growth, glucose would already be depleted when the second growth phase starts.

In addition, GL5 characteristics with extra copies of the plasmid-borne genes *fsaA* or its allele *fsaA*^{A129S} were studied when grown on glucose. GL5/pJF119*fsaA*^{A129S} reached the maximal OD$_{600\,nm}$ in half the time required by GL5, could accumulate DHA and showed a 5-times increase in specific FSA activity. Whereas GL5/pJF119*fsaA* also showed improved characteristics when compared to GL5, it could not reach the same values as GL5/pJF119*fsaA*^{A129S} (see Results Table 5-1, Table 5-3 and Table 5-4). This correlates with the observations made above for GL3/pJF119*fsaA* and GL3/pJF119*fsaA*^{A129S}.

As a consequence of the inability of GL5 to accumulate DHA in the supernatant, the native genes *gldA* (codes for glycerol dehydrogenase; GldA) and *glpK* (codes for glycerol kinase; GlpK) were examined as possible candidates that would support DHA consumption in the cell. GldA can reduce DHA to glycerol, while GlpK can phosphorylate glycerol to Gly3P. It was expected that the deletion of *glpK* from the GL5 chromosome would considerably increase the concentration of DHA and this might enable the formation of glycerol and its accumulation in the medium. The constructed strain was named GL6. Indeed, the deletion of *glpK* allowed GL6 to accumulate DHA in the medium over time with a maximal concentration of 8.8 ± 0.3 mM (29 % of maximal theoretical yield from glucose), nearly three times more than in GL5. Furthermore, the appearance of glycerol in the supernatant of GL6 in the stationary phase with a maximal concentration of 1.9 ± 0.2 mM was confirmed by HPLC. Even though the specific GldA activity in GL6 cell-free extracts was below the detection level, the fact that GldA only needs 0.30 mM DHA to reach half of its specific activity and that this enzyme favours glycerol

formation at physiological pH (Subedi et al., 2008), it can be assumed that GldA activity was present in GL6 (see Results Table 5-2). However, the *gldA* transcript levels in the exponential phase of GL6 during growth on glucose were extremely low (see Results Figure 5-26).

Although 30.8 mM glucose are consumed by GL6 and glycerol is formed from DHA, when both product concentrations (DHA and glycerol) are summed up, only a combined concentration of around 11 mM is reached. This is equivalent to less than 50 % of the maximal theoretical yield from glucose. The missing 50 % DHA might be added to erythrose 4-phosphate or to glycolaldehyde by FSA forming sedoheptulose 7-phosphate (S7P) or xylulose, respectively (Schürmann et al., 2002). DHA might be converted to methylglyoxal (MG; Nomura et al., 2018). Furthermore, FSA can synthesise arabinose 5-phosphate from glyceraldehyde 3-phosphate and glycolaldehyde (see Chapter 6.2). Due to the missing GlpK activity in GL6, glycerol is not an intermediate anymore, but an end-product. Therefore, the production of glycerol from glucose by using DHA as intermediate due to the expression of genes (*gldA*, *fsaA*) that are already present in the *E. coli* chromosome is a novel pathway that can be referred as a "new-to-nature pathway". In this case, a non-native promoter (P_{tac}) and a single amino acid substitution in FSAA in the position Ala129 were required for this novel bypass pathway to be functional (Guitart Font and Sprenger, 2020).

O'Brien and Herschlag (1999) showed that novel activities can be considerably improved with single mutations of a given gene. There are four different codons that code for alanine that by only one base exchange can code for serine, or vice versa. This is the case between FSAA wt and FSAA A129S. In FSAA wt the codon found in the position 129 is GCG (alanine), while in FSAA A129S is UCG (serine). Furthermore, according to Schürmann and Sprenger (2001) there are other microorganisms that have an alanine in the position 129 as well (*Yersinia pestis*, *Salmonella typhi*, *Streptococcus mutans*, *Enterococcus faecalis*), whereas there are others that have instead a serine (*Bacillus subtilis*, *Bacillus stearothermophilus*, *Rhodobacter capsulatus*, *Deinococcus radiodurans*, *Caulobacter crescentus*, *Methanococcus jannaschii*, *Aquifex eolicus*, *Thermotoga maritima*). Therefore, it is feasible that a mutation could have affected *fsaA* in the past resulting in a missense mutation. This would mean, that FSAA might have had a serine in the position 129, but because of a base mutation during the course of evolution, this amino acid was exchanged to alanine.

In the *S. cerevisiae* glycerol pathway, DHAP is converted to Gly3P by glycerol 3-phosphate dehydrogenase. Gly3P is then dephosphorylated to glycerol by the glycerol 3-phosphate phosphatase. Both enzymes are produced in *S. cerevisiae* when the cells are under osmotic stress. The components added into the medium to exercise osmotic stress complicate the

purification of glycerol from the medium (Semkiv et al., 2020). When the yeast glycerol pathway is introduced in *E. coli* (Nakamura and Whited, 2003; Salles et al., 2007; Balagurunathan et al., 2017), it requires 1 mole ATP more than the novel bypass pathway presented in this work due to the phosphorylation step of F6P to F1,6BP before the cleavage of F1,6BP to DHAP and G3P (Guitart Font and Sprenger, 2020; see Figure 6-4). To the best of my knowledge this is a new pathway for glycerol formation.
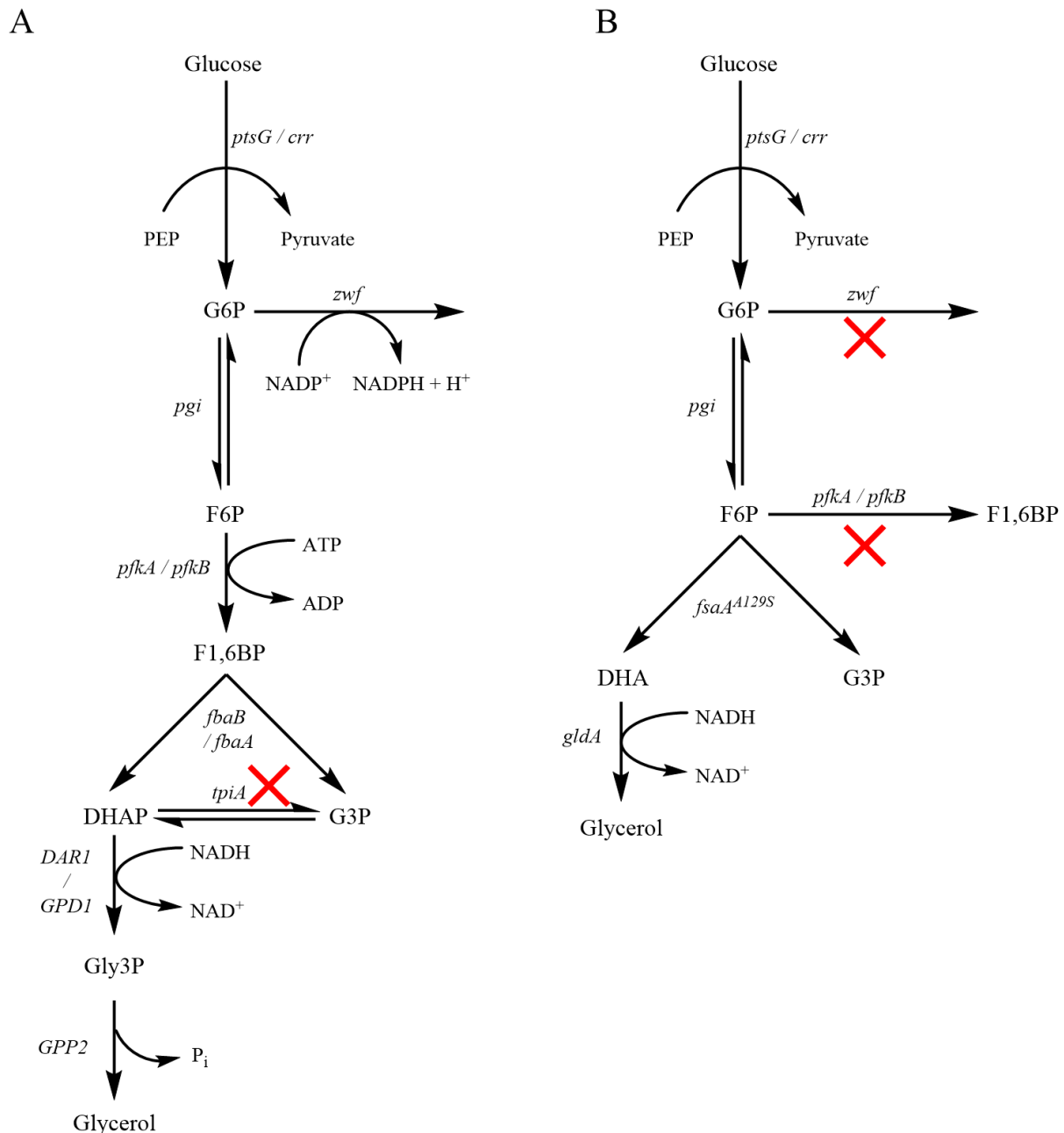
Figure 6-4. Comparison of the yeast glycerol pathway (A) and the novel glycerol pathway presented in this study (B) in *E. coli*. Figure modified after Nakamura and Whited (2003), Salles et al. (2007), Balagurunathan et al. (2017) and Guitart Font and Sprenger (2020).

The appearance of glycerol in the supernatant of GL6 opened the prospect that 1 mole glycerol might be produced from 1 mole glucose via DHA. In theory, this aim could be achieved by

149

overproducing GldA in the cell. Thus, *gldA* under the control of the inducible promoter P*tac* was inserted in the ribose-operon of GL6 chromosome, thereby constructing GL7 (Guitart Font and Sprenger, 2020). During growth on glucose a maximal concentration of DHA of 3.5 ± 0.3 mM was measured in the supernatant of GL7. This concentration is similar to the concentration detected in the supernatant of GL5 and, hence, lower than the concentration in the supernatant of GL6. In contrast to GL5 and GL6, in GL7 this is a consequence of the conversion of nearly all formed DHA to glycerol (21.8 ± 0.0 mM) due to GldA activity (0.4 ± 0.1 U/mg in cell-free extracts; *gldA* expression: 6-fold the expression of *ftsZ*). When the concentrations of DHA and glycerol reached by GL7 are summed up, they make 84 % of the maximal theoretical yield possible with glucose as C-source. However, if a molar ratio of 1:1 is considered between glucose and glycerol+DHA, nearly 5 mM of trioses from 30.2 mM are not accounted for. As mentioned above for GL6, DHA might be converted to other intermediates such as S7P and MG (Schürmann et al., 2002; Nomura et al., 2018). Another possibility is that not all F6P is cleaved to DHA and G3P by FSAA A129S. According to Lee et al. (2017), in the absence of PfkA, FbaA can catalyse the 4-epimerisation of F6P yielding tagatose 6-phosphate (T6P). T6P is known to covalently and irreversibly inhibit FSAA wt and FSAA A129S (Stellmacher et al., 2016). This might also be one of the reasons, why the GL-strains do not reach the same growth rates on glucose as LJ110. Loss of carbon in form of CO_2 can be partly excluded due to the block in the oxidative PPP. However, the GL-strains might have larger energy demand for maintenance reactions (Swanson et al., 2016). Although it was not examined, it is possible that glucose is stored in the GL-strains as glycogen or trehalose (Weiner et al., 2014).

Furthermore, the growth of GL7 was characterised in other C-sources. Similar DHA concentrations could be measured in the GL7 supernatant independently on the C-source used for growth, whereas the maximal reached glycerol concentration was dependent on the C-source (see Results Table 5-3).

6.1.4   Characterisation of the GL-evolved strains

Even though, GL5, GL6 and GL7 can produce DHA and/or glycerol, due to their slow growth rate such a process would not be commercially viable. But, these strains can become the origin of adaptive evolution (Guitart Font and Sprenger, 2020). Adaptive laboratory evolution (ALE) is the response of cells to non-lethal stress conditions to improve their survival. There are many studies that demonstrate that adaptive evolution of *E. coli* cells to a stressful environment can take place through hypermutation of subpopulations of these cells (Sniegowski et al., 1997; Torkelson et al., 1997; McKenzie et al., 2000; Tompkins et al., 2003). These hypermutations

are regulated by the SOS response (McKenzie et al., 2000) and are caused by the error-prone DNA polymerase IV (McKenzie et al., 2000; McKenzie et al., 2001; Tompkins et al., 2003). It has been shown before, that when mutant strains missing relevant metabolic activities (e.g. pyruvate kinase and PEP carboxylase) are put under growth selection pressure, these strains can improve their fitness through adaptive evolution (Feuer et al., 2012). Moreover, improvement in growth on one C-source might also enhance the growth on other C-sources (Fong et al., 2003; Fong and Palsson, 2004). Therefore, GL5, GL6 and GL7 were subject to growth rate selection pressure (see Results Chapter 5.1.7). The evolved faster-growing GL-strains (GL* and GL' strains) were characterised (growth on liquid and solid media, specific FSA and GldA activities and transcript levels of relevant genes) and the data gathered were compared to the data of their parent strains.

Overall, the GL-evolved strains increased their growth rate on glucose with a factor of at least 300 % (see Results Table 5-3). This improvement in growth rate might be a consequence of modifications in the DNA sequence which affect the phenotype of the cells (Cairns et al., 1988; Sniegowski et al., 1997; Torkelson et al., 1997; McKenzie et al., 2000; Tompkins et al., 2003). Adaptive laboratory evolution not only enhanced growth of the GL-evolved strains on glucose, but also restored growth on other C-sources, such as mannitol and glucitol (see Results Table 5-5). Because on MM with glucose and 100 µM IPTG each GL-strain (GL5, GL6 and GL7) had a different $ftsZ/gapA$ ratio and this ratio was only stable within the parent GL-strain and its evolved strains, the mRNA data were only compared between them (e.g. GL5 was only compared to GL5* and GL5').

When comparing the data gathered during growth on glucose of GL5, GL5/ pJF119$fsaA^{A129S}$ and GL5-evolved strains, it can be concluded that GL5* is the fittest of all these strains on glucose (see Results Table 5-3 and Table 5-4). GL5* was selected after growth on liquid MM with glucose. This strain reached on glucose its maximal $OD_{600\,nm}$ after only 54 h incubation. In addition, two times more DHA was measured in the supernatant of GL5* (13.6 ± 0.7 mM) when compared to GL5' (6.3 ± 0.2 mM). Furthermore, the specific FSA activity determined in heat-treated enriched fractions (HT) of GL5* (0.81 ± 0.03 U/mg) was 4-fold higher than the specific activity measured in GL5' HT (0.17 ± 0.04 U/mg). However, no difference in $fsaA/fsaA^{A129S}$ expression (it cannot be distinguished between the expression of both genes) was observed between both evolved strains. It has to be noted that the differences between the transcript levels of $fsaA/fsaA^{A129S}$ and the specific FSA activity could be a consequence of the growth phase chosen for the measurement. The former was determined during the mid-exponential phase ($OD_{600\,nm}$ 0.8-1.4) and the latter at the stationary phase. Therefore, it is

possible that the *fsaA*/*fsaA^{A129S}* transcript levels differ in GL5* and GL5' in the end-exponential phase/stationary phase, that mRNA is longer stable in GL5* than in GL5' (e.g. due to problems with the RNase E), or a type of post-transcriptional regulation takes place impacting the translation of *fsaA*/*fsaA^{A129S}* mRNA differentially in both strains. Each mRNA transcript might be translated between 25 to 36 times (Neidhardt et al., 1990). In fact, it was discovered that the sequence in the chromosome of GL5* between the promoter P$_{tac}$ and the *fsaA^{A129S}* gene has an addition of two bases (5'-GA-3') that might play a role in the *fsaA^{A129S}* mRNA synthesis rate or in the stability of this mRNA. This addition was not observed in the sequences of GL5 and GL5'. Even between GL5 and GL5*, a difference in the expression of *fsaA*/*fsaA^{A129S}* was detected that did not correlate with the difference in specific FSA activity measured: double expression, but ten times more specific FSA activity. Furthermore, the specific FSA activity determined for GL5/pJF119*fsaA^{A129S}* (0.45 ± 0.24 U/mg) is 2.6-fold higher than for GL5', although GL5' has a faster growth on glucose (0.08 ± 0.01 h^{-1} vs. 0.02 ± 0.00 h^{-1}). Therefore, the improvement in fitness of GL5* and GL5' on glucose cannot completely depend on the increase in the total specific FSA activity. This discrepancy might be resolve by changes in the affinity of PTS^{Nag} for glucose. A single mutation in the sequence of the genes *nagE* (codes for PTS^{Nag}) or *nagC* (codes for the repressor protein of PTS^{Nag}) allows PTS^{Nag} to transport glucose with higher affinity (Crigler et al., 2018). The region corresponding to the *nagC* gene in GL5, GL6, GL7 and their corresponding GL-evolved strains was sequenced. In all of the strains mentioned above the base A was missing directly after the stop codon of the *nagC* gene and should have no influence. For this reason, it can be concluded that the glucose uptake rate did not increase in the GL-evolved strains as a result of a single mutation in *nagC*. However, the change in affinity of PTS^{Nag} for glucose due to a single mutation in *nagE* cannot be excluded. Moreover, the expression of *ptsG* was detected in GL5*, but it was below the detection level in GL5 and GL5'. An increase in the expression levels of *ptsG* might result in an increase of PtsG in the inner membrane. Thus, more glucose could be transported into the cell, resulting in dephosphorylated EIIA^{Glc}. Dephosphorylated EIIA^{Glc} in turn inhibits the activity of GlpK, preventing the uptake of DHA from the medium and, therefore, its consumption (Mayer and Boos, 2005; Deutscher et al., 2006; Jahreis et al., 2008; Deutscher et al., 2014). GL5* could reach a higher growth rate on glucose than GL5 and GL5' probably due to the higher amount of PtsG present. Furthermore, a larger DHA concentration could be measured in its supernatant. Besides, the low maximal DHA concentration in the supernatant of GL5 was possibly a result of an increase in the amount of GlpK found in the cell (normalised expression of *glpK* of 2.4 ± 1.4 versus 0.2 for GL5* and 0.1 for GL5'; Hayashi et al., 1967; Jin et al., 1982). Another

possibility for the difference in the maximal concentration of DHA between GL5 and GL5*
could be that during adaptive laboratory evolution a change in the genome occurred, enabling
GL5* to tolerate larger DHA concentration in the medium without them becoming toxic for the
cells. Genome sequencing might resolve this. Although, GlpK is repressed by dephosphorylated
$EIIA^{Glc}$ (Deutscher et al., 2014), DHA still disappeared from the medium in GL5* and GL5'
cultures. Maybe not all $EIIA^{Glc}$ was dephosphorylated in GL5* and GL5', but as a result of their
slow growth on glucose (4 to 6 times the growth rate of GL5, but 5- to 7-fold less than LJ110)
$EIIA^{Glc}$ was present mainly as $P\sim EIIA^{Glc}$. Thus, DHA was still consumed, but at a lower rate
than in GL5 (see Results Figure 5-17 and Appendix Figure 9-6). In the end, a similar amount
of biomass was produced per concentration of glucose consumed (see Results Table 5-3), as a
consequence of the conversion of DHA to DHAP, directly by GlpK or via glycerol and Gly3P,
and the further isomerisation to G3P to enter the lower glycolysis. Thus, in total and in all three
strains (GL5, GL5* and GL5'), a similar ratio of glucose was converted to the intermediate
DHA, but at different conversion rates allowing for strain-specific growth rates.

In comparison with GL6, both GL6* and GL6' had an approximately 3-fold faster growth on
glucose (see Results Table 5-3) and, thus, needed a third of the time to reach their maximal
$OD_{600 \text{ nm}}$ (after only 84 h incubation). Furthermore, a slight increase in the maximal DHA
concentration was measured for both GL6-evolved strains (GL6* with 13.3 ± 0.4 mM and GL6'
with 11.2 ± 1.4 mM), and a 2-fold more specific FSA activity was detected (see Results Table
5-1). In this case, the difference in specific FSA activity was proportional to the increase in the
$fsaA/fsaA^{A129S}$ expression levels. Unexpectedly, in the supernatants of the GL6-evolved strains
a lower glycerol concentration was detected than in GL6, even though more DHA was
available. Therefore, the native GldA activity could be the bottleneck for the production of
glycerol. For all three strains the transcript levels of $gldA$ were similar, but low, and the specific
GldA activity was below detection level. An observation that does not correspond to the faster
growth of GL6' on glucose is that this strain had a nearly 2-fold increase in $sgrS$ expression in
comparison with GL6 and that all three strains (GL6, GL6* and GL6') had similar $ptsG$
transcript levels (see Results Figure 5-26). Therefore, the reason for the faster growth on
glucose of the GL6-evolved strains compared to their parent strain remains unclear and genome
sequencing might elucidate this.

Finally, faster-growing GL7 strains were obtained without compromising the production of
DHA or glycerol. GL7* and GL7' grew 4 times faster on glucose than GL7 and needed a fifth
of the time to reach the maximal $OD_{600 \text{ nm}}$. Yet, between GL7, GL7* and GL7' no considerable
differences were observed regarding DHA or glycerol concentrations. Furthermore, GL7* and

GL7' showed a slightly higher specific GldA activity and a two times increase in specific FSA activity (see Results Table 5-1 and Table 5-2). Again, there is no correlation between the *fsaA*/*fsaA^{A129S}* transcript levels (see Results Figure 5-27) and the specific FSA activity measured. Nguyen and Nevoigt (2009) claimed that *in vitro* GldA from *E. coli* only achieved half the activity measured for Gdh from *Hansenula polymorpha* with glycerol as the substrate. Therefore, a glycerol dehydrogenase from another species might improve the results obtained with GldA from *E. coli*. However, the results reported for these strains (see Results Chapter 5.1.7) indicate that the bottleneck in the growth rate of GL7 is found in the activity of FSAA A129S and not in GldA. Furthermore, GL7* showed a two times higher *ptsG* expression than GL7. More *ptsG* mRNA might result in more glucose transporters (EII^{Glc}) synthesised. Hence, more glucose transporters would allow more glucose to be transported into the cell, which would end in an increase of the growth rate.

6.1.5   Growth characterisation on C-sources other than glucose

It was claimed by Fong et al. (2003) that adaptive evolution on a substrate also might either improve or worsen the growth rate on other substrates. The results of the C-sources tested in this thesis (see Results Chapter 5.1.14) confirm this claim partly. None of the GL-evolved strains showed impaired growth on a C-source that the corresponding parent strain could metabolise. However, growth on mannitol and glucitol was restored after adaptive laboratory evolution on glucose (see Results Table 5-5). Mannitol and glucitol are both transported by the PTS into the cell as mannitol 1-phosphate and glucitol 6-phosphate, respectively. Both phosphorylated sugars enter glycolysis at the level of F6P (Neidhardt, 1996). On the contrary, growth on galactose was only faintly detected for GL5 and GL5-evolved strains. Further, fructose, D,L-lactate and succinate were shown to still be better substrates than glucose for all GL-strains and GL-evolved strains. As it was expected, the deletion of the gene *glpK* abolished the ability of GL6, GL7 and their evolved strains to consume glycerol (see Results Table 5-5; Joyce et al., 2006), even though it was reported by Murarka et al. (2008) that an *E. coli* mutant strain deficient in GlpK activities could still metabolise glycerol. In fact, no growth on glycerol was reported for an *E. coli* mutant strain missing the genes *glpK*, *dhaK*, *pfkA* and *pfkB* and at the same time overexpressing the plasmid-borne genes *gldA* and *fsaA* (Lindner et al., 2020). In contrast to GL7 and its evolved strains, Lindner et al. (2020) used the activity of FSAA wt and not FSAA A129S.

GL7 growth was characterised in liquid media with L-arabinose, galactose or xylose (see Results Table 5-3). These sugars were chosen due to their presence in the hemicellulosic part

of lignocellulosic biomass (abundant renewable resource). GL7 showed the same growth rate on xylose than on L-arabinose (0.12 ± 0.01 h^{-1}), four times faster than on glucose. Xylose and L-arabinose can be transported into the cell either by low-affinity proton symporters, XylE or AraE, or by high-affinity ABC transporters, XylFGH or AraFGH. All these transport systems are regulated by the cAMP receptor protein (CRP; Mayer and Boss, 2005; Luo et al., 2014). Both pentoses enter central carbon metabolism through the non-oxidative branch of the PPP. Furthermore, the growth rate of GL7 on galactose (0.04 ± 0.01 h^{-1}) was slightly higher than on glucose. Two active transport systems exist for the uptake of galactose. One that transports galactose with high-affinity (MglBAC, an ABC transporter) and another with low-affinity (GalP, a proton motive force-dependent transporter; Weickert and Adhya, 1993). Galactose enters glycolysis at the level of G6P. Therefore, it is comprehensible that growth of GL7 on xylose or L-arabinose is faster than on galactose or glucose (not all pentoses end up as F6P, the limiting step in the glycolytic bypass with FSAA A129S). On the other hand, the order regarding the conversion rates of substrate to glycerol is opposite to the order with respect to the growth rates. Glucose with 72 % has the highest conversion rate, followed by galactose with 63 % and finally xylose and L-arabinose both with 40 % each (Guitart Font and Sprenger, 2020).

Another interesting observation was the cell size of LJ110, the GL-strains and the GL-evolved strains after growth on LB medium or on MM with glucose (see Appendix Figure 9-8). The size of *E. coli* cells is known to change in relation to the growth conditions, especially to the availability of nutrients (Westfall and Levin, 2018). In a medium where there is an excess of nutrients, the size of cells is larger than in a medium where the availability of nutrients is limited. This correlates with the growth rate of cells. Cells with slow growth are smaller than cells with larger growth rates (Monahan and Harry, 2016). The length can vary between 1.5 and 5.5 µm, and the width between 0.5 and 1.0 µm. (Nanninga, 1998). Furthermore, UDP-glucose is used as a molecule that signals the nutrient status in *E. coli*. When UDP-glucose binds to the glucosyltransferase OpgH, OpgH blocks cell division by sequestering FtsZ. Increased cell size is the result of delaying cell division (Hill et al., 2013). In nutrient-poor conditions, UDP-glucose is less available, therefore, cell size should decrease. This does not seem to apply to the GL-strains and their evolved strains. Their cells were longer when grown on glucose as sole C-source (poor nutrient conditions, slower growth rate) than on LB medium (rich nutrient conditions, higher growth rate), while LJ110 cell length remained unchanged (see Appendix Figure 9-8). This might have an impact on the OD$_{600\,nm}$ measurements. Furthermore, these differences on length might be a consequence of the accumulation of G6P in the GL-strains and

their evolved strains that results in an increase of the concentration of glucose 1-phosphate, thereby increasing the amount of UDP-glucose present in the cell.

6.1.6   Most promising strains to produce DHA and/or glycerol

The most promising strains to produce DHA and/or glycerol should be defined regarding the parameters growth rate, theoretical yield, genetic stability, C-source and whether the use of antibiotics is required.

The growth of the GL-strains does not have the typical characteristics of a diauxic growth (Moat et al., 2002). During the lag phase that takes place between the two growth steps, glucose has not been completely consumed. This could mean, that the GL-strains have undergone some change, adapting themselves to the new environment to be able to survive. By comparison, the GL-evolved strains do not present this diauxic growth on glucose because they might already have the required characteristics to metabolise glucose at the necessary rate (see Results Figure 5-17, Figure 9-6 and Figure 9-7). Other than the addition of two bases (5'-GA-3') between the promoter P_{tac} and the $fsaA^{A129S}$ gene in GL5*, no other mutations (changes, deletions, insertions) were detected in the sequences of the inserted genes and their promoters when comparing the evolved strains to their parent strains. Furthermore, the region of the promoters of the native $fsaA$ and $fsaB$ genes (P_{fsaA} and P_{fsaB}), and the genes $fsaA$, $fsaB$, $lacI$, $nagC$, $ptsG$, and $sgrS$ were sequenced to evaluate if the difference in fitness between the GL-strains and their evolved strains could lie in a change in one of these regions. Yet, no genetic variability was detected. If adaptive evolution is a result of hypermutation (Sniegowski et al., 1997; Torkelson et al., 1997; McKenzie et al., 2000; Tompkins et al., 2003), the changes in the chromosome of the parent strains might have taken place elsewhere. Therefore, genome sequencing is necessary. Fong et al. (2006) did not observe flux to new pathways in evolved strains. It was claimed that increase of flux at pathways that are also active in the parent strains is the reason for the improved fitness of the evolved strains. Therefore, if this claim is applied to the GL-evolved strains, it would mean that these strains have mainly an increase in flux through the F6P bypass pathway when compared to their parent strains and not on other pathways. This could be explained through the increase in transcript levels of $fsaA/fsaA^{A129S}$ observed in GL5- and GL6-evolved strains when grown on glucose as sole C-source (see Results Chapter 5.1.11), but mainly as a result of the increase on the specific FSA activity in all GL-evolved strains (see Results Table 5-1).

Another possibility that allows evolved strains to reach a higher growth rate on glucose than their parent strains is an increase of the PEP synthetase activity, an enzyme that catalyses the formation of PEP from pyruvate and ATP. Patnaik et al. (1992) showed that the overexpression

of the *ppsA* gene, that encodes for the PEP synthetase, increases the PEP to pyruvate ratio in the cell, which in turn activates the PTS allowing for an increase in glucose uptake. But this assumption is unrealistic for the GL-evolved strains (see Figure 6-2) because these strains do not show a decrease in the amount of biomass when compared to their parent strains, on the contrary, it remains the same or it increases (see Results Table 5-3). In fact, the GL5- and GL6-evolved strains achieved an increase in the product yield (see Table 6-1), even though these strains produced more biomass than their parent strains. This observation contradicts the statement of Shimizu and Matsuoka (2019), that lower growth rates, as a result of lower glucose uptake rates, are energetically more efficient than higher growth rates with larger glucose uptake rates. But, because the growth rates of the GL-evolved strains do not reach the levels of the growth rate of LJ110 on glucose, it can be assumed that there is a negligible or no overflow metabolism in the GL-evolved strains (see Results Table 5-6). Thus, in spite of their growth rates, these strains remain efficient.

In this work, the most promising *E. coli* strain for the production of DHA would be GL5*. GL5* is the fittest strain on glucose in respect to the growth rate, and achieves with 44 % the largest conversion of glucose to DHA, followed by GL6* (43 %). Another *E. coli* strain has been reported to produce DHA from glucose with a molar yield of 87 % (higher than GL5*), but the expression of heterologous genes was required (Jain et al., 2016). Although other microorganisms were reported to reach higher molar yields than the ones reported for the GL-strains and their evolved strains, glycerol instead of glucose was used as the initial substrate for the conversion (see Table 6-1).

Whereas if only the molar yield of glucose to glycerol is regarded, GL7 is with 72 % (theoretically possible 1 mole glycerol per 1 mole glucose) the *E. coli* strain in this work with the best results, followed by GL7* with the best time yield (66 %). Salles et al. (2007) reported an *E. coli* strain that in a fed-batch fermentation was able to convert glucose to glycerol with a 1 mole to 1 mole ratio. However, the expression of heterologous genes was necessary to reach a 100 % yield. In addition, a 100 % yield was obtained in a chemostat with an engineered yeast, *Saccharomyces cerevisiae* (Overkamp et al., 2002). These reported yields are higher than the yield for GL7*. Nevertheless, it has to be remarked that the conditions of the fermentation of GL7* were not optimised. Thus, there is still room for the improvement of the glycerol yield from glucose in GL7*.

Table 6-1. Comparison of the GL-strains and their evolved strains with other reports where DHA or glycerol were produced by microorganisms. Information includes if the expression of heterologous (HE) or homologous (HO) genes was necessary, which substrate was used, which compound was produced and the theoretical molar yield achieved. n.a. = not applicable; a) fed-batch, b) batch, c) biotransformation, d) immobilised cells.

Organism	HE or HO	Substrate	Product	Theoretical molar yield	Reference
Corynebacterium glutamicum	HE	glucose	glycerol	86 %	Li et al., 2022[a]
E. coli GL3/pJF119*fsaA^{A129S}*	HO	glucose	DHA	37 %	this study[b]
E. coli GL4	HO	glucose	DHA	2 %	this study[b]
E. coli GL5	HO	glucose	DHA	10 %	this study[b]
E. coli GL5*	HO	glucose	DHA	44 %	this study[b]
E. coli GL5'	HO	glucose	DHA	21 %	this study[b]
E. coli GL6	HO	glucose	DHA/glycerol	29/6 (35 %)	this study[b]
E. coli GL6*	HO	glucose	DHA/glycerol	43/5 (48 %)	this study[b]
E. coli GL6'	HO	glucose	DHA/glycerol	38/5 (43 %)	this study[b]
E. coli GL7	HO	glucose	DHA/glycerol	12/72 (84 %)	this study[b]
		galactose	DHA/glycerol	12/63 (75 %)	this study[b]
		L-arabinose	DHA/glycerol	12/40 (50 %)	this study[b]
		xylose	DHA/glycerol	10/40 (50 %)	this study[b]
E. coli GL7*	HO	glucose	DHA/glycerol	14/66 (80 %)	this study[b]
E. coli GL7'	HO	glucose	DHA/glycerol	15/64 (79 %)	this study[b]
E. coli	HE	glycerol	DHA	76 %	Zhou et al., 2013[c]
E. coli	HE	glucose	DHA	87 %	Jain et al., 2016[b]
E. coli	HE	glucose	glycerol	100 %	Salles et al., 2007[a]
E. coli	HE	glucose	glycerol	89 %	Balagurunathan et al., 2017[b]
Gluconobacter oxydans	n.a.	glycerol	DHA	90 %	Ma et al., 2010[b]; Hu et al., 2010[a]
Gluconobacter oxydans	n.a.	glycerol	DHA	87 %	Stasiak-Rózanska and Blazejak, 2012[d]
Pichia farinosa	n.a.	glucose	glycerol	59 %	Vijaikishore and Karanth, 1987[a]
Pichia membranifaciens	n.a.	glycerol	DHA	35 %	Liu et al., 2008[b]
Saccharomyces cerevisiae	HE	glucose	DHA	7 %	Nguyen and Nevoigt, 2009[b]
Saccharomyces cerevisiae	n.a.	glucose	glycerol	100 %	Overkamp et al., 2002[b]

Finally, it has to be noted that the DHA production of the GL-strains and their evolved strains could actually be higher as reported here as a result of the precipitation of DHA in the presence of a large amount of salts in the medium (Peiro et al., 2019). This could explain why the glucose to product (DHA and glycerol) ratio is not 1 mole/1 mole.

As mentioned above, an increased growth rate is usually associated with low yields and an increase in biomass formation. Both characteristics are not suitable nor desired for the commercial production (Fisher et al., 2014) because they can hamper the purification of the product and increase the overall cost of production. According to Van Dien (2013) a microbial process can be regarded as commercially viable once the obtained yield is 80 % or more of the theoretical yield. Even though, the glycerol yield in GL7* is not commercially viable yet (<80 %), it could still be improved by adjusting the fermentation conditions (concentration of O_2 in the medium, glucose feed, rotation speed, fed-batch, resting cells, among others).

Taking into account all the reports available, it can be concluded that this work, also partly published by Guitart Font and Sprenger (2020), is the first report of the production of DHA and glycerol from glucose in an *E. coli* strain by the homologous expression of its genes.

6.1.7 Outlook

As mentioned in Chapter 6.1.4, the amount or activity of GldA present in the cells could be the bottleneck during the production of glycerol. Hence, a way to improve the lack of GldA in the cell could be the use of constitutive promoters for the expression of $fsaA^{A129S}$ and *gldA* instead of P_{tac}, so that the use of expensive inducers, such as IPTG, can be avoided (Van Dien, 2013). Another possibility would be the utilisation of promoters that are activated with different inducers, modulating the expression of these genes differently. Thus, one protein would be produced in larger quantities than the other, preventing them to become bottlenecks during growth. Furthermore, the regulation of the expression of key genes by their precursors could be implemented (Woolston et al., 2013). For example: FSAA A129S could be produced depending on the availability of F6P in the cell and GldA on the intracellular concentration of DHA.

Equally important, the transport of glucose can be a limiting step in the GL-strains and their evolved strains. Because it was not possible to delete the *sgrS* gene in GL7 (data not shown), an option could be to generate a PtsG variant which SgrT cannot bind to. Lloyd et al. (2017) claimed that the variant PtsG V12F, discovered by Raina and Storz (2017), is a better fit for this purpose than PtsG P348R (Kosfeld and Jahreis, 2012) because the latter is still inhibited by SgrT. Besides, mutations or deletions in SgrS or in the *ptsG* gene can also considerably affect the translational repression of *ptsG* by SgrS (Kawamoto et al., 2006). Another possibility would

be to use a synthetic 5'-untranslated region (UTR) to control the expression of the *ptsG* gene (Lim and Jung, 2017). Furthermore, instead of aiming for *sgrS*, the glucose PTS could be substituted by another uptake system that does not involve PEP (Gosset, 2005).

As already discussed, DHA can precipitate as a result of salts in the medium. A way to prevent this precipitation after its production is to use a medium with a reduced concentration of salts which can increase the half-life of DHA (Peiro et al., 2019) and, therefore, the amount of DHA available for the conversion to glycerol. Whereas in GL5, GL6 and their respective evolved strains the production of glycerol is not of importance, but only the production of DHA. Hence, in these strains the additional deletion of the *glpF* gene, which codes for the glycerol transporter GlpF, could increase the tolerance to DHA by preventing its transport into the cell by GlpF (Wang et al., 2018). This might help the GL-strains and their evolved strains overcome toxicity and could maybe increase their growth rate on glucose. For GL7 and its evolved strains the co-localisation of FSAA A129S with GldA, for example in a fusion protein or a scaffold (Woolston et al., 2013; Pearsall et al., 2015), might be an option to prevent DHA toxicity towards the cell or DHA loss to the medium as a result of a faster conversion of DHA to glycerol.

A *pfkA* and *pfkB* deficient *E. coli* strain was reported to increase its growth rate on glucose after adaptive evolution as a result of the combination of numerous mutations (Kim et al., 2022). Thus, another information that could be extremely helpful to understand why the GL-evolved strains show an improved fitness on glucose, would be the genetic variability between these strains and their parent strains. It is possible that each evolved strain has other features and that by combining all the features the optimal strain for the production of glycerol can be constructed. For this reason, sequencing all the genomes and comparing them may be key to understand which genetic and/or regulatory modifications are responsible for their differences. Other options to reach better yields would be the silencing or the post-translational control of important genes, such as *pfkA* and *zwf* (Nakashima et al., 2014; Brockman and Prather, 2015) instead of their removal from the chromosome. Furthermore, the co-utilisation of glucose with another C-source when both glycolysis and PPP are blocked is known to increase yields (Shiue et al., 2015; Wang et al. 2022). Glucose can be used for the synthesis of the product of interest and the other C-source for biomass formation. The other C-source should be a non-PTS sugar because it can help the cell to recover from sugar phosphate stress by providing the cell with the necessary amount of PEP (Shimizu and Matsuoka, 2019).

6.2   New arabinose 5-phosphate synthesis pathway

6.2.1   *In vitro* synthesis of arabinose 5-phosphate

In this work, it was reported for the first time that the purified His-tagged FSAA A129S can catalyse the cleavage of arabinose 5-phosphate (A5P) to glyceraldehyde 3-phosphate (G3P) and glycolaldehyde (GoA). So far, only the kinetic parameters of the cleavage of A5P catalysed by FSAA wt had been reported (Garrabou et al., 2009; Lachaux et al., 2019). The K_M for A5P determined with the purified His-tagged FSAA A129S was 1.1 ± 0.2 mM and the V_{max} 5.3 ± 0.5 U/mg (see Results Figure 5-31). These values differ considerably from the K_M (0.6 mM A5P) and V_{max} (0.16 U/mg powder) reported for FSAA wt by Garrabou et al. (2009). On the other hand, Lachaux et al. (2019) used purified His-tagged FSAA wt and reported a K_M of 0.65 mM A5P and V_{max} of 0.26 U/mg. In both cases, it cannot be excluded that the differences between FSAA wt and FSAA A129S are a result of the different assay conditions used (another buffer, a different temperature, or the use of enzyme powder instead of a solution) and not of characteristics that differ between the wild-type enzyme and its variant.

Due to the reversible nature of the reactions catalysed by FSA, it was expected that FSAA A129S can catalyse the formation of A5P from the addition of G3P to GoA. This formation reaction was already performed *in vitro* with FSAA wt by Sánchez-Moreno et al. (2012a), where the yield achieved was 87 %. In addition, Yang et al. (2019) reported that *in vitro* GoA and G3P could be condensed to a pentose 5-phosphate compound by FSAA wt, TalB[F178Y] and the deoxyribose-phosphate aldolase (DeoC), and that the most appropriate enzyme for this reaction was TalB[F178Y], which mainly formed A5P. In this work, the yield achieved at the end of the reaction incubation with FSAA A129S was 32 %, corresponding to 63 ± 1 mM A5P (see Results Chapter 5.2.2). Although, GoA was given in eight portions with 25 mM each, the A5P yield is rather low, most likely as a result of the cross-aldol addition of GoA to threose (Castillo et al., 2010), a side reaction. Szekrenyi et al. (2014) claimed that to reach a saturating GoA concentration in a reaction where GoA acts as the donor, its concentration should stay under 5 mM to favour GoA as the donor substrate and not as the acceptor. Whereas, Hérnandez et al. (2015) reported that in other reactions better results were sometimes achieved with the single addition of GoA instead of a slow incorporation of GoA. In another reaction involving GoA as the acceptor, Yang et al. (2017a) showed that with a four times higher donor concentration, the threose formation rate decreased 4-fold and the product rate increased by 86 %. Even though the amount of DHAP used in the reaction mixture for the synthesis of A5P in the present work should have resulted in an excess of G3P (see Methods Chapter 4.7.11), this was not enough to shift the equilibrium of the reaction towards A5P and

161

prevent the cross-aldol addition of GoA. The K_M for GoA as donor in the formation of threose catalysed by FSAA A129S was reported to be 0.2 mM and the V_{max} of 0.02 U/mg powder (Castillo et al., 2010). However, no K_M values for GoA as the donor in the synthesis of A5P catalysed by FSAA wt or FSAA A129S are available. Garrabou et al. (2009) explained that this gap in the characterisation of FSAA wt was a result of the difficulties to determine this kinetic parameter due to the competing cross-aldol addition of GoA. However, the V_{max} reached by FSAA wt during the synthesis of A5P could be determined. This value in FSAA wt corresponds to 1.5 U/mg powder, while for the formation of threose it is 0.22 U/mg powder (Garrabou et al., 2009). Nevertheless, it cannot be concluded whether the kinetic parameters (K_M and V_{max}) for GoA in the synthesis of A5P catalysed by FSAA A129S are limiting. Or whether these parameters favour the formation of threose over this reaction. Furthermore, the equilibrium in the reaction between threose and GoA goes towards the formation of threose and not its cleavage (Garrabou et al., 2009). If it is assumed that the formation of threose takes place rapidly than the synthesis of A5P and the conversion rate of 1 mole GoA to 1 mole A5P is considered, this could be the reason for the obtained 63 µmole A5P instead of the expected 200 µmole (total µmole GoA in 1 mL synthesis mixture). Another possibility is that DHAP and later G3P were present in excess at the beginning of the reaction but as a result of their instability (phosphorylated compounds), during the reaction, a total of 250 mM were not available for the synthesis of A5P. When adding up the measured end concentrations of A5P, DHAP and G3P (see Results 5.2.2), a total concentration of 97 mM was determined. Therefore, 153 mM were not accounted for.

6.2.2   Characterisation of the A5P auxotroph strain BW25113 Δ*gutQ* Δ*kdsD*::*kan*

In this work, the strain BW25113 was chosen for the deletions of the genes *gutQ* and *kdsD*. These genes code for the arabinose 5-phosphate isomerases (APIs) GutQ and KdsD, respectively. The created strain BW25113 Δ*gutQ* Δ*kdsD*::*kan* is A5P auxotroph because without the external addition of A5P, there is no synthesis of 2-keto-3-deoxymanno-octulosonic acid (KDO; Meredith and Woodard, 2005; Sperandeo et al., 2006).

Furthermore, a "bioassay" was performed to assess the minimal external A5P concentration necessary for the A5P auxotroph strain BW25113 Δ*gutQ* Δ*kdsD*::*kan* to survive on MOPS-MM with glucose and glucose 6-phosphate (G6P; required for the induction of the active transport system for sugar phosphates UhpT). As expected, a positive correlation exists between the initial external A5P concentration and the maximal $OD_{600\,nm}$ reached by the auxotroph strain. The maximal $OD_{600\,nm}$ reached by BW25113 Δ*gutQ* Δ*kdsD*::*kan* in the presence of more than

60 µM external A5P (a value around 3) was similar to the maximal $OD_{600 \, nm}$ reached by the wild-type strain BW25113 in the absence of external A5P. Therefore, when BW25113 Δ*gutQ* Δ*kdsD*::*kan* was supplied with sufficient external A5P during growth on glucose, no growth impairment was observed. Nevertheless, without the external addition of A5P the cells lysed (see Appendix Chapter 9.9). Moreover, microscope photographs could be taken of three BW25113 Δ*gutQ* Δ*kdsD*::*kan* cells that bypassed the lysis due to the absence of external A5P (see Appendix Figure 9-9). One of these cells with more than 20 µm length was unusually elongated when compared to the cell length of around 1 µm in the presence of 100 µM external A5P. In many studies, it was reported that mutant strains form long filaments. On the one hand, Begg and Donachie (1985) and Addinall et al. (1997) proposed that elongated cells are a consequence of the missing FtsZ activity, which prevents the formation of the septum. On the other hand, Taschner et al. (1988) suggested that the cell division machinery might be too slow to make cells with normal average size. Fujishima et al. (2002) indicated that the destabilisation of the structure of the OM as a consequence of the impairment of KDO synthesis impacts the FtsZ-ring formation and, thus, the elongation of cells. A similar statement was made by Harris and Theriot (2016), suggesting that the inhibition of cell surface synthesis postpones cell division resulting in an elongated cell. Whereas, Varma and Young (2004) claimed that long filaments are the result of the connection between minor peptidoglycan-modifying enzymes, the septation apparatus or the incorrect function of FtsZ. In addition, the mechanisms that increase or reduce the time of cell division, mainly through the regulation of the FtsZ activity can be responsible for the form of cells (Young, 2010). However, Coltharp et al. (2016) found out that the proportionality between the rates of cell elongation and of septum closure is affected by FtsI activity and not by FtsZ activity. The elongation of the BW25113 Δ*gutQ* Δ*kdsD*::*kan* cells is most probably caused by the block in the synthesis of KDO. When enough external A5P is available, this auxotroph strain can synthesise KDO and the cells recover their normal length.

Meredith and Woodard (2005) reported that the quantity of LPS determined in an *E. coli* strain deficient in APIs was proportional to the concentration of A5P in the medium. Therefore, it was assumed that a lower concentration of external A5P available to the cells of BW25113 Δ*gutQ* Δ*kdsD*::*kan* would result in a reduced number of KDO molecules produced. However, each *E. coli* cell needs 1.32×10^7 CMP-KDO molecules (Neidhardt et al., 1990) for the formation of the around 1.43×10^6 LPS molecules required during growth on glucose (Neidhardt, 1996). BW25113 Δ*gutQ* Δ*kdsD*::*kan* needed more than 60 µM external A5P for growth, which would correspond to 9.3×10^4 A5P molecules per cell if no intracellular

accumulation takes place. In theory, 1 molecule A5P is equivalent to 1 molecule KDO. Therefore, the number of A5P molecules needed by the A5P auxotroph strain is less than the KDO molecules required per cell. Thus, the reduced availability of KDO might influence the integrity of LPS produced by this strain. As mentioned in the Introduction Chapter 2.5, *E. coli* K-12 has a rough-LPS (no O-antigen; Liu and Reeves, 1994). In addition, defective LPS is known to negatively affect the amount of proteins that are incorporated in the OM (see Introduction Chapter 2.5; Neidhardt et al., 1990). In fact, the synthesis of large amounts of LPS and its export to the OM is known to affect the growth rate and the division of the cell positively (Whitfield and Trent, 2014). Thus, a reduced number of LPS molecules on the surface of the OM in BW25113 Δ*gutQ* Δ*kdsD*::*kan* as a result of the block in the first reaction of the synthesis of KDO might impact the stability of the OM. *E. coli* is known to compensate the loss of LPS molecules by modifying the ratio of LPS molecules to phospholipids present in the OM (estimated to be 0.12:1 in wild type cells; Galloway and Raetz, 1990). This makes the OM significantly sensitive to hydrophobic compounds (Sperandeo et al., 2017). Therefore, the OM can be more readily attacked by lysozyme. When the membrane of a cell is damaged, the proteins in the cell can leak into the medium. Nevertheless, Meredith et al. (2006) and, later, Mamat et al. (2008) isolated KDO-negative *E. coli* strains (deficient in KdsD and GutQ activities) that are viable. The outer membrane of these suppressor strains constituted mainly of lipid IV$_A$. To evaluate the impact that the availability of external A5P has on the OM of the cells of the auxotroph strain, a simple indirect method to test the integrity of LPS (treatment of the cells with lysozyme) was performed (see Methods Chapter 4.7.12). As expected, a correlation between the concentration of external A5P and the relative protein concentration in the supernatant measured after treatment with lysozyme was observed (see Results Chapter 5.2.5). When the concentration of A5P was limited, the relative protein concentration in the supernatant increased, whereas a diminishment of the relative protein concentration was observed, when higher concentrations of A5P were applied. As observed in Results Figure 5-35, it can be concluded, that at concentrations of 50 µM A5P or above the integrity of LPS is ensured, whereas at concentration of or below 20 µM A5P it is at risk. To better understand the relationship between A5P, KDO and LPS more accurate results are required. Therefore, direct methods for the quantification of LPS, such as the purpald assay (Lee and Tsai; 1999) or for the quantification of KDO (Karkhanis et al., 1978) should be performed.

6.2.3   Synthesis of arabinose 5-phosphate *in vivo* and restoration of growth

Previous reports only showed that the API deficiency of an *E. coli* B strain ($\Delta gutQ$ $\Delta kdsD$) could be complemented with the activity of APIs from other organisms, such as Q5LIW1 from *Bacteroides fragilis* (Cech et al., 2014) or CtAPI from *Clostridium tetani* (Cech et al., 2017). Furthermore, there is a very recent report (published after the end of the present study) by Wagner et al (2023) of the *in vivo* synthesis of A5P for other ends than growth complementation, where the *in vitro* synthetic pathway of acetyl-phosphate reported by Yang et al. (2019) is established *in vivo*. This group engineered an *E. coli* strain (API-positive) to use ethylene glycol as a substrate to produce GoA as an intermediate. With the plasmid-based expression of *fsaA*, GoA was added to G3P, thus, forming A5P. A5P was further metabolised to acetyl-phosphate. The last pathway step was the conversion of acetyl-phosphate to acetyl-CoA. In addition, the co-substrate glycerol was used to allow the cells to grow and to replenish G3P required for the synthetic pathway. To examine if the *in vivo* pathway was functional, Wagner et al. (2023) determined the presence of extracellular mevalonate (downstream product of acetyl-CoA when expressing genes from *Lactobacillus casei*). Nevertheless, no *in vivo* study was available regarding growth complementation of an API-deficient *E. coli* strain with enzymes other than APIs.

Since the *in vitro* synthesis of A5P from G3P and GoA can be catalysed by FSAA wt (Sánchez-Moreno et al., 2012a) and by FSAA A129S (see Chapter 6.2.1), it was evaluated if a plasmid-based expression of the genes that code for FSA (*fsaA*, *fsaA^{A129S}* and *fsaB*) would allow for a bypass reaction for the formation of A5P in the BW25113 strain deficient in APIs ($\Delta gutQ$ $\Delta kdsD$). Considering that 1 mole GoA can be added to 1 mole G3P to produce 1 mole A5P and that BW25113 $\Delta gutQ$ $\Delta kdsD$::*kan* only required 0.6 µmole A5P in 10 mL to reach the maximal $OD_{600\,nm}$, it was expected that 1.25 µmole external GoA in 10 mL would be sufficient for the cell to restore its growth in the absence of external A5P. Because there are no kinetic parameters available for this reaction catalysed by the FSA enzymes, it was assumed that to sustain growth enough A5P at the correct rate should be formed. Therefore, the FSA enzymes should have similar or better kinetic parameters than KdsD and GutQ. KdsD has a K_M for Ru5P of 0.35 mM and a k_{cat} of 255 s^{-1} (Meredith and Woodard, 2003) and GutQ of 0.64 mM and 242 s^{-1} (Meredith and Woodard, 2005).

As shown in Results Chapter 5.2.6, the growth of the A5P auxotroph strain was completely impaired in the presence of GoA and the simultaneous absence of external A5P. Whereas, the expression of *fsaA*, *fsaA^{A129S}* or *fsaB* (see Results Figure 5-37) restored the growth of this strain as a result of the synthesis of A5P from externally added GoA. Because the growth of

BW25113 $\Delta gutQ$ $\Delta kdsD$/pJF119$fsaB$ was not impaired, it can be claimed that FSAB, as the other FSA enzymes, can catalyse the aldol addition of GoA and GAP to A5P *in vivo*. Trudeau et al. (2018) reported that FSAA wt or FSAB in combination with KdsD or GutQ and ribulose 5-phosphate kinase was able to produce *in vitro* ribulose 1,5-bisphosphate from GoA and G3P via A5P. Therefore, it had never been shown before that FSAB would enable growth of an A5P auxotroph strain when external A5P was not available to the cell.

As observed in Results Figure 5-37, with increasing GoA concentrations, the maximal $OD_{600\,nm}$ of the BW25113 strain deficient in APIs ($\Delta gutQ$ $\Delta kdsD$) increased as well, regardless of the FSA gene (*fsaA*, *fsaA^{A129S}* or *fsaB*) expressed. The data of the bioassay with external A5P (see Results Chapter 5.2.4) can be linked to the data of the *in vivo* synthesis of A5P (see Results Chapter 5.2.6). If the maximal $OD_{600\,nm}$ determined for each strain in Results Figure 5-37 is used to calculate the concentration of A5P needed to reach this $OD_{600\,nm}$ in Results Figure 5-34, the conversion rate from GoA to A5P can be calculated. It can be concluded that the only strain that reaches a conversion rate close to 1 (1 mole A5P from 1 mole GoA) is BW25113 $\Delta gutQ$ $\Delta kdsD$::*kan*/pJF119$fsaA^{A129S}$. The other tested strains, BW25113 $\Delta gutQ$ $\Delta kdsD$::*kan* with the plasmid-borne expression of *fsaA* (pJF119$fsaA$), BW25113 $\Delta gutQ$ $\Delta kdsD$ with *fsaB* (pJF119$fsaB$), or the expression of the chromosomally inserted gene *fsaA^{A129S}* in the ribose operon (BW25113 $\Delta gutQ$ $\Delta kdsD$ $\Delta rbsK$::P_{tac}-*fsaA^{A129S}*), reached a conversion rate of 0.56, 0.40 and 0.25, respectively. Therefore, *in vivo* the presence of larger amounts of FSAA A129S (expression from a multicopy plasmid) allows the efficient addition of external GoA to the internally formed G3P producing A5P with a 1:1 ratio in BW25113 $\Delta gutQ$ $\Delta kdsD$::*kan*. Whereas, from a stoichiometric point of view FSAA wt, FSAB or a lower amount of FSAA A129S (expression from the chromosome) do not add GoA efficiently to G3P *in vivo* and, thus, the amount of A5P produced is lower. This correlates with the calculated maximal $OD_{600\,nm}$ (see Results Figure 5-37).

Interestingly, the BW25113 strain deficient in APIs ($\Delta gutQ$ $\Delta kdsD$) grew on glucose with the expression of genes that code for FSA (*fsaA*, *fsaA^{A129S}* or *fsaB*) even without the addition of GoA and reached $OD_{600\,nm}$ values above one. Growth was examined under the same conditions as the double mutant strain. Therefore, if growth in the absence of GoA was due to remaining A5P, the double mutant would have shown growth as well. When the $OD_{600\,nm}$ value above one is used in the Michaelis-Menten equation together with the K_S and the maximal $OD_{600\,nm}$ values reported in Results Figure 5-34, the equivalent A5P concentration can be determined. An $OD_{600\,nm}$ value above one corresponds to an A5P concentration of around $10\,\mu M$. Therefore, the A5P auxotroph strain must be able to produce at least $10\,\mu M$ of intracellular GoA

(1 mole A5P = 1 mole GoA) to obtain this $OD_{600\,nm}$ value on glucose. No enzymes in *E. coli* are known to produce GoA during growth on glucose. Therefore, it is unclear how this strain obtained the necessary GoA. Nevertheless, *E. coli* is known to produce GoA from other C-sources and by other pathways than the depletion of glucose. D-arabinose can be further metabolised to DHAP and GoA, but only in *E. coli* K-12 mutants (LeBlanc and Mortlock, 1971; Mayer and Boos, 2005)). In addition, *E. coli* K-12 can utilise ethylene glycol as a substrate for the production of GoA by using a more-oxygen stable propanediol oxidoreductase and by regulating the oxygen concentration (Pandit et al., 2021; Wagner et al., 2023). Furthermore, it has been shown that GoA can be formed *in vitro* by the condensation of two molecules of formaldehyde catalysed by a designed glycolaldehyde synthase. But, the low cell tolerance to formaldehyde is a drawback for the *in vivo* production of GoA (Lu et al., 2019). Another source of GoA is β-hydroxypyruvate (Lam and Winkler, 1990). Besides, Tani and Dempsey (1973) claimed that GoA is the natural precursor of pyridoxal phosphate or it is metabolised to this end in *E. coli* B. Furthermore, it cannot be excluded that the activity of FSA in the cell could produce GoA from the cleavage of 1-deoxyxylulose or xylulose (Schürmann et al., 2002).

To conclude, it has to be mentioned that no direct proof could be found of the formation and excretion of A5P in BW25113 Δ*gutQ* Δ*kdsD*::*kan*. On one hand, the synthesised A5P concentration could not be enzymatically determined due to the large concentrations of A5P needed (at least 50 µM) for this measurement. On the other hand, because the A5P auxotroph strain is dependent on A5P for its survival, any formed A5P in the cell by FSA would most probably be directly used for the synthesis of KDO. However, the present study is the first report that demonstrates the *in vivo* synthesis of A5P from GoA and G3P catalysed by the FSA enzymes (FSAA wt, FSAA A129S and FSAB) through growth complementation of a BW25113 A5P auxotroph strain (Δ*gutQ* Δ*kdsD*).

6.2.4 Outlook

LPS is essential for the survival of most gram-negative bacteria (Whitfield and Trent, 2014; Sperandeo et al., 2017). Even though, KDO is commercially available, it is an expensive molecule. Therefore, it would be of advantage to produce large amounts of KDO at a lower cost. KDO could be employed to study and establish novel strategies to cure infections caused by pathogenic gram-negative bacteria. In fact, there are only a reduced number of publications available regarding the production of KDO or intermediates of its synthesis. Volk (1960) showed that A5P can be chemically synthesised from glucosamine under high temperatures (boiling-water bath). Whereas, the *in vitro* production of KDO 8-phosphate from D-arabinose

and PEP was reported by Bednarski et al. (1988). In addition, the i*n vitro* KDO production from the expensive Ru5P has also been shown (Wen et al., 2016). Furthermore, *E. coli* has been engineered to produce KDO from glucose (Camci-Unal et al., 2012). In the present work a new approach was shown by using an API deficient *E. coli* strain (A5P auxotroph) that was able to synthesise KDO via A5P from the simple compounds G3P and GoA without the need of intermediates of the PPP. This approach could be used for the study of KDO. For example, by using labelled GoA, KDO would end up labelled as well.

Besides, the production of KDO could be improved by using higher concentrations of GoA at once or in steps. GoA can be toxic for *E. coli* cells with concentrations equal or above 5 mM in the medium (see Results Chapter 5.3.1). Another option would be to use other enzymes that display FSA-activity, such as TalB F178Y, *in vivo*. Yang et al. (2019) reported that this enzyme is able to catalyse the formation of A5P from G3P and GoA too.

6.3   Study of the native promoters of the genes *fsaA* and *fsaB* (P*fsaA* and P*fsaB*)

Promoters are a key element in the initiation of transcription. Transcription regulation is complex (Hengge-Aronis, 2002; Typas et al., 2007; Fic et al., 2009; Ishihama, 2010; Lee et al., 2012; Feklístov et al., 2014; Ishihama et al., 2014). In *E. coli*, numerous transcription factors can control the same promoter, thereby modulating its strength, and each transcription factor can control multiple promoters, genes or operons. Approximately 270 different transcription factors bind to DNA, normally to the noncoding regions, and up to 30 bind to RNA polymerase. The seven σ subunits generally regulate the gene selectivity of RNA polymerase (Ishihama, 2010). If a promoter is strong, initiation will take place more often than if a promoter is weak. Furthermore, initiation depends on the sigma factor that interacts with the promoter (Neidhardt et al., 1990). Therefore, the promoters of the *fsaA* and *fsaB* genes (P*fsaA* and P*fsaB*) in *E. coli* were studied to gather information regarding their strength. Such information might help find the physiological function of FSA in *E. coli*.

6.3.1   Strength analysis of the native promoters P*fsaA* and P*fsaB*

To study the strength of the native promoters P*fsaA* and P*fsaB*, two *E. coli* LJ110 reporter strains were constructed (P*fsaA*-*lacZYA* and P*fsaB*-*lacZYA*) and their *β*-galactosidase activities were determined under different conditions (see Results Chapter 5.3.1). When all *β*-galactosidase activities obtained were compared, it was evident that P*fsaA* and P*fsaB* with *β*-galactosidase activities at least 32-fold lower than P*lac* are weak promoters. Whereas in all strength analysis, the *β*-galactosidase activity of P*fsaA* was higher than the activity of P*fsaB*. Consequently, P*lac*

$(3155 \pm 117\ U/OD_{600\ nm}$, Trachtmann, personal comunication) is stronger than P_{fsaA} $(76.7 \pm 10.4\ U/OD_{600\ nm})$, while P_{fsaA} is stronger than P_{fsaB} $(5.3 \pm 1.7\ U/OD_{600\ nm})$.

As explained by Lee et al. (2012), transcription activation can take place when molecules interact with specific promoters, by allowing the presence of other molecules or by preventing the repression of transcription by another molecule. Furthermore, molecules can directly interact with RNA polymerase by changing its preference for specific promoters. Surprisingly, the β-galactosidase activity of P_{fsaA} decreased in the presence of GoA and DHA, both relevant donor substrates of many reactions catalysed by FSAA wt (see Introduction Chapter 2.4.1) and toxic for the cells in higher concentrations (the concentrations used were not toxic for the cells, see Results Chapter 5.3.1). P_{fsaB} showed a higher β-galactosidase activity in the presence of HA. Because the *fsaB* gene is present in the same operon as the *gldA* gene (Reizer et al., 1995), it is plausible that both genes are induced by the same compounds, such as HA (Truniger and Boos, 1994). Furthermore, an increase in β-galactosidase activity was measured when both reporter strains grew on succinate instead of glucose. During growth on succinate the PTS proteins remain phosphorylated, which activates the activity of adenylate cyclase (Deutscher et al., 2006). Therefore, it is possible that the expression of the *fsaA* and *fsaB* genes are controlled by the CRP/cAMP levels in the cell.

6.3.2   Comparison of P_{fsaB} with $P_{fsaB'(mutant)}$

After growth selection of P_{fsaB}-*lacZYA* on lactose, a 6-bases deletion upstream of the -35 motif of the promoter P_{fsaB} (LJ110, $P_{fsaB'(mutant)}$- *lacZYA*; see Appendix Figure 9-3) improved the strength of this promoter by increasing the β-galactosidase activity measured by 3-fold. Furthermore, the addition of 15 mM HA increased the β-galactosidase activity measured for both promoters (native and mutant) by 8-fold (see Results Figure 5-42). Therefore, this sequence deletion upstream of P_{fsaB} most probably do not impact the regulation mechanism where HA might be involved. However, these results showed that this new sequence might allow the binding of other transcription activators upstream of the promoter.

Moreover, to further evaluate which consequences the macrolesion upstream of P_{fsaB} had on the expression of the *lacZ* gene, the parent and mutant reporter strain were grown on MM with lactose in the presence and absence of HA. With this experiment it could be confirmed that the mutated promoter for *fsaB* was responsible for the increase in expression of *lacZ*. While the reporter strain P_{fsaB}-*lacZYA* showed no growth on lactose without the addition of HA, the increased expression of *lacZ* in $P_{fsaB'(mutant)}$-*lacZYA* allowed this strain to grow on lactose. In the presence of HA both reporter strains could grow on lactose. Therefore, it can be concluded that

at least 17 µmole/min/OD$_{600\,nm}$ (β-galactosidase activity measured for P$_{fsaB'(mutant)}$ in the absence of HA) are enough to allow slow growth on lactose (see Results Chapter 5.3.2).

6.4 Possible physiological function of FSA in *E. coli*

The physiological function of FSAA wt and FSAB in *E. coli* is still unknown (Samland and Sprenger, 2014). In the present work it was investigated which reaction catalysed by the FSA enzymes *in vitro* could take place in *E. coli in vivo*. With this purpose, existing pathways were disrupted in *E. coli* preventing the cells to grow. In the first approach, the central carbon metabolism pathways glycolysis and PPP were blocked. Whereas on the other approach, there was a blockade in the KDO biosynthesis pathway. Growth of these mutant *E. coli* strains on glucose was rescued by the activity of FSA. In the former approach, the activity of FSAA wt could not restore growth on glucose, but a novel bypass could be established with the cleavage of F6P to DHA and G3P by the variant FSAA A129S (see Chapter 6.1). While in the latter approach, the addition of external GoA and the activity of FSAA wt, FSAA A129S and FSAB enabled the A5P auxotroph strain to grow on glucose. These recombinant FSA enzymes added GoA to G3P (produced intracellularly from glucose) to form A5P (see Chapter 6.2).

In addition, the native promoters of the *fsaA* and *fsaB* genes were studied. The most relevant finding was that the strength of the promoter P$_{fsaB}$ increased 3-fold by the deletion of 6 bases upstream of the -35 motif, allowing the LJ110 mutant reporter strain P$_{fsaB'(mutant)}$-*lacZYA* to produce the minimum amount of LacZ required to grow on lactose (see Chapter 6.3.2).

Yet, some open questions remained. Whether the expression of *fsaB* under the control of P$_{fsaB'(mutant)}$ would reach transcript levels large enough to allow growth of GL3 on glucose. Or even if the reported activity of FSAB for the cleavage of F6P is sufficient. FSAB has a lower V_{max} for this reaction (1.62 U/mg) in comparison with FSAA wt and FSAA A129S, but the K_M value for F6P with 6.7 mM is located between both FSAA enzymes (Sánchez-Moreno et al., 2012b).

Other groups have reported metabolic engineered pathways where FSA catalysed a key reaction. De Simone et al. (2020) used enzymes belonging to yeast and the overexpression of the native genes *fsaB* and *gldA* to allow the assimilation of methanol in *E. coli*. But the probability that the reaction in this pathway could be the physiological function of FSA in *E. coli* is extremely low because methanol is not a known substrate of this microorganism. Whereas Lachaux et al. (2019) reported a non-natural pathway for the synthesis of glycolic acid in *E. coli* requiring the overproduction of FSAA wt for the cleavage of A5P to GoA and G3P.

This pathway is cyclic and has no added value for *E. coli*, when an essential intermediate for KDO synthesis such as A5P is utilised for other purposes (see Discussion Chapter 6.2.2). However, it cannot be excluded that the cleavage of A5P to GoA and G3P could be the physiological function of FSA. On the other hand, King et al. (2017) reported the biosynthesis of 1-deoxyxylulose 5-phosphate from the aldol addition of GoA to HA catalysed by FSAA wt. This *de novo* pathway restored growth of a glycolate deficient *E. coli* strain on D-arabinose. Therefore, the aldol addition of GoA to HA forming 1-deoxyxylulose might be a candidate reaction for the physiological function of FSA in *E. coli*.

Furthermore, FSAA A129S has been employed in synthetic pathways in *E. coli* to reduce the toxicity of intermediates, such as aldehydes, in the cell by decreasing their concentrations to non-toxic levels (Bayer et al., 2017). In addition, Peiro et al. (2019) showed that while the overexpression of the *fsaB* gene in *E. coli* positively impacts the DHA uptake rate, it does not affect the growth rate on DHA. Whereas the deletion of *fsaB* and *fsaA* in the chromosome of *E. coli* diminish the DHA uptake rate and the growth rate on DHA as well. They concluded that both isoenzymes (FSAA wt and FSAB) are important for DHA consumption and that the concentration of FSAB might be too low in wild-type cells. In fact, the presence of FSAA wt has only been detected twice in wild-type microorganisms. FSAA wt was once detected *in vivo* in the proteome of piglets infected with shiga toxin-producing *E. coli* (O157:H7). It was suggested that *E. coli* used FSAA wt as a bypass for the accumulation of F6P (Pieper et al., 2013). Moreover, it was reported by Hirayama et al. (2022) that four *Methylprofundus* species (methanotrophic bacteria) carry the *fsaA* gene in their chromosome and that two of these species showed large *fsaA* transcription levels. This group suggested that both reactions catalysed by FSAA wt (aldol cleavage of F6P and formation of F6P) are important in these microorganism. Besides, Gao et al. (2021) discovered that the transcription regulator YciT binds within the regulatory region of the *fsaA* gene repressing its expression in *E. coli* MG1655. Yet, why this transcription regulator binds to *fsaA* and under which conditions the unbinding takes place remains unclear. This information would be extremely relevant for the study of the physiological function of FSAA wt in *E. coli*.

In conclusion, in the present work two new artificial pathways have been shown in *E. coli*. These pathways were functional due to reactions catalysed by FSA enzymes: the cleavage of F6P to DHA and G3P in glycolysis and the formation of A5P from GoA and G3P in the biosynthesis of KDO. Even though, much more needs to be investigated, with the knowledge gained within this work, progress has been made towards finding the actual physiological function of FSAA wt and FSAB in *E. coli*.

171

7   Acknowledgments

I would like to thank Prof. Dr. Georg A. Sprenger for giving me the opportunity to do my Ph.D. at the Institute of Microbiology, for the very interesting discussions, for waking up my curiosity, and for not giving up on me.

To apl. Prof. Dr. Martin Siemann-Herzberg, for accepting the role as my second examiner. I really appreciate it.

Many colleagues from the Institute of Microbiology were an important pillar during the nearly 5 years that I spend researching. I would like to thank all of them. Especially Dr. Natalie Trachtmann and Dr. Katrin Gottlieb from the laboratory number 1 supported me, not only on technical aspects, but also on personal grounds. Also my colleagues in the office number 4: Olaf Dickel for being always there, listening and giving support in the good and bad moments; and Erik Eppinger, with whom I shared the practical courses, the up and downs during the Ph.D. and for being a real friend. Janosch Gröning, next to whom I spent many hours supervising practical courses and going together to the canteen He was a big help by taking care of numerous tasks. Dr. Lena Stellmacher for checking on me and on the progress of this thesis every once in a while. And I do not want to forget the people which whom I shared the coffee break: Dr. Jakob Birke, Dr. Leonie Weinmann, Dr. Matthias Schapfl. Their advice and the discussions we had about all imaginable matters where always the highlight of my day.

I would also like to show my appreciation to all the students that I supervised during practical courses. It was fun and refreshing to meet new people with a lot of questions and other ideas.

I would like to acknowledge David Miller. His weekly question about the status of this thesis, even though "annoying", gave me the last push I needed to finish it.

And to the most important people on this journey: my family. I want to thank them for their patience and their understanding. Especially my mother, who has always been there for me and has taught me to always give my best. Thank you. Also a special thanks to Loqui and Sam, our cats, that kept me company while writing the last part of this thesis. And last but not least, I would like to thank the most constant person in this journey, Michael Seiffert, who helped me during the most difficult moments, giving me important reasons not to give up, and always having my back.

A big thank you to all these people. Without them, this would have never been possible.

8   References

Addinall S.G., Cao C., Lutkenhaus J. 1997. Temperature shift experiments with an *ftsZ84*(Ts) strain reveal rapid dynamics of FtsZ localization and indicate that the Z ring is required throughout septation and cannot reoccupy division sites once constriction has initiated. *Journal of Bacteriology* **179**: 4277-4284

Aroua M.K., Cognet P. 2020. Editorial: From glycerol to value-added products. *Frontiers in Chemistry* **8**: 69

Ausubel F.M., Brent R., Kingston R.E., Moore D.D., Seidman J.G., Smith J.A., Struhl. K. 2001. ed. Current protocols in molecular biology. John Wiley & Sons: New York.

Babul J. 1978. Phosphofructokinases from *Escherichia coli*. *The Journal of Biological Chemistry* **253**: 4350-4355

Bächler C., Schneider P., Bähler P., Lustig A., Erni B. 2005. *Escherichia coli* dihydroxyacetone kinase controls gene expression by binding to transcription factor DhaR. *The EMBO Journal* **24**: 283-293

Balagurunathan B., Jain V.K., Tear C.J.Y., Lim C.Y., Zhao H. 2017. In silico design of anaerobic growth-coupled product formation in *Escherichia coli*: experimental validation using a simple polyol, glycerol. *Bioprocess and Biosystems Engineering* **40**: 361-372

Bar-Even A., Flamholz A., Noor E., Milo R. 2012. Rethinking glycolysis: on the biochemical logic of metabolic pathways. *Nature Chemical Biology* **8**: 509-517

Bayer T., Milker S., Wiesinger T., Winkler M., Mihovilovic M.D., Rudroff F. 2017. In vivo synthesis of polyhydroxylated compounds from a "hidden reservoir" of toxic aldehyde species. *ChemCatChem* **9**: 2919-2923

Becker A.-K., Zeppenfeld T., Staab A., Seitz S., Boos W., Morita T., Aiba H., Mahr K., Titgemeyer F., Jahreis K. 2006. YeeI, a novel protein involved in modulation of the activity of the glucose-phosphotransferase system in *Escherichia coli* K-12. *Journal of Bacteriology* **188**: 5439-5449

Bednarski M.D., Crans D.C., DiCosimo R., Simon E.S., Stein P.D., Whitesides G.M., Schneider M.J. 1988. Synthesis of 3-deoxy-D-manno-2-octulosonate-8-phosphate (KDO-8-P) from D-arabinose: generation of D-arabinose-5-phosphate using hexokinase. *Tetrahedron Letters* **29**: 427-430

Begg K.J., Donachie W.D. 1985. Cell shape and division in *Escherichia coli*: experiments with shape and division mutants. *Journal of Bacteriology* **163**: 615-622

Begley M., Gahan C.G.M., Hill C. 2005. The interaction between bacteria and bile. *FEMS Microbiology Reviews* **29**: 625-651

Bennett B.D., Kimball E.H., Gao M., Osterhout R., Van Dien S.J., Rabinowitz J.D. 2009. Absolute metabolite concentrations and implied enzyme active site occupancy in *Escherichia coli*. *Nature Chemical Biology* **5**: 593-599

Benov L., Beema A.F. 2003. Superoxide-dependence of the short chain sugars-induced mutagenesis. *Free Radical Biology & Medicine* **34**: 429-433

Bergmeyer H.U. 1975. New values for the molar extinction coefficients of NADH and NADPH for the use in routine laboratories. *Zeitschrift für Klinische Chemie und Klinische Biochemie* **11**: 507-508

Blangy D., Buc H., Monod J. 1968. Kinetics of the allosteric interactions of phosphofructokinase from *Escherichia coli*. *Journal of Molecular Biology* **31**:13-35

Bledig S.A., Ramseier T.M., Saier Jr. M.H. 1996. FruR mediates catabolite activation of pyruvate kinase (*pykF*) gene expression in *Escherichia coli*. *Journal of Bacteriology* **178**: 280-283

Bobrovskyy M., Vanderpool C.K. 2014. The small RNA SgrS: roles in metabolism and pathogenesis of enteric bacteria. *Frontiers in Cellular and Infection Microbiology* **4**: 61

Boenigk R., Bowien S., Gottschalk G. 1993. Fermentation of glycerol to 1,3-propanediol in continuous cultures of *Citrobacter freundii*. *Applied Microbiology and Biotechnology* **38**: 453-457

Boiteux A., Markus M., Plesser T., Hess B. 1983. Interaction of pyruvate kinase from *Escherichia coli* with fructose 1,6-bisphosphate and calcium ions. *Biochemical Journal* **211**: 631-640

Boulanger E.F., Sabag-Daigle A., Baniasad M., Kokkinias K., Schwieters A., Wrighton K.C., Wysocki V.H., Ahmer B.M.M. 2022. Sugar-phosphate toxicities attenuate *Salmonella* fitness in the gut. *Journal of Bacteriology* **204**: e00344-22

Bradford M.M. 1976. A rapid and sensitive method for the quantification of microgram quantities of protein utilizing the principle of protein-dye binding. *Analytical Biochemistry* **72**: 248-254

Brockman I.M., Prather K.L.J. 2015. Dynamic knockdown of *E. coli* central metabolism for redirecting fluxes of primary metabolites. *Metabolic Engineering* **28**: 104-113

Bustin S.A., Benes V., Garson J.A., Hellemans J., Huggett J., Kubista M., Mueller R., Nolan T., Pfaffl M.W., Shipley G.L., Vandesompele J., Wittwer C.T. 2009. The MIQE guidelines: Minimum Information for Publication of Quantitative real-time PCR Experiments. *Clinical Chemistry* **55**: 611-622

Cairns J., Overbaugh J., Miller S. 1988. The origin of mutants. *Nature* **335**: 142-145

Camci-Unal G., Mizanur R.M., Chai Y., Pohl N.L.B. 2012. Synthesis of a 3-deoxy-D-manno-octulosonic acid (KDO) building block from D-glucose *via* fermentation. *Organic & Biomolecular Chemistry* **10**: 5856-5860

Campos G., Guixé V., Babul J. 1984. Kinetic mechanism of phosphofructokinase-2 from *Escherichia coli*. *The Journal of Biological Chemistry* **259**: 6147-6152

Castillo J.A., Calveras J., Casas J., Mitjans M., Vinardell M.P., Parella T., Inoue T., Sprenger G.A., Joglar J., Clapés P. 2006. Fructose-6-phosphate aldolase in organic synthesis: preparation of D-fagomine, N-alkylated derivatives, and preliminary biological assays. *Organic Letters* **8**: 6067-6070

Castillo J.A., Guérard-Hélaine C., Gutiérrez M., Garrabou X., Sancelme M., Schürmann M., Inoue T., Hélaine V., Charmantray F., Gefflaut T., Hecquet L., Joglar J., Clapés P., Sprenger G.A., Lemaire M. 2010. A mutant of D-fructose-6-phosphate aldolase (Ala129Ser) with improved affinity towards dihydroxyacetone for the synthesis of polyhydroxylated compounds. *Advanced Synthesis & Catalysis* **352**: 1039-1046

Cech D., Wang P.F., Holler T.P., Woodard R.W. 2014. Analysis of the arabinose-5-phosphate isomerase of *Bacteroides fragilis* provides insight into regulation of single-domain arabinose phosphate isomerases. *Journal of Bacteriology* **196**: 2861-2868

Cech D.L., Markin K., Woodard R.W. 2017. Identification of a D-arabinose-5-phosphate isomerase in the Gram-positive *Clostridium tetani*. *Journal of Bacteriology* **199**: e00246-17

Chavarría M., Durante-Rodríguez G., Krell T., Santiago C., Brezovsky J., Damborsky J., de Lorenzo V. 2014. Fructose 1-phosphate is the one and only physiological effector of the Cra (FruR) regulator of *Pseudomonas putida*. *FEBS Open Bio* **4**: 377-386

Chen Z., Liu D. 2016. Toward glycerol biorefinery: metabolic engineering for the production of biofuels and chemicals from glycerol. *Biotechnology for Biofuels* **9**: 205

Cherepanov P.P., Wackernagel W. 1995. Gene disruption in *Escherichia coli*: Tc^R and Km^R cassettes with the option of Flp-catalyzed excision of the antibiotic-resistance determinant. *Gene* **158**: 9–14.

Chotani G., Dodge T., Hsu A., Kumar M., LaDuca R., Trimbur D., Weyler W., Sanford K. 2000. The commercial production of chemicals using pathway engineering. *Biochimica et Biophysica Acta* **1543**: 434-455

Cipolla L., Gabrielli L., Bini D., Russo L., Shaikh N. 2010. Kdo: a critical monosaccharide for bacteria viability. *Natural Product Reports* **27**: 1618-1629

Ciriminna R., Palmisano G., Della Pina C., Rossi M., Pagliaro M. 2006. One-pot electrocatalytic oxidation of glycerol to DHA. *Tetrahedron Letters* **47**: 6993-6995

Clapés P., Fessner W.-D., Sprenger G.A., Samland A.K. 2010. Recent progress in stereoselective synthesis with aldolases. *Current Opinion in Chemical Biology* **14**: 154-167

Coltharp C., Buss J., Plumer T.M., Xiao J. 2016. Defining the rate-limiting processes of bacterial cytokinesis. *Proceedings of the National Academy of Sciences of the USA* E1044-E1053

Concia A.L., Lozano C., Castillo J.A., Parella T., Joglar J., Clapés P. 2009. D-fructose-6-phosphate aldolase in organic synthesis: cascade chemical-enzymatic preparation of sugar-related polyhydroxylated compounds. *Chemistry A European Journal* **15**: 3808-3816

Connstein W., Lüdecke K. 1919. Glyceringewinnung aus Zucker. *Die Naturwissenschaften. Wochenschrift für die Fortschritte der Naturwissenschaft, der Medizin und der Technik* **23**: 403-405

Crigler J., Bannerman-Akwei L., Cole A.E., Eiteman M.A., Altman E. 2018. Glucose can be transported and utilized in *Escherichia coli* by an altered or overproduced *N*-acetylglucosamine phosphotransferase system (PTS). *Microbiology* **164**: 163-172

Daldal F. 1983. Molecular cloning of the gene for phosphofructokinase-2 of *Escherichia coli* and the nature of a mutation, *pfkB1*, causing a high level of the enzyme. *Journal of Molecular Biology* **168**: 285-305

Datsenko K.A., Wanner B.L. 2000. One-step inactivation of chromosomal genes in *Escherichia coli* K-12 using PCR products. *PNAS* **97**: 6640-6645

de Boer M., Broekhuizen C.P., Postma P.W. 1986. Regulation of glycerol kinase by enzyme III^{Glc} of the phosphoenolpyruvate:carbohydrate phosphotransferase system. *Journal of Bacteriology* **167**: 393-395

De Simone A., Vicente C.M., Peiro C., Gales L., Bellvert F., Enjalbert B., Heux S. 2020. Mixing and matching methylotrophic enzymes to design a novel methanol utilization pathway in *E. coli*. *Metabolic Engineering* **61**: 315-325

Deng J., Pan T., Xu Q., Chen M.-Y., Zhang Y., Guo Q.-X., Fu Y. 2013. Linked strategy for the production of fuels via formose reaction. *Scientific Reports* **3**: 1244

Deutscher J., Francke C., Postma P.W. 2006. How phosphotransferase system-related protein phosphorylation regulates carbohydrate metabolism in bacteria. *Microbiology and Molecular Biology Reviews* **70**: 939-1031

Deutscher J., Moussan Désirée Aké F., Derkaoui M., Constant Zébré A., Nguyen Cao T., Bouraoui H., Kentache T., Mokhtari A., Milohanic E., Joyet P. 2014. The bacterial phosphoenolpyruvate:carbohydrate phosphotransferase system: regulation by protein phosphorylation and phosphorylation-dependent protein-protein interactions. *Microbiology and Molecular Biology Reviews* **78**: 231-256

Dower W.J., Miller J.F., Ragsdale C.W. 1988. High efficiency transformation of *E. coli* by high voltage electroporation. *Nucleic Acids Research* **16**: 6127-6145

Erni B., Siebold C., Christen S., Srinivas A., Oberholzer A., Baumann U. 2006. Small substrate, big surprise: fold, function and phylogeny of dihydroxyacetone kinases. *Cellular and Molecular Life Sciences* **63**: 890-900

Feklístov A., Sharon B.D., Darst S.A., Gross C.A. 2014. Bacterial sigma factors: a historical, structural, and genomic perspective. *Annual Review of Microbiology* **68**: 357-376

Feuer R., Gottlieb K., Viertel G., Klotz J., Schober S., Bossert M., Sawodny O., Sprenger G., Ederer M. 2012. Model-based analysis of an adaptive evolution experiment with *Escherichia coli* in a pyruvate limited continuous culture with glycerol. *EURASIP Journal on Bioinformatics and Systems Biology* **2012**: 14

Fic E., Bonarek P., Gorecki A., Kedracka-Krok S., Mikolajczak J., Polit A., Tworzydlo M., Dziedzicka-Wasylewska M., Wasylewski Z. 2009. cAMP receptor protein from *Escherichia coli* as a model of signal transduction in proteins - a review. *Journal of Molecular Microbiology and Biotechnology* **17**: 1-11

Fischer E., Sauer U. 2003. Metabolic flux profiling of *Escherichia coli* mutants in central carbon metabolism using GC-MS. *European Journal of Biochemistry* **270**: 880-891

Fisher A.K., Freedman B.G., Bevan D.R., Senger R.S. 2014. A review of metabolic and enzymatic engineering strategies for designing and optimizing performance of microbial cell factories. *Computational and Structural Biotechnology Journal* **11**: 91-99

Flores N., Leal L., Sigala J.C., de Anda R., Escalante A., Martínez A., Ramírez O.T., Gosset G., Bolivar F. 2007. Growth recovery on glucose under aerobic conditions of an *Escherichia coli* strain carrying a phosphoenolpyruvate:carbohydrate phosphotransferase system deletion by inactivating *arcA* and overexpressing the genes coding for glucokinase and galactose permease. *Journal of Molecular Microbiology and Biotechnology* **13**: 105-116

Folly B.B., Ortega A.D., Hubmann G., Bonsing-Vedelaar S., Wijma H.J., van der Meulen P., Milias-Argeitis A., Heinemann M. 2018. Assessment of the interaction between the flux-signaling metabolite fructose-1,6-bisphosphate and the bacterial transcription factors CggR and Cra. *Molecular Microbiology* **109**: 278-290

Fong S.S., Marcinial J.Y., Palsson B.Ø. 2003. Description and interpretation of adaptive evolution of *Escherichia coli* K-12 MG1655 by using a genome-scale in silico metabolic model. *Journal of Bacteriology* **185**: 6400-6408

Fong S.S., Nanchen A., Palsson B.Ø., Sauer U. 2006. Latent pathway activation and increased pathway capacity enable *Escherichia coli* adaptation to loss of key metabolic enzymes. *The Journal of Biological Chemistry* **281**: 8024-8033

Fong S.S., Palsson B.Ø. 2004. Metabolic gene-deletion strains of *Escherichia coli* evolve to computationally predicted growth phenotypes. *Nature Genetics* **36**: 1056-1058

Fraenkel D.G. 1968. Selection of *Escherichia coli* mutants lacking glucose-6-phosphate dehydrogenase or gluconate-6-phosphate dehydrogenase. *Journal of Bacteriology* **95**: 1267-1271

Fraval H.N.A., McBrien D.C.H. 1980. The effect of methyl glyoxal on cell division and the synthesis of protein and DNA in synchronous and asynchronous cultures of *Escherichia coli* B/r. *Journal of General Microbiology* **117**: 127-134

Fuchs G. 2007. Allgemeine Mikrobiologie. 8. edition. Georg Thieme Verlag: Stuttgart

Fujishima H., Nishimura A., Wachi M., Takagi H., Hirasawa T., Teraoka H., Nishimori K., Kawabata T., Nishikawa K., Nagai K. 2002. *kdsA* mutations affect FtsZ-ring formation in *Escherichia coli* K-12. *Microbiology* **148**: 103-112

Fürste J.P., Pansegrau W., Frank R., Blöcker H., Scholz P., Bagdasarian M., Lanka E. 1986 Molecular cloning of the plasmid RP4 primase region in a multi-host-range *tac*P expression vector. G*ene* **48**: 119-131.

Gabor E., Göhler A.-K., Kosfeld A., Staab A., Kremling A., Jahreis K. 2011. The phosphoenolpyruvate-dependent glucose-phosphotransferase system from *Escherichia coli* K-12 as the center of a network regulating carbohydrate flux in the cell. *European Journal of Cell Biology* **90**: 711-720

Galloway S.M., Raetz C.R.H. 1990. A mutant of *Escherichia coli* defective in the first step of endotoxin biosynthesis. *The Journal of Biological Chemistry* **265**: 6394-6402

Gao Y., Lim H.G., Verkler H., Szubin R., Quach D., Rodionova I., Chen K., Yurkovich J.T., Cho B.-K., Palsson B.O. 2021. Unraveling the functions of uncharacterized transcription factors in *Escherichia coli* using ChIP-exo. *Nucleic Acids Research* **49**: 9696-9710

Garrabou X., Castillo J.A., Guérard-Hélaine C., Parella T., Joglar J., Lemaire M., Clapés P. 2009. Asymmetric self- and cross-aldol reactions of glycolaldehyde catalyzed by D-fructose-6-phosphate aldolase. *Angewandte Chemie* **121**: 5629-5633

Garrabou X., Joglar J., Parella T., Crehuet R., Bujons J., Clapés P. 2011. Redesign of the phosphate binding site of L-rhamnulose-1-phosphate aldolase towards a dihydroxyacetone dependent aldolase. *Advanced Synthesis & Catalysis* **353**: 89-99

Gimpel M., Brantl S. 2016. Dual-function small regulatory RNAs in bacteria. *Molecular Microbiology* **103**: 387-397

Gleizer S., Ben-Nissan R., Bar-On Y.M., Antonovsky N., Noor E., Zohar Y., Jona G., Krieger E., Shamshoum M., Bar-Even A., Milo R. 2019. Conversion of *Escherichia coli* to generate all biomass carbon from CO_2. *Cell* **179**: 1255-1263

Gonzalez R., Murarka A., Dharmadi Y., Yazdani S.S. 2008. A new model for the anaerobic fermentation of glycerol in enteric bacteria: trunk and auxiliary pathways in *Escherichia coli*. *Metabolic Engineering* **10**: 234-245

Gosset G. 2005. Improvement of *Escherichia coli* production strains by modification of the phosphoenolpyruvate:sugar phosphotransferase system. *Microbial Cell Factories* **4**: 14

Gronow S., Brade H. 2001. Lipopolysaccharide biosynthesis: which steps do bacteria need to survive? *Journal of Endotoxin Research* **7**: 3-23

Guérard-Hélaine C., de Berardinis V., Besnard-Gonnet M., Darii E., Debacker M., Debard A., Fernandes C., Hélaine V., Mariage A., Pellouin V., Perret A., Petit J.-L., Sancelme M., Lemaire M., Salanoubat M. 2015. Genome mining for innovative biocatalysts: new dihydroxyacetone aldolases for the chemist's toolbox. *ChemCatChem* **7**: 1871-1879

Guérard-Hélaine C., Debacker M., Clapés P., Szekrenyi A., Hélaine V., Lemaire M. 2014. Efficient biocatalytic processes for highly valuable terminally phosphorylated C5 to C9 D-ketoses. *Green Chemistry* **16**: 1109

Guitart Font E., Sprenger G.A. 2020. Opening a novel biosynthetic pathway to dihydroxyacetone and glycerol in *Escherichia coli* mutants through expression of a gene variant (*fsaA^{A129S}*) for fructose 6-phosphate aldolase. *International Journal of Molecular Sciences* **21**: 9625

Gutknecht R., Beutler R., Garcia-Alles L.F., Baumann U., Erni B. 2001. The dihydroxyacetone kinase of *Escherichia coli* utilizes a phosphoprotein instead of ATP as phosphoryl donor. *The EMBO Journal* **20**: 2480-2486

Hanahan D. 1983. Studies on transformation of *Escherichia coli* with plasmids. *Journal of Molecular Biology* **166**: 557-580

Harris L.K., Theriot J.A. 2016. Relative rates of surface and volume synthesis set bacterial cell size. *Cell* **165**: 1479-1492

Hayashi S.-I., Lin E.C.C. 1967. Purification and properties of glycerol kinase from *Escherichia coli*. *The Journal of Biological Chemistry* **242**: 1030-1035

Hélaine V., Gastaldi C., Lemaire M., Clapés P, Guérard-Hélaine C. 2022. Recent advances in the substrate selectivity of aldolases. *ACS Catalysis* **12**: 733-761

Hélaine V., Mahdi R., Sudhir Babu G.V., de Berardinis V., Wohlgemuth R., Lemaire M., Guérard-Hélaine C. 2015. Straightforward synthesis of terminally phosphorylated L-sugars *via* multienzymatic cascade reactions. *Advanced Synthesis & Catalysis* **357**: 1703-1708

Hengge-Aronis R. 2002. Signal transduction and regulatory mechanisms involved in control of the σ^S (RpoS) subunit of RNA polymerase. *Microbiology and Molecular Biology Reviews* **66**: 373-395

Hernández K., Parella T., Joglar J., Bujons J., Pohl M., Clapés P. 2015. Expedient synthesis of *C*-aryl carbohydrates by consecutive biocatalytic benzoin and aldol reactions. *Chemistry A European Journal* **21**: 3335-3346

Hernández K., Szekrenyi A., Clapés P. 2018. Nucleophile promiscuity of natural and engineered aldolases. *ChemBioChem* **19**: 1353-1358

Higuchi R., Dollinger G., Walsh P.S., Griffith R. 1992. Simultaneous amplification and detection of specific DNA sequences. *Bio/Technology* **10**: 413-417

Hill N.S., Buske P.J., Shi Y., Levin P.A. 2013. A moonlighting enzyme links *Escherichia coli* cell size with central metabolism. *PLOS Genetics* **9**: e1003663

Hirayama H., Takaki Y., Abe M., Imachi H., Ikuta T., Miyazaki J., Tasumi E., Uematsu K., Tame A., Tsuda M., Tanaka K., Matsui Y., Watanabe H.K., Yamamoto H., Takai K. 2022. Multispecies populations of methanotrophic *Methyloprofundus* and cultivation of a likely dominant species from the Iheya North Deep-Sea hydrothermal field. *Applied and Environmental Microbiology* **88**: e00758-21

Hogema B.M., Arents J.C., Bader R., Eijkemans K., Yoshida H., Takahashi H., Aiba H., Postma P.W. 1998. Inducer exclusion in *Escherichia coli* by non-PTS substrates: the role of the PEP to pyruvate ratio in determining the phosphorylation state of enzyme IIA$^{\text{Glc}}$. *Molecular Microbiology* **30**: 487-498

Hollinshead W.D., Rodriguez S., Garcia Martin H., Wang G., Baidoo E.E.K., Sale K.L., Keasling J.D., Mukhopadhyay A., Tang Y.J. 2016. Examining *Escherichia coli* glycolytic pathways, catabolite repression, and metabolite channeling using Δ*pfk* mutants. *Biotechnology for Biofuels* **9**: 212

Holtman C.K., Pawlyk A.C., Meadow N.D., Pettigrew D.W. 2001. Reverse genetics of *Escherichia coli* glycerol kinase allosteric regulation and glucose control of glycerol utilization in vivo. *Journal of Bacteriology* **183**: 3336-3344

Hu, Zhong-Ce, Liu Z.-Q., Zheng Y.-G., Shen Y.-C. 2010. Production of 1,3-dihydroxyacetone from glycerol by *Gluconobacter oxydans* ZJB09112. *Journal of Microbiology and Biotechnology* **20**: 340-345

Inoue T. 2006. Dissertation. Microbial alsolases as C-C bonding enzymes: Investigation of structural-functional characteristics and application for stereoselective reactions. *Universität Stuttgart*

Ishihama A. 2010. Prokaryotic genome regulation: multifactor promoters, multitarget regulators and hierarchic networks. *FEMS Microbiology Reviews* **34**: 628-645

Ishihama A., Kori A., Koshio E., Yamada K., Maeda H., Shimada T., Makinoshima H., Iwata A., Fujita N. 2014. Intracellular concentrations of 65 species of transcription factors with known regulatory functions in *Escherichia coli*. *Journal of Bacteriology* **196**: 2718-2727

Izui K., Taguchi M., Morikawa M., Katsuki H. 1981. Regulation of *Escherichia coli* phosphoenolpyruvate carboxylase by multiple effectors *in vivo*. II. Kinetic studies with a reaction system containing physiological concentrations of ligands. *The Journal of Biochemistry* **90**: 1321-1331

Jahreis K., Pimentel-Schmitt E.F., Brückner R., Titgemeyer F. 2008. Ins and outs of glucose transport systems in eubacteria. *FEMS Microbiology Reviews* **32**:891-907

Jain V.K., Tear C.J.Y., Lim C.Y. 2016. Dihydroxyacetone production in an engineered *Escherichia coli* through expression of *Corynebacterium glutamicum* dihydroxyacetone phosphate dephosphorylase. *Enzyme and Microbial Technology* **86**: 39-44

Jiang Y., Chen B., Duan C., Sun B., Yang J., Yang S. 2015. Multigene Editing in the *Escherichia coli* Genome via the CRISPR-Cas9 System. *Applied and Environmental Microbiology* **81**: 2506-2514

Jin R.Z., Forage R.G., Lin E.C.C. 1982. Glycerol kinase as a substitute for dihydroxyacetone kinase in a mutant of *Klebsiella pneumoniae*. *Journal of Bacteriology* **152**: 1303-1307

Jin R.Z., Lin E.C.C. 1984. An inducible phosphoenolpyruvate: dihydroxyacetone phosphotransferase system in *Escherichia coli*. *Journal of General Microbiology* **130**: 83-88

Joyce A.R., Reed J.L., White A., Edwards R., Osterman A., Baba T., Mori H., Lesely S.A., Palsson B.Ø., Agarwalla S. 2006. Experimental and computational assessment of conditionally essential genes in *Escherichia coli*. *Journal of Bacteriology* **188**: 8259-8271

Karkhanis Y.D., Zeltner J.Y., Jackson J.J., Carlo D.J. 1978. A new and improved microassay to determine 2-keto-3-deoxyoctonate in lipopolysaccharide of gram-negative bacteria. *Analytical Biochemistry* **85**: 595-601

Kawamoto H., Koide Y., Morita T., Aiba H. 2006. Base-pairing requirement for RNA silencing by a bacterial small RNA and acceleration of duplex formation by Hfq. *Molecular Microbiology* **61**: 1013-1022

Kim Y.E., Cho K.H., Bang I., Kim C.H., Ryu Y.S., Kim Y., Choi E.M., Nong L.K., Kim D., Lee S.K. 2022. Characterization of a Entner-Doudoroff pathway-activated *Escherichia coli*. *Biotechnology for Biofuels and Bioproducts* **15**: 120

Kimata K., Tanaka Y., Inada T., Aiba H. 2001. Expression of the glucose transporter gene, *ptsG*, is regulated at the mRNA degradation step in response to glycolytic flux in *Escherichia coli*. *The EMBO Journal* **20**: 3587-3595

King J.R., Woolston B.M., Stephanopoulos G. 2017. Designing a new entry point into isoprenoid metabolism by exploiting fructose-6-phosphate aldolase side reactivity of *Escherichia coli*. *ACS Synthetic Biology* **6**: 1416-1426

Koch J.P., Hayashi S.-I., Lin E.C.C. 1964. The control of dissimilation of glycerol and L-α-glycerophosphate in *Escherichia coli*. *The Journal of Biological Chemistry* **39**: 3106-3108

Kochanowski K., Gerosa L., Brunner S.F., Christodoulou D., Nikolaev Y.V., Sauer U. 2017. Few regulatory metabolites coordinate expression of central metabolic genes in *Escherichia coli*. *Molecular Systems Biology* **13**: 903

Kochanowski K., Volkmer B., Gerosa L., Haverkorn van Rijsewijk B.R., Schmidt A., Heinemann M. 2013. Functioning of a metabolic flux sensor in *Escherichia coli*. *Proceedings of the National Academy of Sciences of the USA* **110**: 1130-1135

Kornberg H.L. 2001. Routes for fructose utilization by *Escherichia coli*. *Journal of Molecular Microbiology and Biotechnology* **3**: 355-359

Kornberg H.L., Smith J. 1970. Role of phosphofructokinase in the utilization of glucose by *Escherichia coli*. *Nature* **227**: 44-46

Kosfeld A., Jahreis K. 2012. Characterization of the interaction between the small regulatory peptide SgrT and the EIICB^{Glc} of the glucose-phosphotransferase system of *E. coli* K-12. *Metabolites* **2**: 756-774

Lachaux C., Frazao C.J.R., Kraußer F., Morin N., Walther T., François J.M. 2019. A new synthetic pathway for the bioproduction of glycolic acid from lignocellulosic sugars aimed at maximal carbon conservation. *Frontiers in Bioengineering and Biotechnology* **7**: 359

Laemmli U.K. 1970. Cleavage of structural proteins during the assembly of the head of bacteriophage T4. *Nature* **227**: 680-685

Lam H.-M., Winkler M.E. 1990. Metabolic relationships between pyridoxine (vitamin B$_6$) and serine biosynthesis in *Escherichia coli* K-12. *Journal of Bacteriology* **172**: 6518-6528

LeBlanc D., Mortlock R.P. 1971. Metabolism of D-arabinose: a new pathway in *Escherichia coli*. *Journal of Bacteriology* **106**: 90-96

Lee C.-H., Tsai C.-M. 1999. Quantification of bacterial lipopolysaccharide by the purpald assay: measuring formaldehyde generated from 2-keto-3-deoxyoctonate and heptose at the inner core by periodate oxidation. *Analytical Biochemistry* **267**: 161-168

Lee D.J., Minchin S.D., Busby S.J.W. 2012. Activating transcription in bacteria. *Annual Review of Microbiology* **66**: 125-152

Lee S.-H., Hong S.-H., An J.-U., Kim K.-R., Kim D.-E., Kang L.-W., Oh D.-K. 2017. Structure-based prediction and identification of 4-epimerization activity of phosphate sugars in class II aldolases. *Scientific reports* **7**: 1934

Levy S.B. 1992. Dihydroxyacetone-containing sunless or self-tanning lotions. *Journal of the American Academy of Dermatology* **27**: 989-993

Li G.-W., Burkhardt D., Gross C., Weissman J.S. 2014. Quantifying absolute protein synthesis rates reveals principles underlying allocation of cellular resources. *Cells* **157**: 624-635

Li W., Zhao X., Zou S., Ma Y., Zhang K., Zhang M. 2012. Scanning assay of β-galactosidase activity. *Applied Biochemistry and Microbiology* **48**: 603-607

Li Z., Dong Y., Liu Y., Cen X., Liu D., Chen Z. 2022. Systems metabolic engineering of *Corynebacterium glutamicum* for high-level production of 1,3-propanediol from glucose and xylose. *Metabolic Engineering* **70**: 79-88

Lim H.G., Noh M.H., Jeong J.H., Park S., Jung G.Y. 2016. Optimum rebalancing of the 3-hydroxypropionic acid production pathway from glycerol in *Escherichia coli*. *ACS Synthetic Biology* **5**: 1247-1255

Lim J.H., Jung G.Y. 2017. A simple method to control glycolytic flux for the design of an optimal cell factory. *Biotechnology for Biofuels* **10**: 160

Lim R., Cohen S.S. 1966. D-phosphoarabinoisomerase and D-ribulokinase in *Escherichia coli*. *The Journal of Biological Chemistry* **241**: 4304-4315

Lindner S.N., Aslan S., Müller A., Hoffart E., Behrens P., Edlich-Muth C., Blombach B., Bar-Even A. 2020. A synthetic glycerol assimilation pathway demonstrates biochemical constraints of cellular metabolism. *The FEBS Journal* **287**: 160-172

Liu D., Reeves P.R. 1994. *Escherichia coli* K12 regains its O antigen. *Microbiology* **140**: 49-57

Liu Z., Hu Z., Zheng Y., Shen Y. 2008. Optimization of cultivation conditions for the production of 1,3-dihydroxyacetone by *Pichia membranifaciens* using response surface methodology. *Biochemical Engineering Journal* **38**: 285-291

Lloyd C.R., Park S., Fei J., Vanderpool C.K. 2017. The small protein SgrT controls transport activity of the glucose-specific phosphotransferase system. *Journal of Bacteriology* **199**: e00869-16

Lovingshimer M.R., Siegele D., Reinhart G.D. 2006. Construction of an inducible, *pfkA* and *pfkB* deficient strain of *Escherichia coli* for the expression and purification of phosphofructokinase from bacterial sources. *Protein Expression and Purification* **46**: 475-482

Lu X., Liu X., Yang Y., Wang S., Wang Q., Wang X., Yan Z., Cheng J., Liu C., Yang X., Luo H., Yang S., Gou J., Ye L., Lu L., Zhang Z., Guo Y., Nie Y., Lin J., Li S., Tian C., Cai T., Zhuo B., Ma H., Wang W., Ma Y., Liu Y., Li Y., Jiang H. 2019. Constructing a synthetic pathway for acetyl-coenzyme A from one-carbon through enzyme design. *Nature Communications* **10**: 1378

Luo X., Ge X., Cui S., Li Y. 2016. Value-added processing of crude glycerol into chemicals and polymers. *Bioresource Technology* **215**: 144-154

Luo Y., Zhang T., Wu H. 2014. The transport and mediation mechanisms of the common sugars in *Escherichia coli*. *Biotechnology Advances* **32**: 905-919

Ma L., Lu W., Xia Z., Wen J. 2010. Enhancement of dihydroxyacetone production by a mutant of *Gluconobacter oxydans*. *Biochemical Engineering Journal* **49**: 61-67

Maki K., Morita T., Otaka H., Aiba H. 2010. A minimal base-pairing region of a bacterial small RNA SgrS required for translational repression of ptsG mRNA. *Molecular Microbiology* **76**: 782-792

Maki K., Uno K., Morita T., Aiba H. 2008. RNA, but not protein partners, is directly responsible for translational silencing by a bacterial Hfq-binding small RNA. *Proceedings of the National Academy of Sciences of the USA* **105**: 10332-10337

Mamat U., Meredith T.C., Aggarwal P., Kühl A., Kirchhoff P., Lindner B., Hanuszkiewicz A., Sun J., Holst O., Woodard R.W. 2008. Single amino acid substitutions in either YhjD or MsbA confer viability to 3-deoxy-D-*manno*-oct-2-ulosonic acid-depleted *Escherichia coli*. *Molecular Microbiology* **67**: 633-648

Mao Y., Yuan Q., Yang X., Liu P., Cheng Y., Luo J., Liu H., Yao Y. Sun H., Cai T., Ma H. 2021. Non-natural aldol reactions enable the design and construction of novel one-carbon assimilation pathways *in vitro*. *Frontiers in Microbiology* **12**: 677596

Matsumoto T., Yamamoto H., Inoue S. 1984. Selective formation of triose from formaldehyde catalyzed by thiazolium salt. *Journal of the American Chemical Society* **106**: 4829-4832

Mayer C., Boos W. 2005. Hexose/pentose and hexitol/pentitol metabolism. *EcoSal Plus* **1**: doi:10.1128/ecosalplus.3.4.1

McKenzie G.J., Harris R.S., Lee P.L., Rosenberg S.M. 2000. The SOS response regulates adaptive mutation. *Proceedings of the National Academy of Sciences of the USA* **97**: 6646-6651

McKenzie G.J., Lee P.L., Lombardo M.-J., Hastings P.J., Rosenberg S.M. 2001. SOS mutator DNA polymerase IV functions in adaptive mutation and not adaptive amplification. *Molecular Cell* **7**: 571-579

Meile L., Rohr L.M., Geissmann T.A., Herensperger M., Teuber M. 2001. Characterization of the D-xylulose 5-phosphate / D-fructose 6-phosphate phosphoketolase gene (*xfp*) from *Bifidobacterium lactis*. *Journal of Bacteriology* **183**: 2929-2936

Meredith T.C., Aggarwal P., Mamat U., Lindner B., Woodard R. 2006. Redifining the requisite lipopolysaccharide structure in *Escherichia coli*. *ACS Chemical Biology* **1**: 33-42

Meredith T.C., Woodard R.W. 2003. *Escherichia coli* YrbH is a D-arabinose 5-phosphote isomerase. *The Journal of Biological Chemistry* **278**: 32771-32777

Meredith T.C., Woodard R.W. 2005. Identification of GutQ from *Escherichia coli* as a D-arabinose 5-phosphate isomerase. *Journal of Bacteriology* **187**: 6936-6942

Meza E., Becker J., Bolivar F., Gosset G., Wittmann C. 2012. Consequences of phosphoenolpyruvate:sugar phosphotransferase system and pyruvate kinase isozymes inactivation in central carbon metabolism flux distribution in *Escherichia coli*. *Microbial Cell Factories* **11**: 127

Mi W., Li Y., Yoon S.H., Ernst R.K., Walz T., Liao M. 2017. Structural basis of MsbA – mediated lipopolysaccharide transport. *Nature* **549**: 233-237

Moat A.G., Foster J.W., Spector M.P. 2002. Metabolism of substrates other than glucose. *Microbial Physiology*. Wiley-Liss, Inc. 394-411

Molin M., Blomberg A. 2006. Dihydroxyacetone detoxification in *Saccharomyces cerevisiae* involves formaldehyde dissimilation. *Molecular Microbiology* **60**: 925-938

Molin M., Norbeck J., Blomberg A. 2003. Dihydroxyacetone kinases in *Saccharomyces cerevisiae* are involved in detoxification of dihydroxyacetone. *The Journal of Biological Chemistry* **278**: 1415-1423

Monahan L.G., Harry E.J. 2016. You are what you eat: metabolic control of bacterial division. *Trends in Microbiology* **24**: 181-189

Mülhardt C. 2009. Die Klonierung von DNA-Fragmente. Der Experimentator: Molekularbiologie / Genomics. Spektrum Akademischer Verlag, Heidelberg 139-168

Mullis K.B., Faloona F.A. 1987. Specific synthesis of DNA *in vitro* via a polymerase-catalyzed chain reaction. *Methods in Enzymology* **155**:335-350

Murarka A., Dharmadi Y., Yazdani S.S., Gonzalez R. 2008. Fermentative utilization of glycerol by *Escherichia coli* and its implications for the production of fuels and chemicals. *Applied and Environmental Microbiology* **74**: 1124-1135

Nakahigashi K., Toya Y., Ishii N., Soga T., Hasegawa M., Watanabe H., Takai Y., Honma M., Mori H., Tomita M. 2009. Systematic phenome analysis of *Escherichia coli* multiple-knockout mutants reveals hidden reactions in central carbon metabolism. *Molecular Systems Biology* **5**: 306

Nakamura C.E., Whited G.M. 2003. Metabolic engineering for the microbial production of 1,3-propanediol. *Current Opinion in Biotechnology* **14**: 454-459

Nakashima N., Ohno S., Yoshikawa K., Shimizu H., Tamura T. 2014. A vector library for silencing central carbon metabolism genes with antisense RNAs in *Escherichia coli*. *Applied and Environmental Microbiology* **80**: 564-573

Nanninga N. 1998. Morphogenesis of *Escherichia coli*. *Microbiology and Molecular Biology Reviews* **62**: 110-129

Neidhardt F.C. 1996. *Escherichia coli* and *Salmonella*. Cellular and Molecular Biology. Second Edition. Volume 1. ASM Press: USA

Neidhardt F.C., Bloch P.L., Smith D.F. 1974. Culture medium for enterobacteria. *Journal of Bacteriology* **119**: 736-747

Neidhardt F.C., Ingraham J.L., Schaechter M. 1990. Physiology of the bacterial cell. A molecular approach. Sinauer Associates: USA

Nguyen H.T.T., Nevoigt E. 2009. Engineering of *Saccharomyces cerevisiae* for the production of dihydroxyacetone (DHA) from sugars: A proof of concept. *Metabolic Engineering* **11**: 335-346

Nikaido H., Vaara M. 1985. Molecular basis of bacterial outer membrane permeability. *Microbiological Reviews* **49**: 1-32

Nomura W., Aoki M., Inoue Y. 2018. Toxicity of dihydroxyacetone is exerted through the formation of methylglyoxal in *Saccharomyces cerevisiae*: effects on actin polarity and nuclear division. *Biochemical Journal* **475**: 2637-2652

Noor E., Eden E., Milo R., Alon U. 2010. Central carbon metabolism as a minimal biochemical walk between precursors for biomass and energy. *Molecular Cell* **39**: 809-820

O'Brien P., Herschlag D. 1999. Catalytic promiscuity and the evolution of new enzymatic activities. *Chemistry & Biology* **6**: R91-R105

Ogawa T., Murakami K., Yoshino M. 2016. Inhibition by fructose 1,6-bisphosphate of transaldolase from *Escherichia coli*. *FEMS Microbiology Letters* **326**: fnw183

Overkamp K.M., Bakker B.M., Kötter P., Luttik M.A.H., van Dijken J.P., Pronk J.T. 2002. Metabolic engineering of glycerol production in *Saccharomyces cerevisiae*. *Applied and Environmental Microbiology* **68**: 2814-2821

Pagliaro M., Ciriminna R., Kimura H., Rossi M., Della Pina C. 2007. From glycerol to value-added products. *Angewandte Chemie International Edition* **46**: 4434-4440

Pandit A.V., Harrison E., Mahadevan R. 2021. Engineering *Escherichia coli* for the utilization of ethylene glycol. *Microbial Cell Factories* **20**: 22

Papenfort K., Sun Y., Miyakoshi M., Vanderpool C.K., Vogel J. 2013. Small RNA-mediated activation of sugar phosphatase mRNA regulates glucose homeostasis. *Cell* **153**: 426-437

Park J.O., Rubin S.A., Xu Y.-F., Amador-Noguez D., Fan J., Shlomi T., Rabinowitz J.D. 2016. Metabolite concentrations, fluxes, and free energies imply efficient enzyme usage. *Nature Chemical Biology* **12**: 482-489

Patnaik R., Roof W.D., Young R.F., Liao J.C. 1992. Stimulation of glucose catabolism in *Escherichia coli* by a potential futile cycle. *Journal of Bacteriology* **174**: 7527-7532

Pearsall S.M., Rowley C.N., Berry A. 2015. Advances in pathway engineering for natural product biosynthesis. *ChemCatChem* **7**: 3078-3093

Peiro C., Millard P., de Simone A., Cahoreau E., Peyriga L., Enjalbert B., Heux S. 2019. Chemical and metabolic controls on dihydroxyacetone metabolism lead to suboptimal growth of *Escherichia coli*. *Applied and Environmental Microbiology* **85**: e00768-19

Peng L., Arauzo-Bravo M.J., Shimizu K. 2004. Metabolic flux analysis for a *ppc* mutant *Escherichia coli* based on ^{13}C-labelling experiments together with enzyme activity assays and intracellular metabolite measurements. *FEMS Microbiology Letters* **235**: 17-23

Persson Ö., Valadi A., Nyström T., Farewell A. 2007. Metabolic control of the *Escherichia coli* universal stress protein response through fructose-6-phophate. *Molecular Microbiology* **65**: 968-978

Petersen A.B., Wulf H.C., Gniadecki R., Gajkowska B. 2004. Dihydroxyacetone, the active browning ingredient in sunless tanning lotions, induces DHA damage, cell-cycle block and apoptosis in cultured HaCaT keratinocytes. *Mutation Research* **560**: 173-186

Piazza I., Kochanowski K., Cappelletti V., Fuhrer T., Noor E., Sauer U., Picotti P. 2018. A map of protein-metabolite interactions reveals principles of chemical communication. *Cell* **172**: 358-372

Pieper R., Zhang Q., Clark D.J., Parmar P.P., Alami H., Suh M.-J., Kuntumalla S., Braisted J.C., Huang S.-T., Tzipori S. 2013. Proteomic view of interactions of Shiga toxin-producing *Escherichia coli* with the intestinal environment in gnotobiotic piglets. *PLOS ONE* **8**: e66462

Pischetsrieder M., Seidel W., Münch G., Schinzel R. 1999. N^2-(1-carboxyethyl) deoxyguanosine, a nonenzymatic glycation adduct of DNA, induces single-strand breaks and increases mutation frequencies. *Biochemical and Biophysical Research Communications* **264**: 544-549

Preiss J. 1984. Bacterial glycogen synthesis and its regulation. *Annual Review of Microbiology* **38**: 419-58

Quispe C.A.G., Coronado C.J.R., Carvalho Jr. J.A. 2013. Glycerol: production, consumption, prices, characterization and new trends in combustion. *Renewable and Sustainable Energy Reviews* **27**: 475-493

Raetz C.R.H., Whitfield C. 2002. Lipopolysaccharide endotoxins. *Annual Review of Biochemistry* **71**: 635-700

Raina M., Storz G. 2017. SgrT, a small protein that packs a sweet punch. *Journal of Bacteriology* **199**: e00130-17

Rale M., Schneider S., Sprenger G.A., Samland A.K., Fessner W.-D. 2011. Broadening deoxysugar glycodiversity: natural and engineered transaldolases unlock a complementary substrate space. *Chemistry – A European Journal* **17**: 2623-2632

Reizer J., Reizer A., Saier M.H. Jr. 1995. Novel phosphotransferase system genes revealed by bacterial genome analysis - a gene cluster encoding a unique Enzyme I and the proteins of a fructose-like permease system. *Microbiology* **141**: 961-971

Reznik E., Christodoulou D., Goldford J.E., Briars E., Sauer U., Segrè D., Noor E. 2017. Genome-scale architecture of small molecule regulatory networks and the fundamental trade-off between regulation and enzymatic activity. *Cell Reports* **20**: 2666-2677

Ricci J.C.D., Hernández M.E. 2000. Plasmid effects on *Escherichia coli* metabolism. *Critical Reviews in Biotechnology* **20**: 79-108

Rice J.B., Balasubramanian D., and Vanderpool C.K. 2012. Small RNA binding-site multiplicity involved in translational regulation of a polycistronic mRNA. *Proceedings of the National Academy of Sciences of the USA* **109:** E2691–2698

Rice J.B., Vanderpool C.K. 2011, The small RNA SgrS controls sugar-phosphate accumulation by regulating multiple PTS genes. *Nucleic Acids Research* **39**: 3806-3819

Richards G.R., Patel M.V., Lloyd C.R., Vanderpool C.K. 2013. Depletion of glycolytic intermediates plays a key role in glucose-phosphate stress in *Escherichia coli. Journal of Bacteriology* **195**: 4816-4825

Riddle V., Lorenz F.W. 1968. Nonenzymic, polyvalent anion-catalyzed formation of methylglyoxal as an explanation of its presence in physiological systems. *The Journal of Biological Chemistry* **243**: 2718-2724

Riddle V.M., Lorenz F.W. 1973. Nonenzymic formation of toxic levels of methylglyoxal from glycerol and dihydroxyacetone in ringer's phosphate suspensions of avian spermatozoa. *Biochemical and Biophysical Research Communications* **50**: 27-34

Riemer S. 2010. Diploma Thesis. Installation of an alternative glycerol pathway in *Escherichia coli* via the glycerol dehydrogenase GLDA and the dihydroxyacetone kinase DHAK$_{Eb}$ of *Escherichia blattae*. *Universität Stuttgart*

Riemer S.A., Rex R., Schomburg D. 2013. A metabolite-centric view on flux distributions in genome-scale metabolic models. *BMC Systems Biology* **7**: 33

Roehl R.A., Vinopal R.T. 1976. Lack of glucose phosphotransferase function in phosphofructokinase mutants of *Escherichia coli*. *Journal of Bacteriology* **126**: 852-860

Roldán R., Sánchez-Moreno I., Scheidt T., Hélaine V., Lemaire M., Parella T., Clapés P., Fessner W.-D., Guérard-Hélaine C. 2017. Breaking the dogma of aldolase specificity: simple aliphatic ketones and aldehydes are nucleophiles for fructose-6-phosphate aldolase. *Chemistry - A European Journal* **23**: 5005-5009

Romeo T., Snoep J.L. 2013. Glycolysis and flux control. In *EcoSal Plus 2013*. ASMScience.org: Washington, DC, USA

Salles I.M., Forchhammer N., Croux C., Girbal L., Soucaille P. 2007. Evolution of a *Saccharomyces cerevisiae* metabolic pathway in *Escherichia coli*. *Metabolic Engineering* **9**: 152-159

Sambrook J., Fritsch E.F., Maniatis T. 1989. Molecular cloning: a laboratory manual. Cold Spring Harbor Laboratory Press: New York

Samland A.K., Rale M., Sprenger G.A., Fessner W.-D. 2011. The transaldolase family: new synthetic opportunities from an ancient enzyme scaffold. *ChemBioChem* **12**: 1454-1474

Samland A.K., Sprenger G.A. 2006. Microbial aldolases as C-C bonding enzymes – unknown treasures and new developments. *Applied Microbiology and Biotechnology* **71**: 253-264

Samland A.K., Sprenger G.A. 2009. Transaldolase: from biochemistry to human disease. *The International Journal of Biochemistry & Cell Biology* **41**: 1482-1494

Samland A.K., Sprenger G.A. 2014. Synthetic potential of dihydroxyacetone-utilizing aldolases. In Industrial Biocatalysis. Pan Stanford Publishing. Singapore. 783–816

Sánchez-Moreno I., Hélaine V., Poupard N., Charmantray F., Légeret B., Hecquet L., García-Junceda E., Wohlgemuth R., Guérard-Hélaine C., Lemaire M. 2012a. One-pot cascade reactions using fructose-6-phosphate aldolase: efficient synthesis of D-arabinose 5-phosphate, D-fructose 6-phosphate and analogues. *Advanced Synthesis & Catalysis* **354**: 1725-1730

Sánchez-Moreno I., Nauton L., Théry V., Pinet A., Petit J.L., de Berardinis V., Samland A.K., Ghérard-Hélaine C., Lemaire M. 2012b. FSAB: A new fructose-6-phosphate aldolase from *Escherichia coli*. Cloning over-expression and comparative kinetic characterization with FSAA. *Journal of Molecular Catalysis B: Enzymatic* **84**: 9-14

Satanowski A., Dronsella B., Noor E., Vögeli B., He H., Wichmann P., Erb T.J., Lindner S.N., Bar-Even A. 2020. Awakening a latent carbon fixation cycle in *Escherichia coli*. *Nature Communications* **11**: 5812

Sauer U., Canonaco F., Heri S., Perrenoud A., Fischer E. 2004. The soluble and membrane-bound transhydrogenase UdhA and PntAB have divergent functions in NADPH metabolism of *Escherichia coli*. *The Journal of Biological Chemistry* **279**: 6613-6619

Sauer U., Lasko D.R., Fiaux J., Hoxhuli M., Glaser R., Szyperski T., Wüthrich K., Bailey J.E. 1999. Metabolic flux ratio analysis of genetic and environmental modulations of *Escherichia coli* central carbon metabolism. *Journal of Bacteriology* **181**: 6679-6688

Sautner V., Friedrich M.M, Lehwess-Litzmann A., Tittmann K. 2015. Converting transaldolase into aldolase through swapping of the multifunctional acid-base catalyst: common and divergent catalytic principles in F6P aldolase and transaldolase. *Biochemistry* **54**: 4475-4486

Schmidt N.G., Eger E., Kroutil W. 2016. Building bridges: biocatalytic C-C bond formation toward multifunctional products. *ACS Catalysis* **6**: 4286-4311

Schnaitman C.A., Klena J.D. 1993. Genetics of lipopolysaccharide biosynthesis in Enteric bacteria. *Microbiological Reviews* **57**: 655-682

Schneider S., Sandalova T., Schneider G., Sprenger G.A., Samland A.K. 2008. Replacement of a phenylalanine by a tyrosine in the active site confers fructose-6-phosphate aldolase activity to the transaldolase of *Escherichia coli* and human origin. *The Journal of Biological Chemistry* **283**: 30064-30072

Schürmann M. 2001. Dissertation. Biochemische Charakterisierung und Struktur-Funktionsbeziehungen bakterieller Transaldolasen und Fruktose-6-Phosphat Aldolasen. Universität Düsseldorf

Schuermann M., Mink D., Hyett D.J. 2008. Isobionics B.V., The Netherlands, WO 2008/067997

Schürmann M., Schürmann M., Sprenger G.A. 2002. Fructose 6-phosphate aldolase and 1-deoxy-D-xylulose 5-phosphate synthase from *Escherichia coli* as tools in enzymatic synthesis of 1-deoxysugars. *Journal of Molecular Catalysis B: Enzymatic* **19-20**: 247-252

Schürmann M., Sprenger G.A. 2001. Fructose-6-phosphate aldolase is a novel class I aldolase from *Escherichia coli* and is related to a novel group of bacterial transaldolases. *The Journal of Biological Chemistry* **276**: 11055-11061

Semkiv M.V., Ruchala J., Dmytruk K.V., Sibirny A.A. 2020. 100 years later, what is new in glycerol bioproduction. *Trends in Biotechnology* **38**: 907-916

Shimada T., Yamamoto K., Ishihama A. 2011. Novel members of the Cra regulon involved in carbon metabolism in *Escherichia coli*. *Journal of Bacteriology* **193**: 649-659

Shimizu K., Matsuoka Y. 2019. Regulation of glycolytic flux and overflow metabolism depending on the source of energy generation for energy demand. *Biotechnology Advances* **37**: 284-305

Shiue E., Brockman I.M., Prather K.L.J. 2015. Improving product yields on D-Glucose in *Escherichia coli* via knockout of *pgi* and *zwf* and feeding of supplemental carbon sources. *Biotechnology and Bioengineering* **112**: 579-587

Siegel J.B., Smith A.L., Poust S., Wargacki A.J., Bar-Even A., Louw C., Shen B.W., Eiben C.B., Tran H.M., Noor E., Gallaher J.L., Bale J., Yoshikuni Y., Gelb M.H., Keasling J.D., Stoddard B.L., Lidstrom M.E., Baker D. 2015. Computational protein design enables a novel one-carbon assimilation pathway. *Proceedings of the National Academy of Sciences of the USA* **112**: 3704-3709

Smyth K.M., Marchant A. 2013. Conservation of the 2-keto-3-deoxymanno-octulosonic acid (Kdo) biosynthesis pathway between plants and bacteria. *Carbohydrate Research* **380**: 70-75

Sniegowski P.D., Gerrish P.J., Lenski R.E. 1997. Evolution of high mutation rates in experimental populations of *E. coli*. *Nature* **387**: 703-705

Sperandeo P., Martorana A.M., Polissi A. 2017. Lipopolysaccharide biogenesis and transport at the outer membrane of Gram-negative bacteria. *Biochimica et Biophysica Acta* **1862**: 1451-1460

Sperandeo P., Pozzi C., Dehò G., Polissi A. 2006. Non-essential KDO biosynthesis and new essential cell envelope biogenesis genes in *Escherichia coli yrbG-yhbG* locus. *Research in Microbiology* **157**: 547-558

Sprenger G.A. 1995. Genetics of pentose-phosphate pathway enzymes of *Escherichia coli* K-12. *Archives of Microbiology* **164**: 324-330

Sprenger G.A. 2017. Glycerol as carbon source for production of added-value compounds. In Engineering of Microorganisms for the Production of Chemicals and Biofuels from Renewable Resources. Springer International Publishing AG. Cham (Switzerland). 93-123

Sprenger G.A., Schörken U., Sprenger G., Sahm H. 1995a. Transketolase A of *Escherichia coli* K12. Purification and properties of the enzyme from recombinant strains. *European Journal of Biochemistry* **230**: 525-532

Sprenger G.A., Schörken U., Sprenger G., Sahm H. 1995b. Transaldolase B of *Escherichia coli* K-12: cloning of its gene, *talB*, and characterization of the enzyme from recombinant strains. *Journal of Bacteriology* **177**: 5930-5936

Stasiak-Rózanska L., Blazejak S. 2012. Production of dihydroxyacetone from an aqueous solution of glycerol in the reaction catalyzed by an immobilized cell preparation of acetic acid bacteria *Gluconobacter oxydans* ATCC 621. *European Food Research and Technology* **235**: 1125-1132

Stellmacher L., Sandalova T., Leptihn S., Schneider G., Sprenger G.A., Samland A.K. 2015. Acid-base catalyst discriminates between a fructose 6-phosphate aldolase and a transaldolase. *ChemCatChem* **7**: 3140-3151

Stellmacher L., Sandalova T., Schneider S., Schneider G., Sprenger G.A., Samland A.K. 2016. Novel mode of inhibition by D-tagatose 6-phosphate through a Heyns rearrangement in the active site of transaldolase B variants. *Acta Crystallographica* **D72**: 467-476

Stincone A., Prigione A., Cramer T., Wamelink M.M.C., Campbell K., Cheung E., Olin-Sandoval V., Grüning N.-M., Krüger A., Alam M.T., Keller M.A., Breitenbach M., Brindle K.M., Rabinowitz J.D., Ralser M. 2015. The return of metabolism: biochemistry and physiology of the pentose phosphate pathway. *Biological Reviews* **90**: 927-963

Subedi K.P., Kim I., Kim J., Min B., Park C. 2008. Role of GldA in dihidroxyacetone and methylglyoxal metabolism of *Escherichia coli* K12. *FEMS Microbiology Letters* **279**: 180-187

Sudar M., Findrik Z., Vasić-Rački D., Clapés P., Lozano C. 2013. Aldol addition of dihydroxyacetone to N-Cbz-3-aminopropanal catalyzed by two aldolases variants in microreactors. *Enzyme and Microbial Technology* **53**: 38-45

Sudar M., Findrik Z., Vasić-Rački D., Soler A., Clapés P. 2015. A new concept for production of (3*S*,4*R*)-6-[(benzyloxycarbonyl)amino]-5,6-dideoxyhex-2-ulose, a precursor of D-fagomine. *RSC Advances* **5**: 69819-69828

Sugiyama M., Hong Z., Liang P.-H., Dean S.M., Whalen L.J., Greenberg W.A., Wong C.-H. 2007. D-fructose-6-phosphate aldolase-catalyzed one-pot synthesis of iminocyclitols. *Journal of the American Chemical Society* **129**: 14811-14817

Suzuki R., Kim B.-J., Shibata T., Iwamoto Y., Katayama T., Ashida H., Wakagi T., Shoun H., Fushinobu S., Yamamoto K. 2010. Overexpression, crystallization and preliminary X-ray analysis of xylulose-5-phosphate/fructose-6-phosphate phosphoketolase from *Bifidobacterium breve*. *Acta Crystallographica* **F66**: 941-943

Swanson M., Reguera G., Schaechter M., Neidhardt F.C. 2016. Microbe. 2nd edition. UK: Wiley

Szekrenyi A., Soler A., Garrabou X., Guérard-Hélaine C., Parella T., Joglar J., Lemaire M., Bujons J., Clapés P. 2014. Engineering the donor selectivity of D-fructose-6-phosphate aldolase for biocatalytic asymmetric cross-aldol additions of glycolaldehyde. *Chemistry - A European Journal* **20**: 12572 - 12583

Tan H.W., Aziz A., Aroua M.K. 2013. Glycerol production and its applications as a raw material: a review. *Renewable and Sustainable Energy Reviews* **27**: 118-127

Tanaka S., Lerner S.A., Lin E.C.C. 1967. Replacement of a phosphoenlopyruvate-dependent phosphotransferase by a nicotinamide adenine dinucleotide-linked dehydrogenase for the utilization of mannitol. *Journal of Bacteriology* **93**: 642-648

Tang C.-T., Ruch F.E., Lin E.C.C. 1979. Purification and properties of a nicotaminamide adenine dinucleotide-linked dehydrogenase that serves an *Escherichia coli* mutant for glycerol catabolism. *Journal of Bacteriology* **140**: 182-187

Tani Y., Dempsey W.B. 1973. Glycolaldehyde is a precursor of pyridoxal phosphate in *Escherichia coli* B. *Journal of Bacteriology* **116**: 341-345

Taschner P.E.M., Huls P.G., Pas E., Woldringh C.L. 1988. Division behavior and shape changes in isogenic *ftsZ*, *ftsQ*, *ftsA*, *pbpB*, and *ftsE* cell division mutants of *Escherichia coli* during temperature shift experiments. *Journal of Bacteriology* **170**: 1533-1540

Tchleu J.H., Norris V., Edwards J.S., Saier Jr. M.H. 2001. The complete phosphotransferase system in *Escherichia coli*. *Journal of Molecular Microbiology and Biotechnology* **3**: 329-346

Teleki A., Sánchez-Kopper A., Takors R. 2015. Alkaline conditions in hydrophilic interaction liquid chromatography for intracellular metabolite quantification using tandem mass spectrometry. *Analytical Biochemistry* **475**: 4-13

Thorell S., Schürmann M., Sprenger G.A., Schneider G. 2002. Crystal structure of decameric fructose-6-phosphate aldolase from *Escherichia coli* reveals inter-subunit helix swapping as a structural basis for assembly differences in the transaldolase family. *Journal of Molecular Biology* **319**: 161-171

Tittmann K. 2014. Sweet siblings with different faces: The mechanisms of FBP and F6P aldolase, transaldolase, transketolase and phosphoketolase revisited in light of recent structural data. *Bioorganic Chemistry* **57**: 263-280

Tompkins J.D., Nelson J.L., Hazel J.C., Leugers S.L., Stumpf J.D., Foster P.L. 2003. Error-prone polymerase, DNA polymerase IV, is responsible for transient hypermutation during adaptive mutation in *Escherichia coli*. *Journal of Bacteriology* **185**: 3469-3472

Torkelson J., Harris R.S., Lombardo M.-J., Nagendran J., Thulin C., Rosenberg S.M. 1997. Genome-wide hypermutation in a subpopulation of stationary-phase cells underlies recombination-dependent adaptive mutation. *The EMBO Journal* **16**: 3303-3311

Trachtmann N., Alvarez Fong K.F., Guitart Font E., Sprenger G.A. 2016. Construction of chromosomally encoded *lacZ* and *gfp* reporter strains of *Escherichia coli* for the study of global regulation of metabolism. *Engineering in Life Sciences* **16**: 675-681

Trudeau D.L., Edlich-Muth C., Zarzycki J., Scheffen M., Goldsmith M., Khersonsky O., Avizemer Z., Fleishman S.J., Cotton C.A.R., Erb T.J., Tawfik D.S., Bar-Even A. 2018. Design and in vitro realization of carbon-conserving photorespiration. *PNAS* **115**: E11455-E11464

Truniger V., Boos W. 1994. Mapping and cloning of *gldA*, the structural gene of the *Escherichia coli* glycerol dehydrogenase. *Journal of Bacteriology* **176**: 1796-1800

Typas A., Becker G., Hengge R. 2007. The molecular basis of selective promoter activation by the σ^S subunit of RNA polymerase. *Molecular Microbiology* **63**: 1296-1306

Van Dien S. 2013. From the first drop to the first truckload: commercialization of microbial processes for renewable chemicals. *Current Opinion in Biotechnology* **24**: 1061-1068

Vanderpool C.K., Gottesman S. 2004. Involvement of a novel transcriptional activator and small RNA in post-transcriptional regulation of the glucose phosphoenolpyruvate phosphotransferase system. *Molecular Microbiology* **54**: 1076-1089

Vanderpool C.K., Gottesman S. 2007. The novel transcription factor SgrR coordinates the response to glucose-phosphate stress. *Journal of Bacteriology* **189**: 2238-2248

Varma A., Young K.D. 2004. FtsZ collaborates with penicillin binding proteins to generate bacterial cell shape in *Escherichia coli*. *Journal of Bacteriology* **186**: 6768-6774

Vijaikishore P., Karanth N.G. 1987. Glycerol production by fermentation: a fed-batch approach. *Biotechnology and Bioengineering* **30**: 325-328

Vogel J., Luisi B.F. 2011. Hfq and its constellation of RNA. *Nature Reviews Microbiology* **9**: 578-589

Volk W.A. 1960. The synthesis of D-arabinose-5-phosphate. *Biochimica et Biophysica Acta* **37**: 365-367

Wadler C.S., Vanderpool C.K. 2007. A dual function for a bacterial small RNA: SgrS performs base pairing-dependent regulation and encodes a functional polypeptide. *Proceedings of the National Academy of Sciences of the USA* **104**: 20454-20459

Wagner N., Bade F., Straube E., Rabe K., Frazão C.J.R., Walther T. 2023. *In vivo* implementation of a synthetic metabolic pathway for the carbon-conserving conversion of glycolaldehyde to acetyl-CoA. *Frontiers in Bioengineering and Biotechnology* **11**: 1125544

Wang K., Wang X., Luo H., Wang Y., Wang Y., Tu T., Qin X., Bai Y., Huang H., Yao B., Su X., Zhang J. 2022. Synergetic fermentation of glucose and glycerol for high-yield N-acetylglucosamine production in *Escherichia coli*. *International Journal of Molecular Sciences* **23**: 773

Wang L., Chauliac D., Rhee M.S., Panneerselvam A., Ingram L.O., Shanmugam K.T. 2018. Fermentation of dihydroxyacetone by engineered *Escherichia coli* and *Klebsiella variicola* to products. *Proceedings of the National Academy of Sciences of the USA* **115**: 4381-4386

Wang Y., San K.-Y., Bennett G.N. 2013. Improvement of NADPH bioavailability in *Escherichia coli* through the use of phosphofructokinase deficient strains. *Applied Genetics and Molecular Biotechnology* **97**: 6883-6893

Waygood E.B., Mort J.S., Sanwal B.D. 1976. The control of pyruvate kinase of *Escherichia coli*. Binding of substrate and allosteric effectors to the enzyme activated by fructose 1,6-bisphosphate *Biochemistry* **15**: 277-282

Weickert M.J., Adhya S. 1993. The galactose regulon of *Escherichia coli*. *Molecular Microbiology* **10**: 245-251

Weiner M., Tröndle J., Albermann C., Sprenger G.A., Weuster-Botz D. 2014. Carbon storage in recombinant *Escherichia coli* during growth on glycerol and lactic acid. *Biotechnology and Bioengineering* **111**: 2508-2519

Wen L., Zheng Y., Li T., Wang P.G. 2016. Enzymatic synthesis of 3-deoxy-D-manno-octulosonic acid (KDO) and its application for LPS assembly. *Bioorganic & Medicinal Chemistry Letters* **26**: 2825-2828

Wendisch V.F., Lindner S.N., Meiswinkel T.M. 2011. Use of glycerol in biotechnological applications. In Biodiesel - Quality, Emissions and By-Products. IntechOpen: London (UK) 305-340

Westfall C.S., Levin P.A. 2018. Comprehensive analysis of central carbon metabolism illuminates connections between nutrient availability, growth rate, and cell morphology in *Escherichia coli*. *PLoS Genetics* **14**: e1007205

Whitfield C., Trent M.S. 2014. Biosynthesis and export of bacterial lipopolysaccharides. *Annual Review of Biochemistry* **83**: 99-128

Winkler H.H., Wilson T.H. 1966. The role of energy coupling in the transport of β-galactosides by *Escherichia coli*. *The Journal of Biological Chemistry* **241**: 2200-2211

Wittgenstein E., Berry H.K. 1960. Staining of skin with dihydroxyacetone. *Science* **132**: 894-895

Wittwer C.T., Herrmann M.G., Moss A.A., Rasmussen R.P. 1997. Continuous fluorescence monitoring of rapid cycle DNA amplification. *BioTechniques* **22**: 130-138

Wolf Jr. R.E., Shea F.M. 1979. Combined use of strain construction and affinity chromatography in the rapid, high-yield purification of 6-phosphogluconate dehydrogenase from *Escherichia coli*. *Journal of Bacteriology* **138**: 171-175

Woolston B.M., Edgar S., Stephanopoulos G. 2013. Metabolic engineering: past and future. *Annual Review of Chemical and Biomolecular Engineering* **4**: 259-288

Xu Y.-F., Amador-Noguez D., Reaves M.L., Feng X.-J., Rabinowitz J.D. 2012. Ultrasensitive regulation of anapleurosis via allosteric activation of PEP carboxylase. *Nature Chemcial Biology* **8**: 562-568

Yang J., Sun S., Men Y., Zeng Y., Zhu Y., Sun Y, Ma Y. 2017a. Transformation of formaldehyde into functional sugars *via* multi-enzyme stepwise cascade catalysis. *Catalysis Science & Technology* **7**: 3459-3463

Yang X., Ye L., Li A., Yang C., Yu H., Gu J., Guo F., Jiang L., Wang F., Yu H. 2017b. Engineering of D-fructose-6-phosphate aldolase A for improved activity towards cinnamaldehyde. *Catalysis Science & Technology* **7**: 382-386

Yang X., Yuan Q., Luo H., Li F., Mao Y., Zhao X., Du J., Li P., Ju X., Zheng Y., Chen Y., Liu Y., Jiang H., Yao Y., Ma H., Ma Y. 2019. Systematic design and *in vitro* validation of novel one-carbon assimilation pathways. *Metabolic Engineering* **56**: 142-153

Yao R., Liu Q., Hu H., Wood T.K., Zhang X. 2015. Metabolic engineering of *Escherichia coli* to enhance acetol production from glycerol. *Applied Microbiology and Biotechnology* **99**: 7945-7952

Yoo G., Dilkaute C., Bong J.-H., Song H.-W., Lee M., Kang M.-J., Jose J., Pyun J.-C. 2017. Autodisplay of the La/SSB protein on LPS-free *E. coli* for the diagnosis of Sjögren's syndrome. *Enzyme and Microbial Technology* **100**: 1-10

Young K.D. 2010. Bacterial shape: two-dimensional questions and possibilities. *Annual Review of Microbiology* **64**: 223-240

Zeppenfeld T., Larisch C., Lengeler J.W., Jahreis K. 2000. Glucose transporter mutants of *Escherichia coli* K-12 with changes in substrate recognition of IICB[Glc] and induction behavior of the *ptsG* gene. *Journal of Bacteriology* **182**: 4443-4452

Zhao J., Baba T., Mori H., Shimizu K. 2004. Effect of zwf gene knockout on the metabolism of *Escherichia coli* grown on glucose or acetate. *Metabolic Engineering* **6**: 164-174

Zhou Y.J., Yang W., Wang L., Zhu Z., Zhang S., Zhao Z.K. 2013. Engineering NAD$^+$ availability for *Escherichia coli* whole-cell biocatalysis: a case study for dihydroxyacetone production. *Microbial Cell Factories* **12**: 103

Zwaig N., Kistler W.S., Lin E.C.C. 1970. Glycerol kinase, the pacemaker for the dissimilation of glycerol in *Escherichia coli*. *Journal of Bacteriology* **102**: 753-759

9   Appendix

9.1   Verification of the constructed strains

9.1.1   Agarose gel electrophoresis of colony PCR results

$\Delta gutQ$ $\Delta kdsD$ $\Delta rbsK$::P$_{tac}$-$fsaA^{A129S}$
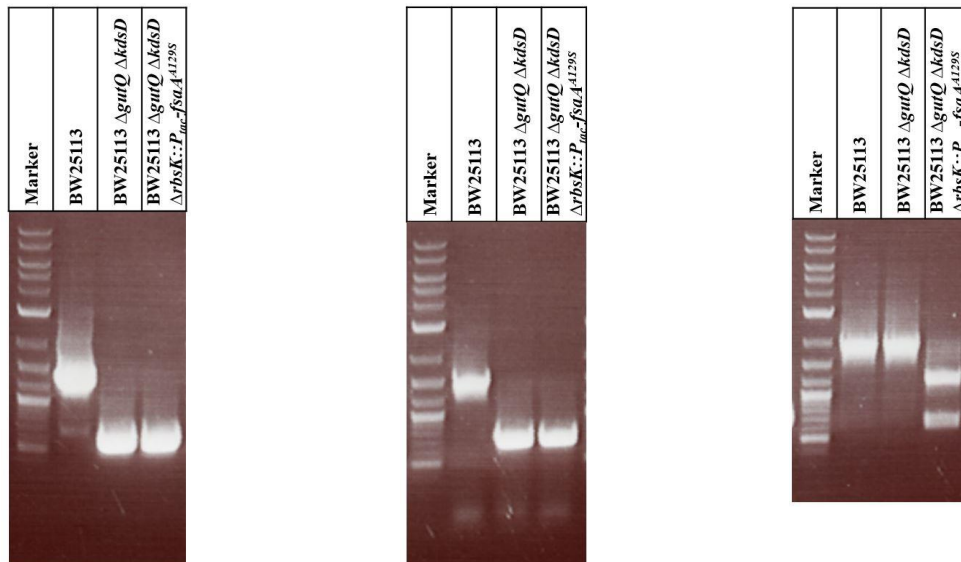
Figure 9-1. Verification of the presence or deletion of the *gutQ*, *kdsD*, *rbsK* genes in the chromosomes of BW25113, BW25113 $\Delta gutQ$ $\Delta kdsD$ and BW25113 $\Delta gutQ$ $\Delta kdsD$ $\Delta rbsK$::P$_{tac}$-$fsaA^{A129S}$ by colony PCR. For the confirmation of $\Delta rbsK$::P$_{tac}$-$fsaA^{A129S}$ a subsequent restriction with EcoR*I* was also necessary. BW25113 was used as a negative control for the deletions and BW25113 $\Delta gutQ$ $\Delta kdsD$ for the integration of P$_{tac}$-$fsaA^{A129S}$ in the ribose-operon. The size of the marker bands can be observed in Figure 9-2. The expected lengths of the amplicons are listed in Table 4-5.

Δ*zwf*
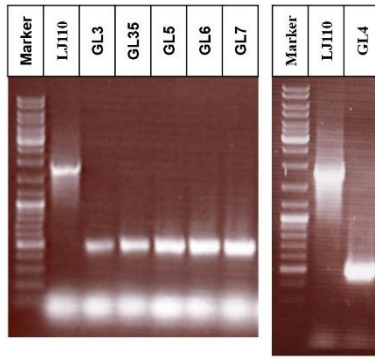
Δ*pfkB*
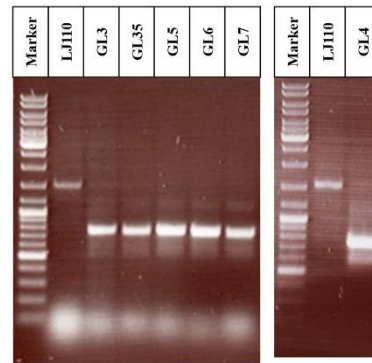
Δ*pfkA*
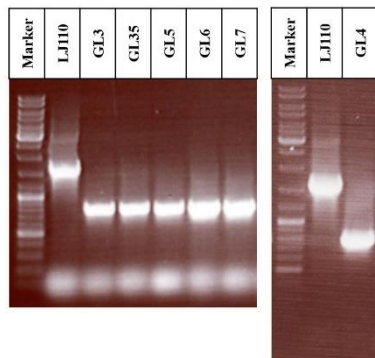
Δ*lacZ*::P*tac*-*fsaA*^{A129S}
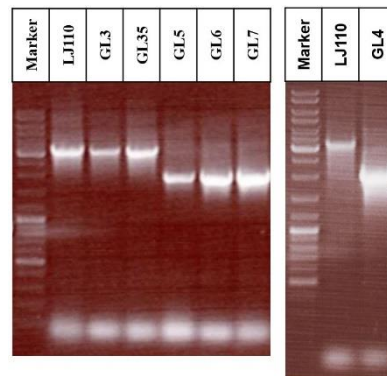
Δ*dhaKLM*
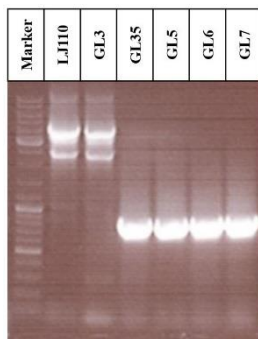
Δ*glpK*
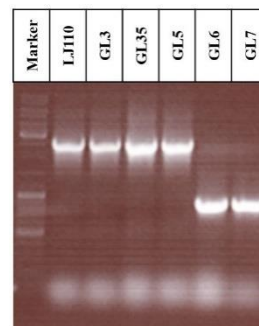
Δ*rbsK*::P*tac*-*gldA*
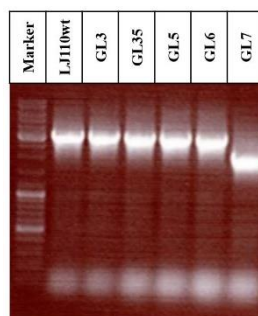
Marker
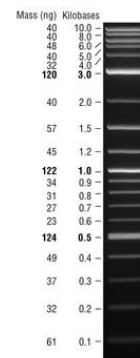
Figure 9-2. Verification of the presence or deletion of the *zwf*, *pfkB*, *pfkA*, *lacZ*, *dhaKLM*, *glpK* and *rbsK* genes in the chromosome of LJ110 and of the GL-strains by colony PCR. LJ110 was used as a negative control for the deletions (Guitart Font and Sprenger, 2020.). The expected lengths of the amplicons are listed in Table 4-5.

9.1.2   Sequence comparison

Figure 9-3. Sequence comparison (3' to 5') between the native promoter of *fsaB* and the evolved mutant promoter of *fsaB* (P*fsaB'(mutant)*). See Chapter 5.3.2 for details.

9.2 Cell dry weight trend lines
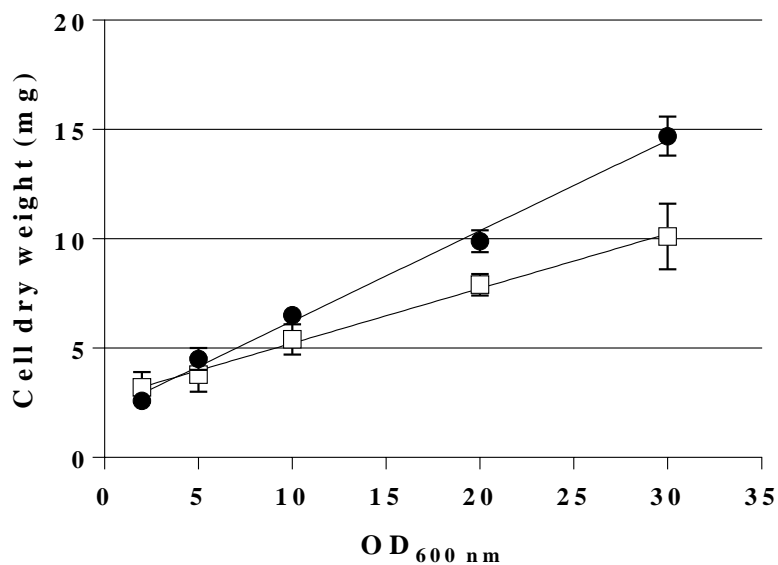
Figure 9-4. Cell dry weight (CDW) of LJ110 (●) and GL3 (□) plotted against the $OD_{600\,nm}$ used. $y = 0.4138x + 2.095$ for LJ110 with a R^2 of 0.9940. $y = 0.2505x + 2.724$ for GL3 with a R^2 of 0.9968. GL3 had at an $OD_{600\,nm}$ of 25 a CDW of 9.0 mg, while LJ110 had at the same $OD_{600\,nm}$ a CDW of 12.4 mg. For details see Chapter 4.8.4.

9.3 DHA or glycerol presence

LJ110
No DHA and no glycerol

GL6'
DHA

GL7'
glycerol
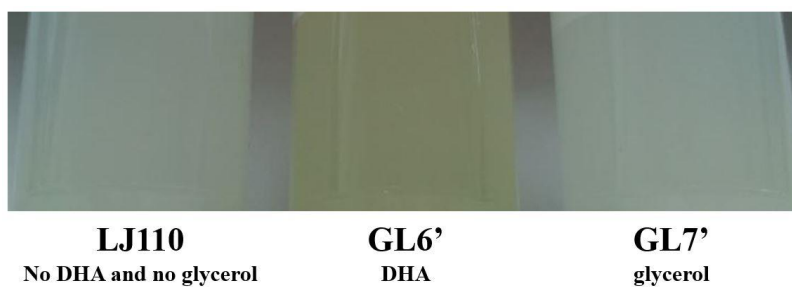
Figure 9-5. LJ110, GL6', GL7' cultures in a test tube after reaching the stationary phase on MM containing glucose and 100 μM IPTG. LJ110 and GL7' cultures presented a white colour, whereas GL6 culture had a yellow colour. This yellow colour was always observed in cultures in which a considerable concentration of DHA was determined in their supernatants.
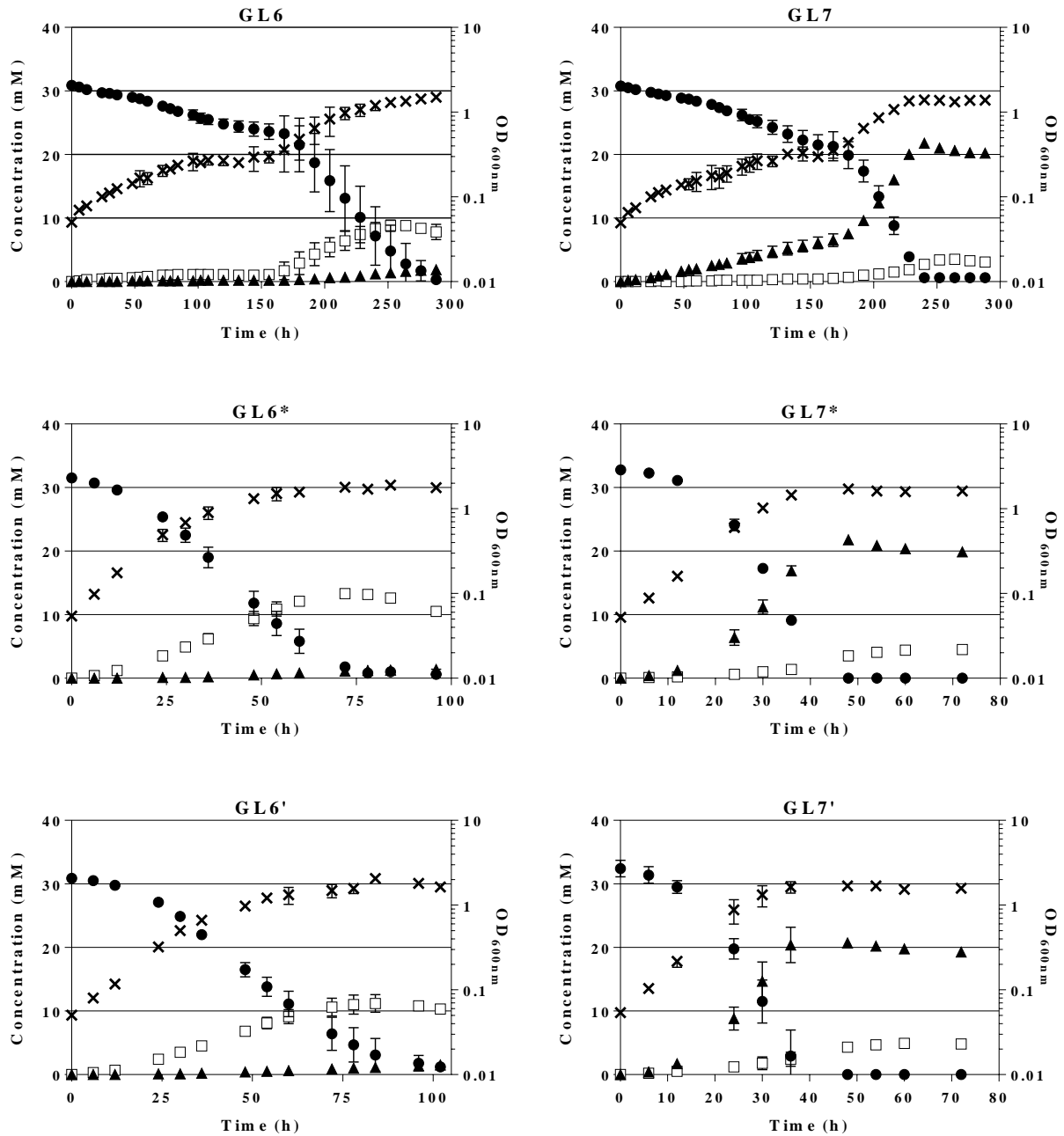
9.4   Glucose, DHA and glycerol concentrations over time
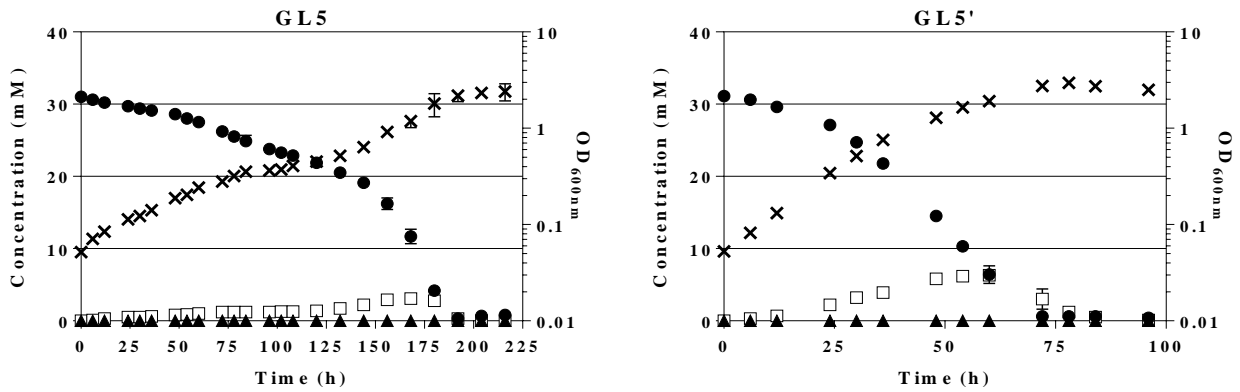
Figure 9-6. Progress over time of the $OD_{600\,nm}$ (✖) and the concentrations of glucose (●), DHA (□) and glycerol (▲) when GL5 and GL5* grew on MM with glucose and 100 μM IPTG. Average of two independent biological replicates. Inoculation of all strains took place from MM fructose with 100 μM IPTG overnight cultures.

207

Figure 9-7. Progress over time of the OD$_{600\,nm}$ (✖) and the concentrations of glucose (●), DHA (□) and glycerol (▲) when GL6, GL6*, GL6', GL7, GL7* and GL7' grew on MM with glucose and 100 μM IPTG. Average of two independent biological replicates. Inoculation of all strains took place from MM fructose with 100 μM IPTG overnight cultures. Data for GL6 and GL7 were reported by Guitart Font and Sprenger (2020).

9.5 Growth rate (μ) and doubling times (Gt)

Table 9-1. Growth rate (μ) and doubling times (Gt) of LJ110, GL-strains and GL-evolved strains on: LB; LB with 100 μM IPTG; LB with 0.1 % deoxycholate; LB with 56 mM glucose; MM with 28 mM fructose; MM with 28 mM fructose and 100 μM IPTG. For details see Chapter 4.5.2.

|		LJ110	GL3	GL4	GL5	GL5*	GL5'	GL6	GL6*	GL6'	GL7	GL7*	GL7'	GL35
LB	μ (h⁻¹)	1.17 ± 0.08	0.59 ± 0.09	0.82 ± 0.01	0.88 ± 0.02	0.88 ± 0.01	0.89 ± 0.01	0.79 ± 0.01	0.84 ± 0.02	0.88 ± 0.05	0.71 ± 0.01	0.70 ± 0.01	0.76 ± 0.11	0.62 ± 0.08
	Gt (min)	36 ± 2	71 ± 11	51 ± 1	47 ± 1	48 ± 1	47 ± 0	53 ± 0	50 ± 1	48 ± 2	59 ± 1	60 ± 1	55 ± 8	67 ± 8
LB + 100 μM IPTG	μ (h⁻¹)	1.17 ± 0.11	0.56 ± 0.17	0.80 ± 0.00	0.91 ± 0.21	0.88 ± 0.01	0.85 ± 0.04	0.85 ± 0.06	0.75 ± 0.05	0.77 ± 0.00	0.72 ± 0.01	0.73 ± 0.00	0.69 ± 0.04	0.57 ± 0.15
	Gt (min)	36 ± 4	78 ± 24	52 ± 0	47 ± 11	48 ± 1	50 ± 1	49 ± 3	56 ± 4	54 ± 0	58 ± 1	58 ± 0	61 ± 4	76 ± 21
LB + 0.1 % deoxycholate	μ (h⁻¹)	1.23 ± 0.01	0.48 ± 0.02	0.35 ± 0.06	0.74 ± 0.01	0.80 ± 0.15	0.79 ± 0.16	0.70 ± 0.06	0.72 ± 0.07	0.69 ± 0.04	0.65 ± 0.06	0.53 ± 0.11	0.57 ± 0.11	0.48 ± 0.03
	Gt (min)	34 ± 0	87 ± 3	120 ± 18	56 ± 0	54 ± 11	54 ± 10	59 ± 4	58 ± 6	51 ± 4	65 ± 5	86 ± 18	75 ± 16	87 ± 6
LB + 56 mM glucose	μ (h⁻¹)	1.34 ± 0.09	0.53 ± 0.01	0.84 ± 0.01	0.85 ± 0.12	0.79 ± 0.13	0.82 ± 0.08	0.73 ± 0.02	0.85 ± 0.03	0.75 ± 0.06	0.68 ± 0.01	0.59 ± 0.07	0.67 ± 0.06	0.52 ± 0.06
	Gt (min)	31 ± 2	79 ± 1	50 ± 1	50 ± 7	54 ± 9	51 ± 6	57 ± 1	49 ± 1	57 ± 5	62 ± 1	74 ± 9	63 ± 7	80 ± 9
MM + 28 mM fructose	μ (h⁻¹)	0.55 ± 0.00	0.27 ± 0.05	0.27 ± 0.01	0.30 ± 0.03	0.26 ± 0.01	0.29 ± 0.01	0.29 ± 0.03	0.32 ± 0.01	0.28 ± 0.02	0.29 ± 0.03	0.28 ± 0.00	0.28 ± 0.00	0.30 ± 0.00
	Gt (min)	75 ± 0	156 ± 27	156 ± 2	139 ± 10	159 ± 8	147 ± 4	146 ± 17	132 ± 6	151 ± 9	143 ± 16	147 ± 1	148 ± 0	140 ± 0
MM + 28 mM fructose + 100 μM IPTG	μ (h⁻¹)	0.55 ± 0.04	0.29 ± 0.05	0.27 ± 0.01	0.30 ± 0.01	0.28 ± 0.01	0.27 ± 0.02	0.29 ± 0.03	0.29 ± 0.01	0.29 ± 0.03	0.28 ± 0.03	0.26 ± 0.00	0.29 ± 0.01	0.27 ± 0.00
	Gt (min)	75 ± 5	147 ± 27	156 ± 7	138 ± 8	149 ± 11	159 ± 12	142 ± 15	144 ± 8	144 ± 16	147 ± 13	159 ± 00	146 ± 3	154 ± 0

9.6 Microscope photographs
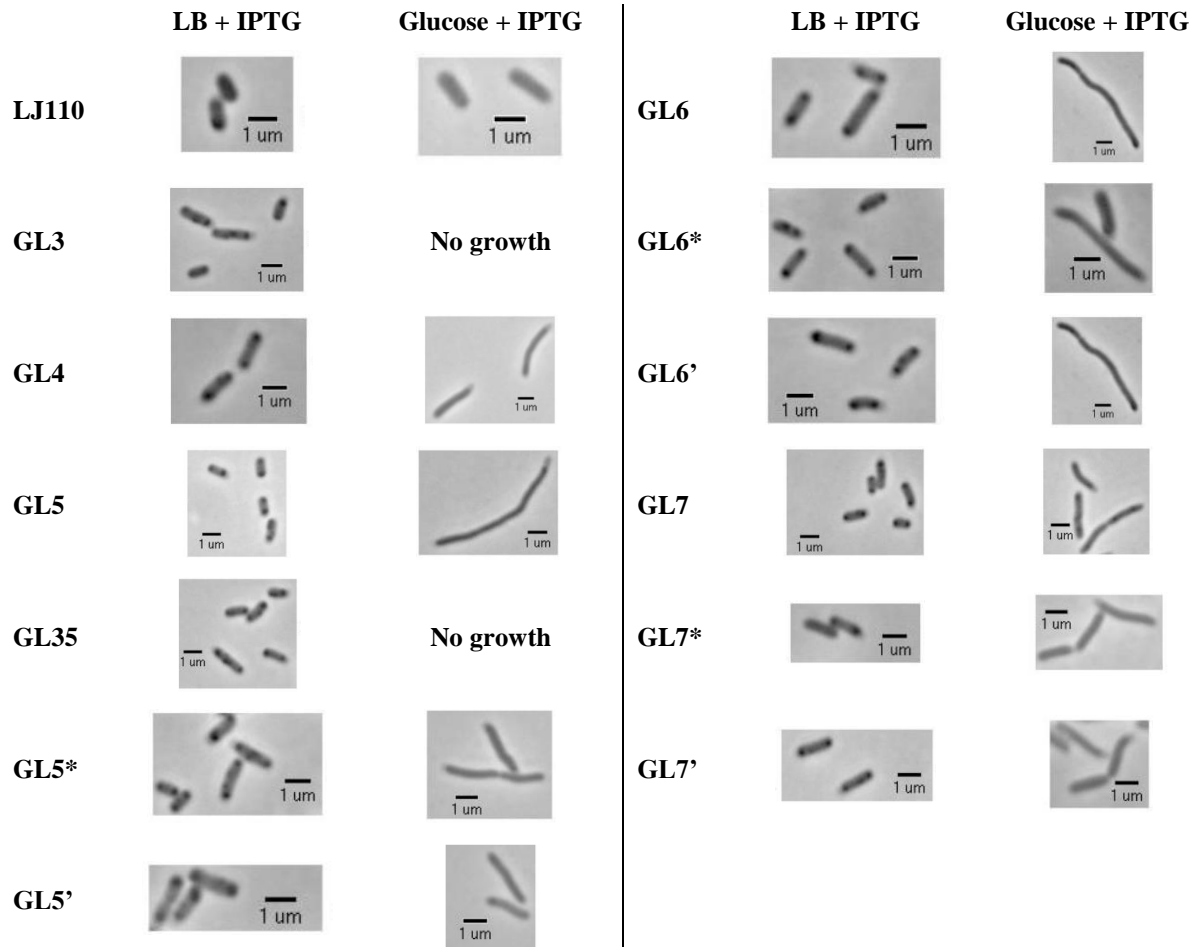
Figure 9-8. Microscope photographs of LJ110, GL-strains and GL-evolved strains. Photos taken after growth on: LB with 100 μM IPTG; and MM containing glucose and 100 μM IPTG. For details see Chapter 4.5.7.

In a 0 µM A5P culture of BW25113 Δ*gutQ* Δ*kdsD*::*kan*, a cell with a considerable length could be photographed with the help of a microscope (see Figure 9-9). It should be noted that, as shown in Table 9-2, nearly all BW25113 Δ*gutQ* Δ*kdsD*::*kan* cells lysed within 24 h incubation and the cultures showed no measurable growth and were not blurry, but many threads could be observed. On the other hand, no lysis was observed for the 0 µM A5P cultures of BW25113 Δ*gutQ* Δ*kdsD* Δ*rbsK*::P*tac*-*fsaA*^{A129S}, because the cells showed minimal growth. For this reason, many cells with a normal length can be observed next to unusually elongated cells in Figure 9-9.
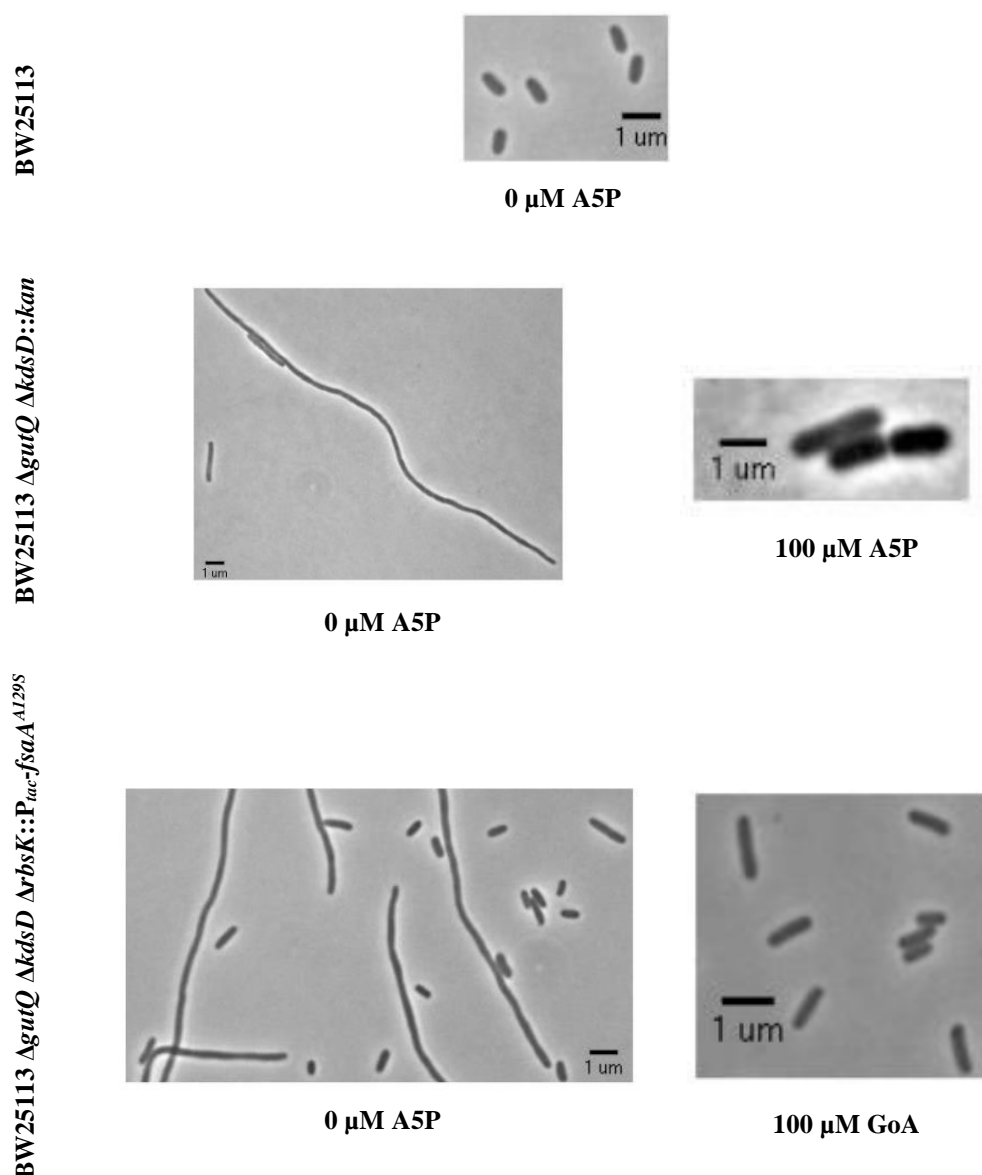

Figure 9-9. Microscope photographs of BW25113, BW25113 Δ*gutQ* Δ*kdsD*::*kan* and BW25113 Δ*gutQ* Δ*kdsD* Δ*rbsK*::P*tac*-*fsaA*^{A129S}. Photos taken after growth on MOPS-MM containing 28 mM glucose. BW25113 Δ*gutQ* Δ*kdsD* Δ*rbsK*::P*tac*-*fsaA*^{A129S} was induced with 100 µM IPTG during growth. For details see Chapter 4.5.7.

9.7   qPCR
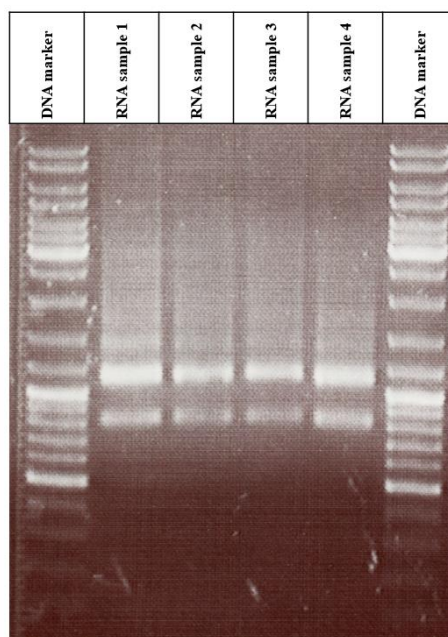
Figure 9-10. Example of an agarose gel electrophoresis after isolation of RNA. All RNA samples were harvested at an OD$_{600\,nm}$ between 0.8 and 1.4. An OD$_{260\,nm}$/OD$_{280\,nm}$ value between 2.07 and 2.17 was measured. All RNA samples used to produce cDNA were free from any DNA contamination (see Chapter 4.6.16). All cDNA samples used for qPCR had an OD$_{260\,nm}$/OD$_{280\,nm}$ value between 1.69 and 1.86.
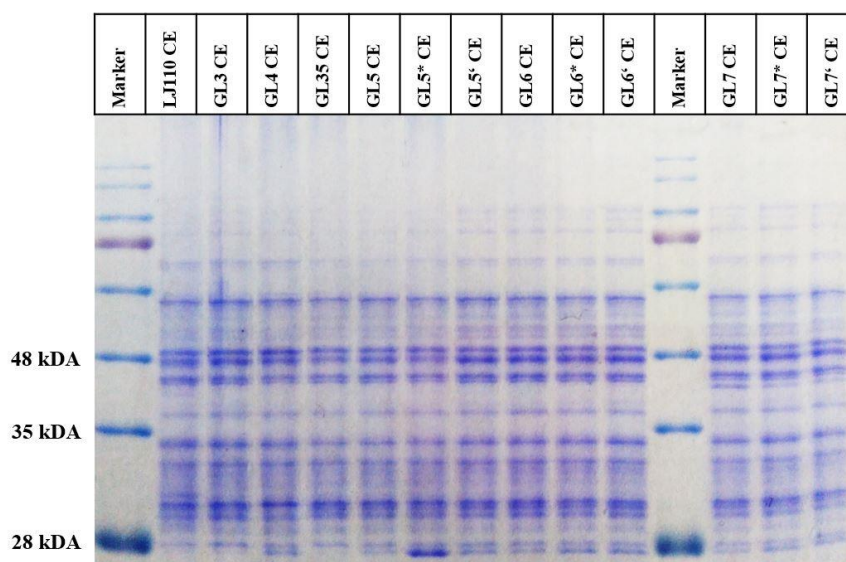
9.8   SDS-PAGE (LB, MM with fructose, and protein purification steps)
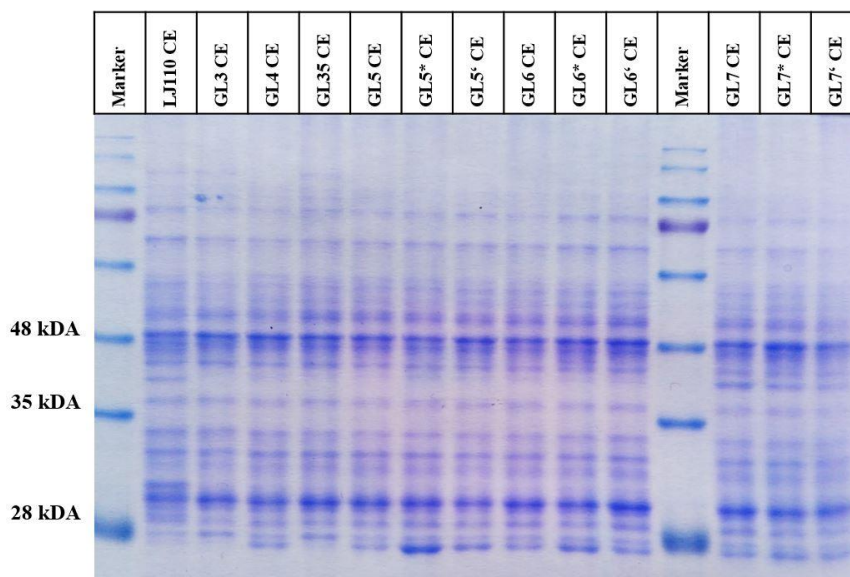
Figure 9-11. SDS-PAGE of cell-free extracts (CE) of LJ110, GL-strains and GL-evolved strains after growth on LB with 100 µM IPTG. Note that to enable the separation of protein bands between 35 kDa and 48 kDa, the SDS-PAGE was stopped after the lower bands of the protein marker had already left the SDS-gel on purpose. 5 µg protein were analysed per sample. + 20 % brightness; + 40 % contrast.
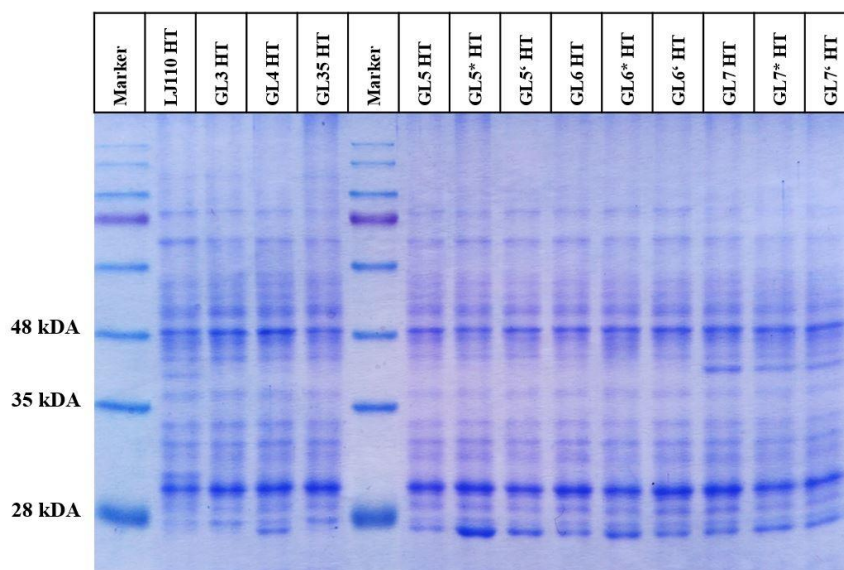
Figure 9-12. SDS-PAGE of heat-treated enriched fractions (HT) of LJ110, GL-strains and GL-evolved strains after growth on LB with 100 µM IPTG. Note that to enable the separation of protein bands around 28 kDa, the SDS-PAGE was stopped after the lower bands of the protein marker had already left the SDS-gel on purpose. 5 µg protein were analysed per sample. + 20 % brightness; + 40 % contrast.

Figure 9-13. SDS-PAGE of cell-free extracts (CE) of LJ110, GL-strains and GL-evolved strains after growt on MM with fructose and 100 µM IPTG. Note that to enable the separation of protein bands between 35 kDa and 48 kDa, the SDS-PAGE was stopped after the lower bands of the protein marker had already left the SDS-gel on purpose. 5 µg protein were analysed per sample. + 20 % brightness; + 40 % contrast.
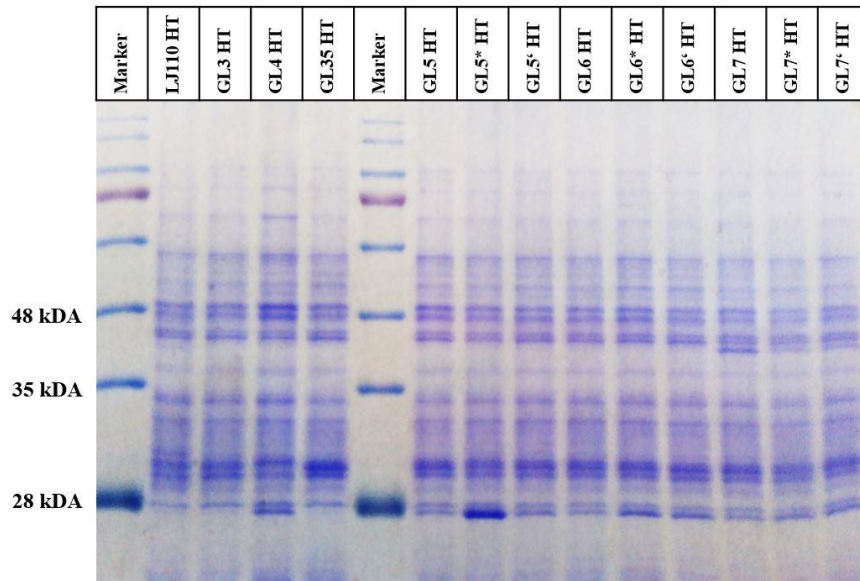
Figure 9-14. SDS-PAGE of heat-treated enriched fractions (HT) of LJ110, GL-strains and GL-evolved strains after growth on MM with fructose and 100 μM IPTG. Note that to enable the separation of protein bands around 28 kDa, the SDS-PAGE was stopped after the lower bands of the protein marker had already left the SDS-gel on purpose. 5 μg protein were analysed per sample. + 20 % brightness; + 40 % contrast.
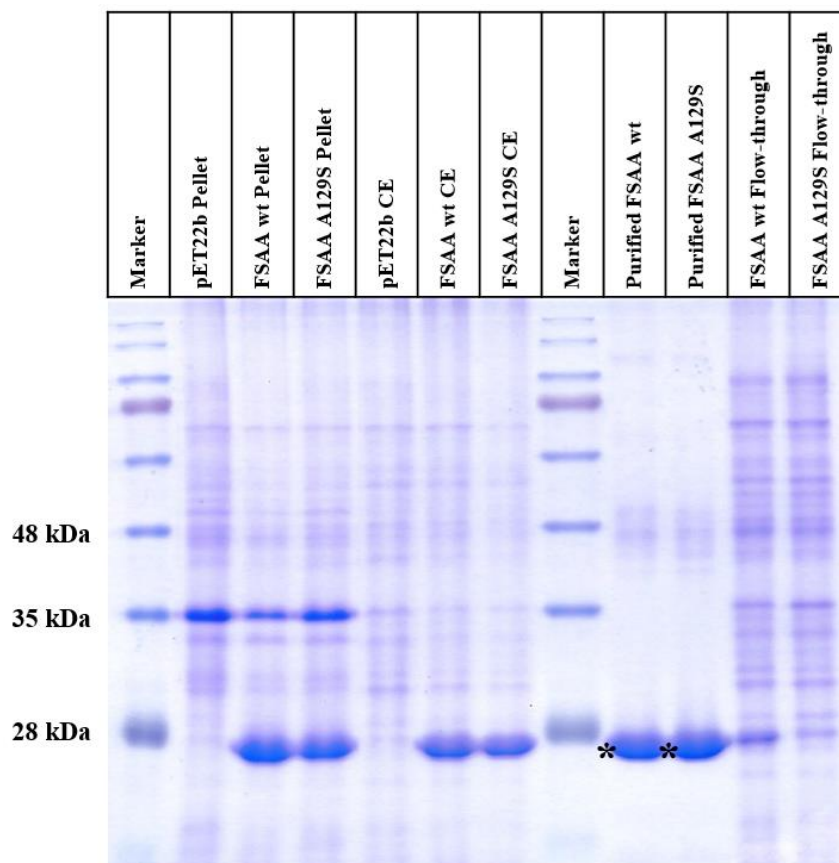

Figure 9-15. SDS-PAGE of the purification steps of the recombinant His-tagged proteins FSAA wt and FSAA A129S. For more details about the purification steps see Chapter 4.7.4. * denotes the bands corresponding to the purified His-tagged FSAA wt and FSAA A129S. Note that to enable the separation of protein bands around 28 kDa, the SDS-PAGE was stopped after the lower bands of the protein marker had already left the SDS-gel on purpose. 5 μg protein were analysed per sample.

9.9 Determination of the best suitable medium to study an A5P auxotroph strain

Meredith and Woodard (2005) used MOPS-MM instead of MM (after Tanaka *et al.*, 1967) because MOPS-MM has a lower P_i concentration. They claimed that low concentrations of P_i would avoid the inhibition of UhpT and, therefore, the A5P transport into the cell would be ensured in the presence of external G6P. It was also reported that the addition of only 15 µM A5P to the preculture was sufficient to allow the cells to grow overnight, but, at the same time, a carryover of A5P to the main culture was prevented. Here, the more suitable combination of minimal media and C-source to study the growth of an A5P auxotroph strain was determined. A suitable medium and C-source would be the ones that only allow an A5P auxotroph strain to grow when external A5P is present in the medium. As observed in Table 9-2, BW25113 Δ*gutQ* Δ*kdsD*::*kan* could not grow without addition of external A5P only on MOPS-MM regardless of the C-source used.

Table 9-2. $OD_{600\ nm}$ reached by BW25113 Δ*gutQ* Δ*kdsD*::*kan* on different media and C-sources. $OD_{600\ nm}$ measured after 24 h incubation at 37°C and 200 rpm.

Medium	C-source	Concentration C-source (w/v)	$OD_{600\ nm}$
MM (after Tanaka et al., 1967)	**Glycerol**	0.1 %	0.334
		0.5 %	partial lysis
	Glucose	0.1 %	0.336
		0.5 %	total lysis
MOPS-MM	**Glycerol**	0.1 %	total lysis
		0.5 %	total lysis
	Glucose	0.1 %	total lysis
		0.5 %	total lysis

9.10 Thin layer chromatography (TLC) of the synthesis of threose
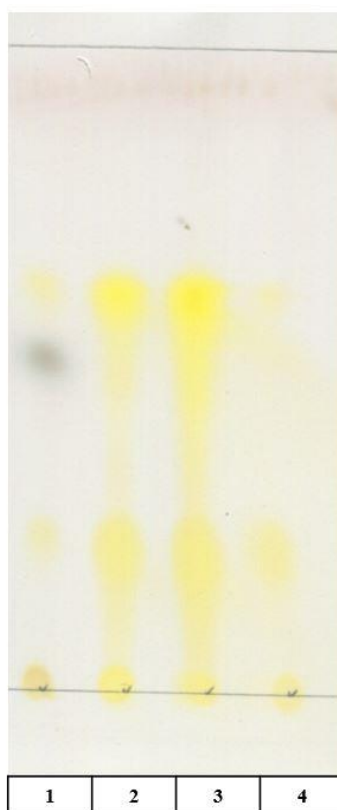
Figure 9-16. Thin layer chromatography (TLC) of the formation of threose due to the cross-aldol addition of GoA catalysed by FSAA A129S. TLC was performed after 24 h incubation of the reaction mixture at 30 °C and 90 rpm. 1) 200 mM GoA; 2) 200 mM D-(-)-threose; 3) 200 mM D-(+)-threose; and 4) 200 mM GoA + 1 U FSAA A129S. - 40 % contrast.

10 Curriculum Vitae

Personal information

Name:	Emma Guitart Font
Date and place of birth:	16.10.1990 in Esplugues de Llobregat (Spain)

Academic career

03/2015 – 02/2019	University of Stuttgart – Institute of Microbiology (Germany)
	Study of the central metabolic pathways and anabolism in *E. coli.*
09/2008 – 07/2013	Universitat Rovira i Virgili, Tarragona (Spain)
	Degree: Diploma in Biotechnology (Llicenciatura)
10/2011 – 09/2012	University of Stuttgart, Stuttgart (Germany)
	Erasmus Program

Work experience

12/2021 –	Lonza AG (Switzerland)
	Associate Principal Scientist QC Microbiology
09/2019 – 11/2021	ALTEN Switzerland AG
	Consultant at Novartis Pharma Stein AG, Stein (Switzerland)
04/2014 – 02/2019	University of Stuttgart – Institute of Microbiology (Germany)
03/2015 – 02/2019	Academic staff
04/2014 – 02/2015	Scientific assistant
11/2012 – 06/2013	Bayer Technology Services GmbH, Leverkusen (Germany)
	Internship in the department of Biochemistry & Biocatalysis
01/2012 – 09/2012	University of Stuttgart – Institute of Microbiology (Germany)
07/2012 – 09/2012	Student research assistant
04/2012 – 06/2012	Diploma thesis
	„Mutagenesis of the *talB* gene with the OmniChange Method"
01/2012 – 03/2012	Student research assistant